

High-spin phenomena in atomic nuclei

M. J. A. de Voigt

Kernfysisch Versneller Instituut, 9747 AA Groningen, The Netherlands

J. Dudek

Institute of Theoretical Physics, Warsaw University, PL-00-681 Warsaw, Poland
and The Niels Bohr Institute, Copenhagen University, DR-2100 Copenhagen, Denmark

Z. Szymański

Institute of Theoretical Physics, Warsaw University, PL-00-681 Warsaw, Poland
and Institut des Sciences Nucléaires, University of Grenoble, 53, av. des Martyrs, F-38026 Grenoble-Cedex, France

A description of high-spin phenomena in atomic nuclei is presented from both the experimental and theoretical points of view. The characteristic features of collective nuclear motion, such as rotational bands, band crossings, and backbending, as well as noncollective aspects, like high-spin isomers and irregular decay patterns, are discussed in detail. Recent achievements of the cranking model including the independent quasiparticle and the shell correction methods are reviewed. Changes in the structure of nuclei excited up to the highest possible angular momenta are analyzed; in particular, angular momentum alignment effects, shape changes, possible phase transitions, and sudden rearrangements in the single-particle structure are discussed. Phenomena related to the nuclear quasicontinuum spectra are also examined.¹

CONTENTS

I. Introduction	950	5. Odd-particle systems	968
A. Historical overview	950	F. A quantal description of noncollective rotation	969
B. Experimental progress in the high-spin region	950	III. High-Spin Nuclear Structure Studied by Means of γ -Ray Spectroscopy; Collective Rotation	972
C. Rotational bands and their crossings in deformed nuclei	951	A. Crossing rotational bands	972
D. Angular momentum alignment in weakly deformed nuclei; yrast traps	951	1. Phenomenological description	972
E. Region of very high spin	952	2. Independent quasiparticles	975
F. Perspectives	952	3. User's instructions for the independent quasiparticle diagrams	989
G. Justification of the review	952	4. The strength of interaction between crossing bands	991
II. Theoretical Aspects of the Nuclear Structure of High-Spin States	953	5. Variation in the pairing gap	992
A. Basic concepts	953	6. Other approaches to nuclear rotation	992
1. Cranking	953	B. Energy correlations in the high-spin spectra of collectively rotating nuclei	993
2. Variational principle and cranking model (an alternative derivation of the cranking model)	953	C. Pairing reduction at high spin and the dynamical moments of inertia	996
3. Signature—a quantum number classifying high-spin rotational spectra	954	D. Multiple Coulomb excitations of high-spin nuclear states	998
B. Single-particle motion and pairing correlations	955	IV. High-Spin Nuclear Structure Studied by Means of γ -Ray Spectroscopy; Noncollective Motion, Yrast Traps	1000
C. The liquid drop model and a classical description of rotation	957	A. Nuclear structure of yrast states; yrast traps	1005
D. The quantal description of collective rotation and the shell correction approach	958	1. The light neutron-deficient nuclei in the rare-earth region	1005
1. Single-particle Routhians	959	2. The hafnium isotopes	1011
2. The phenomenological shell correction approach	960	3. The lead region	1011
E. The independent quasiparticle method and collective rotation	961	4. Collective excitations	1012
1. The Bogolyubov transformation	963	B. Experimental techniques and problems	1015
2. The HFBC equations	963	1. Isotope assignment for yrast traps	1015
3. Symmetries: parity and signature	964	2. Determination of excitation energies and spins	1016
4. The generalized density matrix and the negative quasiparticle Routhians	965	3. Magnetic dipole and electric quadrupole moments	1017
	966	V. The Quasicontinuum Energy Spectrum	1018
		A. Population of the high-spin states	1018
		B. Experimental analysis of the gamma cascades in the quasicontinuum spectra	1020
		C. Nuclear structure information deduced from quasicontinuum spectra	1023
		VI. Summary	1025
		A. Conclusions	1025
		B. Perspectives	1026
		Acknowledgments	1028

¹Specialized material which may be skipped without breaking continuity is set off from the regular text with smaller print and indentation.

Appendix A. Details of Nuclear Potentials	1028
1. The Nilsson average potential	1028
2. The Woods-Saxon average potential	1030
3. Systematic differences between the single-particle spectra of the Nilsson and Woods-Saxon potentials	1032
Appendix B: Transition Probabilities, Lifetimes, and Feeding Times	1036
References	1038

I. INTRODUCTION

A. Historical overview

During the last decade nuclear high-spin states have been the subject of extensive experimental and theoretical studies. Several new methods and ideas have been introduced.

The phenomenon of nuclear rotation was discovered in the early 1950s following pioneering suggestions by A. Bohr (1952, 1953) and Bohr and Mottelson (1953). Early experiments on Coulomb excitation by Huus and Zupančič [(1953); see also Alder *et al.*, 1956], as well as on alpha decay by Asaro and Perlman (1952, 1953), provided firm evidence for nuclear rotational motion. During the 1960s further experiments with the $(\alpha, xn\gamma)$ reactions, initiated by Morinaga and Gugelot (1963), as well as first experiments with heavy ions [see, for example, Stephens *et al.* (1965)], including the in-beam gamma-ray measurements, supplied new material for a systematic analysis of rotational motion especially at relatively high angular momenta. Many peculiar properties of nuclear rotation were discovered and understood in terms of the coupling between rotational and other nuclear degrees of freedom (see the monograph by Bohr and Mottelson, 1969 and 1975).

This article presents further development of roughly the last decade concerning the region of high spins where substantial changes in nuclear structure can be expected as induced by the presence of large quantities of angular momentum.

B. Experimental progress in the high-spin region

The fascinating progress in this new field has been made possible by the essential development in experiments on exciting and detecting the high-spin states in nuclei. Several types of nuclear reactions and processes have been explored to search for the best ways of transferring a large amount of angular momentum to the final nuclear system. Such a transfer can be expected in nuclear reactions initiated by high-energy heavy-ion (HI) projectiles. Fusion reactions and multiple Coulomb excitation have appeared to provide most efficient ways of populating high-spin states.

It is instructive to analyze the decay of a compound nucleus formed after fusion of projectile and target nucleus (see Fig. 1), following from statistical calculations. The upper part of the figure shows that in the reaction con-

STATISTICAL MODEL CALCULATIONS

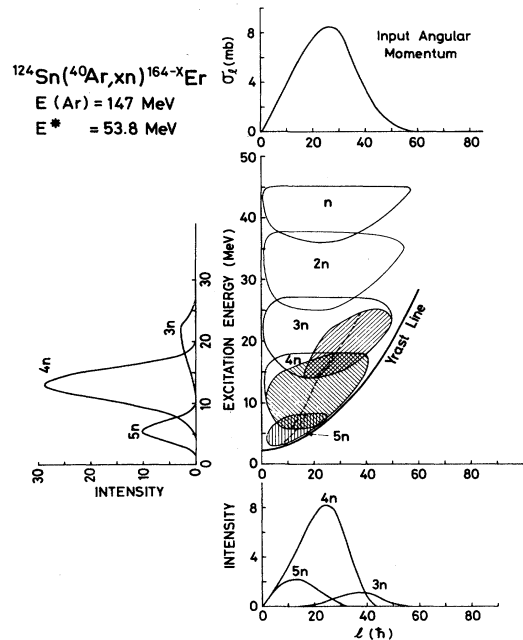


FIG. 1. Statistical model prediction for the decay of the ^{164}Er compound system formed at the excitation energy of 53.8 MeV in the $^{40}\text{Ar} + ^{124}\text{Sn}$ reaction. The assumed population of the ^{164}Er compound system is given as a function of angular momentum at the top part of the figure. Calculated populations are indicated schematically by contour lines as functions of the excitation energy and angular momentum of the system after the emission of 1–5 neutrons. The shaded regions of the $3n$ – $5n$ populations show the ranges where γ -ray emission competes. The entry populations for the $3n$ – $5n$ evaporation residues are also indicated as functions of angular momentum and of the excitation energy at the bottom and at the left-hand side of the figure. The predicted entry line is shown for each γ -ray emitting region (dotted line). The figure is taken from Hillis *et al.* (1979).

sidered a maximum angular momentum of $I \approx 50$ can be transferred, while the cross section reaches its maximum at $I \approx 30$. The central part of Fig. 1 gives the excitation energy E of the nucleus as a function of angular momentum. After the compound nucleus is formed, an equilibration process distributes the energy over all nucleons, some of which can be emitted (in this example, a maximum of five neutrons). An emitted neutron lowers considerably the excitation energy of the system, at least by its separation energy of ~ 8 –10 MeV, but to a much lesser degree the angular momentum (on the average about $1\frac{1}{2}$ unit per neutron). In general, not only neutrons but also charged particles can be emitted from the highly excited nucleus. A state populated by a particle that is emitted last is called an entry state. The set of all entry states forms the entry region. The results presented in the figure suggest that almost the entire initial angular momentum is carried off by the gamma rays.

In the discrete energy region, concentrated at the left

bottom corner of the central part of Fig. 1, the level density is low enough to enable observation of electromagnetic transitions as resolved lines in the γ -ray spectrum. With increasing excitation energies, however, the level density increases exponentially, creating many pathways for the γ rays which constitute a "continuum" in the spectrum. On the other hand, no significant overlap between levels is implied from estimated level densities and widths. Therefore the continuum part is commonly referred to as the quasicontinuum spectrum (qcs). The study of the qcs is a new field in nuclear spectroscopy; a selection of the information on the qcs obtained so far is discussed in Sec. V.

With the possibility of studying experimentally very-high-spin states using HI beams, new techniques have been developed to detect the deexciting γ rays. Enhancement of those γ rays with respect to the background due to the decay of other states, populated in a broad spin range in various reaction channels, has been achieved by using multidetector multiplicity arrays and total γ -ray energy (sum) spectrometers. Combination with conventional, but refined spectroscopic methods has revealed a wealth of new data on the qcs (see Sec. V), and has enabled the observation of "discrete" high-spin states, even up to spin 40 (see Secs. III and IV). This illustrates the difficulty of making a sharp distinction between the discrete energy region and the qcs. In fact, with progress in the selection techniques the maximum spin of a state observed by means of discrete γ lines is expected to increase even further.

C. Rotational bands and their crossings in deformed nuclei

Simultaneously with the vast increase of experimental data on high angular momentum phenomena a certain level of understanding has been achieved in the structure of the underlying nuclear motion.

Deformed nuclei—i.e., those characterized by a nonspherical spatial distribution of nuclear density—are known to exhibit rotational bands in their spectra. In a more detailed, "microscopic" description the rotational motion involves coherent contributions from many nucleons and is thus referred to as a collective motion. It results in a rotation of the nucleus as a whole around an axis different from the nuclear symmetry axis. A schematic example of a collective rotation of a prolate nucleus around an axis perpendicular to the nuclear symmetry axis is given in Fig. 2(a). It was found (cf. Secs. II and III) that the relation between the excitation energy \mathcal{E} and spin I is often a smooth one and, for spins that are not too high, can be approximated by $\mathcal{E} \sim I(I+1)$. The corresponding series of states with consecutively increasing angular momentum is called a rotational band. The lowest state of a band is traditionally referred to as a bandhead. Many states of different intrinsic structure can in principle become bandheads; the band built on the ground state of the nucleus is referred to as the ground-state band. All

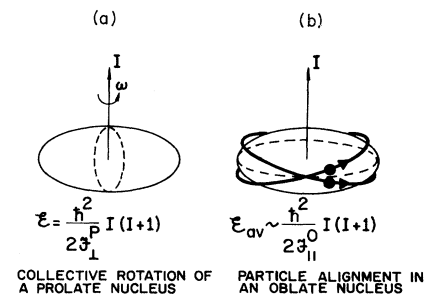


FIG. 2. Two different modes of rotation generating angular momentum. The quantities \mathcal{I}_\perp^P and $\mathcal{I}_{||}^O$ represent the moments of inertia of the two respective rigid bodies rotating around an axis perpendicular to (a) or parallel with (b), the symmetry axis.

other bands are called excited (or sometimes side) bands. The lowest energy state of a given angular momentum is called the yrast state. The sequence of all yrast states (represented in \mathcal{E} vs I plot) is called the yrast line (Swedish: *yr* "dizzy," *yrast* "the dizziest").

It is instructive to represent the rotational bands of a nucleus in the form of \mathcal{E} vs I dependence. Apparently, the different bands can cross in the (\mathcal{E}, I) plane; the first crossing of that type, viz., between the ground state and the first excited rotational band was found by Johnson *et al.* in 1972, in Stockholm. Since then the first excited rotational band in nuclei is often called the Stockholm, or *S* band.

Near the crossing point between the two bands several physical quantities related to the yrast line (e.g., energy, angular momentum, moment of inertia) represented as functions of the rotational frequency ω often show a characteristic multivalued behavior in the form of an *S* shape. This fact is referred to as a backbending effect (see a detailed discussion in Sec. III).

Typical examples of nuclei exhibiting such a collective rotation with crossing bands are provided in the regions of mass number $150 \leq A \leq 190$ (partly overlapping with the rare-earth region) and $A \geq 220$ (actinide region). These nuclei are, in addition, characterized by the existence of the superfluid type (pairing) nucleon-nucleon correlations, which result in an appreciable reduction of the rotational moments of inertia and the quasiparticle (rather than particle-hole) excitations.

D. Angular momentum alignment in weakly deformed nuclei; yrast traps

Another mechanism is likely to exist in spherical or weakly deformed nuclei. Here the alignment in the individual nucleonic orbitals along the nuclear symmetry axis appears to be the only possible mechanism of building up the high angular momentum. This type of nuclear motion (often referred to as a noncollective rotation) is illustrated schematically in Fig. 2(b); in this case a few valence nucleons move in an oblate average potential and populate orbitals with positive angular momentum projec-

tion on the nuclear symmetry axis. It has been discovered that the alignment of the angular momenta of only a few nucleons may be sufficient for producing relatively high nuclear spin. This is the case when the alignment is nearly complete and high-spin orbitals contribute to this phenomenon. We shall argue that this mode of excitation, due to the quantal (shell) structure of the individual-particle spectrum, predominates in spherical nuclei or in those with an oblate axially symmetric deformation (cf. Secs. II.F and IV). The resulting yrast energy spectrum represented as a function of angular momentum forms a considerably irregular sequence [no $I(I+1)$ rule obeyed locally]. However, a remarkable result follows from the quantal structure of the many-nucleon system: nevertheless, the $I(I+1)$ rule is still obeyed on the average over a larger interval in angular momentum.

The various single-particle states may contribute in different ways to the energies and wave functions of yrast states, possibly leading to a retardation in transitions deexciting these states, thus forming isomeric states. High-spin isomers located at the yrast line are commonly called yrast traps, or more specifically energy or structure traps in reference to the two underlying mechanisms (see Sec. II.F). Understanding of the single-particle features responsible for high-spin phenomena emerges from analysis of the vast amount of data on yrast traps.

The discoveries and investigations of the two phenomena, backbending and yrast traps in relation to collective and noncollective rotation, respectively, are among the most important achievements in recent nuclear spectroscopy in the domain of high angular momentum. It should be noted that some high-spin isomeric states had already been discovered about twenty years ago but that only recently has the notion of the yrast trap been introduced (see Sec. IV).

E. Region of very high spin

It is very interesting to analyze the properties of a rotating nucleus at still higher angular momenta in the region where the Coriolis and centrifugal interactions are strong enough not only to destroy the superfluid (pairing) correlations in nuclei but also to modify in an appreciable way the nucleonic motion in the nucleus. The first ideas about nuclear structure in such conditions profited considerably from classical analogies. In the classical description a nucleus is represented as a drop of incompressible liquid with properties adjusted to simulate those of a finite piece of nuclear matter. In addition to the rotational energy such a system is mainly characterized by its shape degrees of freedom determined by the surface tension and Coulomb energy. A detailed analysis of classical properties of rotating nuclei is given by Cohen *et al.* (1974). Later on, Bohr and Mottelson (1974) extended this classical picture, including the quantal description and analyzing various regions of nuclear motion with the increasing angular momentum. An important feature of this treatment, both classical and quantal,

is based on the assumption that the nuclear moment of inertia is in the very-high-spin region close to that of a rigid body.

F. Perspectives

Several challenging questions can be posed concerning the nuclear structure at increasing rotational frequencies. Collective and noncollective modes of excitation may compete and/or combine in various ways, thus generating the observed richness of nuclear phenomena at high angular momenta. One of the intriguing processes possibly occurring at high spin is a substantial change in nuclear shape. The high angular momentum states carry the information on the role of superfluid correlations existing among nucleons and, in particular, on a possible phase transition in the nucleus (from the superfluid to the normal phase). The precise theoretical description of such a phase transition and of the physical effects characteristic of its manifestation are among the interesting, presently unsolved questions on nuclear structure (see Secs. II and III). There are fascinating problems related to the influence of fast rotation and angular momentum alignment on the properties of the average nuclear field. Since a fast rotating nucleus is an intrinsic system in which the time reversal (τ) invariance is broken, new components that are not τ invariant may arise in the average nuclear field.

The possible existence of very large distortions in fast rotating nuclei bears some resemblance to large astronomical objects such as stars or planets. Those objects are held together by long-range gravitational forces, in contrast to atomic nuclei, which are governed by short-range nuclear forces. It is known that slowly rotating astronomical objects acquire a slight oblate deformation as a result of the balance between gravitational and centrifugal forces. At a certain critical angular momentum, however, the rotation is fast enough for a more economic accommodation of energy in an elongated rather than an oblate shape. This effect, called Jacobi instability, may lead to the formation of double stars. We shall see that such a shape transition seems possible in some physical situations involving fast rotation of nuclei (see Sec. V.C). The search for superdeformed shapes in atomic nuclei presently poses one of the challenging problems in nuclear structure.

G. Justification of the review

It is our feeling that combining both the experimental and theoretical aspects of high-spin phenomena in one presentation is particularly relevant at present. During the last decade powerful experimental techniques and theoretical methods were elaborated, due to the growing interest in high-spin nuclear physics. The investigations have provided convincing evidence for collective and noncollective high-spin rotation from both the theoretical and experimental points of view, despite the fact that many questions about the structure of some high-spin nuclear

states are not answered yet. A new class of experiments has just started, based on the gamma-ray detection in a 4π geometry for each reaction event (crystal ball spectrometers). Among the theoretical approaches, the independent quasiparticle description of rotational bands is at present a powerful tool for interpreting a broad class of high-spin phenomena. The independent quasiparticle description promises a degree of generality analogous to that of the Nilsson model which was introduced in the early 1950s to interpret single-particle excitations. This and related methods will be discussed throughout. An elementary treatment of some of the current approaches can be found in a textbook by Szymański (1983).

II. THEORETICAL ASPECTS OF THE NUCLEAR STRUCTURE OF HIGH-SPIN STATES

A. Basic concepts

The occurrence of collective nuclear rotation is closely related to the existence of appreciable deviations from spherical symmetry in nuclear shapes. Although the original nuclear Hamiltonian constructed from two-body nucleon-nucleon forces is rotationally invariant, strong deviations from spherical shape may arise in some nuclei as a result of a spontaneous symmetry breaking mechanism (Bohr and Mottelson, 1975; Bohr, 1976). In this case the average nuclear field acting on individual nucleons—e.g., of the Hartree-Fock type—does not exhibit spherical symmetry either, and its deformation is assumed to follow that of a nuclear-matter distribution.

The rotation of a nucleus about an axis that does not overlap with the symmetry axis induces coupling between the individual nucleonic orbitals and the rotational degrees of freedom of the average nuclear field. This coupling, which tends to align partially each of the nucleonic angular momenta, may be regarded as an effect underlying most of the important phenomena in the domain of rotational excitations.

High angular momentum states in nuclei may also exhibit an altogether different, noncollective nature. They may be created by the complete alignment of angular momenta of only a few individual nucleonic orbitals. Such states are formed most favorably in nuclei with an average nuclear field which is either spherical or axially symmetric with respect to the axis of the angular momentum alignment. They are referred to as states of noncollective rotation.

The two modes of rotation at high angular momentum may coexist and/or compete in various ways. At very high angular momenta the difference between the two excitation modes becomes less and less pronounced, since at extremely high spins all orbitals tend to align their angular momenta completely, regardless of the mode of rotation.

In order to gain a first insight into the average properties of rotating nuclei a description of nuclear rotation in terms of classical motion may be employed as a zeroth

approximation. The nucleus is then thought to have a structure analogous to that of a rotating drop of matter, with its dynamical properties represented by surface tension and the Coulomb energy coefficients. These coefficients are adjusted in order to represent the properties of nuclear matter. The collective rotation of such a drop involves the moment of inertia as the main parameter characterizing the rotational features of the system.

The quantal treatment of nuclear collective and noncollective rotations starts with the introduction of a nuclear Hamiltonian. Throughout this paper its essentially individual-particle character is assumed to dominate in the nuclear motion considered. This corresponds to the leading assumption of many recent investigations providing quantitative results on high-spin states in nuclei. Consequently, the Hamiltonian H will be assumed in the form of an independent-particle term, possibly supplemented by a residual two-body interaction. Either this two-body interaction will be neglected or only the short-range pairing force that produces nuclear superfluid correlations will be adopted.

1. Cranking

In order to account for collective rotation around an axis perpendicular to the symmetry axis the procedure suggested by Inglis (1954, 1955) known as the cranking-model approximation is frequently employed. The nuclear field is rotated externally with constant angular velocity about a fixed axis. The rotation of an average field V , unsymmetric with respect to the rotation axis, introduces an explicit time dependence to the Schrödinger equation. This may, however, be reduced to a stationary equation of motion when the laboratory frame (x, y, z) is transformed into the rotating frame (x', y', z') :

$$\begin{aligned} x' &= x, \\ y' &= y \cos \omega t + z \sin \omega t, \\ z' &= -y \sin \omega t + z \cos \omega t. \end{aligned} \quad (2.1)$$

Here $x' = x$, since the x axis is chosen as the rotation axis. Transforming the original time-dependent Schrödinger equation

$$i\hbar \frac{\partial \psi_{\text{lab}}}{\partial t} = H_{\text{lab}} \psi_{\text{lab}} \quad (2.2)$$

with ψ_{lab} and H_{lab} referring to a nonrotating laboratory coordinate frame, by means of the rotation operator

$$\mathcal{R} = e^{-iJ_x \omega t}, \quad (2.3)$$

where $J_x = J_{x'}$ denotes the x component of the total angular momentum, we obtain

$$\psi_{\text{lab}} = \mathcal{R} \psi_{\text{intr}} \quad (2.4)$$

and

$$H_{\text{lab}} = \mathcal{R} H_{\text{intr}} \mathcal{R}^{-1}. \quad (2.5)$$

The quantities ψ_{intr} and H_{intr} refer to the body-fixed (rotating, intrinsic) coordinate frame. Within this frame one has, after substituting Eqs. (2.4) and (2.5) into Eq. (2.2),

$$i\hbar \frac{\partial \psi_{\text{intr}}}{\partial t} = (H_{\text{intr}} - \hbar\omega J_{x'})\psi_{\text{intr}}, \quad (2.6)$$

with the second term on the right-hand side following from the time derivative of \mathcal{R} . Equation (2.6) is stationary, since the potential entering H_{intr} is now expressed in the rotating coordinate frame (x', y', z') and thus does not depend explicitly on time. It is assumed that the average field V is not affected by rotation. Thus the operation $\mathcal{R}H_{\text{intr}}\mathcal{R}^{-1}$ is equivalent to merely transforming the coordinates from the laboratory to the rotating coordinate systems.

The second term on the right-hand side of Eq. (2.6) is in analogy to the Coriolis and centrifugal forces in classical mechanics.

To demonstrate this analogy let us consider the expressions for the two forces

$$\mathbf{f}_{\text{cor}} = -2m\omega \times \dot{\mathbf{r}}$$

and

$$\mathbf{f}_{\text{cfug}} = -m\omega \times (\omega \times \mathbf{r})$$

in the rotating coordinate frame (x', y', z') . We must construct a classical analogy to the quantal expression (2.6) of the Hamiltonian in a rotating coordinate frame, i.e., a classical Hamiltonian in a rotating frame. We first observe that the centrifugal force $\mathbf{f}_{\text{cfug}} = m(0, -\omega^2 y', -\omega^2 z')$ for $\omega = (\omega, 0, 0)$, and that it can thus be generated by the "potential" $V_{\text{cfug}} = -\frac{1}{2}m\omega^2(y'^2 + z'^2)$. The velocity proportional \mathbf{f}_{cor} , however, has a form which is mathematically identical to that of a Lorentz force acting on a pointlike particle moving in a uniform magnetic field. After redefinition of constants in formulas from electromagnetics the velocity can be described by a "vector potential" $\mathbf{A} = m\omega \times \mathbf{r}'$. Bearing in mind the analogy with electromagnetics, we have

$$\begin{aligned} H_{\text{class}}^{\omega} &= \frac{1}{2m}(\mathbf{p}' - m\omega \times \mathbf{r}')^2 - \frac{1}{2}m\omega^2(y'^2 + z'^2) \\ &= \frac{1}{2m}\mathbf{p}'^2 - \omega L_{x'}, \end{aligned}$$

where $\mathbf{L}' = \mathbf{r}' \times \mathbf{p}'$. The last equality just demonstrates the similarity between the classical and quantal expressions for the Hamiltonian in rotating coordinate frames.

Equation (2.6) may be written as

$$i\hbar \frac{\partial \psi_{\text{intr}}}{\partial t} = H^{\omega}\psi_{\text{intr}}, \quad (2.7)$$

where

$$H^{\omega} = H_{\text{intr}} - \hbar\omega J_{x'} \quad (2.8)$$

is called a cranking Hamiltonian or Routhian. Since H^{ω} does not depend on time, the solution to Eq. (2.7) can be reduced to the eigenvalue problem of H^{ω} . In particular, if H describes a system of independent particles, then so does H^{ω} , because $J_{x'}$ is a one-body operator. Since the

eigenvalues \mathcal{E}_i^{ω} of H^{ω} are not the laboratory-frame energies, one has to transform the eigenfunctions obtained in a rotating coordinate frame back to the laboratory frame [inverse to operation (2.4)] and calculate the expectation values of the Hamiltonian in the laboratory coordinate frame with the transformed wave functions. This is in full analogy to classical mechanics, where the Hamiltonian in a rotating frame of reference H_{class} does not overlap with energy (see, for example, Landau and Lifschitz, 1965).

To perform such a transformation one starts with the eigenvalue problem for the total nuclear Routhian

$$H^{\omega} |\psi\rangle = \mathcal{E}^{\omega} |\psi\rangle. \quad (2.9)$$

Remembering that the total Routhian operator equals the sum of single-particle operators

$$H^{\omega} = \sum_i h^{\omega}(i) = \sum_i [h(i) - \hbar\omega j_{x'}(i)], \quad (2.10)$$

[with $h(i) \equiv h_{\text{intr}}(i)$] one diagonalizes first the problem

$$h^{\omega} |\chi_v^{\omega}\rangle = e_v^{\omega} |\chi_v^{\omega}\rangle. \quad (2.11)$$

Here the eigenvalue e_v^{ω} denotes the corresponding single-particle Routhian. The true energies e_v are defined as the expectation values of the Hamiltonian $h(i)$ [not $h^{\omega}(i)$] with the eigenfunctions $|\chi_v^{\omega}\rangle$ in a body-fixed frame:

$$\begin{aligned} e_v &= e_v(\omega) = \langle \chi_v^{\omega} | h | \chi_v^{\omega} \rangle \\ &= e_v^{\omega} + \hbar\omega \langle \chi_v^{\omega} | j_{x'} | \chi_v^{\omega} \rangle. \end{aligned} \quad (2.12)$$

The total energies are then expressed as sums:

$$\mathcal{E} = \sum_v e_v^{\omega} + \hbar\omega \sum_v \langle \chi_v^{\omega} | j_{x'} | \chi_v^{\omega} \rangle. \quad (2.13)$$

In the ground state the summation over v is understood to include the states with lowest single-particle Routhians e_v^{ω} . In the last relation the approximate equality

$$I \approx I_x = \sum_v \langle \chi_v^{\omega} | j_{x'} | \chi_v^{\omega} \rangle,$$

which is valid in the limit of high spin, is utilized.

2. Variational principle and cranking model (an alternative derivation of the cranking model)

The Hamiltonian of Eq. (2.8) follows from the variational principle. In such a derivation the expectation value of the original Hamiltonian H_{intr} is minimized,

$$\langle H_{\text{intr}} \rangle = \min, \quad (2.14)$$

under the subsidiary condition

$$\langle J_{x'} \rangle = I. \quad (2.15)$$

Here the $J_{x'}$ component of the total nucleonic angular momentum is identified with the total angular momentum I ; such an approximation becomes a good one in the limit of fast rotation. Introducing the Lagrange multiplier $\hbar\omega$, we obtain the wave functions and energies from

the condition

$$\langle H_{\text{intr}} - \hbar\omega J_x' \rangle \equiv \langle H^\omega \rangle = \min, \quad (2.16)$$

where $\hbar\omega$ may be determined from Eq. (2.15). It can be shown that the Lagrange multiplier $\hbar\omega$ divided by \hbar is identical to the angular velocity of rotation. We thus arrive at the same form of the cranking-model Hamiltonian as in Eq. (2.8). Moreover, the variational formulation of the cranking model as described above can be applied to both the collective and noncollective rotational modes.

The cranking-model procedure presented above, with its two derivations (given here and in the preceding section), turns out to be a basic theoretical tool in the analysis of high angular momentum phenomena. This procedure, although known since 1954, was at that time applied in the perturbation approximation up to terms of only the second order in ω , in the calculation of the nuclear moments of inertia. It was not until the early 1970's that the full advantage of the cranking model was realized and applied for determining the nucleonic motion in a rotating system up to all orders in angular velocity ω (Ring *et al.*, 1970; Banerjee *et al.*, 1973; Bengtsson *et al.*, 1975; Andersson *et al.*, 1976; Neergaard *et al.*, 1976; and many works which followed). The derivation, employing the variational principle, remains valid for axially symmetric nuclei and, in particular, for the spherical nuclei, as well. In this case, the cranking model provides a recipe for selecting nucleonic orbitals which are most favorable in creating states with the largest possible angular momenta and with the lowest possible energy. The spherical shell-model calculations which were mainly based on intuitively estimated configurations for high-spin states are also encompassed by the cranking-model procedure, without losing accordance with the variational principle contained in Eqs. (2.14) and (2.15).

The cranking-model approximation is a semiclassical one, since the rotation is imposed externally. It also breaks the rotational invariance, since a fixed rotation axis is adapted. All these features, however, become less important for very fast rotation ($I \gg 1$).

The cranking-model procedure becomes a poor approximation in the immediate vicinity of the crossing frequency (in the \mathcal{E} vs ω plot) between two weakly interacting bands. Problems of this type will be discussed in Sec. II.E (cf. Sec. II.E.4).

3. Signature—a quantum number classifying high-spin rotational spectra

The diagonalization of H^ω in the body-fixed frame is of course greatly simplified after one has made use of its possible symmetries. Obviously, the symmetries in H^ω depend on the symmetries existing in the original nuclear Hamiltonian H . To simplify the notation let us set H equal to H_{intr} . In most cases of interest H is invariant with respect to space inversion \mathcal{P} (parity invariance) and time reversal \mathcal{T} . In addition, in many cases the nuclear deformed average field V entering H is characterized by

even-multipolarity components only—quadrupole, hexadecapole components, etc.—but not by the octupole component, etc. (see also discussion of single-particle potentials in Appendix A). Then the intrinsic Hamiltonian remains invariant with respect to the three rotations \mathcal{R}_κ through angle π around the three principal axes of the nuclear field:

$$\mathcal{R}_\kappa = \exp(-i\pi J_\kappa), \quad (2.17)$$

with $\kappa = x'$, y' , or z' denoting the directions of the three axes. The finite-symmetry group defined by the three operations (2.17) is called D_2 .

Returning to the full cranking Hamiltonian H^ω [Eq. (2.8)], we immediately see that it remains parity invariant (since $[H, \mathcal{P}] = 0$ and $[J_x, \mathcal{P}] = 0$), while both the time-reversal and the full D_2 symmetries are broken (because still $\mathcal{T}H\mathcal{T}^{-1} = H$, while $\mathcal{T}J_x'\mathcal{T}^{-1} = -J_x'$, and, moreover, $\mathcal{R}_y J_x' \mathcal{R}_y^{-1} = -J_x'$ and $\mathcal{R}_z J_x' \mathcal{R}_z^{-1} = -J_x'$). The only symmetry that remains, in addition to the \mathcal{P} symmetry, is the invariance of H with respect to the rotation

$$\mathcal{R}_{x'} = \exp(-i\pi J_{x'}). \quad (2.18)$$

The square of this operator is equivalent to a rotation of the system through the angle 2π , and thus it does not influence the wave function of a system composed of an even number of fermions. On the contrary, systems with an odd number of fermions transform under $(\mathcal{R}_{x'})^2$ like spinors, and consequently the corresponding total wave function changes sign. Thus we can write

$$(\mathcal{R}_{x'})^2 = (-1)^A, \quad (2.19)$$

where A denotes the total number of fermions. Denoting by r the eigenvalues of $\mathcal{R}_{x'}$ and introducing the notation

$$r = \exp(-i\pi\alpha), \quad (2.20)$$

one finds (Bohr and Mottelson, 1975) for integer I

$$r = (-1)^I, \quad (2.21)$$

where I denotes the total nuclear spin. Thus for systems with an even number of nucleons we have

$$r = +1 \quad (\alpha = 0), \quad I = 0, 2, 4, \dots, \quad (2.22a)$$

$$r = -1 \quad (\alpha = 1), \quad I = 1, 3, 5, \dots, \quad (2.22b)$$

while for systems with odd particle number we have

$$r = -i \quad (\alpha = +\frac{1}{2}), \quad I = \frac{1}{2}, \frac{5}{2}, \frac{9}{2}, \dots, \quad (2.23a)$$

$$r = +i \quad (\alpha = -\frac{1}{2}), \quad I = \frac{3}{2}, \frac{7}{2}, \frac{11}{2}, \dots \quad (2.23b)$$

The above four relations can be cast into one equivalent expression:

$$I = \alpha \bmod 2. \quad (2.24)$$

²Here and in the following the symbol df. above the equal sign means "equal by definition."

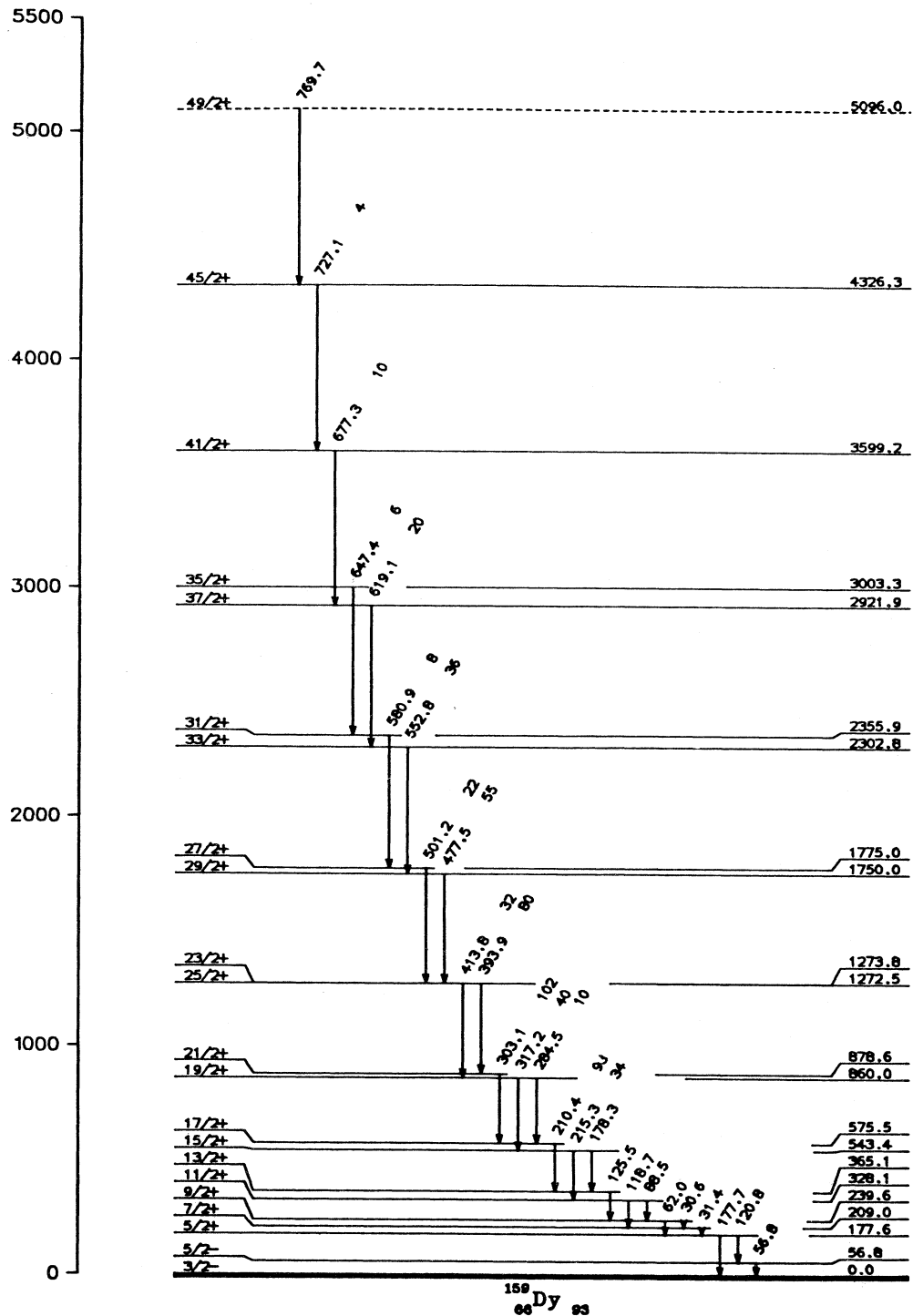


FIG. 3. Experimental level scheme of ^{159}Dy (Lee and Reich, 1979), illustrating the signature splitting in the spectrum of a rotating odd- A nucleus. The odd particle occupies either the lower or the higher of the two orbitals which are degenerated at $\omega=0$ due to Cromers degeneracy. The two orbitals differ in signature ($r=-i$ or $r=+i$) leading to level sequences of $\frac{1}{2}, \frac{5}{2}, \frac{9}{2}, \frac{13}{2}, \dots$, and $\frac{3}{2}, \frac{7}{2}, \frac{11}{2}, \frac{15}{2}, \dots$, respectively (see also Sec. III.A.3 for further explanation).

It also follows from Eqs. (2.19) and (2.20) that the particle-number fulfills the relation

$$A = 2\alpha \bmod 2 . \quad (2.25)$$

The eigenvalue r of the \mathcal{P}_x operator is called the signature. The classification of single-particle states by means of the signature quantum number proved to be, like parity, an important tool for identifying the nucleonic orbitals

in the rotating nuclear potentials (Ring *et al.*, 1969; Goodman, 1974; Faessler *et al.*, 1976; Andersson *et al.*, 1976; Neergaard *et al.*, 1976). The consequences of the \mathcal{P} and \mathcal{R}_x symmetries of the cranking Hamiltonian will be discussed further in Sec. II.E.3. An example of two bands which can be classified by the signatures $r = \pm i$ is given in Fig. 3 for ^{159}Dy (see also experimental level schemes presented in Sec. III).

B. Single-particle motion and pairing correlations

The present understanding of many of the mechanisms in nuclear structure is based almost entirely on the picture of individual nucleons moving in the nuclear average potential. In the domain of high-spin phenomena, like in many others, the rather detailed knowledge of the single-particle orbitals proves to be important. On the other hand, studying the properties of nuclei at high angular momenta may also provide new and valuable information on the properties and distributions of the single-nucleon orbitals in the nucleus. The description of nuclear average potentials can be found in almost every textbook on nuclear physics (see, for instance, Bohr and Mottelson, 1969). In the present paper we shall not discuss it in any detail. However, some of the features that seem to be relevant to the formation of very high-spin nuclear states can be found in Appendix A.

Two approaches are frequently employed to generate the single-particle spectra of deformed as well as spherical nuclei: the Nilsson and Woods-Saxon average field potentials. They are summarized in detail in Appendix A. There also exist other potentials, such as the folded Yukawa potential (Bolsterli *et al.*, 1972) or such potentials as the square-well or harmonic oscillator, which are sometimes used to imitate certain properties of the single-particle nuclear levels. The latter two, although very helpful in model calculations, are too simple for interpreting the experimental data on single-particle excitations for a wide range of nuclei. The folded Yukawa potential provides results on single-particle energies very close to those of the Woods-Saxon potential; thus to some extent the following discussion of the Woods-Saxon spectra (see Appendix A) applies to both potentials.

Knowledge of the correct single-particle spectra is in many cases a prerequisite for analyzing such high-spin phenomena as the alignment effects in nuclei. For their theoretical reproduction it is frequently decisive to start with the correct single-particle level order. In particular, the correct description of the high- j orbitals then plays a special role. Moreover, calculations show that the total energy of a nucleus can be represented as a sensitive function of the single-particle level density. Thus for a correct prediction of, for example, equilibrium deformations, especially at high spins, both properties of the single-particle spectra—i.e., the level order and the level density—have to be reproduced well. This can be achieved by carefully choosing the parameters for the average field potentials.

In addition to the nuclear average potential determining

the properties of the nucleonic single-particle orbitals, a residual two-body interaction must be added in order to account for many specific properties of nuclei. In this paper, the only two-body force that will be discussed is the short-range attractive pairing force. We will limit ourselves to the monopole-pairing component which leads to an interaction only between pairs coupled to angular momentum $I_{12} = 0$. As is well known, the inclusion of the pairing interaction leads to the depression of the nuclear ground state $I = 0$ in even nuclei with respect to the energies of the other states in the nuclear spectrum. It also reduces considerably the nuclear moment of inertia with respect to the rigid-body value.

In solid-state physics such an interaction was considered a long time ago (Bardeen *et al.*, 1957) to explain the effect of superconductivity. Bohr *et al.* (1958) suggested that there may exist an analogy between superfluid systems and finite nuclear systems. And since then the nuclear superfluidity approach (the pairing model) has been proven to be one of the most important elements in nuclear effective interaction theory.

In its simplest version the nuclear Hamiltonian including two-body pairing interactions reads

$$H = \sum_{\nu} e_{\nu} c_{\nu}^{\dagger} c_{\nu} + \frac{1}{4} \sum_{\nu\nu'\mu\mu'} \langle \nu\nu' | v_{\text{pair}} | \mu\mu' \rangle c_{\nu}^{\dagger} c_{\nu'}^{\dagger} c_{\mu'} c_{\mu} . \quad (2.26)$$

The monopole pairing interaction is defined as an interaction that scatters only those pairs of nucleons whose angular momenta are coupled to zero. This implied (see, for instance, Rowe, 1970) that the two-body matrix element has a simple form:

$$\langle \nu\nu' | v_{\text{pair}} | \mu\mu' \rangle = -G \delta_{\nu\bar{\nu}} \delta_{\mu\bar{\mu}} \text{sgn}(\nu) \text{sgn}(\mu) , \quad (2.27)$$

where, in addition, a constant matrix element G is assumed ($G_{\nu\mu} = G = \text{const}$) and $|\bar{\nu}\rangle$ denotes a time reversed state of $|\nu\rangle$.

An approximate solution to the problem of nucleonic motion generated by Hamiltonian (2.26) and (2.27) is obtained after introducing a trial function:

$$|\phi\rangle = \prod_{\nu} (u_{\nu} + v_{\nu} c_{\nu}^{\dagger} c_{\bar{\nu}}^{\dagger}) |0\rangle . \quad (2.28)$$

Here $|0\rangle$ denotes the vacuum state of particles.

The BCS (Bardeen, Cooper, and Schrieffer) trial wave function (2.28) clearly mixes components with various numbers of particles. Consequently one usually requires that the expectation value of the particle number operator fulfills the relation

$$\langle \phi | \hat{N} | \phi \rangle = n , \quad (2.29)$$

where $n = Z$ or N (proton or neutron number, respectively). This equation can be treated as an auxiliary constraint when minimizing the total energy

$$\langle \phi | H | \phi \rangle = \min . \quad (2.30)$$

Minimization in (2.30) with subsidiary condition (2.29) leads to the well-known expressions for the coefficients u_{ν} and v_{ν} of the BCS wave function (2.28); the appropriate considerations will not be repeated here (see, for example,

Bohr and Mottelson, 1975).

The analogy between nuclear pairing correlations and those existing in other superfluid systems may be pursued further. It is well known that strong external influences may destroy the superfluid structure in the system, thus causing a transition from superfluid to normal state (phase transition). Such a mechanism takes place, for example, in the superconducting metals when a strong external magnetic field is applied (Meissner effect). An analogous role is played in the nucleus by the fast rotation. In this case the strong Coriolis force tends to decouple the $I_{12}=0$ pairs and thus to destroy the superfluid correlations. The possibility of a nuclear phase transition following fast rotation of the nucleus was predicted a long time ago (Mottelson and Valatin, 1960). Such a transition is referred to as the Mottelson-Valatin effect. In fact, there are no clear-cut experiments showing evidence for a phase transition in the nucleus (see Sec. III.C).

C. The liquid drop model and a classical description of rotation

In the domain of very fast nuclear rotation one may expect substantial changes in nuclear structure. The strong Coriolis and centrifugal effects acting on nucleons moving in a nuclear field may become dominant factors that compete with the other nuclear interactions and determine the entire picture of nuclear dynamics.

Preliminary insight into the behavior of fast rotating nuclei may be obtained by analyzing the systematic features of the system. Such an analysis emphasizes the classical aspects of nuclear motion and may be based on the picture of a nucleus represented as a drop of incompressible liquid with its properties adjusted as closely as possible to those known from studies of nuclear matter. In such an approach a system is mainly characterized by its shape parameters, and equilibrium is reached for a given value of angular momentum as a result of a balance between the surface and Coulomb energies that compete with the centrifugal energy related to the rotation of the system. In this approximation the total energy of the system can be expressed as

$$\mathcal{E}(\beta, Z, N, I) = \mathcal{E}_{\text{ld}}(\beta, Z, N) + \frac{(\hbar I)^2}{2\mathcal{F}(\beta, Z, N)}, \quad (2.31)$$

where $\mathcal{F}(\beta, Z, N)$ denotes the moment of inertia. Here, $\mathcal{E}_{\text{ld}}(\beta, Z, N)$ denotes the nuclear average binding energy, which is usually calculated from the liquid drop formula (Myers and Świątecki, 1967). In particular, $\mathcal{E}_{\text{ld}}(\beta, Z, N)$ contains the surface energy term, $\mathcal{E}_{\text{surf}}(\beta, Z, N)$ and the Coulomb energy term $\mathcal{E}_{\text{Coul}}(\beta, Z, N)$. These two terms, together with the nuclear moment of inertia $\mathcal{F}(\beta, Z, N)$, depend essentially on the nuclear shape and contribute most significantly to the onset of the nuclear deformation. One should take this into account when expression (2.31) is minimized for fixed angular momentum I . Such an analysis was performed by Cohen *et al.* (1974). Two dimensionless parameters are usually introduced:

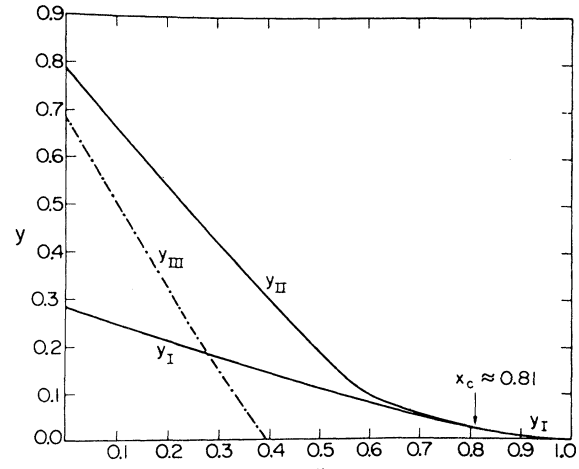


FIG. 4. Various critical rotational parameters y in their dependence on the fissility parameter x . Triaxial shapes appear between y_I and y_{II} . Saddle shapes are stable against reflection asymmetric distortions to the right of the dot-dashed portion of y_{III} . Triaxial shapes are unstable against asymmetry between the dashed portion of y_{III} and y_{II} (from Cohen *et al.*, 1974).

$$x = \frac{\mathcal{E}_{\text{Coul}}(\beta=0, Z, N)}{2\mathcal{E}_{\text{surf}}(\beta=0, Z, N)} \equiv \frac{\mathcal{E}_c^0}{2\mathcal{E}_s^0} \sim \frac{1}{50} \frac{Z^2}{A} \quad (2.32)$$

and

$$y = \frac{(\hbar I)^2 / [2\mathcal{F}_{\text{rigid}}(\beta=0, Z, N)]}{\mathcal{E}_{\text{surf}}(\beta=0, Z, N)} \approx 2 \frac{I^2}{A^{7/3}}. \quad (2.33)$$

They characterize the properties of a nucleus with respect to fission (fissility parameter x) and nuclear rotation (pa-

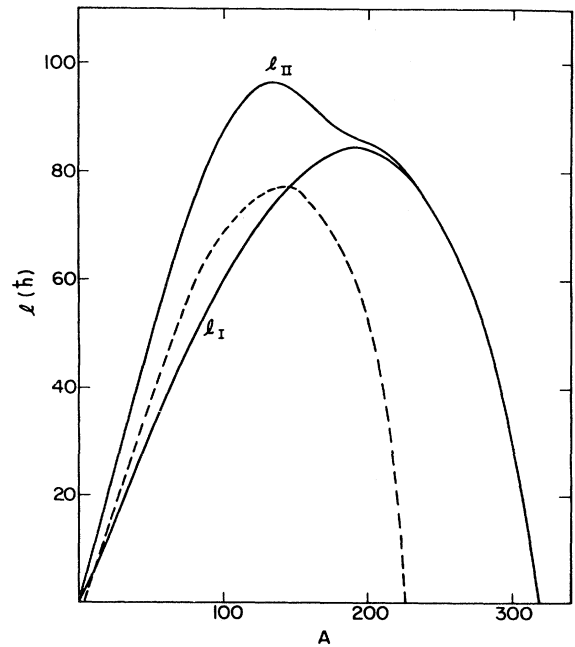


FIG. 5. The maximum angular momentum that can be accommodated in a β -stable rotating nucleus (classical estimates). The figure is taken from Cohen *et al.* (1974). Below the dashed curve the fission barrier is higher than 8 MeV (approximately equal to nucleon binding energy); for further discussion see text.

parameter y .

Figure 4 summarizes the result of the Cohen *et al.* (1974) analysis for various nuclear shapes and instabilities in terms of the parameters x and y . The line y_{II} corresponds to the limit of instability of a drop with respect to fission into separate fragments. The region to the left of y_{III} is characterized by instability with respect to the separation into a two-fragment system with uneven masses (a mass transfer from a light to a heavier fragment). Finally, y_I corresponds to the transition from an oblate equilibrium shape of a rotating drop to a pronounced elongated ("superdeformed") shape; such a transition is analogous to the Jacobi instability known in astrophysics.

Figure 5 illustrates the maximum angular momenta that can be accommodated in beta-stable nuclei. Line l_I forms the border to the superdeformed region above it. Line l_{II} indicates the fission limit. For $A > 100$ the value of l_{II} decreases due to the increasing influence of the Coulomb force favoring fission.

Figure 6 shows a map of the energy surface corresponding to the rotating liquid drop of a system with $Z = 62$ protons and $N = 92$ neutrons (^{154}Sm) in the (ϵ_2, γ)

half-plane between $\gamma = -120^\circ$ and 60° . The four limiting cases, $\gamma = -120^\circ$, -60° , 0° , and 60° , correspond to the possible rotations of axially symmetric shapes with various orientations of the nuclear axes with respect to the rotation axis. The sector defined by $0^\circ \leq \gamma \leq 60^\circ$ describes the rotation about the axis with the largest moment of inertia, and thus such a rotation always leads to the lowest energy for a given deformation parameter ϵ_2 or β_2 . Such an effect seems obvious in the classical description of nuclear motion but does not necessarily have to hold in the quantal description.

D. The quantal description of collective rotation and the shell correction approach

The semiquantitative description of a rotating nucleus is based on the concept of the individual motion of nucleons in a rotating nuclear field. For this purpose the cranking-method procedure (Inglis, 1954, 1955; Bohr and Mottelson, 1955) is frequently applied. The cranking Hamiltonian $H^\omega = H - \hbar\omega j_x$ (see Sec. II.A.1) describes the dynamical coupling of the intrinsic nuclear degrees of freedom with those characterizing nuclear rotation.

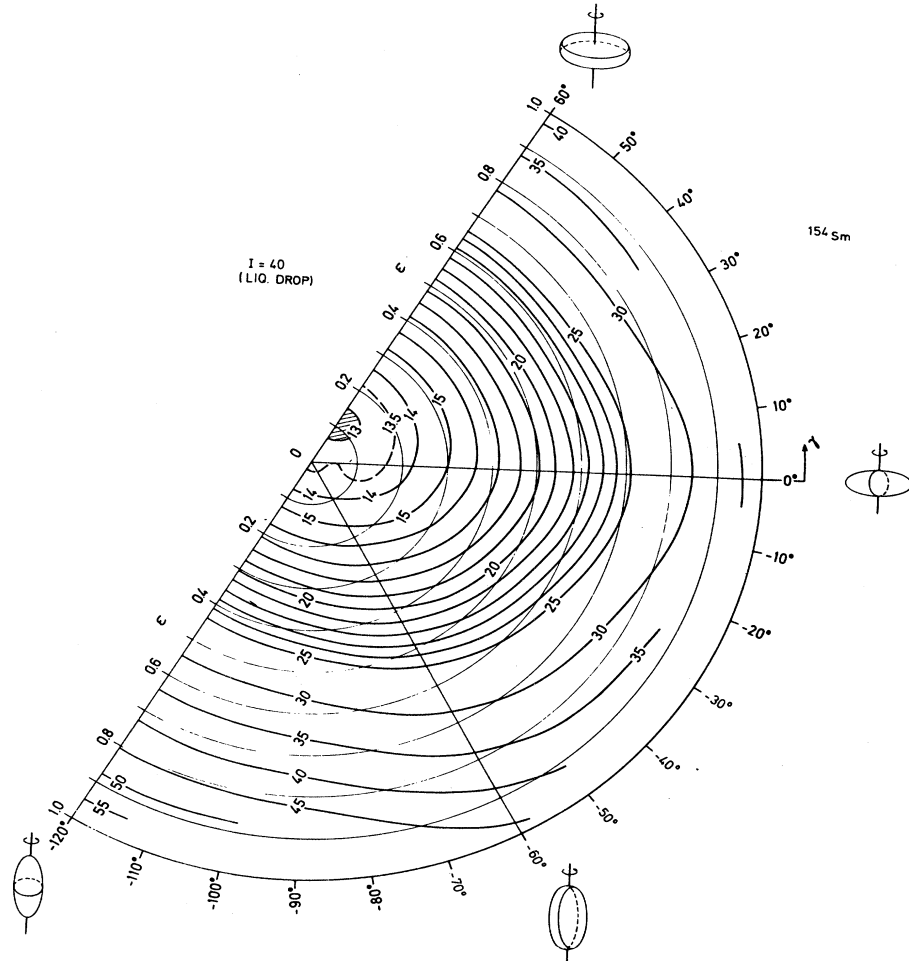


FIG. 6. Example of the liquid-drop model calculations of the total energy for the nucleus ^{154}Sm at $I = 40$. For completeness characteristic shapes and orientations of the axes are also illustrated (from Andersson *et al.*, 1976).

Moreover, if the angular momentum is sufficiently high (e.g., above $I \approx 30$ in the rare-earth nuclei), we may expect, due to the Mottelson-Valatin effect (Mottelson and Valatin, 1960), the short-range pairing correlations pertaining to the superfluid structure to become ineffective in the nucleus and their role in the nuclear Hamiltonian consequently to become negligible. Then the cranking Hamiltonian mainly describes the dynamical competition between the nuclear single-particle structure defined by independent-particle Hamiltonian H and rotation-induced interactions of the Coriolis and centrifugal types.

1. Single-particle Routhians

Figure 7 illustrates the eigenvalues e_v^ω of the cranking Hamiltonian (single-particle Routhians) plotted as func-

tions of angular velocity ω for the Nilsson potential with deformation $\epsilon_2=0.20$ and $\gamma=0^\circ$. The latter value corresponds to the rotation of an axially symmetric nuclear potential about an axis perpendicular to the nuclear symmetry axis. The solid and dashed lines describe states with the signatures $r=-i$ and $r=+i$, respectively (cf. Sec. II.A.3). Those Routhians corresponding to orbitals most sensitive to rotation decrease very steeply with ω and can be approximately characterized by a large angular momentum j [the largest in a given single-particle energy range (major shell)] and by a rather small value of its projection m on the nuclear symmetry axis. They lead to the strongest alignment of the nucleonic angular momenta with the rotation axis. In fact, the aligned angular momentum $\langle v | J_x | v \rangle$ can be seen as directly related to the slope in the curve e_v^ω vs ω :

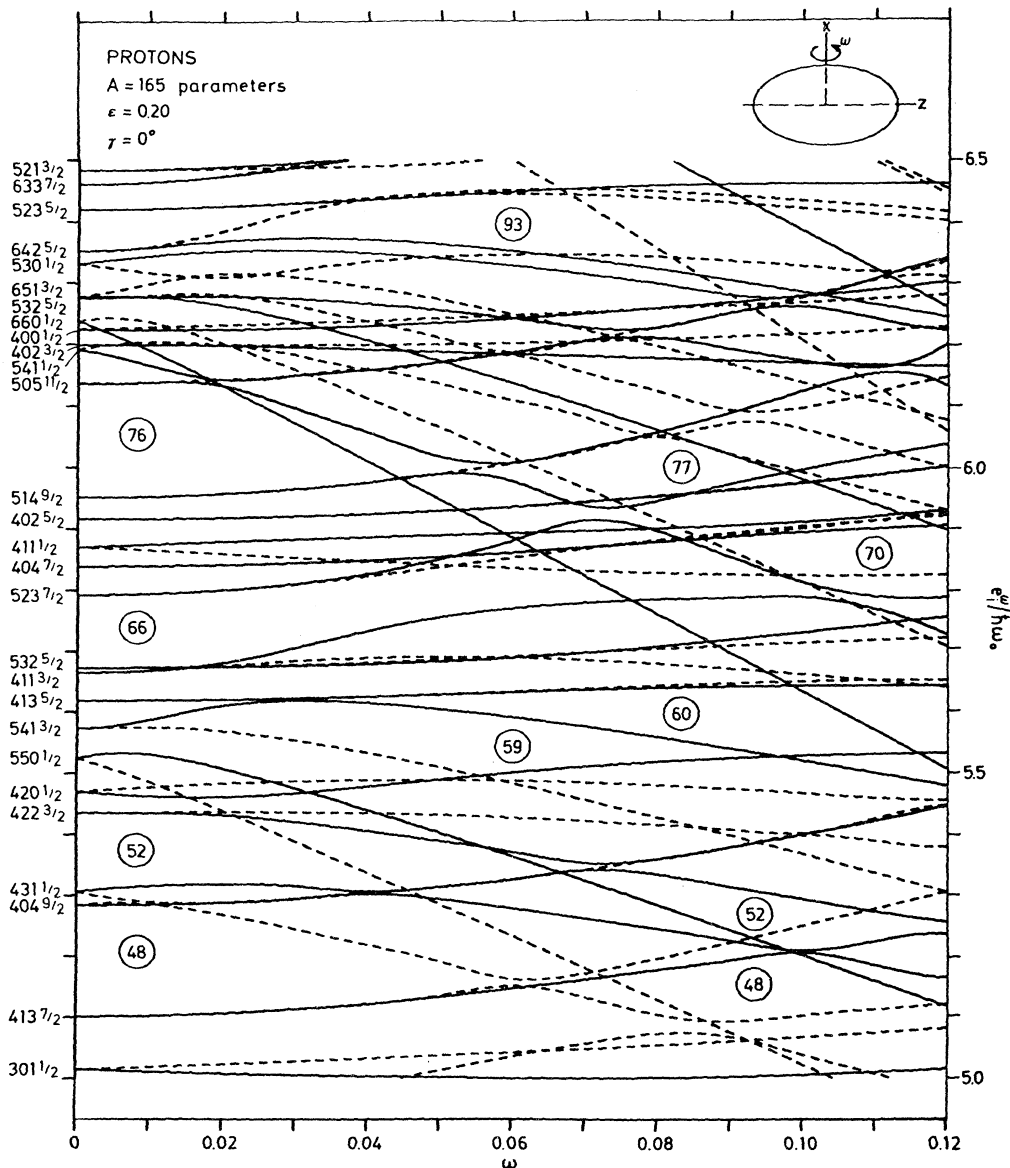


FIG. 7. The single-particle energies in the rotating coordinate frame (single-particle Routhians) as functions of rotational frequency ω calculated with a deformation of $\epsilon=0.20$ and $\gamma=0$ (from Andersson *et al.*, 1976).

$$\frac{de_v^\omega}{d\omega} = -\hbar \langle v | J_x | v \rangle, \quad (2.34)$$

with the minus sign originating from the minus sign in the formula for the Routhian. This equation follows from a direct differentiation of the single-particle eigenvalue e_v^ω of H^ω [cf. Eq. (2.12)] expressed as the expectation value of H^ω within the single-particle state $|v\rangle$. The rotation-sensitive orbitals are found to be the lowest members of high- j multiplets, such as $h_{11/2(1/2)}$, $h_{11/2(3/2)}$, ..., or $i_{13/2(1/2)}, i_{13/2(3/2)}$, ... (in Nilsson notation [550 1/2], [541 3/2], ..., or [660 1/2], [651 3/2], ..., respectively).

The energy of a rotating nucleus can be expressed in terms of cranking-model wave functions. We obtain, then, within the framework of the single-particle picture,

$$\mathcal{E} = \langle \psi | H | \psi \rangle = \mathcal{E}^\omega + \hbar\omega \langle \psi | J_x | \psi \rangle \quad (2.35)$$

[cf. Eq. (2.13)], where $|\psi\rangle$ is the eigenstate of the cranking Hamiltonian H^ω [cf. Eq. (2.9)], while

$$\mathcal{E}^\omega = \langle \psi | H^\omega | \psi \rangle = \sum_{v \text{ occ}} e_v^\omega \quad (2.36)$$

denotes the total nuclear Routhian in the independent-particle approximation; the summation over v extends over all the occupied states. The calculation of the total nuclear energy in the way just described, however, is highly unsatisfactory, as it was recognized a long time ago that the sum of the single-particle eigenvalues does not provide an adequate description of that energy. Until a more fundamental description of nuclear dynamics becomes available, the procedure used so far will be based almost exclusively on the shell correction approach.

2. The phenomenological shell correction approach

We shall not describe here the whole procedure of the shell correction (see, for example, Myers and Świątecki, 1967; Strutinsky, 1967). The main idea of this approach is to calculate the shell correction (by definition) as a difference

$$\delta\mathcal{E}_{\text{shell}} = \mathcal{E} - \tilde{\mathcal{E}} \quad (2.37)$$

between the sum \mathcal{E} of the single-particle energies (here also pairing correlations may be included, thus modifying slightly the expression for \mathcal{E}) and the averaged value $\tilde{\mathcal{E}}$ of this energy. The latter quantity is calculated by replacing the discrete single-particle level energies e_v by certain smoothed energy distributions. For instance, a discrete distribution of levels which is given by a Dirac delta-function density

$$g(e) = \sum_v \delta(e - e_v) \quad (2.38)$$

is replaced by a smooth energy distribution corresponding to the same levels e_v given by

$$\tilde{g}(e) = \sum_v S(e - e_v). \quad (2.39)$$

Here $S(e - e_v)$ represents, for example, a Gaussian function or a combination of several Gaussian functions (Strutinsky, 1967). Alternative approaches can be found, for instance, in Bohr and Mottelson (1969 and 1975) and references quoted therein. Here, we shall not go into more detail in these descriptions. We mention only the characteristic modification of the shell correction method appropriate in the domain of very high angular momenta [cf. Brack and Jennings (1976), Bengtsson *et al.* (1975), Neergaard and Pashkevich (1975), Andersson *et al.* (1976), Neergaard *et al.* (1976)]. In the case of nuclear rotation, the single-particle energies e_v should be replaced by the single-particle Routhians e_v^ω . The new degree of freedom, represented by the rotational frequency ω , introduces a new dependence to the shell correction formula, namely, a dependence on spin. Such a dependence in the total energy formula (2.13) can be represented as the sum $\langle H \rangle + \hbar\omega \langle I_x \rangle$ [see Eq. (2.10)]. This suggests that the Strutinsky smearing procedure should take care of both the level and angular momentum densities [cf. Eq. (2.13)]. In this spirit one defines the level density function by modifying Eq. (2.38) as

$$g_1(e^\omega) = \sum_v \delta(e^\omega - e_v^\omega) \quad (2.40)$$

and the spin-density function as

$$g_2(e^\omega) = \sum_v \langle m_v \rangle \delta(e^\omega - e_v^\omega). \quad (2.41)$$

One then obtains the two corresponding smooth densities $\tilde{g}_1(e^\omega)$ and $\tilde{g}_2(e^\omega)$ [cf. Eq. (2.39)]. Using the two density functions, we find for the nonsmoothed quantities

$$I = \int_{-\infty}^{\lambda} g_2(e^\omega) de^\omega = \sum_{v \text{ occ}} \langle m_v \rangle \quad (2.42)$$

and

$$\mathcal{E} = \int_{-\infty}^{\lambda} g_1(e^\omega) e^\omega de^\omega + (\hbar\omega) I, \quad (2.43)$$

and for the analogous smoothed quantities

$$I = \int_{-\infty}^{\tilde{\lambda}} \tilde{g}_2(e^{\tilde{\omega}}) de^{\tilde{\omega}} \quad (2.44)$$

and

$$\tilde{\mathcal{E}} = \int_{-\infty}^{\tilde{\lambda}} \tilde{g}_1(e^{\tilde{\omega}}) e^{\tilde{\omega}} de^{\tilde{\omega}} + (\hbar\tilde{\omega}) I. \quad (2.45)$$

The shell correction is now defined [cf. Eq. (2.37)] by

$$\delta\mathcal{E}_{\text{shell}}(n, I) = \mathcal{E} - \tilde{\mathcal{E}}, \quad (2.46)$$

with λ and $\tilde{\lambda}$ defined from the corresponding particle number equations. Equation (2.44) implies that $\tilde{\omega}$ in a smoothed case, as opposed to ω in the discrete case, must be used so as to ensure the same value for I in both cases. A more detailed discussion of the generalized shell correction method can be found in Andersson *et al.* (1976), for example.

The final formula for the nuclear energy reads

$$\begin{aligned} \mathcal{E}_{\text{total}}(Z, N; I) &= \mathcal{E}_{\text{ld}} + \delta\mathcal{E}_{\text{shell}}(\text{protons}) \\ &\quad + \delta\mathcal{E}_{\text{shell}}(\text{neutrons}). \end{aligned} \quad (2.47)$$

It is a sensitive function of the nuclear deformation. When combining the results on various deformations and spins, one is able to relate the different nuclear shapes to the minimum energy at a given spin, thus gaining information on the evolution of nuclear shapes with increasing speed of rotation.

In applications of the shell correction method to rotat-

ing nuclei, following the approach suggested by Brack and Jennings (1976) (see, for instance, Bengtsson *et al.*, 1975; Neergaard and Pashkevich, 1975; Neergaard *et al.*, 1977) extensive calculations of the potential energy surfaces as functions of the deformation degrees of freedom were performed for several values of angular momentum. Typical results are shown in Fig. 8 for ^{160}Yb . For spins

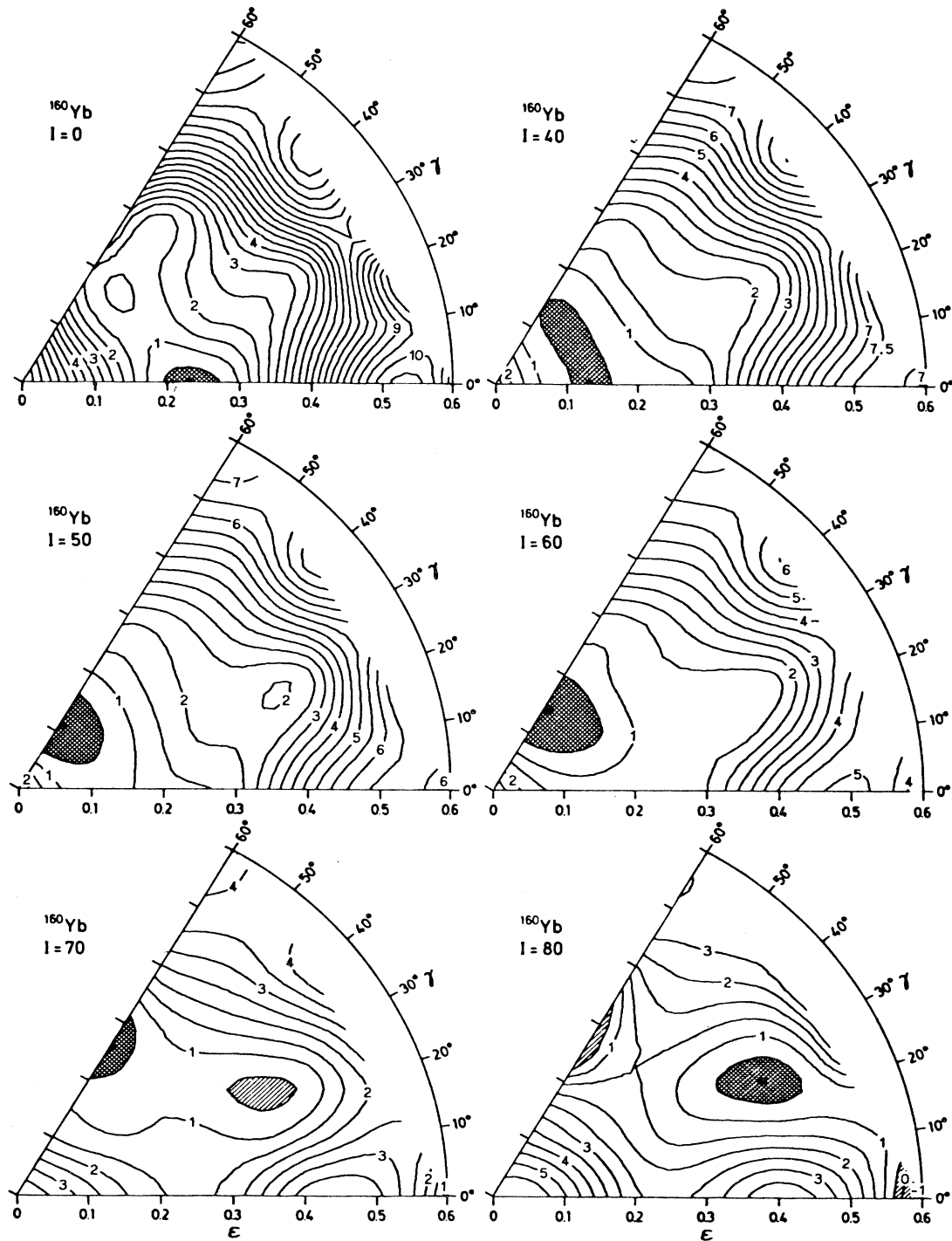


FIG. 8. Typical results of the shell correction method for high-spin rotating nuclei (pairing effects neglected), with the example of ^{160}Yb (from Andersson *et al.*, 1976). Potential-energy surfaces are given in the (ϵ, γ) plane as functions of angular momentum.

between $0\hbar$ and $80\hbar$ drastic changes may occur in equilibrium shape. At low-spin values ^{160}Yb has a weakly elongated (prolate) shape; at higher spins it acquires oblate shapes and finally returns to an elongated shape. The energy maps presented in the figure were calculated with the Nilsson potential; similar results are expected for the Woods-Saxon potential (Neergaard *et al.*, 1977).

The behavior of ^{160}Yb may be typical for neutron-deficient light rare-earth nuclei but not necessarily for nuclei in other regions of the Periodic Table. The only feature common to the nuclear energy landscape investigated so far is the pronounced elongation of shape at very high angular momenta. This may be related to the possible existence of superdeformed nuclei. Today's experimental and theoretical search for superdeformed states at high spin is one of the most interesting endeavors in nuclear structure studies (Åberg *et al.*, 1980; Ragnarsson, 1978; Faber *et al.*, 1979; Bengtsson *et al.*, 1981; Ragnarsson *et al.*, 1980).

In the theoretical predictions for the existence of the superdeformed region the nuclear shell structure plays an important role. At very large deformations—e.g., for ellipsoidal shapes with an axis ratio of 2:1—new magic numbers and shells may emerge, different from those known from spherical shapes (Bohr and Mottelson, 1975; Świętecki *et al.*, 1969; Tsang, 1969; Ragnarsson *et al.*, 1978; Døssing *et al.*, 1977; Dudek *et al.*, 1982).

E. The independent quasiparticle method and collective rotation

Within the last ten years the well-known Hartree-Fock-Bogolyubov (HFB) formalism has been applied to the description of nuclear rotation after employing the cranking-model procedure (Ring *et al.*, 1969; Banerjee *et al.*, 1973; Bhargava, 1973; Bhargava and Thouless, 1973; Goodman, 1974, 1976; Faessler *et al.*, 1976; Hamamoto, 1976; Bengtsson and Frauendorf, 1977, 1979a, 1979b and references cited therein). This formalism known also as the HFBC (HFB cranking) leads to a description of a rotating nucleus in terms of elementary excitations, the so-called independent-quasiparticle energies (Routhians).

In this section we discuss in detail a phenomenological realization of the HFBC method which consists of finding an approximate form of the nuclear spectrum generated by the operator H^ω ,

$$H^\omega = \sum_{vv'} e_{vv'} c_v^\dagger c_{v'} + \frac{1}{4} \sum_{vv'\mu\mu'} v_{vv'\mu\mu'} c_v^\dagger c_{v'}^\dagger c_{\mu'} c_\mu - \hbar\omega \sum_{vv'} (j_x)_{vv'} c_v^\dagger c_{v'} , \quad (2.48)$$

that represents the energy of protons or neutrons in a rotating coordinate frame (Routhian). Here $e_{vv'}$ denotes the kinetic energy plus Nilsson or Woods-Saxon potential term, while $v_{vv'\mu\mu'}$ is taken in the form of a monopole pairing term:

$$v_{vv'\mu\mu'} = -G\delta_{vv'}\delta_{\mu\mu'}\text{sgn}(v)\text{sgn}(\mu) , \quad (2.49)$$

with $\text{sgn}(\bar{v}) = -1$ and $\text{sgn}(v) = +1$ ($|\bar{v}\rangle = \mathcal{T}|v\rangle$). Note that those approaches explicitly employing average nuclear fields should not be mistaken with the fully self-consistent Hartree-Fock method, despite the fact that the name Hartree-Fock-Bogolyubov cranking is frequently applied in the literature to the former, restricted approaches, as well.

Since the HFBC approach provides only an approximate expression $|\psi\rangle$ for the total nuclear wave function, one may not expect it to be an eigenfunction of the particle number operator

$$\hat{N} = \sum_{v=1}^n c_v^\dagger c_v , \quad n = Z \text{ or } N . \quad (2.50)$$

One thus resorts to the requirement that the average value of the operator corresponding to $|\psi\rangle$ be equal to the proton or neutron numbers (Z or N):

$$\langle \psi | \hat{N} | \psi \rangle = n . \quad (2.51)$$

Such an auxiliary condition can be accounted for most easily by a Lagrange multiplier, λ_n (chemical potential), and a new auxiliary operator:

$$H^\omega \rightarrow H^\omega - \lambda_n \hat{N} . \quad (2.52)$$

Since the wave functions generated by H^ω depend on λ_n parametrically, one has to determine from Eq. (2.51) a λ_n value appropriate for n particles. The Routhian in the second quantization representation thus assumes the form

$$H^\omega = \sum_{vv'} [e_{vv'} - \hbar\omega(j_x)_{vv'} - \lambda_n \delta_{vv'}] c_v^\dagger c_v - \frac{1}{4} G \sum_{vv'\mu\mu'} \delta_{vv'} \delta_{\mu\mu'} \text{sgn}(v) \text{sgn}(\mu) c_v^\dagger c_{v'}^\dagger c_{\mu'} c_\mu . \quad (2.53)$$

The summations in Eq. (2.53) extend over the basis states; if the basis is cut—e.g., to p states—then $v, v', \mu, \mu' = 1, 2, \dots, p$.

The first step in the HFBC method consists of transforming operator (2.53) into a quasiparticle picture by making use of the Bogolyubov transformation. The latter leads to the quasiparticle creation and annihilation operators α_i^\dagger and α_j :

$$\alpha_i^\dagger = \sum_{v=1}^p (A_{vi} c_v + B_{vi} c_{v'}^\dagger) , \quad (2.54a)$$

$$\alpha_j = \sum_{v=1}^p (B_{vj}^\dagger c_v + A_{vj}^\dagger c_{v'}^\dagger) . \quad (2.54b)$$

One assumes auxiliary objects—i.e., quasiparticles—to possess fermion properties just as nucleons (i.e., particles) do, and thus by definition

$$\{\alpha_i^\dagger, \alpha_j\} = \delta_{ij} , \quad \{\alpha_i, \alpha_j\} = 0 , \quad \{\alpha_i^\dagger, \alpha_j^\dagger\} = 0 . \quad (2.55)$$

1. The Bogolyubov transformation

The idea behind the transformation into a quasiparticle picture is to introduce a new representation of Hamiltoni-

an (2.53) in which excitations of the system can be constructed from additive building blocks—i.e., quasiparticle energies. Inserting expressions (2.54a) and (2.54b) into Eq. (2.55), and using the anticommutation properties of the operators c^\dagger and c , we obtain the generalized orthonormality relations

$$\sum_{\nu=1}^p (A_{\nu i}^* A_{\nu j} + B_{\nu i}^* B_{\nu j}) = \delta_{ij}, \quad (2.56a)$$

$$\sum_{\nu=1}^p (A_{\nu i} B_{\nu j} + A_{\nu j} B_{\nu i}) = 0, \quad i, j = 1, 2, \dots, p. \quad (2.56b)$$

It is convenient to express the Bogolyubov transformation in matrix notation. Formally, one then has

$$\begin{bmatrix} \alpha^\dagger \\ \alpha \end{bmatrix} = \begin{bmatrix} A^T & B^T \\ B^\dagger & A^\dagger \end{bmatrix} \begin{bmatrix} c^\dagger \\ c \end{bmatrix}, \quad (2.57)$$

with α^\dagger , α , c^\dagger , and c denoting column vectors, e.g.,

$$\alpha^\dagger = \begin{bmatrix} \alpha_1^\dagger \\ \alpha_2^\dagger \\ \vdots \\ \alpha_p^\dagger \end{bmatrix}, \quad c^\dagger = \begin{bmatrix} c_1^\dagger \\ c_2^\dagger \\ \vdots \\ c_p^\dagger \end{bmatrix}. \quad (2.58)$$

Defining

$$Z \equiv \begin{bmatrix} A^T & B^T \\ B^\dagger & A^\dagger \end{bmatrix}, \quad (2.59)$$

one can easily see, using Eqs. (2.56a) and (2.56b), that $Z Z^\dagger = 1$ —i.e., that the matrix Z is unitary. One can now determine the inverse to the Bogolyubov transformation:

$$\begin{bmatrix} c^\dagger \\ c \end{bmatrix} = \begin{bmatrix} A^* & B \\ B^* & A \end{bmatrix} \begin{bmatrix} \alpha^\dagger \\ \alpha \end{bmatrix}. \quad (2.60)$$

It is essential to notice that the new vector space of the operators (c_i^\dagger) or (α_i^\dagger) is of doubled dimensions, i.e., equal to $2p$, as compared to the original basis $\{c_i^\dagger | 0 \rangle, i = 1, 2, \dots, p\}$.

2. The HFBC equations

Using the inverse to the Bogolyubov transformation, Eq. (2.60), one may transform Hamiltonian (2.53) into quasiparticle representation. It is convenient to group the summation terms into sets containing no α operator (H_0), two operators of the type $\alpha^\dagger \alpha$ (H_{11}), two operators of the type $\alpha^\dagger \alpha^\dagger$ and $\alpha \alpha$ (H_{20}), and finally all combinations of the type $\alpha \alpha \alpha$, $\alpha \alpha \alpha^\dagger$, and $\alpha \alpha \alpha^\dagger \alpha^\dagger$ together with their Hermitian conjugates (H_4). After such a grouping one obtains

$$H^\omega \xrightarrow[c \rightarrow \alpha]{} H^\omega = H_0 + H_{11} + H_{20} + H_4, \quad (2.61)$$

where

$$H_0 = \sum_{\alpha\beta} e_{\alpha\beta} \rho_{\alpha\beta} + \frac{1}{2} \sum_{\alpha\beta} \Gamma_{\alpha\beta} \rho_{\alpha\beta} + \sum_{\alpha\beta} \Delta_{\alpha\beta} \chi_{\alpha\beta}, \quad (2.62a)$$

$$H_{11} = \sum_{ij,\alpha\beta} [\nu_{\alpha\beta} (A_{\alpha i}^* A_{\beta j} - B_{\alpha j} B_{\beta i}^*) + \Delta_{\alpha\beta} A_{\alpha i}^* A_{\beta j} + \Delta_{\alpha\beta}^* B_{\alpha i}^* B_{\beta j}] \alpha_i^\dagger \alpha_j, \quad (2.62b)$$

$$H_{20} = \sum_{ij,\alpha\beta} (\nu_{\alpha\beta} A_{\alpha i}^* B_{\beta j}^* + \frac{1}{2} \Delta_{\alpha\beta} A_{\alpha i}^* A_{\beta j}^* + \frac{1}{2} \Delta_{\alpha\beta}^* B_{\beta i}^* B_{\alpha j}^*) \alpha_i^\dagger \alpha_j^\dagger + \text{H.c.} \quad (2.62c)$$

In the equalities (2.62a)–(2.62c) the following standard notation is employed:

$$\rho_{\alpha\beta} = \sum_{i=1}^p B_{\alpha i} B_{\beta i}^* \quad (\rho_{\alpha\beta} = \rho_{\beta\alpha}^*), \quad (2.63)$$

$$\chi_{\alpha\beta} = \sum_{i=1}^p A_{\beta i} B_{\alpha i}^* \quad (\chi_{\alpha\beta} = -\chi_{\beta\alpha}), \quad (2.64)$$

$$\Delta_{\alpha\beta} = 2 \sum_{\gamma\delta} \nu_{\alpha\beta\gamma\delta} \chi_{\gamma\delta}, \quad (2.65)$$

$$\Gamma_{\alpha\gamma} = 4 \sum_{\beta\delta} \nu_{\alpha\beta\gamma\delta} \rho_{\beta\delta}, \quad (2.66)$$

$$\nu_{\alpha\beta} = \varepsilon_{\alpha\beta} + \Gamma_{\alpha\beta} \quad [\varepsilon_{\alpha\beta} = e_{\alpha\beta} - \lambda_n \delta_{\alpha\beta} - \hbar\omega(j_x)_{\alpha\beta}], \quad (2.67)$$

We make use of the freedom in the coefficients of the A and B matrices that are still undefined and require that

$$H_{20} = 0. \quad (2.68)$$

Simultaneously, we also require that the summation over α and β in Eq. (2.62b) can be reduced to the form

$$\sum_{\alpha\beta} [\nu_{\alpha\beta} (A_{\alpha i}^* A_{\beta j} - B_{\alpha j} B_{\beta i}^*) + \Delta_{\alpha\beta} A_{\alpha i}^* B_{\beta j} + \Delta_{\alpha\beta}^* B_{\alpha i}^* A_{\beta j}] = E_i^\omega \delta_{ij}, \quad (2.69)$$

where E_i^ω ($i = 1, 2, \dots, p$) represent some real numbers.

Until now all the transformations were exact. The approximation in the method consists of neglecting the four-operator term H_4 . This is equivalent to saying that we hope that the expectation values of H_4 are small as compared to those of the remaining terms in the Hamiltonian.

One can show that the requirements (2.68) and (2.69) are equivalent to the following system of nonlinear equations for A and B :

$$\sum_{\beta=1}^p (\nu_{\alpha\beta} A_{\beta i} + \Delta_{\alpha\beta} B_{\beta i}) = +E_i^\omega A_{\alpha i}, \quad i = 1, 2, \dots, p, \quad (2.70a)$$

$$\sum_{\beta=1}^p (\nu_{\alpha\beta}^* B_{\beta i} + \Delta_{\alpha\beta}^* A_{\beta i}) = -E_i^\omega B_{\alpha i}, \quad i = 1, 2, \dots, p, \quad (2.70b)$$

The nonlinearity of this set of equations follows from the fact that both $\nu_{\alpha\beta}$ and $\Delta_{\alpha\beta}$ depend on A and B . Equations (2.70a) and (2.70b) are called the HFBC equations. The quantities $\nu_{\alpha\beta}$ and $\Delta_{\alpha\beta}$ expressed in terms of A 's and B 's

satisfying Eqs. (2.70a) and (2.70b) [see Eqs. (2.65) and (2.67)] are called the self-consistent single-particle Routhian and the self-consistent pairing field, respectively. The auxiliary matrices $\rho_{\alpha\beta}$ and $\chi_{\alpha\beta}$ are called the single-particle density and the pair density, respectively.

Note that in Eqs. (2.70a) and (2.70b) there is a dependence on the rotational frequency ω , since $v_{\alpha\beta}$ contains the $[-\omega(j_x)_{\alpha\beta}]$ term.

The requirements (2.68) and (2.69) can be interpreted as follows:

(i) We assume that the Bogolyubov-transformed Hamiltonian describes the ground-state band of the system via Eq. (2.62a) and that this band corresponds to zero-quasiparticle configurations (such a zero-quasiparticle state is frequently referred to as a quasiparticle vacuum state). This ground state depends on the rotational frequency ω ; for higher rotational frequencies the quasiparticle vacuum states may differ from the states of the ground-state band.

(ii) The excitations of the system are given by E_i^ω . The excitation term is straightforwardly related to the number of quasiparticles excited in the system, n_{excit} , since after solving Eqs. (2.70a) and (2.70b), one obtains

$$H_{11} = \sum_{i=1}^{n_{\text{excit}}} E_i^\omega \alpha_i^\dagger \alpha_i . \quad (2.71)$$

Using E_i^ω as additive quantities, one can thus construct from the solutions to the HFBC equations all multiquasiparticle excitations.

The iterative procedure applied to the HFBC equations aims at finding the matrices A and B and simultaneously the quasiparticle Routhians E_ν^ω that fulfill Eqs. (2.70a) and (2.70b). Once these quantities have been found, one can calculate the total angular momentum and total energy from the relations

$$I \approx I_x = \sum_{\alpha\beta} (j_x)_{\alpha\beta} \rho_{\alpha\beta} \quad (2.72)$$

and

$$\mathcal{E} = \sum_{\alpha\gamma} \left[e_{\alpha\gamma} + 2 \sum_{\beta\delta} v_{\alpha\beta\gamma\delta} \rho_{\beta\delta} \right] \rho_{\alpha\gamma}^* + \frac{1}{2} \sum_{\alpha\beta} \chi_{\alpha\beta}^* \Delta_{\alpha\beta} , \quad (2.73)$$

and in principle compare these results with experimental data in the form of $[I, \mathcal{E}(I)]$ bands. In fact, one can obtain much more information about rotating nuclei from the HFBC approach than only the \mathcal{E} -vs- I dependence, as discussed below and in Sec. III.

3. Symmetries: parity and signature

The Hamiltonian that is used to describe high-spin states in nuclei can in most cases be treated as parity invariant because the quadrupole and hexadecapole deformations describe sufficiently well the nuclear distortions of fast rotating nuclei along their yrast lines. The parity-nonconserving collective degrees of freedom, such as the octupole deformations or deformations of multipolarity

five, which were proven to be important for fission, are less important for high-spin excitations. Consequently, we have for the Routhian (2.53)

$$[H^\omega, \mathcal{P}] = 0 , \quad (2.74)$$

from which it follows that the solution to the HFBC equations [see, for example, (2.70a) and (2.70b)] can be denumerated by the parity quantum number $\pi = +1$ or -1 and that the size of the matrix representation of H^ω can be significantly reduced.

The presence of the $(-\omega j_x)$ term in the Routhian apparently breaks the initial time reversal invariance of the nuclear Hamiltonian and thus removes the Cramers degeneracy. As discussed in Sec. II.A, however, the Routhian is invariant with respect to \mathcal{R}_x [cf. Eq. (2.18)], and thus the corresponding signature quantum number r can be used together with parity π to denote the quasi-particle states. This also considerably simplifies the HFBC equations.

Consider a single-particle basis generated by some single-particle Hamiltonian obeying axial symmetry. Let us denote the corresponding single-particle basis states by $|k, \Omega_k\rangle$, where Ω_k denotes the single-particle angular momentum projection onto the symmetry axis. Generally, these states are at least doubly degenerate, and thus $|k, \Omega_k\rangle$ and its time-reversed image $\mathcal{T}|k, \Omega_k\rangle = |k, \bar{\Omega}_k\rangle$ belong to the same eigenenergy. Adopting the phase convention, according to which

$$\mathcal{R}_x |k, \Omega_k\rangle = i(-1)^{\Omega_k - 1/2} |k, \bar{\Omega}_k\rangle \quad (2.75)$$

and

$$\mathcal{R}_x |k, \bar{\Omega}_k\rangle = i(-1)^{\Omega_k - 1/2} |k, \Omega_k\rangle , \quad (2.76)$$

one can transform the representation of the basis in which Ω is a good quantum number into one in which the signature is a good quantum number (Goodman transformation):

$$|K\rangle = \frac{1}{\sqrt{2}} [-|k, \Omega_k\rangle + (-1)^{\Omega_k - 1/2} |k, \bar{\Omega}_k\rangle] , \quad (2.77a)$$

$$|\tilde{K}\rangle = \frac{1}{\sqrt{2}} [(-1)^{\Omega_k - 1/2} |k, \Omega_k\rangle + |k, \bar{\Omega}_k\rangle] . \quad (2.77b)$$

By representing all the operators that appear in the HFBC approach by matrices with their matrix elements taken within the states of Eqs. (2.77a) and (2.77b), one achieves the following important simplifications:

$$\Delta_{KK'} = 0, \quad \Delta_{\tilde{K}\tilde{K}'} = 0 , \quad (2.78)$$

$$v_{KK'} = 0, \quad v_{\tilde{K}\tilde{K}'} = 0 , \quad (2.79)$$

$$(j_x)_{KK'} = 0, \quad (j_x)_{\tilde{K}\tilde{K}'} = 0 ,$$

and

$$A_{KK'} = 0, \quad A_{\tilde{K}\tilde{K}'} = 0 , \quad (2.80)$$

$$B_{KK'} = 0, \quad B_{\tilde{K}\tilde{K}'} = 0 ,$$

while

$$(j_x)_{\tilde{K}\tilde{K}'} = -(j_x)_{KK'} \quad (2.81)$$

and

$$\nu_{KK'} = \nu_{\tilde{K}\tilde{K}'} \quad (2.82)$$

In this new representation the HFBC equations split into two systems of equations, each characterized by a given signature value. For system I

$$\sum_{K',r=-i} (\nu_{KK'} A_{K'L} + \Delta_{KK'} B_{K'L}) = (+E_L^\omega) A_{KL}, \quad (2.83a)$$

$$\sum_{K',r=-i} (\nu_{\tilde{K}\tilde{K}'} B_{\tilde{K}'L} + \Delta_{\tilde{K}\tilde{K}'} A_{\tilde{K}'L}) = (-E_L^\omega) B_{\tilde{K}L}, \quad (2.83b)$$

and for system II

$$\sum_{K',r=+i} (\nu_{KK'} A_{K'L} + \Delta_{KK'} B_{K'L}) = (+E_L^\omega) A_{\tilde{K}L}, \quad (2.84a)$$

$$\sum_{K',r=+i} (\nu_{\tilde{K}\tilde{K}'} B_{\tilde{K}'L} + \Delta_{\tilde{K}\tilde{K}'} A_{\tilde{K}'L}) = (-E_L^\omega) B_{KL}. \quad (2.84b)$$

Replacing $A_{K'L}$, $B_{\tilde{K}'L}$, and $(+E_L^\omega)$ in system I by $B_{K'L}$, $A_{\tilde{K}L}$, and $(-E_L^\omega)$, respectively, transforms that system into system II. It is thus sufficient to solve only one of the two systems, since the solutions to the second are given by the above simple transformation. The presence of the \mathcal{R}_x symmetry thus simplifies considerably the effort of finding pairing self-consistent solutions to the HFBC equations.

The splitting [(2.83a) \rightarrow (2.84a), (2.83b) \rightarrow (2.84b)] of the HFBC equations can be also be illustrated using the generalized density matrix.

4. The generalized density matrix and the negative quasiparticle Routhians

Some important properties of the HFBC approach can be presented in a most compact way by matrix notation. For this purpose one employs the matrix Z ,

$$Z = \begin{bmatrix} A^T & B^T \\ B^\dagger & A^\dagger \end{bmatrix},$$

which was proven to be unitary (Sec. II.E.1), i.e., $ZZ^\dagger = 1$. In this section we confine our considerations to systems with even numbers of protons and neutrons (the odd-particle number system can be described after some simple modifications of the formalism). Recalling the definitions of the density and pair-density matrices ρ and χ [Eqs. (2.63) and (2.64)], we can define an auxiliary matrix \mathcal{X} of double dimensions (with respect to the dimensions of ρ or χ), viz.,

$$\mathcal{X} = \begin{bmatrix} \rho & \chi \\ -\chi^* & 1-\rho^* \end{bmatrix}, \quad (2.85)$$

which fulfills

$$\mathcal{X}^2 = \mathcal{X}, \quad (2.86)$$

the latter equality being equivalent to

$$\rho^2 - \chi\chi^* = \rho, \quad (2.87a)$$

$$\rho\chi - \chi\rho^* = 0. \quad (2.87b)$$

The last two relations can easily be proven after employing the unitarity of Z and the definitions of ρ and χ . Let us also define the so-called HFB matrix:

$$\mathcal{M} = \begin{bmatrix} \nu & \Delta \\ -\Delta^* & -\nu^* \end{bmatrix}. \quad (2.88)$$

Using the definitions of matrices A , B , and \mathcal{M} , we can rewrite the HFBC equations [Eqs. (2.70a) and (2.70b)] as

$$\mathcal{M} \begin{bmatrix} A_{(i)} \\ B_{(i)} \end{bmatrix} = E_i^\omega \begin{bmatrix} A_{(i)} \\ B_{(i)} \end{bmatrix}, \quad (2.89)$$

with $A_{(i)}$ and $B_{(i)}$ denoting the i th column of matrices A and B , respectively. Note that the similarity between Eq. (2.89) and the eigenvalue problem is only formal, since \mathcal{M} depends on A and B and since the equations are apparently nonlinear. Nevertheless, we conventionally refer to Eq. (2.89) as to the eigenvalue problem. Inserting the solutions $A_{(i)}$ and $B_{(i)}$ of Eq. (2.89) into \mathcal{M} and \mathcal{X} , one can show that

$$[\mathcal{X}, \mathcal{M}] = 0. \quad (2.90)$$

Simple algebraic operations on the system of HFBC equations (2.70a) and (2.70b) prove that once $(+E_i^\omega)$ is an eigenvalue of \mathcal{M} to the eigenvector $(\begin{smallmatrix} A_{(i)} \\ B_{(i)} \end{smallmatrix})$, then $(-E_i^\omega)$ is also an eigenvalue of \mathcal{M} to the eigenvector $(\begin{smallmatrix} B_{(i)}^* \\ A_{(i)}^* \end{smallmatrix})$. From the unitarity of Z it follows that if

$$\mathcal{X} \begin{bmatrix} A_{(i)} \\ B_{(i)} \end{bmatrix} = k_i \begin{bmatrix} A_{(i)} \\ B_{(i)} \end{bmatrix}, \quad (2.91)$$

then

$$\mathcal{X} \begin{bmatrix} B_{(i)}^* \\ A_{(i)}^* \end{bmatrix} = (1-k_i) \begin{bmatrix} B_{(i)}^* \\ A_{(i)}^* \end{bmatrix}. \quad (2.92)$$

From Eq. (2.86) it follows, however, that the eigenvalues of \mathcal{X} can only be $k_i = 0$ or 1 , while Eq. (2.90) ensures that there always exists a representation of the matrices \mathcal{X} and \mathcal{M} in which both are diagonal. Consequently, \mathcal{X} and \mathcal{M} can always be represented in such a way that in the ground-state configuration

$$\mathcal{X} = \begin{bmatrix} 0 & & & & & & & \\ & 0 & & & & & & \\ & & \ddots & & & & & \\ & & & 0 & & & & \\ \cdots & & & & \cdots & & & \\ & & & & & 1 & & \\ & & & & & & 1 & \\ & & & & & & & \ddots \\ & & & & & & & & 1 \end{bmatrix}, \quad (2.93)$$

while (for $E_i^\omega > 0$ ordered in decreasing sequence along the diagonal)

$$\mathcal{M} = \begin{pmatrix} E_p^\omega & & & & \\ & E_{p-1}^\omega & & & \\ & \ddots & \ddots & & \\ & & E_1^\omega & & 0 \\ & & & -E_1^\omega & \\ & & & & -E_2^\omega \\ & & & & \\ & 0 & & & -E_p^\omega \\ & & \ddots & & \\ & & & -E_p^\omega & \end{pmatrix} \quad (2.94)$$

Due to the \mathcal{P} invariance the matrix representation of Routhian (2.53) reduces in most of the cases studied to two submatrices denumerated by parity $\pi = -1$ or $+1$ (see Sec. II.E.3). Hence matrices A and B and hence also \mathcal{M} and \mathcal{K} split into $\pi = \pm 1$ submatrices:

$$\mathcal{K} \rightarrow \{\mathcal{K}_{\pi+}, \mathcal{K}_{\pi-}\}, \quad \mathcal{M} \rightarrow \{\mathcal{M}_{\pi+}, \mathcal{M}_{\pi-}\}, \quad (2.95)$$

whose structure resembles strictly that in representations (2.93) and (2.94).

Taking into account the \mathcal{R}_x invariance and its consequences for the structure of the HFBC equations [cf. Eqs. (2.83a), (2.83b) and (2.84a), (2.84b)] we find that, within both parities separately, for each quasiparticle Routhian E_L^ω that belongs to the solution of set I of signature $r = -i$ there exists the quasiparticle Routhian $E_L^\omega = -E_L^\omega$ that belongs to the solution of set II of opposite signature ($r = +i$). Quasiparticle Routhians of both signatures are thus present on the diagonal of \mathcal{K}_π . It is illustrative to

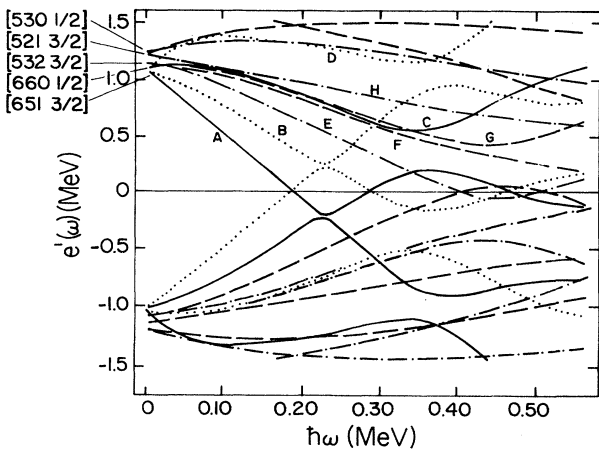


FIG. 9. The quasiparticle Routhians—eigenvalues to the HFBC operator of Eq. (2.88) with the Nilsson model average potential. Here both the negative and the positive eigenvalues are plotted, despite the fact that due to the symmetry of the HFBC equations, essential information is repeated. This figure represents graphically Eq. (2.94). [The figure is obtained from Riedinger (1980).]

combine the information about quasiparticle Routhians of both parities and both signatures in one plot. In Fig. 9, a pictorial representation of Eq. (2.94), E_i^ω are plotted as functions of the rotational frequency ω .

Recall that in this section we confine ourselves to systems with even particle number. Relations (2.91) and (2.92) ensure that in both parities half the total number of eigenvalues of \mathcal{K}_π are equal to zero and the other half equal to one. In this way one discovers that the configurations of the system of particles are represented within the HFBC approach by a set of quasiparticle levels [cf. Eq. (2.94) and Fig. 9], out of which one half has negative and the other half positive values for a not too large ω (see also Sec. III). Excitations of the system above the quasiparticle vacuum-state energy [Eq. (2.62b)] in the rotating coordinate frame are given only in terms of the positive eigenvalues E_i^ω [cf. Eq. (2.71)]. If the eigenvalues k_i that correspond to positive E_i^ω are all equal to zero, there is no quasiparticle excitation in the system. Thus one can say that the corresponding quasiparticle vacuum configuration is represented by all negative E_i^ω “occupied” [$(1-k_i)=1$] and all positive E_i^ω “empty” ($k_i=0$) [Eq. (2.93)]. All possible two-quasiparticle, four-quasiparticle, etc., excited configurations can easily be obtained by proper permutations of zeros and unities in the diagonal of the matrix \mathcal{K}_π in Eq. (2.93); one has to remember only that if a positive eigenvalue ($+E_i^\omega$) is occupied by a quasiparticle, its negative eigenvalue partner ($-E_i^\omega$) of opposite signature must be unoccupied [cf. Eqs. (2.91) and (2.92)]. For instance, the lowest two-quasiparticle band (in many nuclei this is the Stockholm band) can be represented by

$$\mathcal{K}_{\pi+}^{(s)} = \begin{pmatrix} 0 & & & & & & & \\ & 0 & & & & & & \\ & & \ddots & & & & & \\ & & & 1 & & & & \\ & & & & 1' & & & \\ & & & & & \ddots & & \\ & & & & & & 0 & \\ & & & & & & & 0 \\ & & & & & & & & 1 \\ & & & & & & & & & 1 \\ & & & & & & & & & & 1 \\ & & & & & & & & & & & 1 \\ & & & & & & & & & & & & 1 \end{pmatrix}$$

or

$$\mathcal{K}_{\pi-}^{(s)} = \begin{pmatrix} 0 & & & & & & & \\ & 0 & & & & & & \\ & & \ddots & & & & & \\ & & & 1 & & & & \\ & & & & 1' & & & \\ & & & & & \ddots & & \\ & & & & & & 0 & \\ & & & & & & & 0 \\ & & & & & & & & 1 \\ & & & & & & & & & 0 \\ & & & & & & & & & & 1 \\ & & & & & & & & & & & 1 \\ & & & & & & & & & & & & 1 \end{pmatrix} \quad (2.96)$$

In fact, the presence of negative eigenvalues in Eq. (2.94) which results from the doubled dimensions introduced by the Bogolyubov transformation (cf. Secs. II.E.1 and II.E.2) can simply be ignored, since the vacuum configuration corresponds to all negative states occupied by quasiparticles. It is thus sufficient to use only the upper half of the matrices ($\mathcal{M}_{\pi+}, \mathcal{M}_{\pi-}, \mathcal{K}_{\pi+}, \mathcal{K}_{\pi-}$) just by employing [cf. Eq. (2.96) as an example]

$$\mathcal{K}_\pi^> = \begin{pmatrix} 0 & & & \\ & 0 & & \\ & & \ddots & \\ & & & 0 \\ & & & & 1 \\ & & & & & 1 \end{pmatrix}, \quad (2.97)$$

together with $\mathcal{M}_\pi^>$, which is equal to

$$\mathcal{M}_\pi^> = \begin{pmatrix} \cdot & & \\ & E_C^\omega & \\ & E_B^\omega & \\ & & E_A^\omega \end{pmatrix} \quad (2.98)$$

for $\pi = +1$ and -1 each. Any two-quasiparticle excitation is now obtained by selecting two diagonal elements of $\mathcal{K}_{\pi}^>$ that are equal to one [either both in $\mathcal{K}_{\pi+}^>$ or both in $\mathcal{K}_{\pi-}^>$ (positive-parity excitation) or else one in $\mathcal{K}_{\pi+}^>$ and one in $\mathcal{K}_{\pi-}^>$ (negative-parity excitation)]. Sometimes one says that two quasiparticles occupy two states. The generalization for multiquasiparticle configurations is straightforward. We want to emphasize once more that the above argument is valid for ω sufficiently small that no eigenvalue E_v^ω which is positive at $\omega=0$ becomes negative.

These simple rules become slightly complicated for higher ω values, where some of the quasiparticle Routhians cross in function of ω . Then the vacuum may become degenerate (gapless superconductivity) at a certain $\omega = \omega^*$, and thus for higher rotational frequencies the original quasiparticle vacuum configuration is no longer a

ground-state configuration. Such a situation will be discussed further in Sec. III, where a comparison to the experimental data is given. Here we wish to present only the simplified form of the quasiparticle diagrams in which all those quasiparticle Routhians that are negative at $\omega \approx 0$ are disregarded, Fig. 10. The figure illustrates the behavior of $M_\pi^>$ of Eq. (2.98) as a function of ω . At certain rotational frequencies crossings between quasiparticle levels do in fact occur. Since, however, the contributions to the total spin that originate from individual quasiparticle Routhians are

$$\langle i | j_x | i \rangle = -\frac{dE_i^\omega}{d\omega} , \quad (2.99)$$

one can immediately see that the crossings of the occupied quasiparticle levels leading to a change of sign of the derivatives in Eq. (2.99) may also lead to the discontinuities in angular momentum as function of ω corresponding to significant changes in nuclear alignment. In the case of weak interaction between the crossing bands the immediate vicinity of the crossing frequency (in the E -vs- ω plot) is rather poorly described by the cranking model. This fact is mainly caused by the large angular momentum fluctuations which occur near the crossing frequency. Hamamoto (1976) has suggested that the band interaction obtained within the cranking model should be regarded rather as unphysical in this case. This problem has also been discussed by Marshalek and Goodman (1978), Grümmer *et al.* (1978), and Faessler *et al.* (1981).

5. Odd-particle systems

The systems of protons and neutrons with odd-particle numbers n can be treated analogously to the one described in Sec. II.E.4. The only modification consists of first defining an auxiliary system of, for example, $(n-1)$ particles [$(n-1)$ is an even number now] and treating the odd particle in terms of a one-quasiparticle excitation of the vacuum. Thus after one has solved the HFBC equations, the generalized density matrix becomes

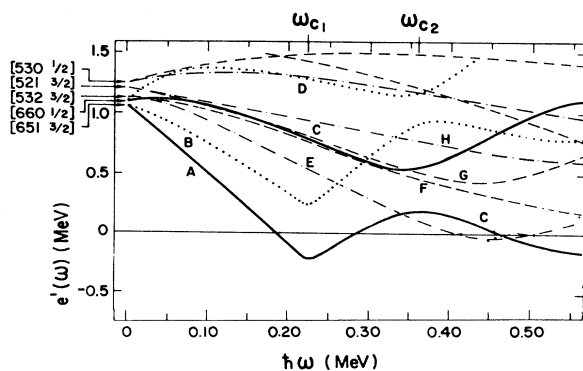


FIG. 10. Results similar to those in Fig. 9; here, however, only those quasiparticle Routhians positive at $\omega \approx 0$ are plotted. In this way, the superfluous information from Fig. 9 is not taken into account. This figure represents graphically Eq. (2.98).

as a representative for the ground-state configuration.

The results, as discussed in Secs. II.E.4 and II.E.5, at the same time prove the theorem according to which the

quasiparticle excitations of an even-particle system consist of an even number of quasiparticle eigenvalues and those of odd-particle systems of an odd number of quasiparticle eigenvalues.

F. A quantal description of noncollective rotation

For axially symmetric nuclei with their angular momenta aligned with the symmetry axis—e.g., the x axis—the nucleonic orbitals are not influenced by rotation about the x axis of the nuclear potential. Therefore, in contrast to the situation discussed in Sec. II.E, collective rotation about that axis is not possible, and the system can increase its angular momentum only by means of nucleonic configuration changes. In many nuclei the alignment of individual nucleonic orbitals does in fact occur and is the basic mechanism in structuring the angular momentum (see Sec. IV). We shall argue that this mechanism predominates in spherical nuclei or those characterized by an oblate, (or sometimes prolate), axially symmetric deformation.

Let us first regard the classical aspects of the motion of an ellipsoidally deformed nucleus. Simple geometrical considerations lead to the following sequence of classical moments of inertia (see, for instance, Stephens, 1979, and Fig. 11):

(i) For an oblate deformed body rotating about the symmetry axis

$$\mathcal{J}_{o-s} \approx \mathcal{J}_0 \left[1 + 0.6 \frac{\Delta R}{R} \right], \quad (2.101)$$

(ii) for a prolate deformed body rotating about an axis perpendicular to the symmetry axis

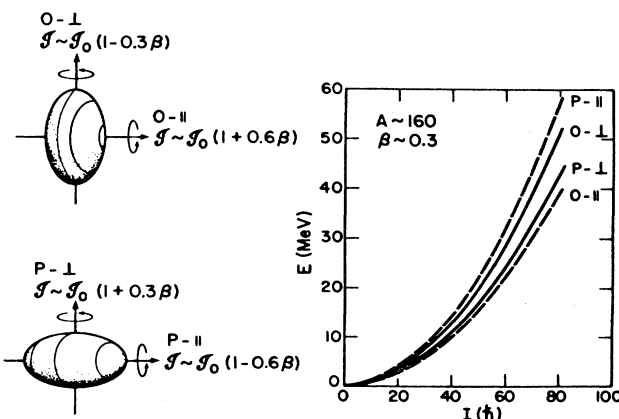


FIG. 11. Characteristic modes of rotation and the corresponding energies as functions of spin represented for prolate (P) and oblate (O) deformed nuclei, with the rotation axis parallel (\parallel) or perpendicular (\perp) to the symmetry axis (Stephens, 1979).

$$\mathcal{F}_{p-\perp} \approx \mathcal{F}_0 \left[1 + 0.3 \frac{\Delta R}{R} \right], \quad (2.102)$$

(iii) for an oblate deformed body rotating about an axis perpendicular to the symmetry axis

$$\mathcal{F}_{o-\perp} \approx \mathcal{F}_0 \left[1 - 0.3 \frac{\Delta R}{R} \right], \quad (2.103)$$

(iv) for a prolate deformed body rotating about the symmetry axis

$$\mathcal{F}_{p-s} \approx \mathcal{F}_0 \left[1 - 0.6 \frac{\Delta R}{R} \right]. \quad (2.104)$$

Here the deformation is expressed by $\Delta R/R$, with ΔR representing the difference between the longer and the shorter semiaxes, and \mathcal{F}_0 the classical moment of inertia of a spherical nucleus.

Obviously, the rotation about the symmetry axis (i) in oblate nuclei corresponds to higher moments of inertia, and consequently to lower energy, than the rotation perpendicular to symmetry axis (iii). In the quantal description one assumes that the mechanism of classical rotation about symmetry axis (i) is replaced by the mechanism of alignment of individual orbitals, while the rotation about an axis perpendicular to symmetry axis (iii) is understood as a collective one.

On the average the alignment of angular momenta in individual orbitals leads to the average moment of inertia $\mathcal{F} \approx \mathcal{F}_{\text{rigid}}$, at least in simple nuclear models (Bohr and Mottelson, 1969). This gives support to the existence of some correspondence between the classical rotation about the symmetry axis and the quantal alignment of individual orbitals with this axis. Thus one may generally expect the collective bands to lie above the noncollective yrast states in oblate nuclei. For prolate nuclei the opposite is valid; the collective band is expected to lie below those states formed by the alignment of individual orbitals [cf. (ii)–(iv)].

Generally, shell effects do not modify any of the above considerations significantly. The only known exception is the region around the prolate ^{176}Hf nucleus, where a very strong negative shell correction shifts the noncollective states below the collective band (see discussion in Sec. IV.A.2). Several nuclei were found experimentally whose yrast, and also higher excitations reveal a very irregular dependence on spin (see examples in Sec. IV). In addition, one also expects a very irregular dependence of the state decay probabilities (lifetimes) on spin. Consequently, some yrast states may become particularly long lived. They are usually referred to as yrast isomers or yrast traps (see Sec. IV for possible reasons for and mechanisms prevalent in yrast traps).

Most of these properties were predicted by Bohr and Mottelson (1974). Although several nuclei with irregular excitation patterns were known experimentally before 1974, the great wealth of experimental information on this excitation mode and high-spin isomeric states that

now exists has been gained during the last five years. Since these states may also be interpreted in terms of shell-model configurations (spherical or deformed), recently developed high-spin spectroscopy may furnish valuable information on the single-particle structure in excited nuclei.

For an axially symmetric nuclear field with $\gamma=60^\circ$ or -120° the individual-particle Routhians e_v^ω are given by a simple expression [cf. Eq. (2.12)]:

$$e_v^\omega = e_v - (\hbar\omega)m_v, \quad (2.105)$$

where m_v denotes the projection of the particle angular momentum onto the rotation, and at the same time symmetry axis, and e_v is the single-particle energy in the case of no rotation.

In independent-particle systems the filling of the nucleonic orbitals may be studied either by means of plots of the single-particle Routhians e_v^ω vs ω , e_v^ω given by Eq. (2.105), or by minimizing the sum of the single-particle energies e_v (i.e., the eigenvalues of the original Hamiltonian H , not H^ω) under the constraint that the total angular momentum I and the number of particles be fixed for neutrons and protons separately. Frequently one assumes the projection of I to be approximately equal to I itself; this is a good approximation for high-spin states. The minimization of the sum of the energies $\sum e_v$ under these conditions may easily be illustrated by the geometrical method that represents all the energies e_v of a given kind of particle (neutrons or protons) as points in the (m, e) plane (Bohr and Mottelson, 1975). The projection m_v of the individual nucleonic angular momenta is a good quantum number in this case, as follows from the axial symmetry. The minimization procedure for the sum

$$\mathcal{E} = \sum_{v \text{ occ}} e_v \quad (2.106)$$

[with the constraint for given angular momentum; cf. Eq. (2.109) below] with respect to the selection of the set of occupied states v occ is equivalent to including in Eq. (2.106) only those points (m_v, e_v) that lie below a straight line

$$e = \lambda + (\hbar\omega)m \quad (2.107)$$

in the (m, e) plane (tilted Fermi surface).

Generally, one can find the single-particle yrast configurations by (i) constructing all possible particle-hole excited states, and (ii) finding the yrast states for consecutive spin values by minimizing the energy with respect to a certain configuration at a given spin. Such an approach is easy to formulate. Considering only the bound single-particle states, however—i.e., neglecting the possibility that some single-particle excitations may involve the positive energy part of the spectrum (resonances)—we have for the neutrons in medium-heavy nuclei about 100 bound states and as, for example, in ^{152}Dy , about 86 neutrons residing in these states. One thus has to take into account all possible ways for 86 particles to occupy 100 levels. This amounts to $({}^{100}_{43}) \sim 10^{30}$. Consequently, steps (i) and

(ii) go beyond any computer ability, and a reformulation is needed. From the mathematical point of view, our problem is to find a minimum,

$$\sum_{v \text{ occ}} e_v = \min, \quad (2.108)$$

for a given spin I ,

$$I \approx I_x = \sum_{v \text{ occ}} m_v, \quad (2.109)$$

and for a given nucleus,

$$\sum_{v \text{ occ}} 1 = A. \quad (2.110)$$

Since in the independent-particle approach the lowest (yrast) energies of the nucleus are composed of lowest-energy neutron and proton contributions, we can limit our considerations to one kind of particle first. We will then combine the proton and neutron contributions. In order to find the energy minimum in Eq. (2.108) under the subsidiary conditions (2.109) and (2.110) formulated now for the two kinds of particles separately, let us apply the well-known Lagrange multiplier method. According to the Lagrange method, one defines an auxiliary expression

$$\sum_{v \text{ occ}} e_v^\omega = \sum_{v \text{ occ}} [e_v - (\hbar\omega)m_v - \lambda] \quad (2.111)$$

and then applies the theorem, which states that finding the minimum of Eq. (2.108) under the subsidiary conditions (2.109) and (2.110) is equivalent to finding the usual, i.e., unconstrained, minimum of the auxiliary expression (2.111), i.e.,

$$\sum_{v \text{ occ}} e_v^\omega = \min. \quad (2.112)$$

The two yet unknown parameters $\hbar\omega$ and λ are called the Lagrange multipliers. They can be calculated from Eqs. (2.109) and (2.110) after finding the minimum of Eq. (2.112), which in turn is equivalent to finding the n lowest-lying Routhians e_v^ω or, in other words, the set of $\{e_v^\omega\}$ for which

$$e_v - \hbar\omega m_v \leq \lambda. \quad (2.113)$$

One can thus formulate the following theorem. Finding a constrained minimum in Eq. (2.108) is equivalent to the geometrical problem of finding on the (m, e) plane n of those and only of those points e which lie below the straight line given by Eq. (2.107). The set of these points defines the so-called optimal or Lagrange configurations. The particular spin values for which a solution to the Lagrange problem exists play an especially important role in such an analysis.

The method of employing the tilted Fermi surface and the distinction between optimal and nonoptimal configurations can best be visualized with an example. Figure 12 illustrates a few solutions to the problem (2.108) for the lowest spin configurations for $N=83$ and $Z=64$ particles. Not for any pair of the Lagrange multipliers λ and $\hbar\omega$ do there exist exactly n e_v^ω 's such that

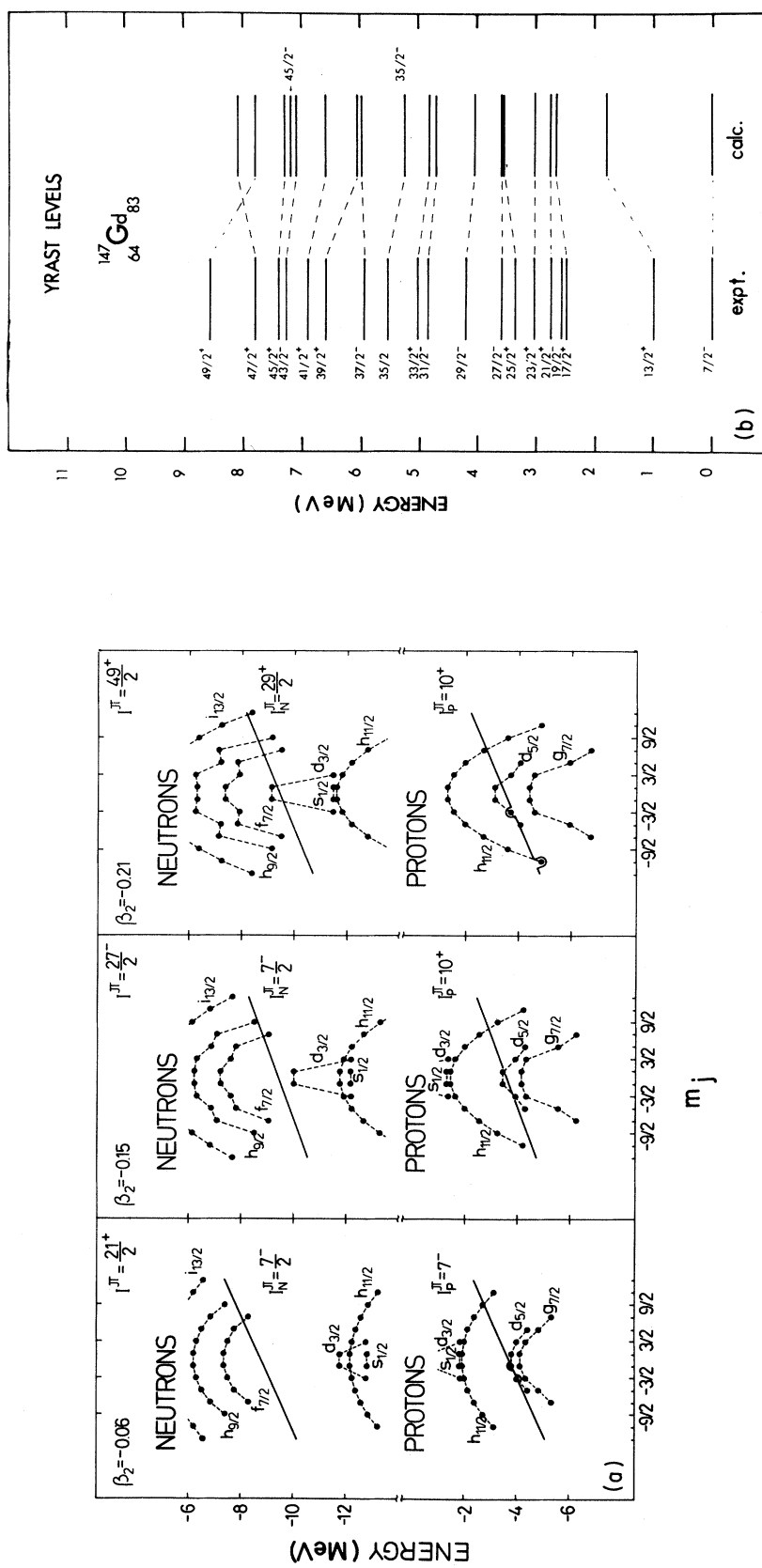


FIG. 12. (a) Tilted Fermi surfaces corresponding to the isomers observed in ^{147}Gd : 4.8 ns $I^\pi = \frac{21}{2}^+$ isomer, 27 ns $I^\pi = \frac{27}{2}^-$ isomer, and the 530 ns $I^\pi = \frac{49}{2}^+$ isomer (Dudek *et al.*, 1981). (b) Comparison between the experimental level scheme of ^{147}Gd and the calculations based on the deformed Woods-Saxon potential.

$e_\nu \leq (\hbar\omega)m_\nu + \lambda$. In other words, the Lagrange multiplier method [Eqs. (2.108)–(2.110)] offers solutions only for some spin values [in Fig. 12(a) these values are $I_N = \frac{7}{2}$ and $\frac{29}{2}$; $I_Z = 7$ and 10].

Finding the Lagrange configurations for a sequence of several spin values for both neutrons and protons facilitates the finding of all other lowest-energy configurations. For calculating all the yrast line configurations it is sufficient to consider the one-particle—one-hole and two-particle—two-hole configurations, defined with respect to the consecutive tilted Fermi surfaces of Eq. (2.107) that specify the Lagrange configurations. The result of such a calculation is illustrated in Fig. 12(b).

The above conclusions are valid for even and odd particle numbers. The Lagrange multiplier method, with its geometrical interpretation, facilitates the task of finding the lowest-energy particle-hole configurations; its application demonstrates how to select only a few most important configurations using diagrams, such as the ones in Fig. 12(a).

The procedure described above establishes the yrast line of an axially symmetric nucleus. Possible isomeric states can also be predicted. The latter emerge as a result of an irregular single-particle structure in the nucleonic configurations, as discussed above. The high-spin isomers may then appear either as energy yrast traps—i.e., as either local minima in the yrast line or states decaying by very-low-energy transitions—or as structure yrast traps—i.e., as states differing to such an extent from their neighbors that the transitions deexciting one into another are strongly retarded. In experiments, energy yrast traps rarely appear as local minima along the yrast line; they often decay via electric quadrupole transitions.

The Lagrange multiplier method, known also as the tilted Fermi surface method, has been applied in several papers: by Andersson *et al.* (1976, 1978), Andersson and Krumlinde (1977), Døssing *et al.* (1977, 1980, 1981), Cerfaski *et al.* (1977, 1979), Matsuyanagi *et al.* (1978), Leander *et al.* (1979), Åberg *et al.* (1979), Dudek *et al.* (1981, 1982a). Some of the calculations also take into account the pairing that leads to the superfluid correlations in nuclei which may modify some properties of the nuclear spectrum (e.g., Andersson and Krumlinde, 1977); see Sec. IV.

Another method of analyzing the yrast line is based on the spherical shell model (see Blomqvist, 1979, and references cited therein). In this approach the deformation is neglected, but instead residual interaction between the valence nucleons is introduced. This interaction is usually more general than the pairing force utilized frequently in calculating a deformed field. The interaction supplementing the spherical shell-model Hamiltonian also includes a long-range component responsible for static deformations. This method, which can be regarded as merely an extension of the shell-model approach, was successfully applied to nuclei in the vicinity of ^{208}Pb and also in the heavy rare-earth region around ^{146}Gd , the latter being treated as another nucleus with doubly closed shells (Kleinheinz, Lunardi *et al.*, 1978; Kleinheinz, Ogawa *et al.*, 1978;

Ogawa, 1978, Kleinheinz *et al.*, 1979; Broda, Kleinheinz, Lunardi, and Blomqvist, 1979; Kleinheinz, 1979, and references therein).

III. HIGH-SPIN NUCLEAR STRUCTURE STUDIED BY MEANS OF γ -RAY SPECTROSCOPY; COLLECTIVE ROTATION

In this section we discuss selected aspects of nuclear collective rotation at high angular momenta together with theoretical and experimental ideas employed recently in studies of collective nuclear structure. In Sec. III.A the interpretation of yrast-state properties will be discussed in terms of band crossings; related properties of excited rotational bands will also be illustrated. In Sec. III.B the γ - γ energy correlations in the high-spin spectra of collectively rotating nuclei are discussed. The effect of nuclear pairing correlations in the high-spin states and the related pairing reduction due to Coriolis effects are the subject of Sec. III.C. In Sec. III.D the multiple Coulomb excitations of high-spin states are discussed from the point of view of nuclear structure studies. In Appendix B, elementary information on the electromagnetic transition probabilities, lifetimes, and feeding times is collected.

A. Crossing rotational bands

1. Phenomenological description

In this section we discuss the properties of collective rotational bands in nuclei which are appreciably deformed. We shall see that the typical behavior observed and analyzed in such nuclei is strongly related to the crossings between different rotational bands along the yrast line.

We begin our discussion by recalling the typical quantities important in the description of collective rotational bands. The bands are defined in terms of state energies \mathcal{E} as functions of angular momentum I ; we know (cf. Sec. II) that the nuclear states belonging to a given band are characterized by a definite (common) parity and signature. Furthermore, bands of the same parity and signature can be distinguished with the help of other, additional quantum characteristics—the number of quasiparticles, the number of phonons, etc. The band identity (the fact that we can define bands) follows from the fact that in most of the cases the intraband electric quadrupole transitions (cf. Appendix B) are much faster than the related interband transitions. Typical many-band level schemes are illustrated in Figs. 13(a) and 13(b) (these level schemes will also be discussed in more detail below).

A crossing of any two bands [in the (\mathcal{E}, I) plane] means that at certain $I = I_{\text{cross}}$ the energies of the corresponding two states belonging to different bands are approximately equal. In particular, a crossing of any two bands which form a portion of the yrast line leads apparently to a rearrangement in the intrinsic structure in the deexciting nucleus. Such a rearrangement is sometimes very abrupt.

We first introduce the angular velocity of rotation us-

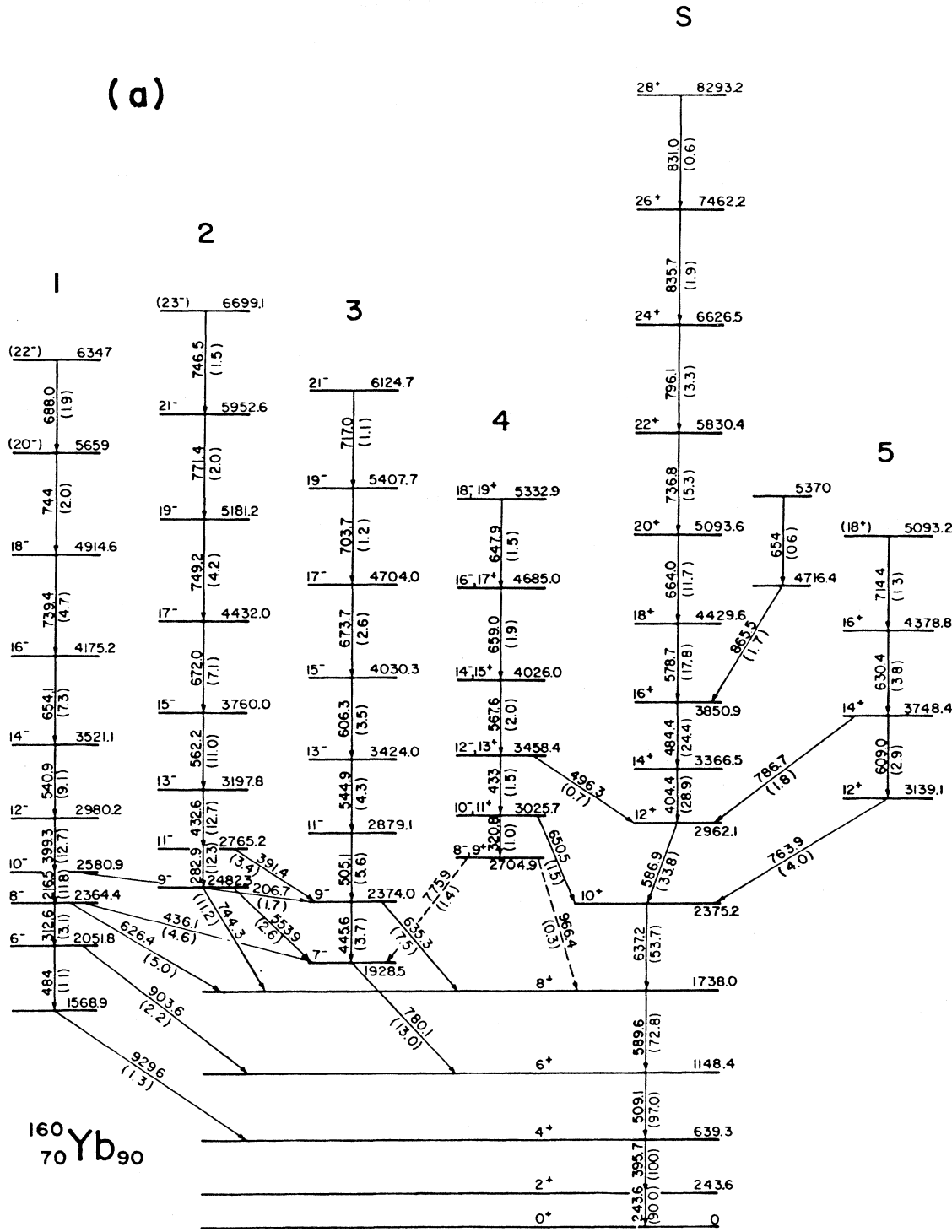


FIG. 13. Collective rotational bands in ^{160}Yb (a) and in ^{161}Yb (b) as deduced from the reactions $^{147,148}\text{Sm}(^{16}\text{O},3n)^{160,161}\text{Yb}$ (Riedinger *et al.*, 1980, and of Gaardhøye *et al.*, 1980). The yrast sequence is composed of the ground-state band (gsb) ($I^\pi = 0^+, 2^+, \dots, 10^+$) and of the excited (Stockholm) band (for $I^\pi = 12^+, 14^+, \dots, 28^+$) marked with *S*.

ing an analogy with classical physics. For a rotation about a fixed axis (O_x) we define

$$\omega(I) = \frac{1}{\hbar} \frac{d\mathcal{E}(I)}{dI_x}, \quad (3.1)$$

where I_x denotes the component of angular momentum along the axis of rotation. An approximate relation between I_x and the total angular momentum I is often employed:

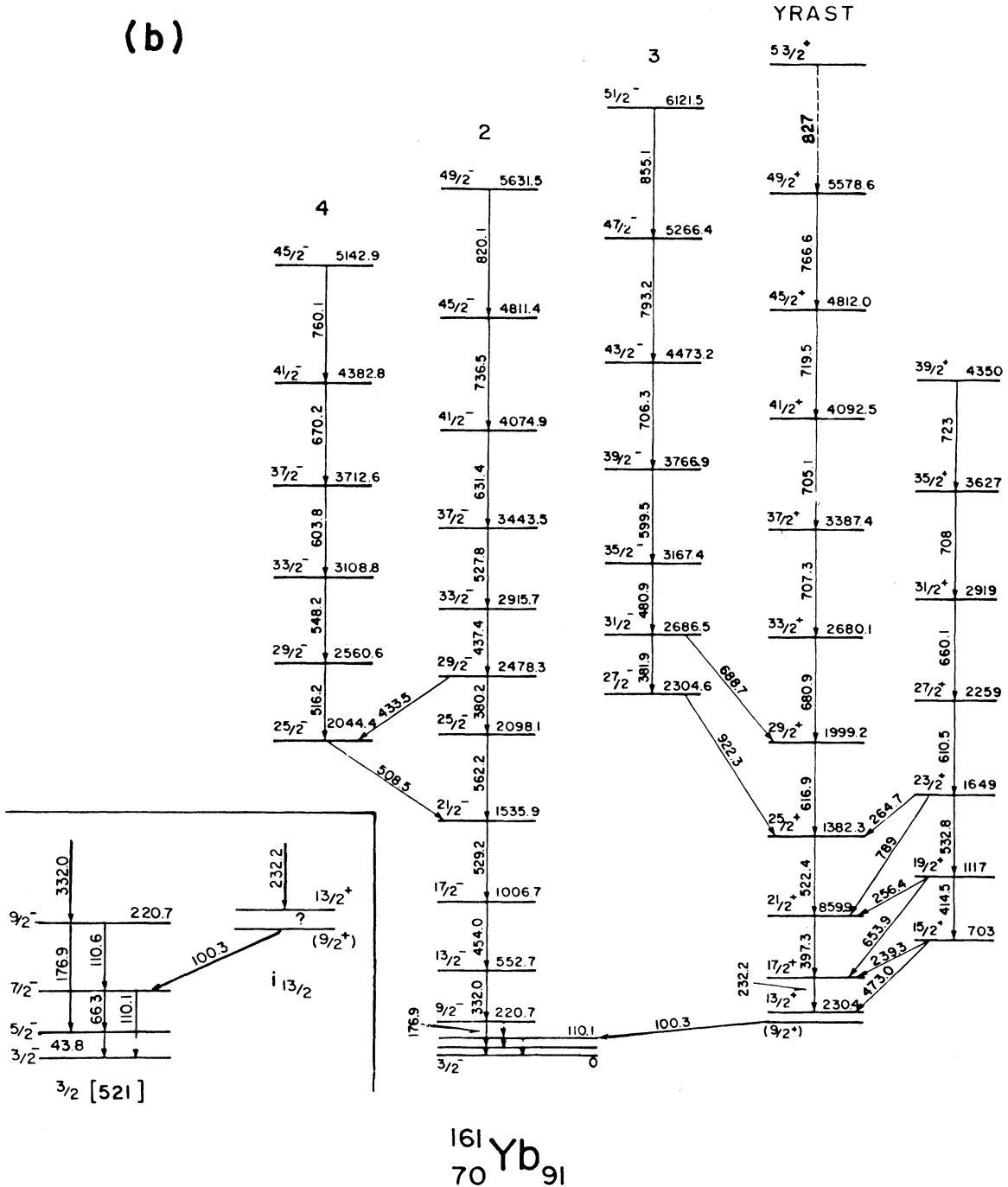


FIG. 13. (Continued.)

$$I_x = [I(I+1) - K^2]^{1/2} \approx [(I + \frac{1}{2})^2 - K^2]^{1/2}. \quad (3.2)$$

In Eq. (3.2) K denotes the component of I along the nuclear symmetry axis, say, 0_z . The appearance of the $I(I+1)$ term in the square brackets in Eq. (3.2) takes into account the three-dimensional character of rotation. However, since for high spins the distinction between $\sqrt{I(I+1)}$ and I is not essential, one can often write $\sqrt{I(I+1)} \sim I$.

Next, important quantities introduced are the nuclear moments of inertia. Following Bohr and Mottelson (1981), we introduce (assuming the maximum O_x axis alignment, $I_x \sim I$)

$$\mathcal{F}^{(1)} \equiv \left[\frac{2}{\hbar^2} \frac{d\mathcal{E}(I)}{d(I^2)} \right]^{-1} = \hbar \frac{I}{\omega(I)} , \quad (3.3)$$

referred to as the "kinematical" moment of inertia, and

$$\mathcal{F}^{(2)} \equiv \left[\frac{1}{\hbar^2} \frac{d^2 \mathcal{E}(I)}{dI^2} \right]^{-1} = \hbar \frac{dI}{d\omega} \quad (3.4)$$

referred to as the "dynamical" moment of inertia. We shall see later that the above two quantities reflect two different physical aspects of nuclear structure; in particular, the dynamical moment of inertia is related to the curvature of the $\mathcal{E}(I)$ line. For a rigid-body rotation the two quantities coincide.

Let us also introduce the aligned angular momentum $i(\omega)$, defined as the difference between the actual yrast angular momentum $I_x(\omega)$ and an auxiliary $I_{\text{ref}}(\omega)$, the latter quantity describing the angular momentum of the so-called reference rotor, i.e.,

$$i(\omega) = I_x(\omega) - I_{\text{ref}}(\omega) \quad (3.5)$$

(Bohr and Mottelson, 1977; see also below). The above quantity depends on how precisely $I_{\text{ref}}(\omega)$ is defined; we will discuss a possible choice later.

Consider a nucleus deexciting along its yrast line. If in a certain spin range two rotational bands cross at the yrast line, it is equivalent to say that the nucleus changes its intrinsic structure. This corresponds to a transition from one band to the other (see Fig. 14). The situation of a sharp crossing is illustrated in Fig. 14(a). It can immediately be seen that the angular velocity of rotation

which is related to the slope in the curve of \mathcal{E} vs I [cf. Eq. (3.1)] must decrease at the crossing point $I = I_{\text{cross}}$, whereas I increases. This means physically that a part of angular momentum is transferred into the intrinsic degrees of freedom, thus leading to a slowing down of the collective rotation.

The graphical representation of the band crossing effect looks much more dramatic if ω instead of I is used as an independent variable. In such a representation all the important physical quantities—energy, angular momentum, aligned angular momentum, moments of inertia, etc.—exhibit a multivalued behavior; the latter was discovered experimentally for the first time by Johnson *et al.* (1972) and is often called a backbending effect. Figure 14(b) shows that a strong interaction ("repulsion") between the bands may smooth out the dramatic effect of band crossing.

Detailed spectroscopic information on the ground-state and excited bands in nuclei exists at present. A small fraction of this extensive information concerning the yrast bands of even-even rare-earth nuclei has been chosen (cf. Table I) in order to illustrate the band crossing dependence on proton and neutron numbers. Additional information can be found in the compilations of Lieder and Ryde (1978), Lederer and Shirley (1978), Sayer *et al.* (1975), Saethre *et al.* (1973), and Madjakov (1982), while more recent experimental data on $N=96$ isotones are summarized by Michel and Vervier (1981). From the above experimental evidence it is clear that in many nuclei, at least, one band crossing (along the yrast line) has been detected. In the following section we will argue for the interpretation of this effect in terms of crossings between the ground-state and neutron quasiparticle bands. However, the second crossing along the yrast lines in a few nuclei has already been found experimentally—for the first time by Lee *et al.* (1977) in ^{158}Er at $I=28$ (cf. Table I). In this experiment the $^{122}\text{Sn}(^{40}\text{Ar},4n)^{158}\text{Er}$ reaction was employed at 166-MeV beam energy. Observation of the $4n$ channel in this reaction was enhanced detecting coincidences between two Ge(Li) detectors with one NaI(Tl) detector or more out of six. This selection technique was quite effective, due to relatively low γ -ray multiplicities in the competing $5n$ and $6n$ channels; thus the above setup played the role of a multiplicity filter.

The second backbending in the yrast line of ^{156}Er was also found (Byrski *et al.*, 1980), using the reaction $^{141}\text{Pr}(^{19}\text{F},4n)^{156}\text{Er}$. The data were obtained with an array of three Ge(Li) detectors used for the γ - γ coincidence measurements.

2. Independent quasiparticles

We have seen (cf. Sec. II) that the collective rotational motion can be approximately described in terms of the nuclear cranking model. Since the nuclear coupling scheme involves the two-body pairing (nuclear superfluid) correlations, the appropriate derivation led to the expression of the relevant physical quantities in terms of independent quasiparticles rather than simply particles.

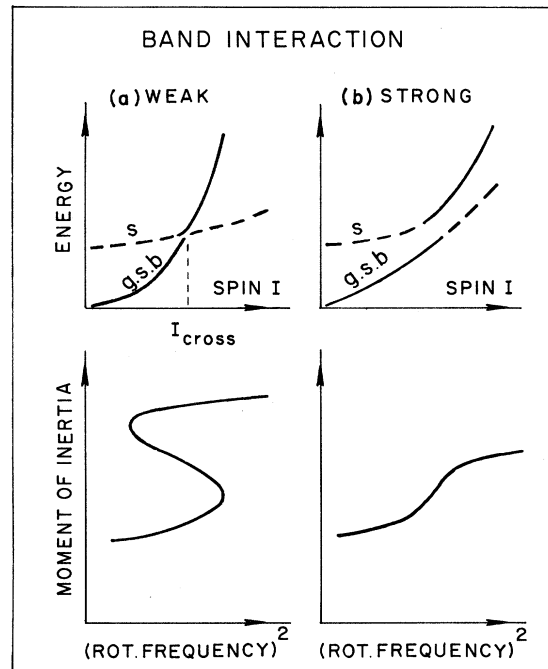


FIG. 14. Schematic illustration of the band interaction [(a) weak and (b) strong], leading to two different curvatures of the yrast lines and consequently to two different shapes of the moment of inertia curves. The distance of the closest approach of the two curves is related to the interaction strength $|V|$ discussed in the text (up to a good approximation, this distance is equal to $2|V|$).

TABLE I. Properties of even rare-earth nuclei.

E_x	I^π	$\tau_{1/2}$	$E_\gamma(I \rightarrow I-2)$	$B(E2; I \rightarrow I-2)$	$B(E2; \text{rot})^a$	$\frac{B(E2)}{B(E2)_{\text{rot}}}$	$2\mathcal{F}/\hbar^2 b$	$\hbar^2 \omega^2 c$
(keV)		(ps)	(keV)	($e^2 b^2$)			(MeV $^{-1}$)	(MeV 2)
$^{152}_{64}\text{Gd}_{88}$							Zolnowski <i>et al.</i> , 1980	
344	2+	29 ± 2	344	0.39 ± 0.03			17.4	0.039
755	4+		411				34.1	0.045
1227	6+		472				46.6	0.046
1747	8+		520				57.7	0.069
2300	10+		553				68.7	0.076
2884	12+		584				78.8	0.085
3499	14+		615				87.8	0.095
4143	16+		644				96.3	0.104
$^{154}_{64}\text{Gd}_{90}$							Gono and Sugihara, 1974; Sie <i>et al.</i> , 1977	
123	2+	1190 ± 20	123	0.77 ± 0.02	0.77	1	48.8	0.005
371	4+	46.0 ± 1.5	248	1.18 ± 0.04	1.11	1.06	56.5	0.016
718	6+	7.9 ± 0.4	347	1.38 ± 0.06	1.22	1.13	63.4	0.031
1145	8+	2.6 ± 0.2	427	1.53 ± 0.08	1.28	1.20	70.3	0.046
1638	10+	1.1 ± 0.2	493	1.7 ± 0.2	1.31	1.30	77.1	0.061
2185	12+		547				84.1	0.075
2778	14+		593				91.1	0.088
3405	16+		627				99.0	0.098
4088	18+		683				102	0.117
$^{156}_{64}\text{Gd}_{92}$							Sie <i>et al.</i> , 1977	
89	2+	2220 ± 40	89	0.92 ± 0.03	0.92	1	67.4	0.0026
288	4+	114 ± 2	199	1.29 ± 0.02	1.31	0.98	70.3	0.010
584	6+	18 ± 3	296	1.47 ± 0.04	1.45	1.01	74.3	0.022
964	8+	4.4 ± 0.3	380	1.57 ± 0.25	1.51	1.04	78.9	0.037
1415	10+	1.87 ± 0.11	451	1.59 ± 0.09	1.56	1.02	84.3	0.051
1923	12+	1.10 ± 0.10	508	1.51 ± 0.15	1.59	0.95	91.0	0.065
$^{158}_{64}\text{Gd}_{94}$							Kearns <i>et al.</i> , 1977	
80	2+	2530 ± 50	80	0.97 ± 0.03	0.97	1	75.0	0.0021
261	4+	162 ± 13	181	1.28 ± 0.10	1.41	0.91	77.3	0.0087
539	6+		278				79.1	0.020
904	8+	5.1 ± 0.4	365	1.60 ± 0.15	1.60	1.00	82.2	0.034
1351	10+	1.80 ± 0.10	447	1.74 ± 0.10	1.64	1.06	85.0	0.050
1867	12+	0.98 ± 0.08	516	1.57 ± 0.16	1.67	0.94	89.1	0.067
$^{154}_{66}\text{Dy}_{88}$							Davidson <i>et al.</i> , 1974; Marchie van Voorhuisen <i>et al.</i> , 1977	
335	2+	40 ± 4	335	0.29 ± 0.03	0.29		17.9	0.037
747	4+	12 ± 2	412	0.52 ± 0.09	0.42		33.9	0.045
1224	6+	5.0 ± 1.5	477	0.61 ± 0.18	0.46		46.1	0.060
1747	8+		523				57.4	0.069
2304	10+		557				68.2	0.078
2893	12+		589				78.1	0.087
3509	14+		616				87.7	0.095
4091	16+		582				106	0.085
4638	18+		547				129	0.074
5250	20+		612				127	0.094
							Pakkanen <i>et al.</i> , 1982	
5935	22+		685				126	0.12
6691	24+		756				124	0.14
7514	26+		823				124	0.17
8401	28+		887				124	0.20
9137	30+		736				160	0.14
9942	(32+)		805				157	0.16

TABLE I. (Continued.)

E_x (keV)	I^π	$\tau_{1/2}$ (ps)	$E_\gamma(I \rightarrow I-2)$ (keV)	$B(E2; I \rightarrow I-2)$ ($e^2 b^2$)	$B(E2; \text{rot})^a$	$\frac{B(E2)}{B(E2)_{\text{rot}}}$	$2\mathcal{F}/\hbar^2$ ^b (MeV ⁻¹)	$\hbar^2 \omega^2$ ^c (MeV ²)
¹⁵⁶ ₆₆ Dy ₉₀								
138	2 ⁺	840±40	138	0.76±0.02	0.76	1	43.5	0.006
404	4 ⁺	29±3	266	1.33±0.06	1.10	1.21	52.6	0.019
770	6 ⁺	9.1±0.7	366	0.91±0.07	1.20	0.76	60.1	0.033
1216	8 ⁺	2.21±0.14	446	1.46±0.05	1.25	1.17	67.3	0.050
1715	10 ⁺	0.89±0.06	509	1.85±0.06	1.28	1.45	74.7	0.065
2286	12 ⁺	0.46±0.09	561	2.2±0.4	1.31	1.67	82.0	0.080
2887	14 ⁺	0.51±0.07	601	1.4±0.2	1.32	1.08	89.9	0.090
Ward <i>et al.</i> , 1979; Bjerregaard <i>et al.</i> , 1963								
3499	16 ⁺	0.79±0.10	612	1.7±0.2	1.34	1.30	101	0.094
4025	18 ⁺	0.92±0.05	526	1.52±0.09	1.35	1.13	133	0.069
4635	20 ⁺	0.49±0.04	610	1.36±0.12	1.35	1.00	128	0.093
5319	22 ⁺	0.35±0.06	684	1.09±0.19	1.36	0.80	126	0.117
6069	24 ⁺	0.39±0.06	750	0.61±0.09	1.36	0.45	125	0.141
6877	26 ⁺	0.21±0.07	808	0.8±0.3	1.37	0.6	126	0.163
7738	28 ⁺	0.16±0.06	861	0.8±0.3	1.37	0.6	128	0.185
8650	30 ⁺	0.12±0.05	912	0.8±0.3	1.38	0.6	129	0.208
Emling, 1981								
¹⁵⁸ ₆₆ Dy ₉₂								
Emling <i>et al.</i> , 1981; Funk <i>et al.</i> , 1966								
99	2 ⁺	1942±17	99	0.934±0.008	0.93	1	60.6	0.003
317	4 ⁺	71±5	218	1.39±0.09	1.35	0.99	64.2	0.013
638	6 ⁺	9.1±1.0	321	1.74±0.19	1.47	1.20	68.5	0.026
1044	8 ⁺	2.9±0.6	406	1.8±0.4	1.53	1.15	73.9	0.041
1520	10 ⁺	1.41±0.19	476	1.6±0.2	1.57	1.04	79.8	0.057
2050	12 ⁺	0.85±0.16	530	1.6±0.3	1.60	0.99	86.8	0.070
2613	14 ⁺	0.73±0.15	563	1.4±0.3	1.62	0.85	95.9	0.079
3191	16 ⁺	0.63±0.09	578	1.4±0.2	1.64	0.85	107	0.084
3782	18 ⁺	0.55±0.08	591	1.4±0.2	1.65	0.86	118	0.087
4408	20 ⁺	0.40±0.08	626	1.6±0.3	1.66	0.93	125	0.098
5086	22 ⁺	0.33±0.09	678	1.1±0.3	1.66	0.66	127	0.115
Sunyar, 1979								
5822	24 ⁺	0.28±0.10	736	0.84±0.3	1.66	0.51	128	0.135
6613	26 ⁺	0.17±1.10	791	1.2±0.7	1.67	0.73	129	0.156
7454	(28 ⁺)		841				131	0.177
¹⁶⁰ ₆₆ Dy ₉₄								
Johnson <i>et al.</i> , 1972; Sayer <i>et al.</i> , 1974;								
Lopiparo, 1972								
87	2 ⁺	2000±20	87	1.01	1.01	1	69.0	0.002
284	4 ⁺		197	1.39±0.14	1.46	0.95	71.1	0.010
581	6 ⁺		297	1.23±0.06	1.60	0.77	74.1	0.022
Kearns <i>et al.</i> , 1977								
967	8 ⁺	3.4±0.3	386	1.84±0.18	1.67	1.10	77.7	0.038
1429	10 ⁺	1.50±0.10	462	1.77±0.15	1.71	1.04	82.3	0.053
1951	12 ⁺	0.93±0.07	522	1.56±0.12	1.74	0.90	88.1	0.068
2515	14 ⁺	0.6±0.2	564	1.7±0.6	1.75	0.94	95.7	0.080
Sayer <i>et al.</i> , 1974;								
Kurfess and Scharenberg, 1967								
81	2 ⁺	2190±40	81	1.03	1.03	1	74.1	0.0022
266	4 ⁺		185	1.47±0.13	1.49	0.98	75.7	0.009
549	6 ⁺		283	1.38±0.06	1.63	0.85	77.7	0.020
Kearns <i>et al.</i> , 1977								
921	8 ⁺	4.1±0.4	372	1.84±0.18	1.70	1.08	80.6	0.035
1375	10 ⁺	1.57±0.12	454	1.86±0.16	1.74	1.07	83.7	0.052
1903	12 ⁺	0.93±0.06	528	1.48±0.10	1.77	0.84	87.1	0.069

TABLE I. (Continued.)

E_x (keV)	I^π	$\tau_{1/2}$ (ps)	$E_\gamma(I \rightarrow I-2)$ (keV)	$B(E2; I \rightarrow I-2)$ ($e^2 b^2$)	$B(E2; \text{rot})^a$	$\frac{B(E2)}{B(E2)_{\text{rot}}}$	$2\mathcal{F}/\hbar^2 b$ (MeV $^{-1}$)	$\hbar^2 \omega^2 c$ (MeV 2)
¹⁶⁴ ₆₆ Dy ₉₈								
73	2 ⁺	2390±40	73	1.08	1.08	1	82.2	0.0017
242	4 ⁺		169	1.14±0.06	1.55	0.73	82.8	0.0076
501	6 ⁺		259	1.43±0.08	1.71	0.84	84.9	0.017
							Kurfess and Scharenberg, 1967	
844	8 ⁺	6.2±1.0	343	1.9±0.3	1.78	1.04	87.4	0.030
1261	10 ⁺	2.34±0.18	417	1.90±0.15	1.83	1.05	91.1	0.043
1745	12 ⁺	1.14±0.10	484	1.86±0.18	1.86	1.00	95.0	0.059
2290	14 ⁺	0.66±0.05	545	1.88±0.14	1.88	1.00	99.0	0.74
							Kearns et al., 1977	
¹⁵⁶ ₆₈ Er ₈₈								
344	2 ⁺	33.2±1.7	344	0.33±0.02	0.33	1	17.4	0.040
797	4 ⁺	5.4±0.7	453	0.53±0.06	0.47	1.13	30.9	0.054
1340	6 ⁺	1.1±0.7	543	1.0±0.6	0.52	1.92	40.5	0.074
1959	8 ⁺		619				48.5	0.095
2633	10 ⁺		674				56.4	0.114
3315	12 ⁺		682				67.4	0.116
3837	14 ⁺		522				104	0.068
4381	16 ⁺		544				114	0.074
5006	18 ⁺		625				112	0.098
5717	20 ⁺		711				110	0.126
6489	22 ⁺		772				111	0.149
7316	24 ⁺		827				114	0.171
8082	26 ⁺		766				133	0.147
8764	(28 ⁺)		682				161	0.116
9530	(30 ⁺)		766				154	0.147
10330	(32 ⁺)		800				157	0.160
¹⁵⁸ ₆₈ Er ₉₀								
							Diamond et al., 1969;	
							Lee et al., 1977	
192	2 ⁺	300±15	192	0.55±0.03	0.55	1	31.1	0.012
527	4 ⁺	14.4±0.7	335	0.87±0.04	0.79	1.1	41.7	0.030
970	6 ⁺	2.8±0.5	443	1.14±0.19	0.87	1.31	49.5	0.050
1494	8 ⁺	1.2±0.5	524	1.2±0.5	0.91	1.32	57.3	0.069
2074	10 ⁺	0.8±0.4	580	1.1±0.5	0.92	1.20	65.6	0.084
2683	12 ⁺	<0.7	609	>1.0	0.95		75.7	0.092
3193	14 ⁺	2.1±0.5	510	0.8±0.3	0.96	0.83	106	0.065
3666	16 ⁺	1.7±0.6	473	1.4±0.5	0.97	1.44	131	0.056
4233	18 ⁺	<1.5	567	>0.6	0.97		124	0.080
4892	20 ⁺		659				120	0.108
5632	22 ⁺		740				117	0.136
6438	24 ⁺		806				117	0.162
7284	26 ⁺		846				121	0.179
8143	28 ⁺		859				128	0.184
9020	30 ⁺		877				135	0.192
9927	32 ⁺		907				139	0.206
							Burde et al., 1982	
10887	34 ⁺		960				140	0.230
11906	36 ⁺		1019				139	0.260
12967	38 ⁺		1061				141	0.281
¹⁶⁰ ₆₈ Er ₉₂								
							Diamond et al., 1969;	
							Lieder et al., 1972;	
							Davidson et al., 1972;	
							Ryde et al., 1973	
126	2 ⁺	920±50	126	0.83±0.04	0.83	1	47.6	0.0052

TABLE I. (Continued.)

E_x (keV)	I''	$\tau_{1/2}$ (ps)	$E_\gamma(I \rightarrow I-2)$ (keV)	$B(E2; I \rightarrow I-2)$ ($e^2 b^2$)	$B(E2; \text{rot})^a$	$\frac{B(E2)}{B(E2)_{\text{rot}}}$	$2\mathcal{F}/\hbar^2 b$ (MeV $^{-1}$)	$\hbar^2 \omega^2 c$ (MeV 2)
390	4 ⁺	34.5±1.7	264	1.16±0.06	1.19	0.97	53.0	0.018
765	6 ⁺	5.4±0.5	375	1.34±0.12	1.31	1.02	58.5	0.036
1229	8 ⁺	2.2±0.5	464	1.18±0.27	1.37	0.86	64.5	0.054
1761	10 ⁺	1.2±0.5	532	1.05±0.40	1.40	0.75	71.4	0.071
2340	12 ⁺		579				79.4	0.083
2931	14 ⁺		591				91.4	0.087
3465	16 ⁺		534				116	0.071
4021	18 ⁺		556				126	0.077
4661	(20 ⁺)		640				122	0.102
 ¹⁶² ₆₈ Er ₉₄								
102	2 ⁺		102				Johnson <i>et al.</i> , 1972; Fenzl <i>et al.</i> , 1975	
330	4 ⁺		228				58.8	0.0034
667	6 ⁺		337				61.4	0.014
1097	8 ⁺		430				65.3	0.029
1603	10 ⁺		506				70.0	0.047
2165	12 ⁺		562				75.1	0.064
2746	14 ⁺		581				81.9	0.079
3292	16 ⁺		546				92.9	0.084
3847	18 ⁺		555				114	0.075
4463	20 ⁺		616				126	0.077
							127	0.095
 ¹⁶⁴ ₆₈ Er ₉₆								
91	2 ⁺	1430±0.18	91.4	1.02±0.07	1.02	1	Yates <i>et al.</i> , 1980; Fossan and Herskind, 1963; Ben-Zvi <i>et al.</i> , 1968	0.0028
299	4 ⁺	86±8	208.1	1.39±0.14	1.48	0.94	65.6	0.011
614	6 ⁺		315.0		1.61		67.3	0.025
1025	8 ⁺	3.69±0.18	410.2	1.86±0.09	1.68	1.11	73.2	0.042
1518	10 ⁺	1.46±0.09	493.5	1.91±0.12	1.72	1.11	77.0	0.061
2083	12 ⁺	0.8±0.06	564.7	1.75±0.13	1.75	1.00	81.5	0.080
2703	14 ⁺		619.8	2.33±0.32	1.77	1.32	87.1	0.096
3263	16 ⁺		560.5	≤2.8	1.80		111	0.079
3769	18 ⁺		505.5				138	0.064
4346	(20 ⁺)		577.1				135	0.083
5000	(22 ⁺)		654.4				131	0.107
(5729)	(24 ⁺)		729.0				132	0.133
 ¹⁶⁶ ₆₈ Er ₉₈								
81	2 ⁺	1870±30	81	1.00±0.02	1.0	1	West <i>et al.</i> , 1976	0.002
265	4 ⁺	117±7	184	1.63±0.10	1.45	1.12	74.1	0.009
545	6 ⁺		280		1.58		76.0	0.026
911	8 ⁺	4.2±0.4	366	1.97±0.19	1.65	1.19	78.6	0.035
1350	10 ⁺	1.68±0.15	439	2.05±0.18	1.69	1.21	Kearns <i>et al.</i> , 1977	81.9
1847	12 ⁺	0.93±0.07	497	2.00±0.15	1.72	1.16	86.6	0.049
2390	14 ⁺		543		1.74		92.6	0.063
2969	(16 ⁺)		579		1.76		99.4	0.074
							107	0.084
 ¹⁶⁸ ₆₈ Er ₁₀₀								
80	2 ⁺	1860±20	80	1.18±0.02	1.18	1	Domingos <i>et al.</i> , 1972; Erb <i>et al.</i> , 1972	0.002
264	4 ⁺	119±7	184	1.71±0.10	1.71	1.0	75.0	0.009
549	6 ⁺		285				76.1	0.021
928	8 ⁺	3.4±0.3	380	2.0±0.2	1.95	1.03	77.2	0.036
1404	10 ⁺	1.42±0.08	469	1.74±0.10	1.98	0.88	Kearns <i>et al.</i> , 1977	81.0
							88.9	0.055

TABLE I. (Continued.)

E_x (keV)	I^π	$\tau_{1/2}$ (ps)	$E_\gamma(I \rightarrow I-2)$ (keV)	$B(E2; I \rightarrow I-2)$ ($e^2 b^2$)	$B(E2; \text{rot})^a$	$\frac{B(E2)}{B(E2)_{\text{rot}}}$	$2\mathcal{F}/\hbar^2$ ^b (MeV ⁻¹)	$\hbar^2 \omega^2$ ^c (MeV ²)
1942	12 ⁺	0.62±0.04	547	1.86±0.12	2.02	0.92	84.0	0.075
¹⁷⁰ ₆₈ Er ₁₀₂							Domingos <i>et al.</i> , 1972	
79	2 ⁺	1880±50	79	1.04±0.03	1.04	1	75.7	0.002
261	4 ⁺		182				77.3	0.009
540	6 ⁺		279				78.9	0.019
							Kearns <i>et al.</i> , 1977	
913	8 ⁺	3.6±0.3	373	2.1±0.2	1.72	1.22	80.4	0.035
1374	10 ⁺	1.48±0.10	461	1.83±0.12	1.75	1.05	82.4	0.053
1916	12 ⁺	0.57±0.04	542	2.11±0.15	1.76	1.20	84.9	0.073
¹⁶⁰ ₇₀ Yb ₉₀							Riediner <i>et al.</i> , 1980;	
							Bochev <i>et al.</i> , 1976;	
							Beck <i>et al.</i> , 1979;	
							Johnson, 1982	
243	2 ⁺	114±6	243	0.50±0.03	0.50	1	24.7	0.019
639	4 ⁺	8.1±0.4	396	0.69±0.04	0.72	0.96	35.4	0.042
1148	6 ⁺	1.9±0.2	509	0.86±0.09	0.79	1.19	43.2	0.065
1738	8 ⁺	0.9±0.2	590	0.9±0.2	0.83	1.18	50.8	0.088
2375	10 ⁺	0.6±0.3	637	0.9±0.5	0.85	1.18	59.6	0.101
2962	12 ⁺		587		0.86		78.4	0.086
3366	14 ⁺	7.6±0.7	404	0.70±0.07	0.87	0.80	134	0.041
3850	16 ⁺	1.9±0.2	484	1.07±0.11	0.88	1.22	128	0.058
4429	18 ⁺	2.1±0.2	579	0.41±0.04	0.89	0.46	121	0.089
5092	20 ⁺	1.2±0.2	663	0.37±0.04	0.89	0.42	118	0.109
5829	22 ⁺	0.69±0.14	737	0.29±0.5	0.89	0.32	117	0.136
6625	24 ⁺		796				118	0.158
7461	26 ⁺		836				122	0.175
8292	28 ⁺		831				132	0.173
9129	30 ⁺		837				141	0.175
10007	32 ⁺		878				144	0.193
10960	(34 ⁺)		953				141	0.227
¹⁶² ₇₀ Yb ₉₂							Riedinger <i>et al.</i> , 1980;	
							Bochev <i>et al.</i> , 1976	
166	2 ⁺	400±60	166	0.73±0.11	0.73	1	35.9	0.009
487	4 ⁺	14±2	321	1.12±0.17	1.05	1.07	43.8	0.027
923	6 ⁺	3.2±0.6	436	1.1±0.2	1.15	0.96	50.5	0.048
1445	8 ⁺	1.4±0.5	522	1.0±0.4	1.21	0.83	57.6	0.068
2023	10 ⁺		578				65.7	0.083
2634	12 ⁺		611				75.2	0.093
3256	14 ⁺		623				86.7	0.097
3877	16 ⁺		621				99.8	0.096
4493	18 ⁺		616				114	0.095
5146	20 ⁺		653				119	0.107
5863	(22 ⁺)		717				120	0.129
¹⁶⁴ ₇₀ Yb ₉₄							Lieder <i>et al.</i> , 1972;	
							Davidson <i>et al.</i> , 1972;	
							Bochev <i>et al.</i> , 1976	
123	2 ⁺	880±40	123	0.92±0.04	0.92	1	48.8	0.005
386	4 ⁺	30±11	263	1.36±0.05	1.31	1.04	53.2	0.018
761	6 ⁺	5.0±0.2	375	1.46±0.05	1.44	1.01	58.7	0.035
1224	8 ⁺	1.5±0.5	463	1.7±0.5	1.51	1.13	64.8	0.054
1754	10 ⁺	0.8±0.3	530	1.6±0.5	1.55	1.03	71.7	0.070
2331	12 ⁺	0.6±0.2	577	1.6±0.6	1.58	1.01	79.7	0.083
2901	14 ⁺	0.7±0.2	570	1.3±0.4	1.60	0.81	94.7	0.081
3391	16 ⁺	1.8±0.4	490	1.1±0.2	1.62	0.68	126	0.060

TABLE I. (Continued.)

E_x (keV)	I^π	$\tau_{1/2}$ (ps)	$E_\gamma(I \rightarrow I-2)$ (keV)	$B(E2; I \rightarrow I-2)$ ($e^2 b^2$)	$B(E2; \text{rot})^a$	$\frac{B(E2)}{B(E2)_{\text{rot}}}$	$2\mathcal{F}/\hbar^2 b$ (MeV $^{-1}$)	$\hbar^2 \omega^2 c$ (MeV 2)
3934	18 $^+$	0.7 \pm 0.4	543	1.6 \pm 0.7	1.63	0.98	129	0.074
4566	20 $^+$		632				123	0.100
5279	22 $^+$		713				121	0.127
$^{166}_{70}\text{Yb}_{96}$								
102	2 $^+$	1240 \pm 60	102	1.05 \pm 0.05	1.05	1	58.8	0.003
330	4 $^+$	53 \pm 17	228	1.47 \pm 0.05	1.50	0.98	61.4	0.014
668	6 $^+$	7.9 \pm 0.3	338	1.56 \pm 0.06	1.65	0.95	65.0	0.029
1098	8 $^+$	2.1 \pm 0.2	430	1.7 \pm 0.2	1.73	0.98	69.8	0.046
1606	10 $^+$	1.0 \pm 0.5	508	1.6 \pm 0.8	1.78	0.90	74.8	0.065
2176	12 $^+$	0.6 \pm 0.3	570	1.4 \pm 0.7	1.81	0.77	80.7	0.081
2779	14 $^+$	0.5 \pm 0.3	603	1.4 \pm 0.8	1.83	0.77	89.6	0.091
3274	16 $^+$	1.1 \pm 0.3	495	1.6 \pm 0.4	1.85	0.86	125	0.061
3783	18 $^+$		509				138	0.065
4372	20 $^+$		589				132	0.087
5038	22 $^+$		666				130	0.111
5777	24 $^+$		739				127	0.137
$^{168}_{70}\text{Yb}_{98}$								
88	2 $^+$	1550 \pm 70	88	1.26 \pm 0.06			Johnson <i>et al.</i> , 1972;	
287	4 $^+$		199				Dracoulis <i>et al.</i> , 1977	
585	5 $^+$		298				68.4	0.0026
970	8 $^+$		385				70.4	0.010
1425	10 $^+$		455				73.6	0.022
1936	12 $^+$		511				78.0	0.037
2489	14 $^+$		553				83.4	0.052
3073	16 $^+$		584				90.1	0.065
3687	18 $^+$		614				97.7	0.076
4337	20 $^+$		650				106	0.085
							114	0.094
							120	0.106
$^{170}_{70}\text{Yb}_{100}$								
84	2 $^+$	1600 \pm 20	84	1.12 \pm 0.14	1.12	1	Saethre <i>et al.</i> , 1973	
278	4 $^+$		194				71.2	0.0023
573	6 $^+$		295				72.4	0.010
							74.4	0.022
963	8 $^+$	3.0 \pm 0.3	390	2.0 \pm 0.2	1.85	1.08	Kearns <i>et al.</i> , 1977	
1437	10 $^+$	1.16 \pm 0.08	474	2.00 \pm 0.14	1.89	1.06	77.0	0.038
1983	12 $^+$	0.77 \pm 0.07	546	1.51 \pm 0.15	1.93	0.78	80.2	0.056
2580	14 $^+$		597				84.3	0.074
3196	16 $^+$		616				90.4	0.089
3808	18 $^+$		612				101	0.095
							114	0.094
$^{172}_{70}\text{Yb}_{102}$								
79	2 $^+$	1680 \pm 60	79	1.16 \pm 0.04	1.16	1	Sayer <i>et al.</i> , 1970	
260	4 $^+$	115 \pm 80	181	1.8 \pm 1.3	1.68	1.07	76.2	0.002
540	6 $^+$	17.1 \pm 0.9	280	1.76 \pm 0.09	1.83	0.96	77.1	0.009
							78.6	0.020
912	8 $^+$	3.5 \pm 0.3	372	2.18 \pm 0.19	1.91	1.14	Kearns <i>et al.</i> , 1977	
1370	10 $^+$	1.32 \pm 0.08	458	2.08 \pm 0.13	1.96	1.06	80.8	0.034
1896	12 $^+$	0.52 \pm 0.07	526	2.6 \pm 0.4	2.00	1.3	82.9	0.052
							85.5	0.072
$^{174}_{70}\text{Yb}_{104}$								
76	2 $^+$	1740 \pm 90	76	1.18 \pm 0.07	1.18	1	Funk <i>et al.</i> , 1966;	
							Sayer <i>et al.</i> , 1970;	
							Ward <i>et al.</i> , 1976	
							78.9	0.002

TABLE I. (Continued.)

E_x (keV)	I^π	$\tau_{1/2}$ (ps)	$E_\gamma(I \rightarrow I-2)$ (keV)	$B(E2; I \rightarrow I-2)$ ($e^2 b^2$)	$B(E2; \text{rot})^a$	$\frac{B(E2)}{B(E2)_{\text{rot}}}$	$2\mathcal{F}/\hbar^2 b$ (MeV ⁻¹)	$\hbar^2 \omega^{2c}$ (MeV ²)
253	4 ⁺	135±20	177	1.68±0.12	1.71	0.98	79.1	0.008
526	6 ⁺	14±4	273	2.4±0.3	1.9	1.26	80.6	0.019
889	8 ⁺	3.6±0.5	363	2.3±0.2	2.0	1.15	82.6	0.033
1337	10 ⁺	1.52±0.14	448	2.10±0.10	2.0	1.05	84.8	0.050
1862	12 ⁺	0.66±0.07	525	2.20±0.12	2.1	1.05	87.6	0.069
2458	14 ⁺	0.42±0.10	596	1.8±0.2	2.1	0.86	90.6	0.089
3118	16 ⁺		660				93.9	0.109
3837	18 ⁺		719				97.4	0.129
4611	20 ⁺		774				101	0.150
¹⁷⁶ Yb ₁₀₆								
							Sayer <i>et al.</i> , 1970;	
							Ward <i>et al.</i> , 1976;	
							Tippie and Scharenberg, 1966	
82	2 ⁺	1760±50	82	1.06±0.02	1.06	1	73.1	0.002
272	4 ⁺	110±10	189	1.57±0.08	1.54	1.02	74.1	0.009
565	6 ⁺	13±4	293	1.9±0.3	1.7	1.12	75.1	0.021
954	8 ⁺	3.1±0.5	389	2.00±0.16	1.8	1.11	77.1	0.038
1431	10 ⁺	1.20±0.10	477	1.91±0.08	1.8	1.01	79.7	0.057
1985	12 ⁺	0.59±0.06	554	1.84±0.10	1.9	0.97	83.0	0.077
2602	14 ⁺	0.38±0.07	617	1.66±0.15	1.9	0.87	87.5	0.095
3270	16 ⁺		668				92.8	0.112
3979	18 ⁺		709				98.7	0.126
¹⁶⁴ Hf ₉₂								
							Riedinger, 1981	
211	2 ⁺		211				28.4	0.015
588	4 ⁺		377				37.1	0.038
1086	6 ⁺		498				44.2	0.062
1670	8 ⁺		584				51.4	0.085
2306	10 ⁺		636				59.7	0.101
2874	12 ⁺		568				81.0	0.080
3213	14 ⁺		339				159	0.028
3681	16 ⁺		468				132	0.055
4265	18 ⁺		584				120	0.085
4941	20 ⁺		676				115	0.114
5702	22 ⁺		761				113	0.145
6548	24 ⁺		846				111	0.178
7465	26 ⁺		917				111	0.210
¹⁶⁶ Hf ₉₄								
							Bochev <i>et al.</i> , 1977	
159	2 ⁺	497±30	159	0.70±0.03	0.7	1	37.7	0.008
470	4 ⁺	16.8±1.0	311	1.06±0.07	1.00	1.06	45.0	0.026
897	6 ⁺	3.5±0.5	427	1.09±0.15	1.10	0.99	51.5	0.046
1406	8 ⁺	1.2±0.5	509	1.3±0.5	1.15	1.12	58.9	0.066
1970	10 ⁺	0.7±0.5	564	1.5±1.1	1.19	1.25	67.3	0.079
2564	12 ⁺	0.9±0.7	594	0.8±0.7	1.21	0.70	77.4	0.088
3177	(14 ⁺)		613				88.1	0.094
¹⁶⁸ Hf ₉₆								
							Bochev <i>et al.</i> , 1977;	
							Janssens <i>et al.</i> , 1981	
124	2 ⁺	890±40	124	0.84±0.04	0.84	1	48.5	0.005
386	4 ⁺	36±4	262	1.15±0.12	1.20	0.96	53.5	0.018
757	6 ⁺	5.9±0.6	371	1.30±0.13	1.32	0.99	59.3	0.034
1214	8 ⁺	1.98±0.19	457	1.40±0.13	1.38	1.01	65.7	0.052
1736	10 ⁺	1.00±0.15	522	1.4±0.2	1.42	1.00	72.8	0.068
2306	12 ⁺	0.51±0.18	570	1.8±0.6	1.44	1.23	80.7	0.081
2858	14 ⁺	0.84±0.18	552	1.3±0.3	1.46	0.89	97.7	0.076
3311	16 ⁺	1.8±0.2	453	1.60±0.18	1.47	1.09	137	0.051

TABLE I. (Continued.)

E_x (keV)	I^π	$\tau_{1/2}$ (ps)	$E_\gamma(I \rightarrow I-2)$ (keV)	$B(E2;I \rightarrow I-2)$ ($e^2 b^2$)	$B(E2;\text{rot})^a$	$\frac{B(E2)}{B(E2)_{\text{rot}}}$	$2\mathcal{F}/\hbar^2 b$ (MeV $^{-1}$)	$\hbar^2 \omega^2 c$ (MeV 2)
3833	18 $^+$		522				134	0.068
4440	20 $^+$		607				128	0.092
5125	22 $^+$		685				126	0.118
5875	24 $^+$		750				125	0.141
6687	26 $^+$		812				126	0.165
7560	(28 $^+$)		873				126	0.191
$^{170}_{72}\text{Hf}_{98}$								
100	2 $^+$	1230 \pm 30	100	1.0 \pm 0.2	1.0	1	59.8	0.003
321	4 $^+$	62 \pm 7	221	1.43 \pm 0.15	1.45	0.98	63.4	0.013
642	6 $^+$	10.8 \pm 0.9	321	1.43 \pm 0.12	1.58	0.89	68.7	0.026
1042	8 $^+$	3.2 \pm 0.3	400	1.68 \pm 0.16	1.65	1.00	75.0	0.040
1504	10 $^+$	1.52 \pm 0.19	462	1.7 \pm 0.2	1.69	1.00	82.3	0.053
2015	12 $^+$	1.00 \pm 0.10	511	1.6 \pm 0.2	1.72	0.90	90.0	0.065
2565	14 $^+$	0.66 \pm 0.15	551	1.7 \pm 0.4	1.74	0.94	98.1	0.076
3150	16 $^+$	\sim 0.45	585	\sim 1.8	1.76	\sim 1.0	106	0.085
3765	18 $^+$	\sim 0.35	615	\sim 1.8	1.77	\sim 1.0	114	0.094
4420	20 $^+$	\sim 0.25	655	\sim 2.0	1.78	\sim 1.1	119	0.107
Lisle <i>et al.</i> , 1981								
5130	22 $^+$		710				121	0.126
5902	24 $^+$		772				122	0.149
6739	26 $^+$		837				122	0.175
$^{172}_{72}\text{Hf}_{100}$								
Skaali <i>et al.</i> , 1975; Walker <i>et al.</i> , 1980								
95	2 $^+$	1550 \pm 100	95	0.82 \pm 0.05			63.1	0.003
309	4 $^+$		214				65.4	0.012
628	6 $^+$		319				69.0	0.025
1037	8 $^+$		409				73.4	0.042
1521	10 $^+$		484				78.6	0.058
2065	12 $^+$		544				84.7	0.074
2654	14 $^+$		589				91.6	0.087
3276	16 $^+$		622				99.5	0.097
3918	18 $^+$		642				109	0.103
4575	20 $^+$		657				119	0.107
5273	22 $^+$		698				123	0.121
$^{174}_{72}\text{Hf}_{102}$								
Jett and Lind, 1970								
91	2 $^+$		91				65.9	0.003
297	4 $^+$		206				67.8	0.011
608	6 $^+$		311				70.8	0.024
1009	8 $^+$		401				74.8	0.040
1486	10 $^+$		477				79.8	0.057
2020	12 $^+$		534				86.0	0.071
2597	14 $^+$		577				93.7	0.083
$^{176}_{72}\text{Hf}_{104}$								
Saethre <i>et al.</i> , 1973								
88	2 $^+$	1390 \pm 40	88	1.09 \pm 0.03			67.9	0.0025
290	4 $^+$		202				69.4	0.011
597	6 $^+$		307				71.7	0.023
998	8 $^+$		401				74.8	0.040
1481	10 $^+$		483				78.6	0.058
2035	12 $^+$		554				83.1	0.077
Khoo <i>et al.</i> , 1976								
2647	14 $^+$		612				88.3	0.094
3308	16 $^+$		661				93.7	0.109
4010	18 $^+$		702				99.7	0.123

TABLE I. (Continued.)

E_x (keV)	I^π	$\tau_{1/2}$ (ps)	$E_\gamma(I \rightarrow I-2)$ (keV)	$B(E2; I \rightarrow I-2)$ ($e^2 b^2$)	$B(E2; \text{rot})^a$	$\frac{B(E2)}{B(E2)_{\text{rot}}}$	$2\mathcal{F}/\hbar^2 b^2$ (MeV $^{-1}$)	$\hbar^2 \omega^2 c$ (MeV 2)
Khoo and Løvhøiden, 1977								
$^{178}_{72}\text{Hf}_{106}$							64.4	0.0029
93	2 $^+$	1460 \pm 30	93	0.97 \pm 0.02			65.6	0.012
307	4 $^+$		214				67.6	0.026
632	4 $^+$		325				70.4	0.045
1059	8 $^+$		427				74.2	0.066
1571	10 $^+$		512				79.3	0.084
2151	12 $^+$		580				86.1	0.098
2778	14 $^+$		627					
Gujrathi and Dania, 1971								
$^{180}_{72}\text{Hf}_{108}$							64.3	0.003
93	2 $^+$	1520 \pm 20	93	0.93 \pm 0.02	0.93	1	65.0	0.012
309	4 $^+$	57 \pm 10	216	1.4 \pm 0.2	1.35	1.04	66.2	0.028
641	6 $^+$		332				67.7	0.049
1084	8 $^+$		443					
Walker <i>et al.</i> , 1976; Michel <i>et al.</i> , 1980								
$^{170}_{74}\text{W}_{96}$							38.3	0.008
157	2 $^+$	497 \pm 10	157	0.700 \pm 0.014	0.70	1	45.8	0.025
462	4 $^+$	21.0 \pm 1.4	305	0.93 \pm 0.06	1.00	0.93	53.3	0.043
875	6 $^+$	4.5 \pm 0.4	413	1.00 \pm 0.08	1.10	0.91	61.5	0.059
1363	8 $^+$		488				70.6	0.072
1901	10 $^+$		538				81.8	0.079
2464	12 $^+$		563				125	0.047
2897	14 $^+$		433				139	0.050
3343	16 $^+$		446				132	0.070
3873	18 $^+$		530				127	0.095
4489	20 $^+$		616				125	0.117
5175	22 $^+$		686					
Walker <i>et al.</i> , 1976								
$^{172}_{74}\text{W}_{98}$							48.8	0.003
123	2 $^+$		123				55.1	0.017
377	4 $^+$		254				62.8	0.031
727	6 $^+$		350				71.6	0.044
1146	8 $^+$		419				80.9	0.055
1616	10 $^+$		470				89.8	0.066
2129	12 $^+$		513				98.5	0.075
2677	14 $^+$		548				108	0.083
3254	16 $^+$		577				117	0.089
3852	18 $^+$		598				120	0.104
4497	20 $^+$		645					
Walker <i>et al.</i> , 1976								
$^{174}_{74}\text{W}_{100}$							53.6	0.004
112	2 $^+$		113				57.6	0.016
355	4 $^+$		243				63.0	0.030
704	6 $^+$		349				69.4	0.047
1137	8 $^+$		433				76.3	0.062
1635	10 $^+$		498				83.5	0.076
2186	12 $^+$		551				90.9	0.088
2780	14 $^+$		594				101	0.093
3392	16 $^+$		612				120	0.084
3973	18 $^+$		581				124	0.099
4602	20 $^+$		629				121	0.126
5311	(22 $^+$)		709					
Walker <i>et al.</i> , 1976								
$^{176}_{74}\text{W}_{102}$							55.2	0.004
109	2 $^+$		109				58.4	0.015
349	4 $^+$		240				62.7	0.031
699	6 $^+$		350					

TABLE I. (Continued.)

E_x (keV)	I^π	$\tau_{1/2}$ (ps)	$E_\gamma(I \rightarrow I-2)$ (keV)	$B(E2; I \rightarrow I-2)$ ($e^2 b^2$)	$B(E2; \text{rot})^a$ ($e^2 b^2$)	$\frac{B(E2)}{B(E2)_{\text{rot}}}$	$2\mathcal{F}/\hbar^2 b$ (MeV $^{-1}$)	$\hbar^2 \omega^2 c$ (MeV 2)
1140	8 $^+$		441				68.1	0.048
1640	10 $^+$		508				74.8	0.065
2206	12 $^+$		558				82.5	0.078
2802	14 $^+$		596				90.7	0.089
3427	16 $^+$		625				99.3	0.097
4002	18 $^+$		575				122	0.083
 $^{178}_{74}\text{W}_{104}$								
106	2 $^+$		106				56.5	0.004
343	4 $^+$		237				59.1	0.014
695	6 $^+$		352				62.6	0.031
1142	8 $^+$		447				67.1	0.050
1666	10 $^+$		524				72.5	0.069
2245	12 $^+$		579				79.4	0.084
2859	14 $^+$		614				87.9	0.094
3489	16 $^+$		630				98.4	0.099
4102	18 $^+$		613				114	0.094
 $^{180}_{74}\text{W}_{106}$								
103	2 $^+$	1220 \pm 30	103	0.89 \pm 0.02			Bernthal <i>et al.</i> , 1976	
337	4 $^+$		234				59.8	0.015
688	6 $^+$		351				62.7	0.031
1138	8 $^+$		450				66.7	0.051
1664	10 $^+$		526				72.2	0.069
2236	12 $^+$		572				80.5	0.082
2825	14 $^+$		589				91.7	0.087
3416	16 $^+$		591				105	0.087
4021	18 $^+$		605				116	0.092
 $^{182}_{74}\text{W}_{108}$								
100	2 $^+$	1380 \pm 20	100	0.91 \pm 0.02	0.91	1	Bernthal <i>et al.</i> , 1976;	
329	4 $^+$	64 \pm 5	229	1.17 \pm 0.09	1.31	0.89	Milner <i>et al.</i> , 1971	
680	6 $^+$	8.7 \pm 0.9	351	1.20 \pm 0.13	1.44	0.83	59.9	0.003
1144	8 $^+$		464				61.1	0.014
1712	10 $^+$		568				62.7	0.031
2373	12 $^+$		661				64.7	0.054
(3113)	(14 $^+$)		(740)				67.0	0.080
							69.6	0.109
							72.9	0.137
 $^{172}_{76}\text{Os}_{96}$								
228	2 $^+$		228				Durell <i>et al.</i> , 1982	
607	4 $^+$		379				26.3	0.017
1056	6 $^+$		449				36.9	0.038
1527	8 $^+$		471				49.0	0.051
2027	10 $^+$		500				63.7	0.055
2568	12 $^+$		541				76.0	0.063
3105	14 $^+$		537				85.0	0.073
3593	16 $^+$		488				101	0.072
4181	18 $^+$		588				127	0.060
4837	20 $^+$		656				119	0.086
5533	(22 $^+$)		696				119	0.108
6259	(24 $^+$)		726				124	0.121
							129	0.132
 $^{174}_{76}\text{Os}_{98}$								
159	2 $^+$		159				Durell <i>et al.</i> , 1982	
435	4 $^+$		276				37.8	0.0083
							50.7	0.020

TABLE I. (Continued.)

E_x (keV)	I^π	$\tau_{1/2}$ (ps)	$E_\gamma(I \rightarrow I-2)$ (keV)	$B(E2; I \rightarrow I-2)$ ($e^2 b^2$)	$B(E2; \text{rot})^a$	$\frac{B(E2)}{B(E2)_{\text{rot}}}$	$2\mathcal{F}/\hbar^2$ ^b (MeV ⁻¹)	$\hbar^2 \omega^2$ ^c (MeV ²)
778	6 ⁺		343			64.1	0.030	
1173	8 ⁺		395			75.9	0.039	
1619	10 ⁺		446			85.2	0.050	
2115	12 ⁺		496			92.7	0.062	
2658	14 ⁺		543			99.4	0.074	
3242	16 ⁺		584			106	0.085	
3864	18 ⁺		622			113	0.097	
4527	20 ⁺		663			118	0.110	
5236	22 ⁺		708			121	0.125	
5989	(24 ⁺)		754			125	0.142	
6788	(26 ⁺)		799			128	0.160	
$^{176}_{76}\text{Os}_{100}$								
135	2 ⁺		135			44.4	0.0060	
395	4 ⁺		260			53.8	0.018	
742	6 ⁺		347			63.4	0.031	
1157	8 ⁺		415			72.2	0.044	
1633	10 ⁺		476			79.8	0.057	
2167	12 ⁺		534			86.1	0.071	
2754	14 ⁺		587			92.0	0.086	
3381	16 ⁺		627			102	0.098	
4018	18 ⁺		637			110	0.101	
4682	20 ⁺		664			117	0.110	
5396	22 ⁺		714			120	0.127	
6144	(24 ⁺)		748			126	0.140	
$^{178}_{76}\text{Os}_{102}$								
132	2 ⁺		132			45.5	0.0057	
398	4 ⁺		266			52.6	0.019	
761	6 ⁺		363			60.6	0.033	
1193	8 ⁺		432			69.4	0.047	
1682	10 ⁺		488			77.9	0.060	
2219	12 ⁺		538			85.5	0.072	
2804	14 ⁺		585			92.3	0.086	
3429	16 ⁺		625			99.2	0.098	
4020	18 ⁺		591			118	0.087	
4663	20 ⁺		643			121	0.103	
5382	22 ⁺		719			120	0.129	
6154	24 ⁺		772			122	0.149	
$^{180}_{76}\text{Os}_{104}$								
132	2 ⁺		132			45.5	0.0057	
409	4 ⁺		277			50.5	0.020	
796	6 ⁺		387			56.8	0.038	
1258	8 ⁺		462			64.8	0.054	
1768	10 ⁺		510			74.4	0.065	
2309	12 ⁺		541			85.0	0.073	
2875	14 ⁺		566			95.4	0.080	
Neskakis <i>et al.</i> , 1982								
3495	16 ⁺		620			100	0.096	
4135	18 ⁺		640			109	0.102	
4822	20 ⁺		687			113	0.118	
5552	22 ⁺		730			118	0.133	
6326	(24 ⁺)		774			121	0.150	
7096	(26 ⁺)		770			132	0.148	
7823	(28 ⁺)		727			151	0.132	
8556	(30 ⁺)		733			161	0.134	
(9382)	(32 ⁺)		(826)			(152)	(0.170)	

TABLE I. (Continued.)

E_x (keV)	I^π	$\tau_{1/2}$ (ps)	$E_\gamma(I \rightarrow I-2)$ (keV)	$B(E2; I \rightarrow I-2)$ ($e^2 b^2$)	$B(E2; \text{rot})^a$	$\frac{B(E2)}{B(E2)_{\text{rot}}}$	$2\mathcal{F}/\hbar^2 b$ (MeV $^{-1}$)	$\hbar^2 \omega^2 c$ (MeV 2)
$^{182}_{76}\text{Os}_{106}$								
127	2 $^+$	813 ± 11	127	0.810 ± 0.10			47.2	0.0053
400	4 $^+$		273				51.2	0.020
793	6 $^+$		393				55.9	0.039
1277	8 $^+$		484				62.0	0.059
1811	0 $^+$		534				71.2	0.071
2345	2 $^+$		534				86.1	0.071
2839	4 $^+$		494				109	0.061
3318	16 $^+$		479				129	0.057
3855	18 $^+$		537				130	0.072
4478	20 $^+$		623				125	0.096
5189	22 $^+$		711				121	0.126
5984	24 $^+$		795				118	0.158
$^{184}_{76}\text{Os}_{108}$								
120	2 $^+$	1184 ± 13	120	0.640 ± 0.010	0.64	1	50.0	0.005
384	4 $^+$	46 ± 13	264	0.9 ± 0.2	0.93	0.97	53.0	0.018
774	6 $^+$		390				56.4	0.038
1275	8 $^+$		501				59.9	0.063
1870	10 $^+$		595				63.9	0.088
2546	12 $^+$		676				68.0	0.114
3259	14 $^+$		713				75.7	0.127
3787	16 $^+$		528				117	0.070
4342	18 $^+$		555				126	0.076
4998	20 $^+$		656				119	0.107
5738	22 $^+$		740				116	0.137
$^{186}_{76}\text{Os}_{110}$								
137	2 $^+$	820 ± 30	137	0.62 ± 0.02	0.62	1	43.8	0.006
434	4 $^+$	24	297	1.0	0.90	1.11	47.2	0.023
869	6 $^+$	3.1	435	1.17	0.94	1.24	50.6	0.047
1421	8 $^+$		552				54.4	0.076
2069	10 $^+$		648				58.7	0.105
2782	12 $^+$		713				64.5	0.127
3440	14 $^+$		658				82.0	0.108
3934	16 $^+$		494				125	0.061
(4494)	(18 $^+$)		(560)				125	0.078

$$^a B(E2; \text{rot}) = \frac{\langle I020 | (I-2)0 \rangle^2}{\langle 2020 | 00 \rangle^2} B^{\text{expt}}(E2; 2 \rightarrow 0) = 5 \langle I020 | (I-2)0 \rangle^2 B^{\text{expt}}(E2; 2 \rightarrow 0).$$

$$^b \frac{2\mathcal{F}}{\hbar^2} = \frac{4I-2}{E_\gamma}.$$

$$^c \hbar^2 \omega^2 = \frac{I^2 - I + 1}{(2I-1)^2} E_\gamma^2 \quad (\approx \frac{1}{4} E_\gamma^2 \text{ for } I > 6).$$

The corresponding picture is based on the Hartree-Fock-Bogolyubov method (Ring *et al.*, 1969; Banerjee *et al.*, 1973; Bhargava, 1973; Bhargava and Thouless, 1973; Goodman, 1974, 1976; Faessler *et al.*, 1976; Hamamoto, 1976; Bengtsson and Frauendorf, 1977; Cwiok *et al.*, 1980).

Below, we shall briefly outline an analysis of the collective rotational bands at high angular momenta in terms of independent quasiparticles (for the description of other approaches see Sec. III.A.6), as suggested by Bohr and Mottelson (1977), as well as by Bengtsson and Frauendorf (1979a, 1979b) (see also Bengtsson and Frauendorf, 1981;

Faessler *et al.*, 1981; Cwiok *et al.*, 1980). The procedure consists of calculating the nuclear quantities for fixed angular momentum using solutions of the cranking Hamiltonian [cf. Eq. (2.8) in Sec. II]. However, as already discussed in Sec. II, the single-quasiparticle solutions do not specify the energies but rather the single-quasiparticle Routhians (i.e., energies in a rotating frame). Instead of calculating the true energies $\mathcal{E}(I)$ and comparing them with experiments, Bohr and Mottelson (1977) and Bengtsson and Frauendorf (1977, 1979a, 1979b) suggest a different procedure. The experimental data are first transformed to the rotating frame of reference (i.e., the

"experimental" Routhians are determined from data on true energies) and then compared with the results of the calculation. The advantage of this formulation lies in the possibility of a direct test for the calculated independent quasiparticle diagrams (i.e., individual quasiparticle Routhians plotted versus angular velocity ω). In order to achieve this goal one employs the relation for the Routhians of a nucleus [cf. Eq. (2.13)]

$$\mathcal{E}^\omega(I) = \mathcal{E}(I) - \hbar\omega(I)I_x(I). \quad (3.6)$$

Remembering that the rotational frequency of a nucleus, $\omega = \omega(I)$ can be defined according to Eq. (3.1) only in terms of differences in discrete points, we realize that

$$\hbar\omega(I) = \frac{\mathcal{E}(I+1) - \mathcal{E}(I-1)}{I_x(I+1) - I_x(I-1)}, \quad (3.7)$$

which reflects the discrete nature of angular momentum I . We can rewrite Eq. (3.6) in the form

$$\mathcal{E}_{\text{expt}}^\omega(I) = \frac{1}{2}\{\mathcal{E}(I+1) + \mathcal{E}(I-1)\} - \hbar\omega(I)I_x(I). \quad (3.8)$$

In the last relation we approximated the energy \mathcal{E} of Eq. (3.6) by the average between the neighboring experimental values; we also added the subscript "expt" to stress the fact that all the quantities entering (3.8) are deduced from experimental data.

In the analysis by means of the independent quasiparticles we are not interested in the absolute energies or

Routhians but rather in the excitation spectra—i.e., in the differences between the actual total physical quantities and the reference ones. The latter quantities are defined properly so as to characterize a selected rotational band, usually the ground band. For the ground band it is convenient to introduce the kinematical moment of inertia $\mathcal{F}_{\text{ref}}^{(1)}$. The corresponding expression is usually assumed to be linear in ω^2 :

$$\mathcal{F}_{\text{ref}}^{(1)} = \mathcal{F}_0^{(1)} + \mathcal{F}_2^{(1)}\omega^2, \quad (3.9)$$

which makes it equivalent to the VMI model (variable moment of inertia model) [i.e., the two-parameter Harris formula—cf. Harris (1965), Mariscotti *et al.* (1969)]. Here the constants $\mathcal{F}_0^{(1)}$ and $\mathcal{F}_2^{(1)}$ have to be adjusted for each nucleus separately. The corresponding angular momentum is given by

$$I_{\text{ref}}(\omega) = (\mathcal{F}_0^{(1)} + \mathcal{F}_2^{(1)}\omega^2)\omega/\hbar \quad (3.10)$$

[angular momentum I equals $\mathcal{F}^{(1)}\omega/\hbar$; cf. Eq. (3.3)]. Any contribution to the total spin $I(\omega)$ of the nucleus possibly originating from the nucleon that aligned its angular momentum with the axis of rotation will manifest itself by a deviation from the smooth increase described by Eq. (3.10). The value of I_{ref} can then be used as the reference quantity in Eq. (3.5). Figure 15 gives examples of the aligned angular momenta $i(\omega)$ for various bands in some even- and odd- A isotopes of Yb ($^{160,161}\text{Yb}$) following

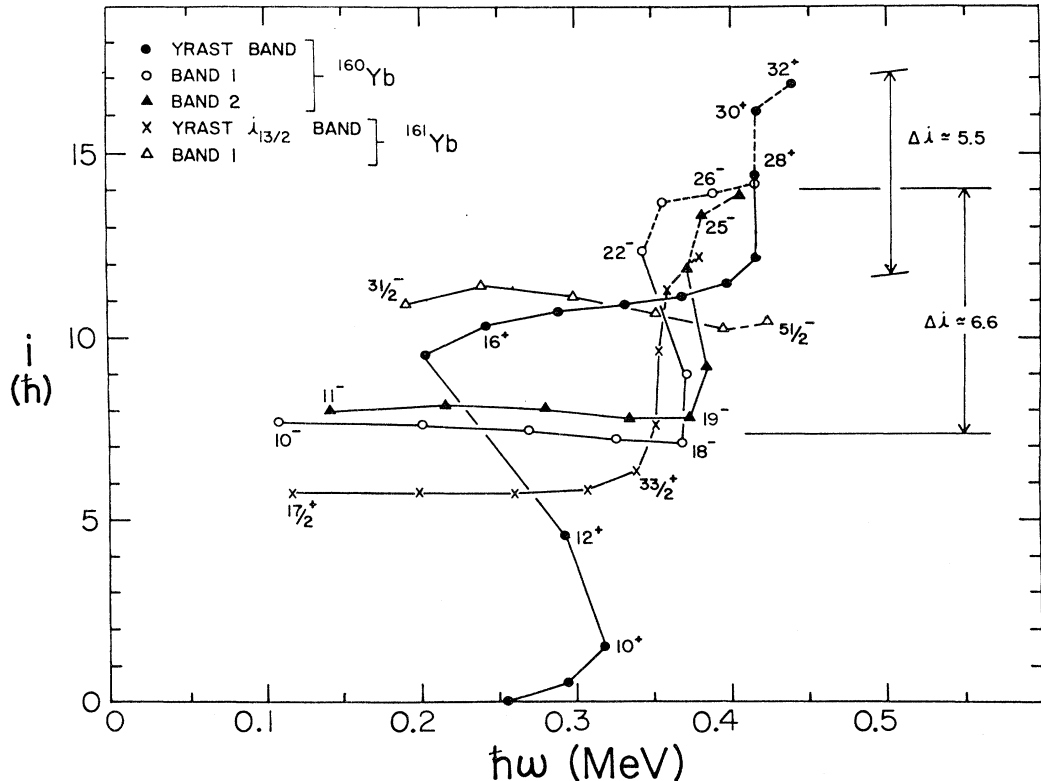


FIG. 15. Plot of the aligned angular momentum vs rotational frequency for the various bands in $^{160,161}\text{Yb}$. For the band labels see notation of Fig. 13. The various crossing frequencies (where the curves show an up- or backbend) and the gains in aligned angular momentum Δi are discussed in the text (Sec. III.A.3). The figure is from Riedinger (1980) and Gaardhøye *et al.*, (1980).

directly from experiment.

In analogy with the aligned angular momentum $i(\omega)$ [cf. Eq. (3.5)] we can now introduce the relative energy $E^*(I)$ as the difference between the total Routhian $\mathcal{E}_{\text{expt}}(I)$ and the reference quantity $\mathcal{E}_{\text{ref}}^\omega$

$$E^*(I) = \mathcal{E}_{\text{expt}}^\omega(I) - \mathcal{E}_{\text{ref}}^\omega(I). \quad (3.11)$$

Here the latter quantity can be calculated as [cf. Eqs. (3.8) and (3.10)]

$$\begin{aligned} \mathcal{E}_{\text{ref}}^\omega &= -\hbar \int I_{\text{ref}}(\omega) d\omega = - \int \omega \mathcal{F}^{(1)}(\omega) d\omega \\ &= -\frac{1}{2} \mathcal{F}_0 \omega^2 - \frac{1}{4} \mathcal{F}_2^{(1)} \omega^4 + \hbar^2 / (8 \mathcal{F}_0^{(1)}), \end{aligned} \quad (3.12)$$

where the constant $\hbar^2 / (8 \mathcal{F}_0^{(1)})$ has been added to assure approximately vanishing $\mathcal{E}_{\text{ref}}^\omega(0)$ at $I=0$ (cf. Bengtsson and Frauendorf, 1979a, 1979b). The derivation of Eq. (3.12) is based on the fact that the derivative of the Routhian with respect to ω is simply proportional to the angular momentum with negative sign [cf. Eq. (2.34)]. In the even-even nucleus the quantity $E^*(I)$ determined by Eq. (3.11) is close to zero in the region of $\omega < \omega^*$ (with ω^* denoting the angular velocity at the band crossing). For $\omega > \omega^*$, $E^*(I)$ corresponds to the excitation of two quasiparticles.

In odd-mass nuclei relation (3.11) has to be modified. For the odd- N (odd- Z) nuclear system the lowest excitation energy of neutrons (protons) is given by a one-quasiparticle excitation, and thus $E^*(I)$ in this case can be interpreted as the experimental quasiparticle Routhian (for an odd- A nucleus). The quantity $\mathcal{E}_{\text{ref}}^\omega(I)$ is usually approximated by an arithmetical average between the analogous quantities corresponding to two neighboring even-even nuclei. Hence

$$\begin{aligned} E^*(I) &= \mathcal{E}_{\text{expt, odd } A}^\omega(I) \\ &- \frac{1}{2} (\mathcal{E}_{\text{ref}, A-1}^\omega + \mathcal{E}_{\text{ref}, A+1}^\omega) + \delta. \end{aligned} \quad (3.13)$$

Here, δ denotes an even-odd mass difference that enters Eq. (3.13) for the energy in the odd- A nucleus (with respect to the energies in its even-even adjacent nuclei). An independent quasiparticle diagram has been shown in Fig. 9 for neutrons in the ^{160}Yb nucleus.

Figure 9 exhibits all the solutions to the corresponding HFB equations. There, solid (dotted) lines denote positive parity solutions with signature $-i$ ($+i$), while dotted-dashed (dashed) lines correspond to the negative parity solutions with signature $-i$ ($+i$). Since the picture appears to be symmetric with respect to the abscissa axis (however, together with a reflection a simultaneous change in signature is required), it suffices to plot only one-half of the whole picture, i.e., including only the “physical” Routhians, those that are positive at $\omega=0$ (Fig. 10). The calculated curves in Fig. 10 can be directly compared with the experimental single-quasiparticle Routhians determined from Eq. (3.13) for the system with odd particle numbers. The experimental Routhians for the even system are determined as sums of pairs AB , AE , BE , etc., representing the two-particle configurations (cf. Fig. 10). One can immediately see that levels with the

highest slopes, such as levels A and B in Fig. 10, play an important role in the behavior of the rotating system, as they are easiest to align [cf. Eq. (2.34)]. For the rare-earth neutrons these are the $[660\frac{1}{2}]$, $[651\frac{3}{2}]$, $[642\frac{5}{2}]$, ..., orbitals (in the Nilsson notation, which is, however, not valid for $\omega \neq 0$) originating from the high- j multiplet. Let us now analyze a rather sharp crossing of two bands in the quasiparticle picture. In the range of small ω all the “unphysical” levels (i.e., those deleted in Fig. 10 as compared to Fig. 9) may be considered occupied, while those included in Fig. 10 (the “physical” levels) can be thought of as empty. At the point $\omega = \omega^* = 0.23$ MeV/ \hbar an abrupt change in the slope in levels A and B occurs simultaneously. This corresponds to the rearrangement in the vacuum and the exchange in the properties of two quasiparticles which is better visible in Fig. 9. Let us put aside for the moment the interaction between the HFB solutions that leads to the repulsion between the curves. We shall come back to this question in Sec. III.A.4. We are then left for the moment with a sharp crossing. The abrupt change in the slope corresponds to a rapid increase in nuclear alignment, and—when translated into the (ω, \mathcal{E}) plane—to the backbending. For the odd-neutron system the presence of the odd particle occupying the lowest level (say, level A in Fig. 10) prevents the sudden jump in angular momentum. Indeed, for the odd system level A is occupied, while level B is empty. It then follows from the properties of the HFB solutions (cf. Sec. II.E.4) that in this case the unphysical image of level A [deleted from Fig. 10, but still present in Fig. 9; let us call it $(-A)$] is empty. For the same reason, the unphysical image of level B (say, $-B$) is occupied. In this situation the “gain” in alignment coming from the change in slope of $(-B)$ is compensated exactly by the “loss” in level $(+A)$. We thus see that there is no jump in angular momentum and consequently no backbending. This phenomenon is often referred to as blocking of the backbending on the yrast line by the odd particle. Similar blocking may occur in the excited bands (sidebands) if they are built on two orbits (say, AE in Fig. 10), one of which (say, A) is involved as a bandhead configuration of the sideband. We shall discuss this behavior in more detail below in connection with the “user’s instructions” providing simple rules for employing the independent quasiparticle diagrams.

3. User’s instructions for the independent quasiparticle diagrams

In order to facilitate the application of the independent quasiparticle diagrams we present below “user’s instructions,” similar to those formulated by Bengtsson and Frauendorf (1979a, 1979b). Their diagrams, however, contain both positive- and negative-energy solutions to the HFBC equations [cf. Eq. (2.83) and our Fig. 9]. Due to the symmetry of the diagrams, such a presentation repeats essential information. We thus prefer to include in the diagrams only those curves above zero at $\omega=0$ (cf. Fig. 10).

The independent-quasiparticle diagrams are composed

of only those quasiparticle levels which are positive at $\omega=0$. Each level is characterized by parity $\pi=+1$ or -1 and by signature $r=+i$ or $-i$; alternatively, one can use the signature exponent $\alpha=-\frac{1}{2}$ or $+\frac{1}{2}$ related to r by $r=e^{-i\pi\alpha}$. The vacuum state is defined for even particle numbers only as the state in which all levels in the diagram are unoccupied by quasiparticles. The vacuum-state energy, spin, etc., undergo variations with increasing rotational frequency. They are described in more detail below. The total signature of the vacuum is $r_{\text{vac}}=+1$ ($\alpha_{\text{vac}}=0$), and the total parity $\pi_{\text{vac}}=+1$.

Instruction 1: The excitations of the even (odd) particle number systems are constructed from an even (odd) number of quasiparticles.

Instruction 2: The excitation energy (with respect to the vacuum) is obtained as the sum of appropriate quasiparticle contributions E_v^ω [$v=(\pi,r,x)$, with x denoting all further quantum numbers needed to identify the levels uniquely].

Instruction 3: The total parity, total signature, total spin, etc., of the excited configurations are given by the corresponding product of parities, product of signatures, sum of spins, etc., of the contributing quasiparticles and the contribution from the vacuum.

Instruction 4: The angular momentum contributions to the total spin-projection on the axis of rotation originating from each occupied level v can be calculated from the slopes of the curves in the diagram

$$\langle v | j_x | v \rangle = -\frac{1}{\hbar} \frac{dE_v^\omega}{d\omega}. \quad (3.14)$$

Instruction 5: If the total-signature exponent in a given configuration is α_{tot} , then spins within the corresponding rotational band obey the relation $I=\alpha_{\text{tot}} \text{mod} 2$ and the total number of particles $N=2\alpha_{\text{tot}} \text{mod} 2$.

Instruction 6: If the slopes of the two lowest-lying quasiparticle Routhians of opposite signature change sign (cf. Fig. 10 for illustration) at some rotational frequency ω [strictly $(d/d\omega)(E_v^\omega + E_{\bar{v}}^\omega)$ changes sign], the vacuum undergoes structural rearrangement,³ and the vacuum contribution to the total angular momentum increases (often rapidly) by the amount given by the change in slope according to Instruction 4.

Instruction 7 (blocking effect): If only one of two opposite-signature levels which are degenerated at $\omega=0$ is occupied by a quasiparticle, a possible crossing (cf. Instruction 6 and its footnote) at frequency ω^* is blocked—

i.e., no structural rearrangements in the bands and in the vacuum (and thus no backbending) are possible at ω^* .

Examples for the application of the quasiparticle diagram are given below. The excited bands (i.e., in contrast to the ground-state band, those bands built on certain two-quasiparticle excited states) and their crossings are described in terms of quasiparticle Routhians.

The two nuclei, ^{160}Yb and ^{161}Yb , provide a good example for the rotational band analysis. In the measurements by Riedinger *et al.* (1980) and Riedinger (1980) yrast states were observed up to $I^\pi=32^+$ and four excited bands were identified up to at least $I=18$ in ^{160}Yb . In the measurement by Gaardhøye *et al.* (1980) the yrast band of ^{161}Yb was observed up to $\frac{49}{2}^+$, and, in addition, four excited bands were found. The detailed decay schemes are presented in Figs. 13(a) and 13(b) for ^{160}Yb and ^{161}Yb , respectively.

In the work of Riedinger *et al.* (1980) the reaction $^{147}\text{Sm}(^{16}\text{O},3n)^{160}\text{Yb}$ was employed with beam energies up to 82 MeV. Data were taken with an array of four Ge(Li) detectors in coincidence with at least one out of three NaI detectors. With the use of a 108-MeV ^{20}Ne beam and of a $25 \times 25\text{-cm}^2$ NaI(Tl) sum spectrometer it was possible to extend the yrast band beyond the second backbending (at $I^\pi=28^+$) up to 32^+ (Riedinger, 1980). In addition, two negative-parity side bands were extended with at least two transitions each.

Investigation of odd-mass nuclei may often reveal which quasiparticle configurations are responsible for certain observed features in the adjacent even-mass nucleus. It is thus instructive to compare the results on ^{160}Yb with the results of the simultaneous investigation of ^{161}Yb performed using the $(^{16}\text{O},3n)$ reaction and applying the same technique as the one applied for the ^{160}Yb measurement (Gaardhøye *et al.*, 1980). In ^{160}Yb a sharp backbending in the yrast band is observed at $\hbar\omega_c \approx 0.27$ MeV, a value close to those of the first backbending in most of the rare-earth nuclei. The three negative-parity bands in ^{160}Yb and the two bands in ^{161}Yb are observed to bend up at a somewhat higher frequency, $\hbar\omega_c \approx 0.36$ MeV (see Fig. 15). The $r^\pi=-i^-$ band (3) in ^{161}Yb shows an up-bend at the still higher frequency $\hbar\omega_c \approx 0.42$ MeV, a similar value as that of the second backbending in ^{158}Er and ^{160}Yb . The gain in angular momentum at the first backbending in ^{160}Yb is approximately 10.6, while the negative parity bands (1 and 2) gain about 6.6 units at the crossing frequency. The newest data on the second backbending in ^{160}Yb allow an estimate of the alignment gained at the crossing frequency $\hbar\omega_c \approx 0.42$ MeV of $\Delta i=5.5$ (Riedinger, 1980). Detailed analysis (see below) provides evidence that the $h_{11/2}$ protons are responsible for the second backbending, as suggested by Faessler and Ploszajczak, 1978; cf. also Bengtsson and Frauendorf, 1979a, 1979b. Detailed cranking-model calculations yield fair agreement for the above-given crossing frequencies and aligned angular momentum in the yrast bands of $^{160},^{161}\text{Yb}$ and the negative parity bands in ^{160}Yb (cf. Riedinger, 1980). The resulting quasiparticle diagram (see below) indicates that the corresponding first backbending

³Such a change occurs for ω close to the value at which the lowest two-quasiparticle excitation energy is equal to zero, i.e., when the two-quasiparticle state and the vacuum degenerate. Since this often happens while the pairing superfluid correlations are still present in the nucleus, although the excitation energy gap has disappeared, the whole effect is referred to as nuclear “gapless superfluidity.” As already discussed above, the corresponding crossing between the ground-state and the excited bands frequently leads to backbending.

can be attributed to the alignment of $i_{13/2}$ neutrons.

The high- j orbitals closest to the Fermi level of ^{160}Yb are $i_{13/2,3/2}$ and $i_{13/2,1/2}$ (in Nilsson notation $[651\frac{3}{2}]$ and $[660\frac{1}{2}]$, respectively). The corresponding quasiparticle Routhians are illustrated in Fig. 10 as functions of rotational frequency. A strong signature splitting (fast removal of Cramers degeneracy present at $\omega=0$) can be seen from the figure; the corresponding opposite signature partners are denoted by (A,B) and (C,D).

The excitation of $^{70}\text{Yb}_{90}$ must be composed of an even number of quasiparticle levels (Instruction 1); in particular, the Stockholm-band configuration is defined by levels A and B (occupied by quasiparticles). The excitation energy of the Stockholm band (more exactly, Routhians) is given by the sum $(E_A^\omega + E_B^\omega)$ (Instruction 2). The parity of the Stockholm band configuration $\pi_s = (+1)(+1)\pi_{\text{vac}} = 1$ and signature $r_s = (+i)(-i)r_{\text{vac}} = 1$ (Instruction 3). Note that parity and signature of the S band are always $(+1)$ and $(+1)$, respectively. The contributions to the S band aligned angular momentum are given by

$$-\frac{1}{\hbar} \left[\frac{dE_A^\omega}{d\omega} + \frac{dE_B^\omega}{d\omega} \right] \approx 5.3 + 4.1 = 9.4$$

and are practically independent of rotational frequency (for not too high ω). Since $r_S = 1$, or $\alpha_S = 0$, $I = \alpha_S \bmod 2 = 0, 2, 4, \dots$ (even numbers only for the Stockholm band; Instruction 5). At $\omega^* = 0.23 \text{ MeV}/\hbar$ the slopes of curves A and B change sign (cf. Instruction 6); moreover, the total excitation of the S band equals $E_A^{\omega^*} + E_B^{\omega^*} \approx 0$ and thus the S band crosses the ground-state band at $\omega = \omega^*$. This crossing frequency agrees well with the average derived from the aligned angular momentum plot (Fig. 15). Apparently, at $\omega = \omega^*$ the roles of the vacuum configuration and the Stockholm configuration interchange, the latter becoming the yrast.

The lowest negative-parity bands result from a configuration in which only one of the A and B levels is occupied. The second occupied quasiparticle level is one of the two lowest negative-parity levels (E, F displayed in Fig. 10, for complete illustration see Fig. 9, where the negative-parity levels mentioned are denoted also E and F). Since only one quasiparticle level out of two (E_A and E_B) is occupied in this configuration, no band crossing (or backbending) is possible in these bands at $\omega = \omega^* = 0.23 \text{ MeV}/\hbar$, which illustrates the effect of blocking, Instruction 7.

The blocking effect can also be demonstrated using $^{161}\text{Yb}_{91}$ data. Here the lowest neutron excited bands are of one-quasiparticle character (Instruction 1). The ground-state band configuration in this nucleus is defined by the vacuum state (identical to the vacuum state in ^{160}Yb , since the vacuum is defined only for even particle numbers) and the lowest one-quasiparticle excitation. The quasiparticle level (denoted by A in Fig. 10) has the signature $r = -i$ ($\alpha = +\frac{1}{2}$), and thus the corresponding yrast band is composed of spins $I = \frac{1}{2} \bmod 2 = \frac{1}{2}, \frac{5}{2}, \frac{9}{2}, \frac{13}{2}, \dots$ (Instruction 5). The band corresponding to level B occupied is characterized by signature $r = +i$ ($\alpha = -\frac{1}{2}$) and the spin sequence $I = \frac{3}{2}, \frac{7}{2}, \frac{11}{2}, \dots$ (according to Instruc-

tion 5). According to Instruction 7, neither of the two bands can produce any backbending effect at $\omega = \omega^*$.

In contrast to the blocking effect at $\hbar\omega = 0.23 \text{ MeV}$, no blocking-type limitations apply to the configurations involving either E_A^ω or E_B^ω at $\omega = 0.36 \text{ MeV}/\hbar$ (cf. Fig. 10). Consequently a backbending could occur in the corresponding excited bands at this frequency for ^{161}Yb . A more detailed analysis of the $^{160,161}\text{Yb}$ data can be found in the work of Riedinger (1980).

4. The strength of interaction between crossing bands

The absolute value of the interaction strength $|V|$ is obtained from the two solutions of the HFB equations with the same signature and parity as the closest distance between the two corresponding curves in the quasiparticle diagram. This quantity can be read directly from the diagram as half of the distance at $\omega = \omega^* = 0.23 \text{ MeV}/\hbar$ between curve B and the reflection of A in Fig. 9, or as half of the algebraic sum of ordinates in the curves A and B at $\omega = \omega^*$ if Fig. 10 is used. In other words,

$$|V| = \frac{1}{2}(E_B^\omega + E_A^\omega) = \frac{1}{2}(|E_B^\omega| - |E_A^\omega|) \quad (3.15)$$

at $\omega = \omega^*$.

The quantity $|V|$ determined in this way corresponds to the nonphysical interaction of the two bands for equal values of ω . It was analyzed by Bengtsson and Frauendorf (1979a, 1979b), who suggested that the “true” interaction of the two bands corresponding to states with the same angular momenta equals approximately V . The magnitude of $|V|$ appears to be crucial for the existence (or nonexistence) of backbending. Large values of $|V|$ lead to the strong repulsion of the bands, and it can be seen from Fig. 14 that in this case the backbending may disappear.

A remarkable property of $|V|$ has been noticed by

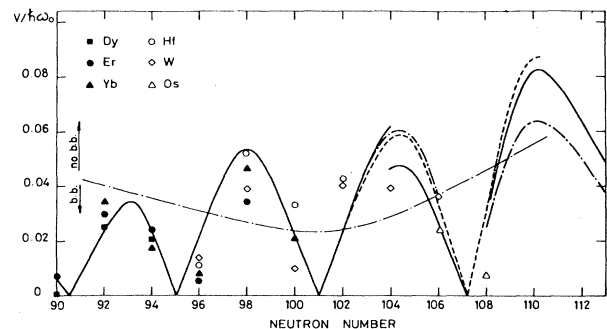


FIG. 16. The strength $|V|$ of the interaction between the gsb and the Stockholm (S) band as a function of the neutron number for the rare-earth nuclei (Bengtsson, 1980). The characteristic oscillatory behavior was obtained using the HFB cranking model after assuming that the band interaction strength can be approximated from Eq. (3.15). The dash-dotted line shows the limit for the backbending (points lying below this line correspond to nuclei which will produce a backbending effect according to the calculations).

Bengtsson, Hamamoto, and Mottelson (1978), who calculated the quantity $|V|$ in a simple model of a large j shell. It follows from the quantal interference effects in the wave function that $|V|$ exhibits oscillatory behavior as a function of the location of the Fermi surface λ relative to the members of the high- j multiplet (split by the deformation in the nuclear potential) exhibiting $j - \frac{3}{2}$ zeros. These zeros correspond to sharp crossings. The behavior of $|V|$ as a function of the Fermi surface (and thus of particle number) is illustrated in Fig. 16. The analysis using this feature of the oscillatory behavior of V by Bengtsson and Frauendorf (1979a, 1979b) and others (Grümmer *et al.*, 1979; Faessler *et al.*, 1981; Bengtsson, 1980; Dudek, Nazarewicz, and Szymański, 1981) shows generally a very good agreement with experiment.

5. Variation in the pairing gap

It seems to be worth mentioning that calculations that include the possible variations in the gap parameter Δ (self-consistent) in the HFB scheme (cf. Sec. II.E), together with a thorough choice of the single-particle level scheme and proper deformation, seem to improve greatly the detailed agreement with experiment (Cwiok *et al.*, 1980; Dudek, Nazarewicz, and Szymański, 1981). Figure 17 illustrates an example of the $\mathcal{F}^{(1)}$ vs ω^2 curve calculated with the self-consistent gap parameter Δ . The good agreement with experiment is due largely to the self-consistency in Δ as well as "realistic" single-particle spectrum (cf. discussion in Appendix A Sec. 3).

The important role of variation in the gap parameter Δ seems to be in line with recent observations by Garrett

et al. (1982) and Garrett and Frauendorf (1982), who performed a systematic analysis of the crossing frequency ω^* in even- and odd-mass nuclei. A pronounced odd-even effect has been observed in ω^* , which may be attributed to the influence of the odd-even difference in the gap parameter Δ . The search for the disappearance of the pairing correlations due to rotation will be discussed in Sec. III.C.

6. Other approaches to nuclear rotation

The independent quasiparticle approach based on the cranking model described in Sec. II and this section (III.A) seems to be the only existing theoretical scheme applied successfully on a large scale to the problem of high-spin collective rotation up to now. Various corrections and improvements of this scheme based mostly on the Hartree-Fock-Bogolyubov method have been suggested and tested in many detailed calculations (see, e.g., Faessler *et al.*, 1976a; Goodman, 1979; Fleckner *et al.*, 1979; Egido and Ring, 1982, 1982a; Hara *et al.*, 1982; Praharaj, 1982). A considerable effort has been devoted to the elimination of possible inaccuracies due to the nonconservation of the particle number N and angular momentum I in the HFB cranking method. Attempts were also made to use the HFB method in its possibly most self-consistent form. The calculations with N -projected HFB wave functions should in principle lead to more realistic descriptions of actual nuclei. They lead in particular to a much more smooth transition from the superfluid to the normal nuclear state. However, it seems still to be an open question whether the variational principle with the N -projected wave functions constitutes the best way of correcting for the nonconservation of the particle number in the HFB approximation. The method consisting of projection of total angular momentum out of the Slater determinants built from the individual-nucleon wave functions in the deformed nuclear potential could be considered an alternative procedure (see, for example, Bohr and Mottelson, 1975). However, this method has been explored up to now only in light nuclei and for relatively low angular momenta (see, however, Hara *et al.*, 1982 and Praharaj, 1982). Another method, the interacting boson approximation (IBA model in the various versions of Arima and Iachello 1976, 1978, 1979, and Scholten *et al.*, 1978) has been used to describe rotational and vibrational features reflected in various bands of many nuclei. However, it is not certain whether the interacting boson approximation which seems to be valid at low angular momenta (depending on the number of bosons) would provide an adequate description for the nuclear response to the fast rotation. This model has been used by Morrison *et al.* (1981) as a description of the nuclear core for the calculation of the high-spin spectra in transitional Hg nuclei. Further discussions of these problems fall outside the scope of the present article.

We have based all our discussions of nuclear rotation on the concept of the cranking model (cf. Sec. II.A). Another basis could be provided by the model of valence

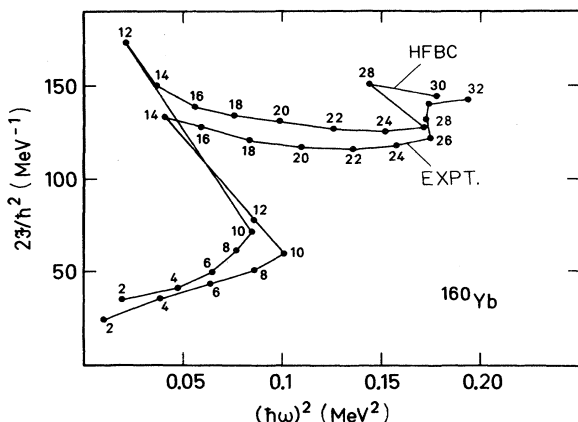


FIG. 17. The double backbending effect in ^{160}Yb reproduced theoretically within the pairing self-consistent HFBC method (cf. Sec. II.E) using the Woods-Saxon single-particle potential. The experimental data are taken from Beck *et al.* (1979), with the 30^+ and 32^+ data points from Riedinger (1980, 1981), and the calculated results from Cwiok *et al.* (1980). The main difference between this approach and that of Bengtsson and Frauendorf (1979a, 1979b) lies in the fact that the proton and neutron pairing Δ values are calculated from the HFBC equations at each rotational velocity in the former approach, while in the latter, Δ values are assumed to be constant.

particles coupled to the nuclear rotor core (Bohr and Mottelson, 1975). This model which is not fully equivalent to the cranking model has been discussed recently in several papers (Bohr and Mottelson, 1980; Almberger *et al.*, 1979, 1980a, 1980b; Hilton *et al.*, 1981). It may provide an interesting alternative for the calculation of nuclear properties at high angular momentum.

Finally, let us observe that the pseudospin [or, more general, pseudo-SU(3)] symmetry introduced a long time ago by Hecht and Adler (1969), Arima *et al.* (1969), Ratna Raj'u *et al.* (1973) may also be employed as a promising tool for the investigation of nuclear properties at high angular momenta (Bohr *et al.*, 1982; see also Draayer *et al.*, 1981).

B. Energy correlations in the high-spin spectra of collectively rotating nuclei

An experimental technique particularly useful for the studies of the γ -ray energy correlations was developed by Andersen *et al.* (1979), Garrett and Herskind (1979), and Herskind (1980). It consists in registering coincidences between γ quanta with the help of at least two detectors (more elaborate setups have been described, for instance, in the above references). A convenient means of representing the results of such a coincidence experiment is to plot the number of coincidences N_γ vs E_{γ_1} , and simultaneously versus E_{γ_2} , the energies of the coincident quanta registered by the first and the second detector, respectively. Such a two-dimensional plot is sometimes referred to as a correlation matrix.

To illustrate the advantage of the two-dimensional rep-

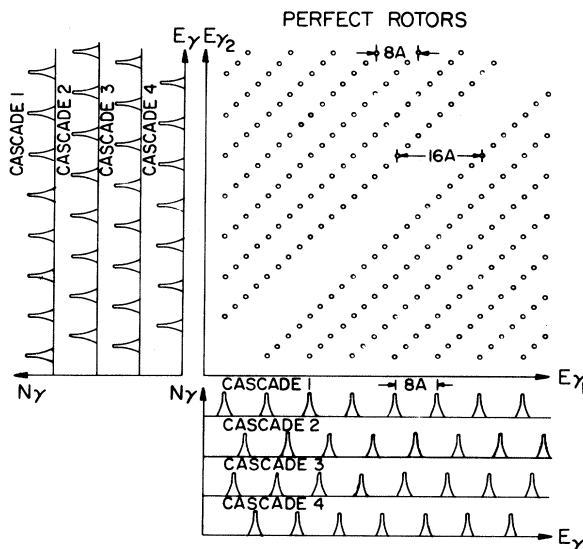


FIG. 18. A model for an E_γ - E_γ correlation matrix (coincidence intensity pattern) in the case of an ideal rotor with four bands of constant $\mathcal{F}_{\text{band}}$. The spacing between adjacent ridges on each side of the diagonal correspond to $\Delta E_\gamma = 8A$, with $A = \hbar^2 / 2\mathcal{F}_{\text{band}}$, and the width of the central valley equal to $16A$. [From Herskind (1980).]

resentation let us first consider the E_{γ_1} - E_{γ_2} correlation pattern due to radiation from an ideal rotor. We define an ideal rotor as an object generating the spectrum

$$\mathcal{E}(I) = \frac{\hbar^2}{2\mathcal{F}_{\text{rig}}} I(I+1), \quad (3.16)$$

with a constant \mathcal{F}_{rig} , called the rigid rotor moment of inertia. The corresponding transition energies, $E_\gamma(I)$, are given by

$$\begin{aligned} E_\gamma(I) &= \mathcal{E}(I) - \mathcal{E}(I-2) \\ &= \frac{\hbar^2}{2\mathcal{F}_{\text{rig}}} (4I-2). \end{aligned} \quad (3.17)$$

The ideal rotor generates an "ideal coincidence spectrum" like the one illustrated in Fig. 18. Open circles in the figure represent the sharp maxima of $N_\gamma = N_\gamma(E_{\gamma_1}, E_{\gamma_2})$ situated at points with the coordinates $E_{\gamma_1} = E_\gamma(I)$, $E_{\gamma_2} = E_\gamma(I')$ [cf. Eq. (3.17)]. Note that in the idealized example there are no counts for energies different from those defined by $E_\gamma(I)$ and $E_\gamma(I')$.

Since a given γ quantum cannot be in coincidence with itself, the main diagonal in the correlation matrix contains no counts.

Apparently, atomic nuclei do not, in general, resemble closely perfect rotors, and thus in more realistic considerations one has to expect deviations from the simple pattern of Fig. 18. In particular, transition energies different from the one given by Eq. (3.17) (and also various line intensities) may contribute strongly to such deviations (cf. the schematic illustration in Fig. 19). Moreover, from the discussion in previous sections it follows that in the case of backbending (multivalued behavior of total energy versus ω) the valley can be locally filled by the nonzero

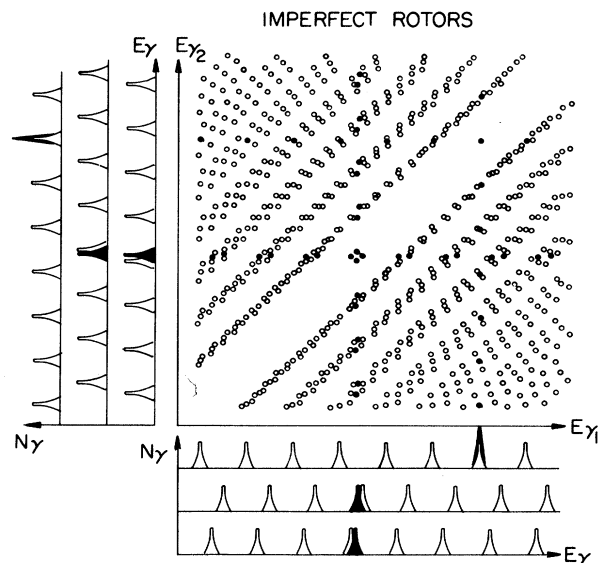


FIG. 19. The same matrix as in Fig. 18, but, in addition, with four bands with a 10% larger and four bands with a 10% smaller $\mathcal{F}_{\text{band}}$. Also, backbending features are indicated by black peaks and dots. [From Herskind (1980).]

counts in the diagonal, since there may be two or more γ rays corresponding to different spins but to the same rotational frequencies. Such a piling up of coincidence counts in some place at the main diagonal is often referred to as a "bridge." The presence of valleys in the $E_{\gamma_1} - E_{\gamma_2}$ plots is thus a signature of collective rotation, while the presence of bridges can be related to the band crossings and backbending effects.

In the correlation method we are interested only in the registration of the full energies of the emitted γ rays. Unfortunately the response of commonly used γ -ray detectors limits the registration of the full energy only to the so-called photopeak, which contains a certain fraction of the total number of events. Owing to this limited (photopeak/total) efficiency, which amounts to $\sim 50\%$ for large NaI crystals and to $\sim 15\%$ for Ge(Li) detectors,

the number of full-energy coincidences between two detectors covers only $\sim 25\%$ and $\sim 2\%$, respectively, of all coincidence events. Subtraction techniques were proposed (Andersen *et al.*, 1979; Herskind, 1980) to remove the uncorrelated background of events which are not due to full-energy coincidences (for instance, Compton-scattering events). An example of an $E_{\gamma_1} - E_{\gamma_2}$ contour plot obtained with the reaction $^{159}\text{Tb}(^{14}\text{N},xn)^{173-x}\text{Hf}$ at 95 MeV (de Voigt *et al.*, 1981) is presented in Fig. 20. Two anti-Compton spectrometers were used with a photopeak/total efficiency of $\sim 60\%$ each and thus the remaining $\sim 40\%$ of the total number of counts were spread in the region of the Compton edge. The probabilities for the various detection combinations using two detectors in coincidence follow from these efficiency numbers; full energy events in both detectors $\sim 36\%$,

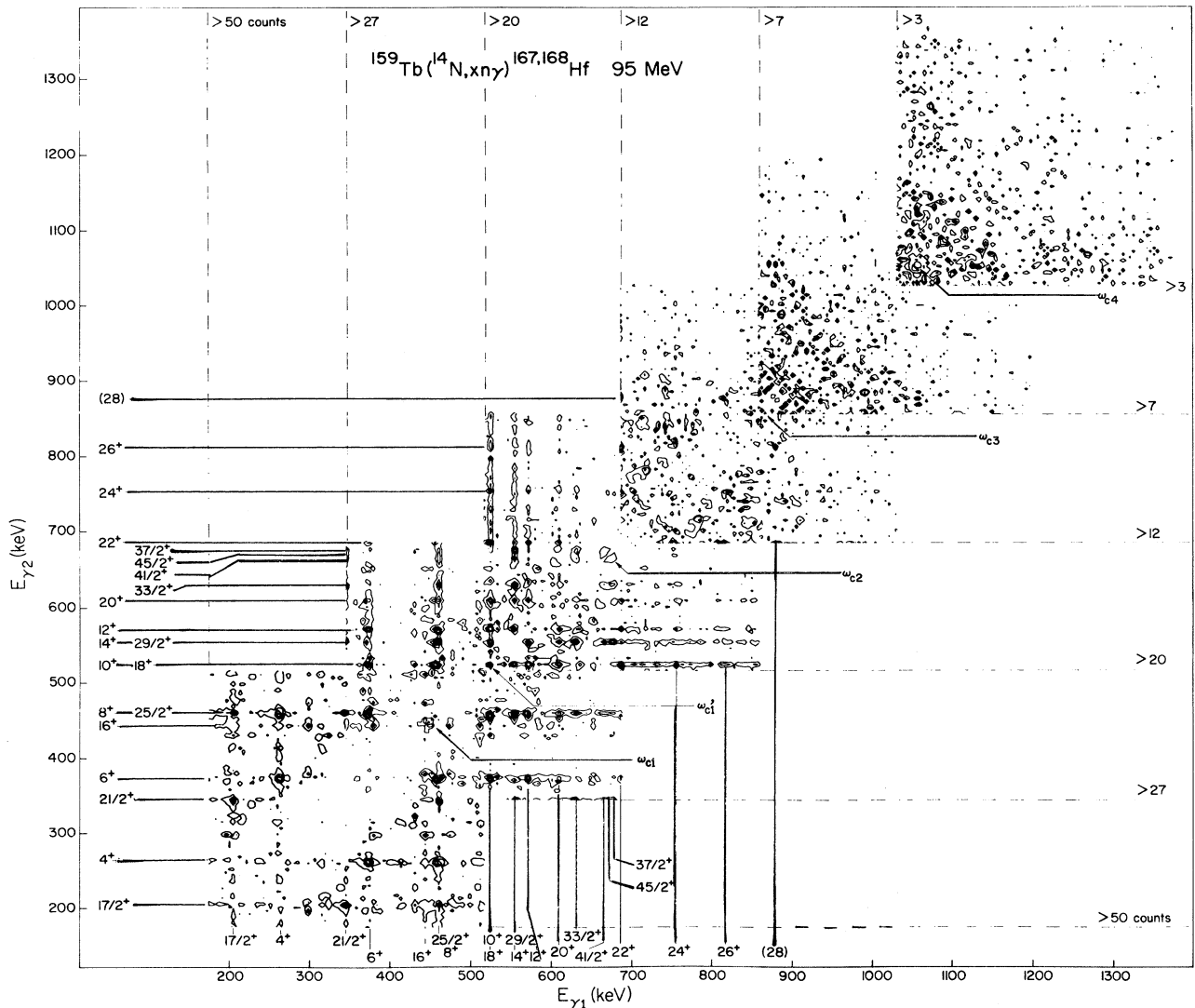


FIG. 20. Contour plot of the symmetrized γ - γ correlation matrix. Six different intensity thresholds are indicated by the numbers at the dashed lines. Enhanced intensities in the valley are indicated by $\omega_{c1}, \dots, \omega_{c4}$. The first two at ω_{c1} and ω_{c2} are due to known backbending effects in ^{168}Hf and ^{167}Hf , respectively. The known discrete yrast-band transitions in these nuclei are indicated on the left and in the bottom part by the spin of the initial levels (de Voigt *et al.*, 1981).

Compton in one detector and full energy in the other one and vice versa $\sim(2 \times 24)\%$, and Compton events only $\sim 16\%$. The valley along the diagonal is clearly seen to about 900 keV. The known band crossings are identified in the lower energy range, but several more "bridges" across the valley are seen at higher γ -ray energies. The enhanced intensities in the central valley, as indicated in Fig. 20, occur at the rotational frequencies of $\hbar\omega=0.23-0.26, 0.34, 0.42$, and 0.52 MeV. The first two were identified as due to the crossings of the $v_{13/2}$ two-quasiparticle S band with the ground-state band (gsb) in ^{168}Hf and ^{167}Hf , known from conventional spectroscopy (Janssens *et al.*, 1981). The two higher frequencies were attributed to crossings of bands which may involve $\pi h_{11/2}$ or higher orbitals. The frequency of $\hbar\omega_3=0.42$ MeV is the same as in ^{158}Er (Lee *et al.*, 1977) and in ^{160}Yb (Beck *et al.*, 1979), where the second backbending was attributed to $h_{11/2}$ protons. The highest crossing frequency $\hbar\omega_4=0.52$ MeV in $^{167,168}\text{Hf}$ is close to the one reported by Deleplanque *et al.* (1980) at 0.55 MeV in erbium nuclei. In this energy region, however, the statistics seem rather poor.

At a given fixed energy of, say, E_{γ_1} the maxima along the straight line given by equation $E=E_{\gamma_1}$ appear at the intervals

$$\Delta E_{\gamma}(I)=E_{\gamma}(I)-E_{\gamma}(I-2)=8\left[\frac{\hbar^2}{2\mathcal{F}_{\text{rig}}}\right] \quad (3.18)$$

in the simplified case of an ideal rotor (cf. Fig. 18). It also becomes apparent that the width of the central "valley" is simply related to the rotational constant $A=\hbar^2/2\mathcal{F}_{\text{rig}}$ —i.e., the width equals $16A$ (cf. Fig. 18) measured along the E_{γ} axis. From the example considered one also learns that the width of the valley is straightforwardly related to the second derivative of the excitation energy with respect to spin, since (for $\Delta I=2$ transitions)

$$E_{\gamma}(I)=2\left[\frac{\mathcal{E}(I)-\mathcal{E}(I-2)}{2}\right]=2\frac{d\mathcal{E}}{dI}, \quad (3.19)$$

and similarly

$$\Delta E_{\gamma}=4\frac{d^2\mathcal{E}}{dI^2}. \quad (3.20)$$

The latter quantity is related to $\mathcal{F}^{(2)}$ [cf. Eq. (3.4)]. We also notice that the central valley is determined by coincidence counts coming from adjacent transitions, presumably belonging to one rotational band. The width of the valley at a certain point is thus related to the dynamical moment of inertia $\mathcal{F}_{\text{band}}^{(2)}$ characteristic for one band.

The width of the central valley in the correlation matrix was reported to decrease smoothly with E_{γ} (see Fig. 20) in the work of de Voigt *et al.* (1981). This seems to be in contrast with the finding of Deleplanque *et al.* (1980), who observed an increasing width of the valley at the highest frequencies. On the other hand, the ^{14}N data on ^{168}Hf show a behavior quite similar to those obtained by Lisle *et al.* (1981) who studied ^{170}Hf with an 80-MeV

^{16}O beam on ^{158}Gd . The correlation pattern for ^{170}Hf showed a decreasing valley width at the highest frequencies $\hbar\omega\approx 0.37$ MeV. The corresponding average dynamical moment of inertia values increased to about that of a rigid sphere, an observation interpreted as being due to a decrease of pairing. Such a conclusion was also reached by Białkowski *et al.* (1981) on the basis of correlation data from the reaction $^{124}\text{Te}(^{12}\text{C},6n)^{130}\text{Ce}$ at 118-MeV bombarding energy. They observed an approximately constant value of the valley width around $\hbar\omega\approx 0.4$ MeV and a decrease at the highest frequencies 0.5–0.6 MeV. The Coriolis antipairing may be responsible for that decrease (cf. Sec. III.C). However, as mentioned above, the determination of the valley width and the interpretation of features seen in the correlation matrix are far from unambiguous at present. Refinement of the technique and analysis methods are required (besides better statistics) before detailed nuclear structure information can be extracted.

Theoretical interest in the $E_{\gamma_1}-E_{\gamma_2}$ correlations is reflected in the calculations of correlation patterns for γ -ray cascades using, for example, particle-rotor spectra (Leander *et al.*, 1981). Some details of the calculation are given in Sec. V.C. In Fig. 21 a calculated $\gamma-\gamma$ energy correlation pattern corresponding to a certain mixture of spectra of the ^{165}Yb and ^{166}Yb nuclei is given. It is seen that the correlation pattern reproduces some typical features occurring in the corresponding observed coincidence patterns, such as the existence of the valley at the diagonal, and some bridges across the valley, related to

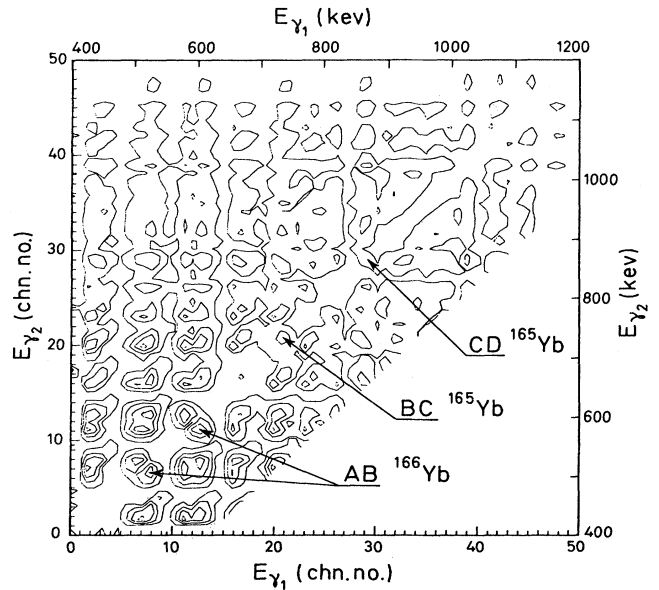


FIG. 21. Gamma-correlation plot from cascades through particle-rotor spectra calculated for ^{165}Yb and ^{166}Yb . The contour lines are for 150, 600, 1200, and 1800 "coincidences" per (16×16) -keV bin. Bridges across the central valley are marked with the cranking-model crossings, with A , B , C , and D denoting quasiparticle states that lie lowest at small ω (from Leander *et al.*, 1981).

the crossings between various bands. These results illustrate that the $E_{\gamma_1} - E_{\gamma_2}$ energy correlations provide information on both the discrete and quasicontinuum γ -ray spectrum and thus provide a link between the two corresponding regions of excitation.

Some further implications of the fast rotation on the properties of band dynamical moments of inertia at moderately high spins are discussed in Sec. III.C.

C. Pairing reduction at high spin and the dynamical moments of inertia

There is no doubt at present that the nuclear pairing correlations decrease at high rotational frequencies and that the state of nuclear superfluidity eventually disappears at some critical frequency ω_{crit} . Although several authors attempted description of this phenomenon using various versions of the cranking model, very little is known at present about possibilities of its quantitative description. One of the main difficulties is the problem of extracting the information on the pairing collapse (pairing phase transition) directly from the experimental data. In this section first attempts to attack this problem are briefly discussed.

One of the most relevant physical quantities in discussing the phase transition effect seems to be the dynamical moment of inertia $\mathcal{F}^{(2)}$ as suggested by Bohr and Mottelson (1981). They also pointed out that for rotational frequencies slightly below the critical frequency the dynamical moment of inertia should exceed the corresponding rigid-body value. Bohr and Mottelson discuss, in fact, the expected qualitative behavior of the yrast moment of inertia, thus stressing mostly the characteristic “average” properties of the yrast line in the vicinity of the phase transition.

The evidence for the pairing phase transition drawn directly from experimental data is, however, strongly obscured by the effect of the band crossing and the accompanying alignment in individual angular momenta (cf. Sec. III.A). Indeed, in the region of backbending the angular momentum I plotted versus ω exhibits a typical S-shaped curve (similar to that of the moment of inertia $\mathcal{F}^{(1)}$ vs ω^2 —cf. the bottom part of Fig. 14). The dynamical moment of inertia $\mathcal{F}^{(2)}$ would then exhibit violent changes in the vicinity of the crossing frequency. This behavior clearly indicates that the dynamical moment of inertia as a quantity related to the second-order derivative is far too sensitive to describe sharp crossings between the levels. In the search for the pairing phase transition one would like to get rid of the very rapid fluctuations of $\mathcal{F}^{(2)}$ vs ω caused by ordinary bandcrossings and to concentrate on the probably less violent behavior underlying the pairing collapse.

One way to achieve this goal is to study the dynamical moment of inertia $\mathcal{F}^{(2)}$ along one selected band without leaving it at its crossings. This may be possible, for instance, if the members of the ground band are known way up beyond the crossing. The part of the band above the

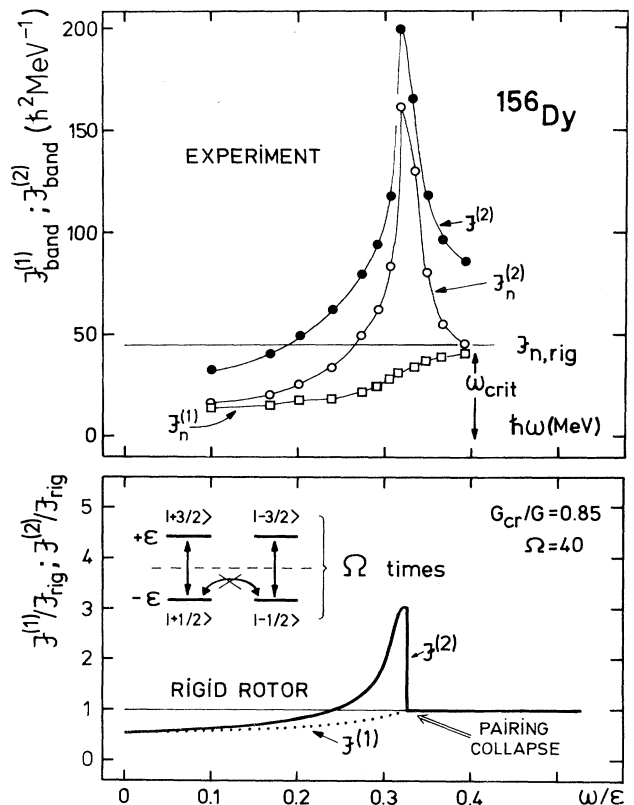


FIG. 22. The experimental values of the $\mathcal{F}^{(2)}$ moment of inertia for the gsb in ^{156}Dy (solid circles). In this particular nucleus both the yrast band and the continuation of the gsb have been measured up to $I^\pi = 30^+$ and 28^+ , respectively (cf. Ward *et al.*, 1979). Here the data of the gsb were selected since they correspond to a higher collective rotational velocity than that in the yrast states. The open circles correspond to the neutron $\mathcal{J}_n^{(2)}$ values [obtained by subtracting the theoretical proton $\mathcal{J}_p^{(2)}$ values]. Open squares correspond to the neutron moments of inertia $\mathcal{J}_n^{(1)}$ obtained similarly—i.e., $\mathcal{J}_n^{(1)} = \mathcal{J}_{\text{expt}}^{(1)} - \mathcal{J}_{p,\text{calc}}^{(1)}$. Note that $\mathcal{J}_n^{(1)} \approx \mathcal{J}_n^{(2)}$ at the highest ω value. The theoretical results for the $\mathcal{F}^{(1)}$ and $\mathcal{F}^{(2)}$ moments of inertia calculated within the Ω times degenerate two-level model are indicated at the bottom.

crossing—which lies, of course, above the yrast line—is characterized by a rather large angular velocity of rotation (compared to that on the yrast line) and may thus be a very good test ground for the study of the pairing correlations. In this region the pairing-destroying trend in the Coriolis interaction is the strongest.

Figure 22 presents the experimental data for ^{156}Dy for which the ground-state band is known up to $I^\pi = 28^+$, showing the experimental values of the kinematical and dynamical moments of inertia as a function of the rotational frequency. For comparison, also the degenerate model [with two levels—cf. Valatin (1961), Krumlinde and Szymanski (1973), and Szymanski (1977)] calculation results are presented to stress striking qualitative similarities between experimental and the simplified model results. In Fig. 23 the “realistic” HFBC model results with the Woods-Saxon potential are compared to the same ex-

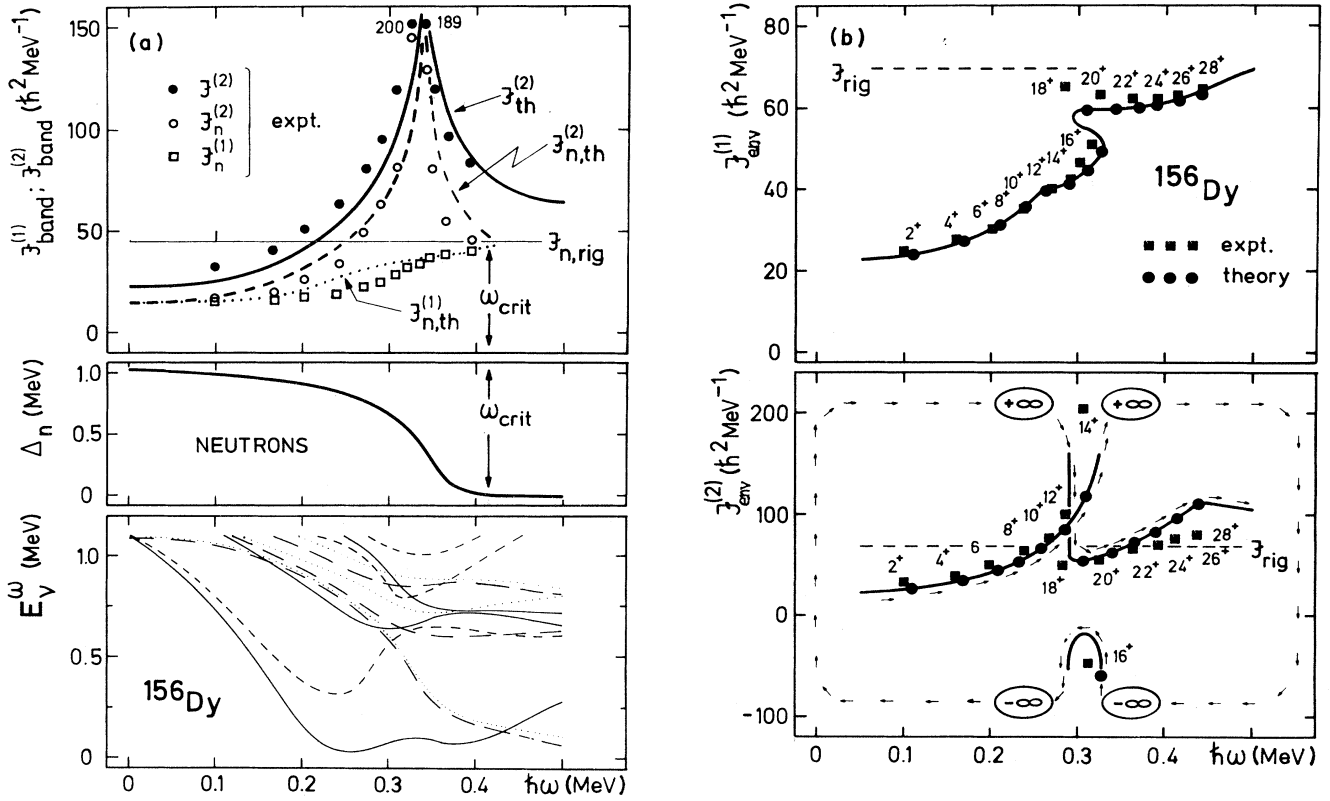


FIG. 23. (a) Comparison between the experimental data from Fig. 22 and the pairing self-consistent HFBC calculations with the Woods-Saxon potential for the $\mathcal{F}^{(1)}$ and $\mathcal{F}^{(2)}$ moments of inertia. The middle part shows the calculated “self-consistent” neutron pairing Δ as a function of ω . The bottom part displays the relevant neutron quasiparticle Routhians. The frequency at which the calculated pairing Δ collapses corresponds very well to the point at which $\mathcal{F}_{n,\text{expt}}^{(1)} \approx \mathcal{F}_{n,\text{expt}}^{(2)} \approx \mathcal{F}_{n,\text{rig}}$. The behavior of quasiparticle Routhians reveals characteristic differences when compared with the diagrams of Bengtsson and Frauendorf (1979a, 1979b), with constant Δ , the latter overstressing the alignment behavior. (b) The experimental (squares) and calculated (circles) moments of inertia $\mathcal{F}^{(1)}$ (upper part) and $\mathcal{F}^{(2)}$ (bottom part) for the yrast states of ^{156}Dy . Note that the multivalued behavior of $\mathcal{F}^{(1)}$ for the yrast states results in singularities of $\mathcal{F}^{(2)}$ as it follows from the relation $\mathcal{F}^{(2)} = \mathcal{F}^{(1)} + \omega d\mathcal{F}^{(1)}/d\omega$ [cf. Eqs. (3.3) and (3.4)].

perimental data. Calculations indicate clearly that the positions of maxima of the moment of inertia $\mathcal{F}^{(2)}$ are strongly correlated to the disappearance of the neutron pairing (the corresponding neutron \mathcal{F} values are also displayed in the figure).

From the above results one can conclude that the qualitative description of not only the kinematical but also the dynamical moments of inertia is possible for fast rotating nuclei by making use of the HFBC method of Sec. II.E with the Woods-Saxon potential. Moreover, good quantitative description of the experimental data suggests the possibility of interpreting characteristic behavior of $\mathcal{F}^{(1)}$ and $\mathcal{F}^{(2)}$ moments of inertia in terms of the pairing collapse mechanism although the latter may be initiated by alignment.

On the other hand, one has to take into account that the band interactions and crossings may also be reflected by rapid variation of $\mathcal{F}^{(2)}$ with rotational frequency. In fact, the two mechanisms, viz., the rotational alignment and the pairing collapse, are strongly related. Alignment

of individual nucleonic angular momenta gives rise to breaking of the nucleonic pairs, which in turn diminishes the role of pairing interactions and leads, according to the calculations, to a pairing collapse.

The rotational bands whose states carry minimum alignment of individual nucleonic angular momenta are among the best “candidates” to reveal the pairing phase transition at relatively low spin (see discussion above). Such bands are often nonyrast at higher rotational frequencies, and their states are most likely interacting with the states of the other multiquasiparticle excited bands. The related possible irregularities in the kinematical moment of inertia in the form of so-called upbendings give an indication for the possible band interactions. Smooth behavior of $\mathcal{F}^{(2)}$, on the other hand, indicates very strong (or no) interaction of the band with the neighboring bands. If this happens, the characteristic “bump” in the $\mathcal{F}^{(2)}$ vs ω curve can more likely be related to a rapid reduction or even collapse of the pairing correlations in nuclei.

D. Multiple Coulomb excitations of high-spin nuclear states

Coulomb excitation induced by heavy projectiles is known as a very selective process of populating rotational states. The excitation process is caused by the electromagnetic field of impinging charged projectiles. For projectile energies not too high the distance of closest approach between the two ions remains larger than the range of nuclear forces (due to Coulomb repulsion). In such a case the intrinsic nuclear properties enter the expression of the excitation cross section only via electromagnetic multipole moments. One can show in particular (see, e.g., Alder *et al.*, 1956) that the cross section for the excitation via an $E\lambda$ ($M\lambda$) transition is proportional to the corresponding nuclear reduced transition probability $B(E\lambda)$ [$B(M\lambda)$] (see Appendix B). Therefore the measurement of these cross sections provides important experimental information on $B(E\lambda)$ [$B(M\lambda)$] and thus also on the nuclear structure.

For heavy ions of sufficiently high energies the Coulomb excitation passes consecutively via a series of many rotational states (multiple Coulomb excitation) reaching possibly high spins. One can estimate, for instance, that using ^{238}U as a target, states of up to $I \approx 6$ can be populated with ^{16}O projectiles with an energy of 73 MeV, states of up to $I \approx 14$ with 185-MeV ^{40}Ar , those up to $I \approx 26$ with 605-MeV ^{132}Xe , and those up to $I \approx 32$ with 1000-MeV ^{208}Pb beams, respectively. The energy of the beam particles should be sufficiently high that possibly the highest spins are reached. On the other hand, this energy should not exceed the relative potential barrier E_c of the colliding ions, since otherwise the nuclear interactions disturb the "clean" Coulomb excitation mechanism. One can estimate that

$$E_c \approx 1.44Z_1Z_2/1.16(A_1^{1/3} + A_2^{1/3} + 2). \quad (3.21)$$

The limitation (see above) for the beam energies leads to a limitation for the projectile velocities (v/c significantly smaller than 1). One can show that for v/c relatively small, magnetic-type excitations can be neglected as compared to those of electric type and that the latter are dominated by quadrupole transitions. Therefore in the multiple Coulomb excitations one can preferably populate ground-state bands; this property is sometimes stressed by calling multiple Coulomb excitation a clean, or selective mechanism.

Since the target nuclei must be relatively long living (the nuclei not too far from the beta-stability line) the multiple Coulomb excitation process can be used to study nuclei often not accessible via (HI, xn) reactions, the latter leading mostly to the neutron-deficient isotopes. Examples of the high-spin spectroscopic studies using the Coulomb excitation can be found in Ward *et al.* (1976) on $^{174,176}\text{Yb}$ excited with ^{86}Kr and ^{136}Xe beams from the Berkeley Super-Hilac, in Grosse (1979), Emling *et al.* (1981), and Grosse *et al.* (1981) on $^{156,158}\text{Dy}$ and ^{238}U excited with ^{208}Pb beams from the Darmstadt (GSI) Unilac, and in Simon *et al.* (1980) on ^{235}U and ^{237}Np nuclei.

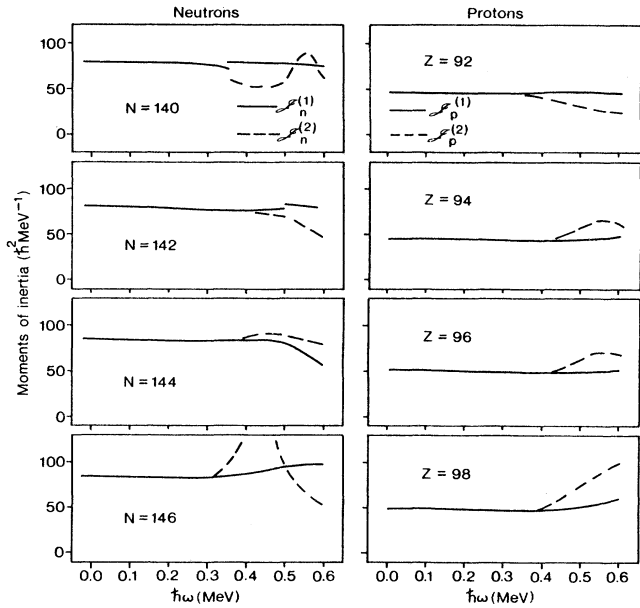


FIG. 24. Comparison between the $\mathcal{F}^{(1)}$ and $\mathcal{F}^{(2)}$ moments of inertia calculated for selected neutron and proton numbers in actinide nuclei. In this calculation the pairing effect was arbitrarily set equal to zero. Calculations performed at the equilibrium deformations of the corresponding nuclei indicate that $\mathcal{F}^{(1)} = \mathcal{F}^{(2)}$ in all the cases for $\hbar\omega \leq 0.3$ MeV. Therefore if the pairing collapses for $\hbar\omega \leq 0.3$ MeV, the relation $\mathcal{F}^{(1)} = \mathcal{F}^{(2)} = \mathcal{F}_{\text{rig}}$ at ω_{crit} should be expected for these nuclei. At higher rotational velocities the effect of alignment splits the $\mathcal{F}^{(1)}$ and $\mathcal{F}^{(2)}$ values, since $\mathcal{F}^{(2)} = \mathcal{F}^{(1)} + \omega d\mathcal{F}^{(1)}/d\omega$.

The measurements for actinide nuclei seem to provide particularly interesting data on the interplay between the individual-nucleonic alignment effect and the collective effect of pairing collapse (see Sec. III.C). In the preceding section we discussed the possibility of analyzing the possible pairing reduction and/or collapse in terms of the $\mathcal{F}^{(1)}$ and $\mathcal{F}^{(2)}$ moments of inertia. Such an analysis may be complicated by the fact that angular momentum alignment originating from one nucleonic pair may give rise to a characteristic maximum very similar to that produced by the pairing collapse. From the equality

$$\mathcal{F}^{(2)}(\omega) = \mathcal{F}^{(1)}(\omega) + \omega \frac{d\mathcal{F}^{(1)}}{d\omega} \quad (3.22)$$

and the relation

$$I(\omega) = I_{\text{bulk}}(\omega) + i_{2qp}(\omega) \quad (3.23)$$

[$I_{\text{bulk}}(\omega)$ refers to the angular momentum generated by the $A - 2$ nucleons, while $i_{2qp}(\omega)$ denotes the contribution from a decoupling pair] one finds that

$$\mathcal{F}^{(2)}(\omega) = \mathcal{F}_{\text{bulk}}^{(1)}(\omega) + \omega \frac{d\mathcal{F}_{\text{bulk}}^{(1)}}{d\omega} + \frac{di_{2qp}(\omega)}{d\omega}. \quad (3.24)$$

Thus it becomes clear that increase in $\mathcal{F}_{\text{bulk}}^{(1)}$ due to pairing decrease (or collapse) or increase in $i_{2qp}(\omega)$ due to strong alignment will give rise to a pronounced maximum

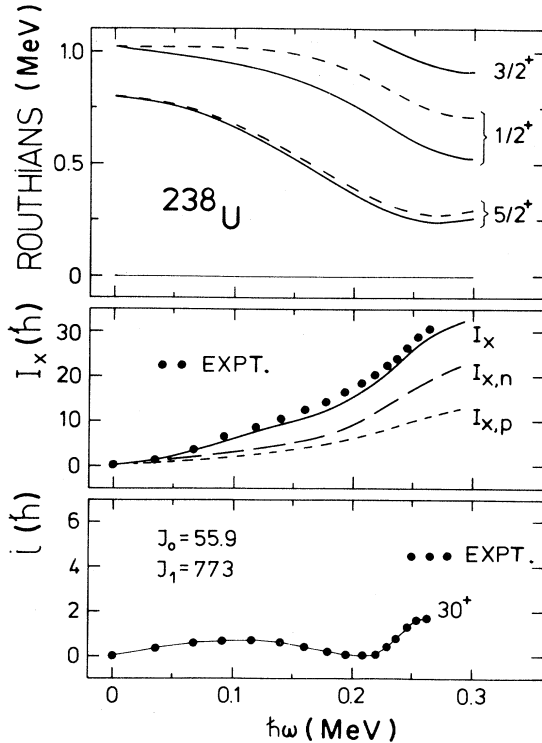


FIG. 25. Quasiparticle Routhians (top), the total angular momentum $I_x(\omega)$ (middle), and the aligned angular momentum $i(\omega)$ (bottom) for the ^{238}U nucleus. Note that even subtle variations in I_x vs ω are reproduced by the pairing self-consistent HFBC calculations with the Woods-Saxon potential (cf. Sec. II.E). The experimental data (points) are from Grosse *et al.* (1981). The increase in aligned angular momentum is correlated with the change in slope of the Routhian curves in the quasiparticle diagram. The small value of the aligned angular momentum can be understood in terms of the strong band interaction $|V| \sim 0.4$ MeV and the smooth behavior of the Routhians as a function of the rotational velocity.

in $\mathcal{F}^{(2)}$ vs ω . For most of the actinide nuclei studied until now the deformation seems to be relatively stable during the deexcitation process (at least for $I \leq 30$). Thus most of the variation in $\mathcal{F}_{\text{bulk}}^{(1)}$ is expected to originate from the variation of pairing. At normal configurations (i.e., after pairing collapse) one may expect that

$$\mathcal{F}^{(2)}(\omega) \approx \mathcal{F}_{\text{bulk}}^{(1)}(\omega) \approx \mathcal{F}^{(1)}(\omega), \quad (3.25)$$

provided that the contribution from the aligning nucleons can be neglected. Figure 24 shows that indeed for $\omega \leq 0.35-0.40$ MeV/ \hbar both moments of inertia $\mathcal{F}^{(1)}$ and $\mathcal{F}^{(2)}$ calculated from the Woods-Saxon spectra are nearly identical ($\Delta_n = \Delta_p = 0$ was set in this auxiliary calculation). The results of Fig. 25 show that (according to the calculations) the effect of the last term in Eq. (3.24) is generally small in most of the discussed frequency range.

Figure 26 shows a comparison between calculated and experimental moments of inertia for ^{238}U ; the lower part of the figure displays also the calculated proton and neu-

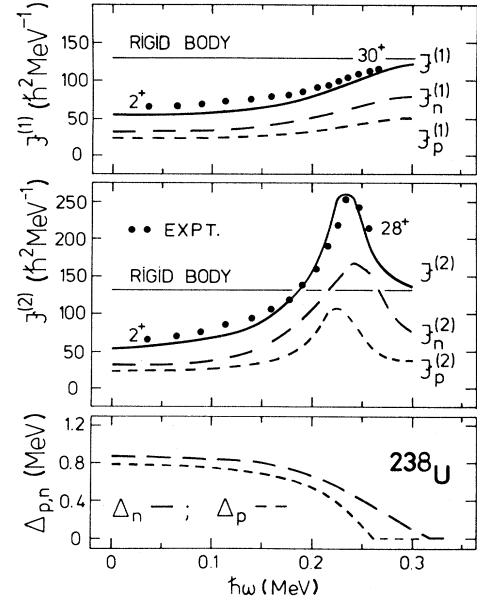


FIG. 26. Comparison between the calculated and the experimental values of the moments of inertia: $\mathcal{F}^{(1)}$ (top) and $\mathcal{F}^{(2)}$ (middle) for the ^{238}U nucleus [the data points are from Grosse *et al.* (1981)]. At the bottom the corresponding proton and neutron pairing energy gaps are also displayed as a function of the rotational velocity. Note that the pairing collapse frequencies are correlated with the characteristic maxima revealed by $\mathcal{F}^{(2)}$ (cf. comments in the caption of Fig. 24).

tron pairing gaps as a function of rotational frequency. The maxima in the moments of inertia $\mathcal{F}^{(2)}$ are clearly correlated with the decrease in pairing correlations. A characteristic behavior of $\mathcal{F}^{(1)}$ and $\mathcal{F}^{(2)}$ (monotonic increase in $\mathcal{F}^{(1)}$ and a pronounced maximum in $\mathcal{F}^{(2)}$), common values at $\omega \approx 0$ [cf. Eqs. (3.22) and (3.24)], and a tendency for the two to merge at some $\omega \sim 0.28$ MeV/ \hbar

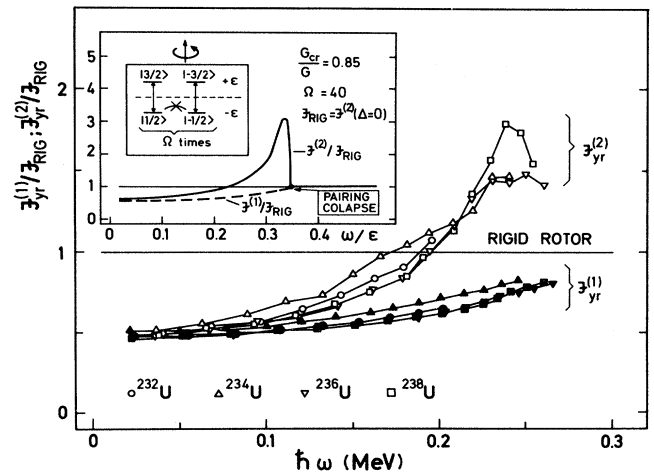


FIG. 27. Comparison between the experimental values of $\mathcal{F}^{(1)}$ (solid symbols) and $\mathcal{F}^{(2)}$ (open symbols) moments of inertia for four uranium nuclei. The inset illustrates the results of the calculation based on the Ω times degenerate two-level model [for experimental data see Grosse *et al.* (1981)].

deserve notice. This behavior is similar for some other actinide nuclei; cf. Fig. 27, where the experimental data for $^{232-234-236-238}\text{U}$ are shown.

Unfortunately, most of the analyses of the alignment effect in actinide nuclei based on the subtraction of the reference-rotor contribution from the total angular momentum contain both effects, i.e., the alignment due to two quasiparticles and that due to reduction in pairing simultaneously. This can be demonstrated by splitting the angular momentum $I(\omega)$ into two parts [cf. Eq. (3.23)]: (a) $i_{2qp}(\omega)$ —contributed by the pair of aligning nucleons, and (b) $I_{\text{bulk}}(\omega)$ —contributed by the rest of the nucleus. Calculating then the “aligned angular momentum,” $i(\omega)$, by

$$\begin{aligned} i(\omega) &= I(\omega) - I_{\text{ref}}(\omega) \\ &= i_{2qp} + [I_{\text{bulk}}(\omega) - (\mathcal{F}_0 + \mathcal{F}_2(\omega)^2)\omega], \end{aligned} \quad (3.26)$$

one includes in $i(\omega)$ the contribution from the square brackets in Eq. (3.26), as well; the latter quantity may in general be different from zero in the actinide nuclei, although in the rare-earth nuclei, where the dramatic alignment often occurs, it can be neglected in the first approximation.

Recent information on the alignment effect in actinide nuclei has been deduced from g -factor measurements in ^{232}Th and ^{238}U employing ^{127}I and ^{142}Nd beams (Häusser *et al.*, 1982). An increase of the g factor from ~ 0.3 to ~ 0.5 in the spin region $I = 18-24$ in both nuclei was interpreted as evidence for the onset of proton effect. More information on g -factor measurements is contained in Sec. IV.B.3 and in Appendix B.

IV. HIGH-SPIN NUCLEAR STRUCTURE STUDIED BY MEANS OF γ -RAY SPECTROSCOPY; NONCOLLECTIVE MOTION, YRAST TRAPS

The observation of high-spin (> 10) isomeric yrast states initiated extensive theoretical studies mainly focused on the explanation of the observed phenomena in terms of noncollective rotation. We have argued in Sec. II.F that such a motion of axially symmetric nuclei with their angular momenta aligned with the symmetry axis results from quantum effects. The calculations lead first of all to the assignment of a nucleonic configuration to each state. In addition, some other properties of nuclear spectra, such as electric quadrupole and magnetic dipole moments, were calculated and compared with the measured values.

An overall characteristic of the spectrum is provided by the average slope of the curve representing the yrast energies as functions of I^2 or $I(I+1)$. In a relatively large range of angular momentum the curve is almost a straight line, when the low-spin part of the spectrum ($I \leq 15$) is neglected. Although there is no collective rotation in this case, we may introduce the moment of inertia $\mathcal{F}_{\text{env}}^{(1)}$ that characterizes this slope according to Eq. (3.3). It is denoted $\mathcal{F}^{(1)}$, since it is determined over a rather large interval in angular momentum. On the other hand, the subscript

“env” has been added to indicate the average over many different configurations (an envelope). This definition appears to be a limiting case of a more general notion of \mathcal{F}_{env} introduced in Sec. V.C. The noncollective character of the motion manifests itself in a particularly irregular excitation pattern which contrasts with the characteristic $\mathcal{E} \sim I(I+1)$ smooth energy-spin dependence in collectively rotating nuclei (cf. Fig. 32 below). Nevertheless, the envelope moment of inertia is of interest, since it describes the ability of the system to increase its angular momentum by means of configuration rearrangements. For simple systems of nucleons moving in a static potential $\mathcal{F}_{\text{env}}^{(1)}$ appears to be of the order of the rigid-body value, $\mathcal{F}_{\text{rigid}}$ (Bohr and Mottelson, 1969).

Owing to an irregular dependence of \mathcal{E} on I the γ -ray energies E_γ of transitions deexciting some yrast states are particularly low. Since the corresponding transition probabilities are $\sim E_\gamma^{2\lambda+1}$ (λ is the transition multipolarity), the corresponding yrast states become long living. The decay of some yrast states may also be hindered because of the local energy minima appearing along the yrast line. Both mechanisms give rise to the existence of yrast isomers referred to as energy traps. Another mechanism possibly leading to occurrence of isomers is due to significant differences in the intrinsic structure between the initial and possible final states involved in the γ -ray transitions. The latter isomers are also called structure traps.

High-spin isomeric states are of particular interest for the study of nuclear structure, because (i) they may serve as reference states helpful for the study of still higher-lying quasicontinuum states (cf. Sec. V) and of discrete states and (ii) they provide information about the single-particle structure at high-spin excitations (the topic of this section).

The $E2$ transitions deexciting the isomeric states are all strongly retarded with respect to rotational values, which may exhibit enhancement factors of 200 W.u. (Weisskopf units). This is a clear indication that they stem from rearrangements in the occupation of single-particle orbitals rather than from collective transitions.

The existence of the high-spin ($I > 10$) isomeric states has been known for a long time near the $Z = 82$, $N = 126$ closed shells ($^{211,212}\text{Po}$). In some of the shell-model calculations (Glendenning, 1962; Auerbach and Talmi, 1964) attempts were made to relate the existence of these isomers to the single-particle level spectrum and the nucleonic residual interaction. A few years later, in a series of pioneering papers Grover and Gilat (Grover and Gilat, 1967a–1967c; Grover, 1967) initiated an extensive study of nuclear properties and decay modes at large angular momenta. In particular, an attempt was made (Grover, 1967) to construct high angular momentum states out of many shell-model orbitals with nucleonic angular momenta aligned parallel to the nuclear symmetry axis.

New interest in the possible existence of yrast traps was initiated by Bohr and Mottelson (1974) who emphasized the importance of the axial symmetry in the potential for the formation of noncollective high-spin states in nuclei. A search for possible regions of nuclei possessing axially

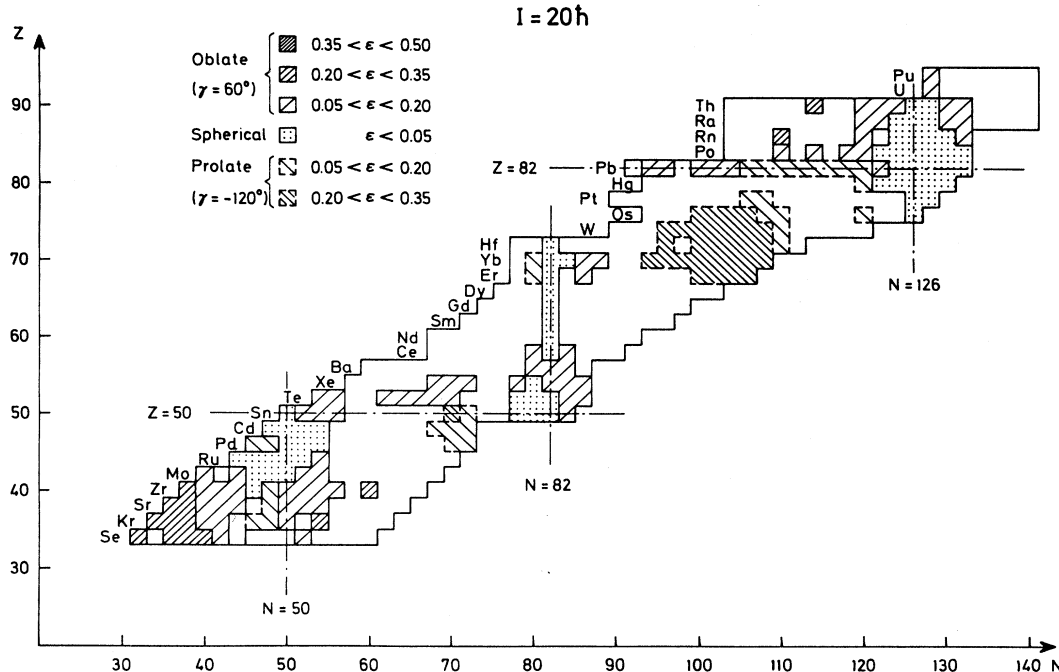


FIG. 28. Various types of nuclear axially symmetric shapes in the (Z, N) plane for spin $I = 20$. Calculations have been performed using the Nilsson potential. The shadowed regions correspond to those areas where yrast traps might *a priori* be expected. Regions which are left blank are most favorable for the collective rotation, and yrast traps are highly unlikely there [from Andersson *et al.* (1978)].

symmetric shapes at high-spin excitations was also carried out by Andersson *et al.* (1978). The results are presented in Figs. 28 and 29, where possible types of nuclear axially symmetric shapes are located in the (N, Z)

plane. Three regions that have been explored most extensively so far are the neutron deficient rare-earth region of $58 \leq Z \leq 70$ and $80 \leq N \leq 88$, the doubly magic ^{208}Pb region of $Z \sim 82$ and $N \sim 126$, and the relatively light nuclei

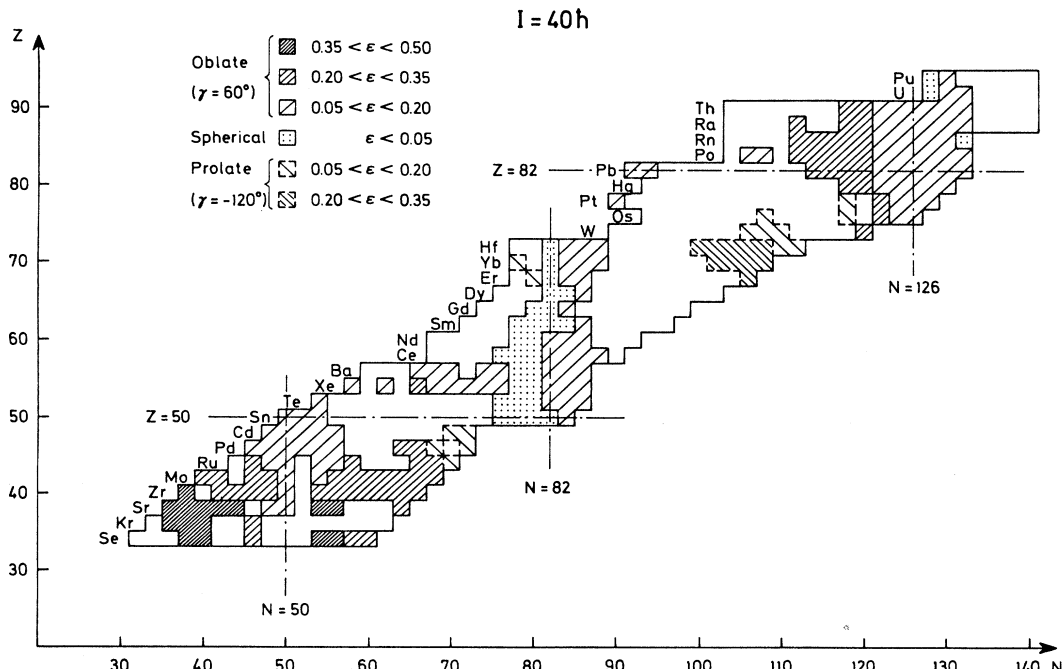


FIG. 29. The same as Fig. 1 but for spin $I = 40$ [from Andersson *et al.* (1978)].

TABLE II. Observed high-spin yrast isomers with $T_{1/2} \gtrsim 1\text{ ns}$ and $I \geq 10$ or $M_r > 5$ in rare-earth nuclei.

Nucleus	E_x (MeV)	$T_{1/2}$ (ns)	M_r	I^π	g	$ \mathbf{M}(L) ^2$ (Wu)	Particle configuration	References
$^{146}_{63}\text{Eu}$	2.5 3.45 ± 0.15	8 135 ± 25	4 6.0 ± 1.0	14 10^+	1.276 ± 0.014	$\pi(d_{5/2}^2 h_{11/2}^1)_{10+} \nu(d_{3/2}^2)_{0^+}$	Hageman, 1981 Borggreen <i>et al.</i> , 1980	
$^{146}_{64}\text{Gd}$	8.916	4.0			≤ 20 0.63 ± 0.09	see Table V	Häusser, 1979 Neergaard <i>et al.</i> , 1981	
$^{147}_{63}\text{Gd}$	2.760	4.8 ± 1.4		$\frac{21}{2}^+$ 0.72 ± 0.11	$E2; 1.6 \pm 0.5$	see Table V	Broda <i>et al.</i> , 1979 Haas <i>et al.</i> , 1981 Neergaard <i>et al.</i> , 1981	
$^{147}_{65}\text{Tb}$	3.582 ^a	27.0 ± 0.7		$\frac{27}{2}^-$ 0.840 ± 0.017	see Table V		Broda <i>et al.</i> , 1978 Haas <i>et al.</i> , 1981 Neergaard <i>et al.</i> , 1981	
$^{148}_{66}\text{Dy}$	8.590 ^a	530 ± 30	12 ± 2	$\frac{49}{2}^+$ 0.446 ± 0.008	$E2; 0.02$ $E3; 2.4$	see Table V	Dössing <i>et al.</i> , 1980 Häusser <i>et al.</i> , 1980 Borggreen <i>et al.</i> , 1980 Broda <i>et al.</i> , 1979 Haas <i>et al.</i> , 1981 Neergaard <i>et al.</i> , 1981	
$^{149}_{66}\text{Gd}$	10.996 3.388	0.80 ± 0.01 6.0 ± 0.5		$(\frac{39}{2}^-)$ $(\frac{27}{2}^+)$	$(E2; 0.006)$ $(E2; 12.0 \pm 1.0)$	see Table V	Dössing <i>et al.</i> , 1980 Häusser <i>et al.</i> , 1980 Baklander <i>et al.</i> , 1982 Haas <i>et al.</i> , 1981 Piparinen <i>et al.</i> , 1980	
$^{147}_{65}\text{Tb}$	2.992	3.5		$(\frac{23}{2}, \frac{25}{2}^+)$	$E3; 44 \pm 11$		Broda, Kleinheinz, Daly, <i>et al.</i> , 1979 Borggreen <i>et al.</i> , 1980 Broda, Kleinheinz, Daly, <i>et al.</i> , 1979 Jastrzebski <i>et al.</i> , 1980 Daly, <i>et al.</i> , 1979 Gui <i>et al.</i> , 1982 Haas <i>et al.</i> , 1981 Daly <i>et al.</i> , 1978	
$^{146}_{66}\text{Dy}$	2.936	150 ± 20 ms	1300 ± 500	13.5 ± 1.0	30 ± 5			
$^{148}_{66}\text{Dy}$	2.918	470 ± 20						

TABLE II. (Continued.)

Nucleus	E_x (MeV)	$T_{1/2}$ (ns)	M_γ	I^π	g	$ \mathbf{M}(L) ^2$ (W.u)	Particle configuration	References
^{149}Dy	2.661	500 ± 30 ms		$\frac{27}{2}^-$			$\pi(h_{11/2}^2)_{10^+} \nu f_{7/2}$	Daly <i>et al.</i> , 1980 Daly <i>et al.</i> , 1980
	7.410+Δ	29 ± 3	7.50 ± 0.5	$\frac{47}{2} \pm 1$				Stefanini <i>et al.</i> , 1976a, 1976b Haas <i>et al.</i> , 1981 Jastrzębski <i>et al.</i> , 1980 Hageman <i>et al.</i> , 1979a, 1979b Kleinheinz, 1979
^{150}Dy	3.026	1.1 ± 0.3		10 ⁺			$\pi(h_{11/2}^3)_{10^+}$	Lunardi <i>et al.</i> , 1979
	4.567	1.7 ± 0.2		16 ⁺			$\pi(h_{11/2})_{10^+} \nu(f_{7/2}^2)_6^+$	Lunardi <i>et al.</i> , 1979
^{151}Dy	2.959	1.3 ± 0.6		$\frac{27}{2}^-$			see Table III	Piiparinen <i>et al.</i> , 1979
	4.904	6.1 ± 1.0		$\frac{41}{2}(-)$			see Table III	Haas <i>et al.</i> , 1981 Piiparinen <i>et al.</i> , 1979 Lister <i>et al.</i> , 1979 Khoo, 1979
	6.032	12.6 ± 0.5	11.0 ± 0.5	$\frac{49}{2}^+$		(M_1 ; 0.16 ± 0.01)	see Table III	Borggreen <i>et al.</i> , 1980 Haas <i>et al.</i> , 1981 Hageman <i>et al.</i> , 1979a, 1979b Piiparinen <i>et al.</i> , 1979 Lister <i>et al.</i> , 1979 Khoo, 1979
^{152}Dy	3.161	4.3 ± 0.9	11	11 ⁻				Nagai <i>et al.</i> , 1980 Haas <i>et al.</i> , 1981 Jansen <i>et al.</i> , 1979 Nagai <i>et al.</i> , 1980 Haas <i>et al.</i> , 1979 Khoo <i>et al.</i> , 1978 Merding <i>et al.</i> , 1979
	5.088	6.0 ± 4		17 ⁺		E2; 16.0 ± 1.0	see Table III	Haas <i>et al.</i> , 1981 Jansen <i>et al.</i> , 1979 Haas <i>et al.</i> , 1979 Khoo <i>et al.</i> , 1978 Merding <i>et al.</i> , 1979
	6.129	9.5 ± 0.7		21 ⁻	0.55 ± 0.08	E2; 0.90 ± 0.08	see Table III	Haas <i>et al.</i> , 1981 Jansen <i>et al.</i> , 1979 Haas <i>et al.</i> , 1979 Khoo <i>et al.</i> , 1978 Merding <i>et al.</i> , 1979
	7.882	1.6 ± 0.2		27 ⁻		E2; 12 ± 2	see Table III	Haas <i>et al.</i> , 1981 Haas <i>et al.</i> , 1979 Khoo <i>et al.</i> , 1978

TABLE II. (Continued.)

Nucleus	E_x (MeV)	$T_{1/2}$ (ns)	M_γ	I^π	g	$ \mathbf{M}(L) ^2$ (Wu)	Particle configuration	References
$^{149}_{67}\text{Ho}$	(2.737)	59 ± 4		($\frac{27}{2}^-$)		$E2; 1.9 \pm 0.2$	$(h_{11/2}^3)_{27/2} -$	Merdinger <i>et al.</i> , 1979
$^{150}_{67}\text{Ho}$	2.625	92 ± 8	6 ± 1	17+		$E2; 3.5 \pm 0.3$	$(h_{11/2}^3)_{27/2} - f_{7/2}$	Hippi <i>et al.</i> , 1982
								Borggreen <i>et al.</i> , 1980
								Jastrzębski <i>et al.</i> , 1980
								Hageman <i>et al.</i> , 1979a,b
								Wilson <i>et al.</i> , 1981
								Borggreen <i>et al.</i> , 1980
								Hageman <i>et al.</i> , 1979a,b
								Jastrzębski <i>et al.</i> , 1980
								Jastrzębski <i>et al.</i> , 1981
								Borggreen <i>et al.</i> , 1980
								Hageman, 1981
								Jastrzębski <i>et al.</i> , 1980
								Jastrzębski <i>et al.</i> , 1980
								Borggreen <i>et al.</i> , 1980
								Hageman, 1981
								Jastrzębski <i>et al.</i> , 1980
								Borggreen <i>et al.</i> , 1980
								Jastrzębski <i>et al.</i> , 1980
								Jastrzębski <i>et al.</i> , 1980
								Radford, 1980
								Jastrzębski <i>et al.</i> , 1980
								Siefanini <i>et al.</i> , 1976a,b
								Hippi <i>et al.</i> , 1982
								Broda, Kleinheinz,
								Daly, <i>et al.</i> , 1979
								Baba <i>et al.</i> , 1981
								Bastin <i>et al.</i> , 1980
								Baba <i>et al.</i> , 1981
								Bastin <i>et al.</i> , 1980
								Borggreen <i>et al.</i> , 1980
								Jastrzębski <i>et al.</i> , 1980
								Baba <i>et al.</i> , 1981
								Borggreen <i>et al.</i> , 1980
								Jastrzębski <i>et al.</i> , 1980
								Holzman <i>et al.</i> , 1980
								Borggreen <i>et al.</i> , 1980
								Jastrzębski <i>et al.</i> , 1980
								Hageman <i>et al.</i> , 1979a,b
								Horn <i>et al.</i> , 1980

TABLE II. (Continued.)

Nucleus	E_x (MeV)	$T_{1/2}$ (ns)	M_γ	I^π	g	$ M(L) ^2$ (Wu)	Particle configuration	References
$^{151}_{51}\text{Tm}$	(2.655)	270 ± 20	9.0 ± 1.0	$(\frac{41}{2} - \frac{45}{2})$				Carlén <i>et al.</i> , 1982
$^{151}_{69}\text{Tm}$	(5.201 + Δ)							Borggreen <i>et al.</i> , 1980
$^{156}_{70}\text{Yb}$	3.028	470 ± 50	6.0 ± 0.5	$(\frac{27}{2}^+)$				Jastrzębski <i>et al.</i> , 1980
$^{154}_{70}\text{Er}$	3.016 + Δ	50 ± 5	5.0 ± 1.0	(10 ⁻ , 11 ⁻)				Hageman <i>et al.</i> , 1979a, 1979b
								Horn <i>et al.</i> , 1980
								Carlén <i>et al.</i> , 1979
								Foin <i>et al.</i> , 1982
								Auger <i>et al.</i> , 1979
								Sunyar, 1979
								Heppi <i>et al.</i> , 1982
								Lister <i>et al.</i> , 1981

^aMeasured quadrupole moments: $|Q| = 1.26 \pm 0.08 \text{ e b}$ for the 3.58-MeV state, and $|Q| = 3.14 \pm 0.17 \text{ e b}$ for the 7.50-MeV state (Häusser *et al.*, 1980).

in the vicinity of Te, Xe, and Ba, with Z ranging from 52 to 56 (cf. Ragnarsson *et al.*, 1975; Andersson *et al.*, 1976; Pomorski and Nerlo-Pomorska, 1977). In the above three papers no definite predictions of the yrast traps are given. The method used was essentially the shell correction method with two level densities (cf. Secs. II.D and II.F). The pairing correlations were not taken into account by these authors. Such an approximation is expected to be good only in the high-spin limit. The region $A=40-80$ has been analyzed by Åberg and Leander (1979). Here again no predictions for definite isomers have been made, although there seems to exist a non-negligible chance for the occurrence of isomers in some nuclei in this region.

The recently increased experimental efforts were in fact triggered by the systematic search for nuclei with high-spin isomers in the region between Ba and Pb carried out by the Copenhagen-Darmstadt collaboration (Pedersen *et al.*, 1977). Delayed γ -ray cascades of high multiplicity were measured by this group after the formation of compound systems with ^{40}Ar , ^{50}Ti , and ^{65}Cu beams from the Unilac at GSI, Darmstadt. A new technique of enhancing high multiplicity (spin) events by means of a multiplicity filter composed of sixteen $5 \times 5 \text{ cm}^2$ NaI(Tl) detectors was employed. In many experimental studies this technique was applied; sometimes use was also made of a sum spectrometer to select the high-energy long (high multiplicity) γ -ray cascades. Those investigations yielded in recent years a wealth of information on the properties of isomeric yrast states, not only concerning final nuclei, excitation energies, spins, and parities, but also electromagnetic transition rates and magnetic dipole and electric quadrupole moments. Detailed quasiparticle structure of yrast states cannot be deduced from electromagnetic transition probabilities only; such details are rather to be expected from the measurements of the magnetic dipole moments of long-lived yrast traps. The quadrupole moments for high-spin states have been explored less; they give supplementary information on the nuclear deformation of yrast traps for which magnetic moments appear to be rather irrelevant.

We will compare experimental data obtained in three mass regions with theoretical results in Sec. IV.A. Selections of isomeric states and their main properties in the rare-earth, hafnium, and lead regions are collected in Tables II, VII, and VIII, respectively, below, as an illustration rather than an attempt to be complete. Technical and experimental details and problems are discussed in Sec. IV.B.

A. Nuclear structure of yrast states; yrast traps

1. The light neutron-deficient nuclei in the rare-earth region

The most intensive searches for yrast traps have been carried out in this mass region. (The results are collected in Table II.) Initial experimental (Pedersen *et al.*, 1977)

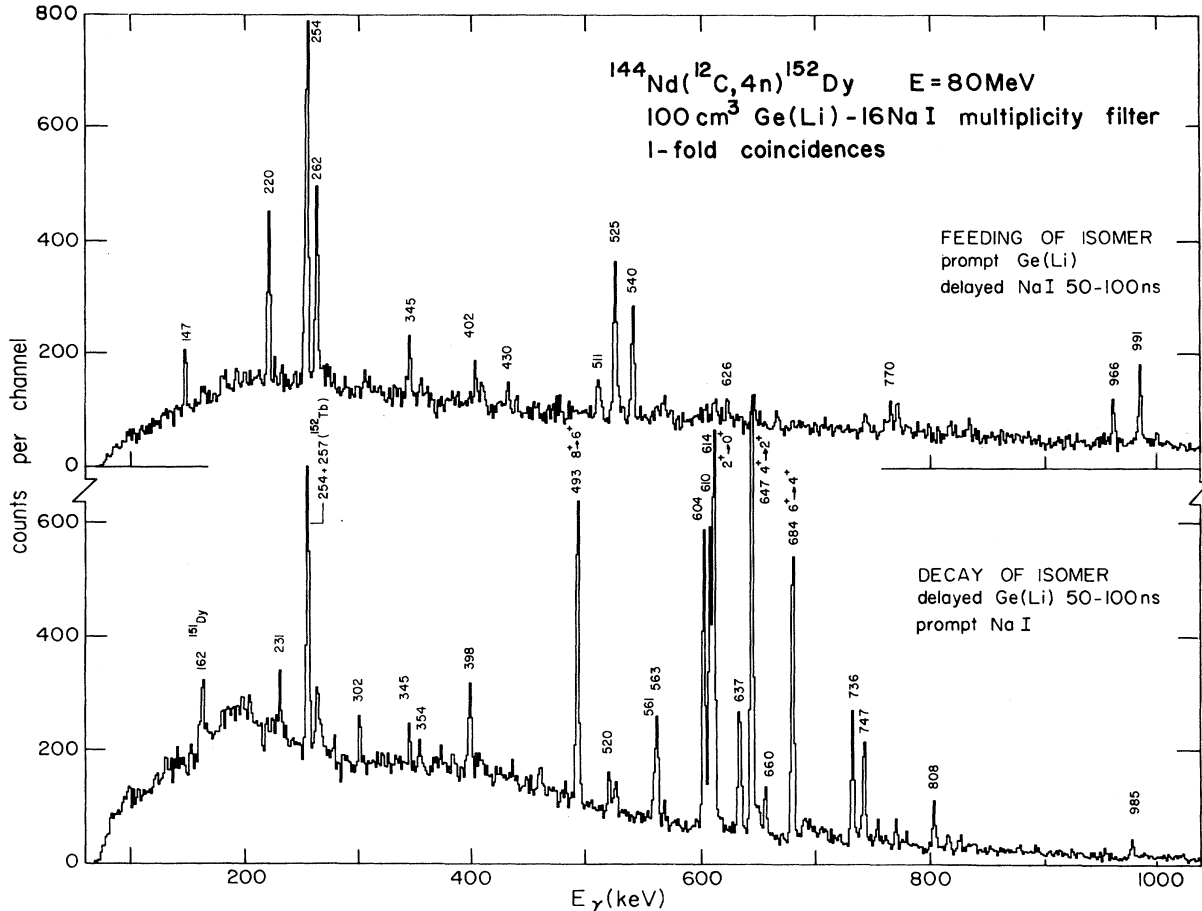


FIG. 30. Illustration of time selection on γ rays with a multiplicity filter. Gamma rays in ^{152}Dy feeding (top) and deexciting (bottom) the 60-ns isomer, as observed with a Ge(Li) detector in coincidence with one out of sixteen NaI(Tl) detectors using a 100-MeV ^{12}C beam (Jansen *et al.*, 1979).

and theoretical (Andersson *et al.*, 1978) searches provided indications for the existence of high-spin isomeric states here.

Experimental setups have always been designed in such a way that the time difference between γ rays feeding and deexciting the isomer could be observed. Depending on the details of the applied technique, the energies E_γ^{del} and multiplicities M_γ^{del} of the delayed transitions could also be measured. From these quantities the excitation energy and spin of the isomeric states have been estimated; from measurements with a sum spectrometer (see Sec. IV.B), in particular, the excitation energies of isomers have been found.

An example of the selection of γ rays feeding and deexciting the 60-ns isomer in ^{152}Dy with the 16 NaI(Tl) detector multiplicity array of the Groningen group is given in Fig. 30. The quantity $\bar{M}_\gamma^{\text{del}}$ is deduced from the Ge(Li) spectra taken in coincidence with one to, say, six NaI(Tl) detectors (out of sixteen) after imposing the proper time restrictions on these detectors. The quantity $\bar{E}_\gamma^{\text{del}}$ is obtained from simultaneously generated NaI(Tl) energy spectra. The work performed with this multiplicity setup

supplemented an extensive conventional γ -ray spectroscopic study of ^{152}Dy (Jansen *et al.*, 1976), which established the decay scheme up to the second isomeric state with $T_{1/2} = 10$ ns at $\mathcal{E}_x = (6077 + \delta)$ keV (Jansen *et al.*, 1979). This nucleus has been a subject of extensive experimental investigations also by several other groups. The Argonne-Chalk River-Strasbourg collaboration (Khoo *et al.*, 1978; Haas *et al.*, 1979, 1981) extended the discrete level scheme to $\mathcal{E}_x = 12.650$ MeV, $I = 37$, including a third isomer in the nanosecond region and seven isomers in the picosecond region. This work included the measurement of linear polarizations with a three-Ge(Li) Compton polarimeter in coincidence with a four-NaI(Tl) detector multiplicity array. A Strasbourg-Cracow collaboration (Merdinger *et al.*, 1979) investigated discrete states up to $I \sim 28$, including the three isomers (in the nanosecond region), and measured also the linear polarizations of γ rays above the first isomer. Moreover, they determined the g factor of the 10-ns isomer as $g = +0.55 \pm 0.06$. Finally, the Jülich group (Nagai *et al.*, 1980) settled the long-standing question (Jansen *et al.*, 1976) about the unobserved isomeric transition δ and es-

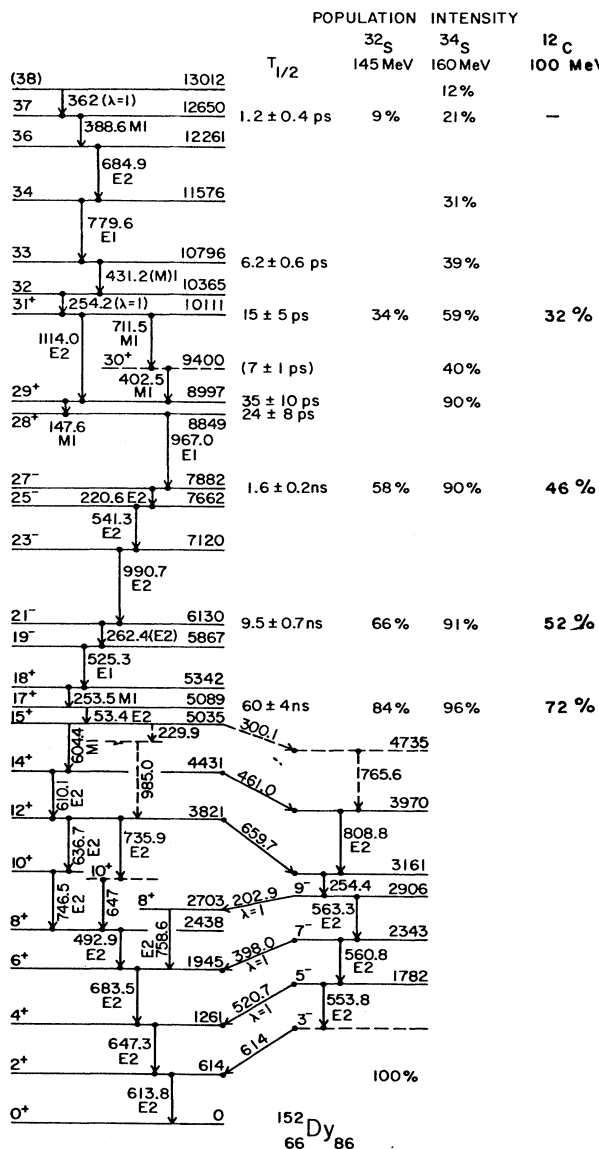


FIG. 31. The level scheme of ^{152}Dy as deduced from the combined evidence of several experiments (Jansen *et al.*, 1976, 1979; Khoo *et al.*, 1978; Haas *et al.*, 1979, 1981; Merdinger *et al.*, 1979). The spin's parities are obtained above the 60-ns isomer and are taken from Haas *et al.* (1979, 1981), using the $M1$ assignment to the 604-keV transition of Nagai *et al.* (1980). The isomeric transition $\delta=53.3$ keV with $E2$ character was measured by Nagai *et al.* (1980). The population intensities refer to reactions induced by ^{32}S and ^{34}S beams (Haas *et al.*, 1981) and by a ^{12}C beam (Hageman, 1981).

tablished its energy as 53.3 keV and its character as $E2$. This finding was confirmed by Haas *et al.* (1981). It establishes the spin and parity of the (60-ns) isomeric state in ^{152}Dy as $I^\pi=17^+$, a result based also on the $M1$ character of the 604.4-keV transition (Nagai *et al.*, 1980). The results of all these investigations on ^{152}Dy are presented in Fig. 31, which illustrates refined γ -ray spec-

troscopic work revealing many yrast traps. It is worth noting that the observation of those very-high-spin states has been facilitated by the use of various heavy-ion beams such as ^{12}C , ^{16}O , and ^{32}S . The level scheme of ^{152}Dy (Fig. 33) deviates from that of Haas *et al.* (1981) only in the sense that in the latter no parity assignments are given for the $I=15$ and higher spin states.

The high-spin spectrum in this nucleus with several isomers has been used by many authors as a test for various versions of theoretical calculations. Table III gives a comparison of some theoretical estimates for single-particle configurations with both deformed and spherical orbitals in ^{151}Dy and ^{152}Dy . Figure 32 illustrates some of the attempts of explaining the yrast line in ^{152}Dy with several different versions of the calculation in comparison with experiment. It can be seen that the discrepancy between theory and experiment in the slope of the yrast line is rather large if no pairing correlations are taken into account (Cerkaski *et al.*, 1979). Leander *et al.* (1979) suggests that the discrepancy may disappear if the pairing correlations are included. The other groups (Faessler and Ploszajczak, 1980; Dudek, 1980; Døssing *et al.*, 1981) emphasize the role of the proper reproduction of the single-particle levels. This may be more important than the inclusion of pairing for a good fit, especially for $I>20$. Finally, the assignments of the spherical shell model (Kleinheinz, 1979) seem to show that the results for ^{151}Dy are similar to those obtained by the use of deformed orbitals (cf. Table III). This agreement is not so surprising, because the deformation arises from the residual interactions, and thus the deformed field simulates the effect of those interactions used in the spherical shell model (Matsuyanagi *et al.*, 1978). Calculations of magnetic dipole moments of isomeric states in ^{152}Dy were performed by Cerkaski *et al.* (1979). The results given in Table IV show among others a value of $g=0.66$ for the 21^- state ($T_{1/2}=10$ ns) which agrees reasonably well with the experimental value of 0.55 ± 0.06 .

An interesting possibility arises in the interpretation of the characteristically irregular pattern for nuclei with spin aligned with the symmetry axis. It consists in decomposing the spectrum of high-spin states into multiplet substructures as discussed below. In the calculation based on deformed single-particle orbitals (cf. Sec. II.F) one may consider in particular the set of particle-hole states in which the particle state is fixed, while the hole states run over the whole j multiplet, or vice versa. In the weakly deformed field of oblate shape, energies $e_\nu(m_\nu)$ lie approximately on inverted parabolas (cf. Fig. 35 below). This is easily seen from the single-particle energies of a $j(m_\nu)$ multiplet in the case of a deformed quadrupole field with the strength parameter κ ; $e_\nu=-\kappa[3m^2-j(j+1)]/[j(j+1)]^{1/2}$. Consequently, the yrast line would reflect this dependence. Figure 33 illustrates this possibility for the analysis of the spectrum in ^{150}Dy . Indeed, one can distinguish the existence of smooth parabolalike branches in the yrast line with the characteristic $E2$ transitions deexciting states within the branch. Moreover, occurrence of isomers is noted on top and at

TABLE III. Configuration assignments of some isomeric states in ^{151}Dy and ^{152}Dy on the basis of deformed and spherical orbitals. Some of the labels include quantum number m , in addition to l and j [for example, $(h_{11/2})_{7/2}$ denotes $l=5, j=\frac{11}{2}$, and $m=\frac{7}{2}$].

^{151}Dy		
I^π	Deformed orbitals (Dudek, 1980)	Spherical shell model (Piiparinen <i>et al.</i> , 1979; Lister <i>et al.</i> , 1979)
$\frac{27}{2}^-$	$\pi(h_{11/2}^2)_{10} + \nu(f_{7/2}^3)_{7/2}^-$	$\pi(h_{11/2}^2)_{10} + \nu(f_{7/2}^3)_{7/2}^-$
$\frac{41}{2}^-$	$\pi(h_{11/2}^2)_{10} + \nu(h_{9/2})_{7/2}^-$	$\pi(h_{11/2}^2)_{10} + \nu(f_{7/2}^2 h_{9/2})_{21/2}^-$
$\frac{49}{2}^+$	$\pi(h_{11/2}^2)_{10} + \nu(f_{7/2} h_{9/2} i_{13/2})_{29/2}^+$	

^{152}Dy		
I^π	Deformed orbitals (Døssing <i>et al.</i> , 1980)	Deformed orbitals (Cerkaski <i>et al.</i> , 1979)
17^-	$\pi(h_{11/2}^2)_0 \nu(f_{7/2}^2 h_{9/2} i_{13/2})_{17}^-$	$\pi\{(h_{11/2})_{9/2}(d_{5/2}^{-1})_{1/2} -\} \nu\{(i_{13/2})_{13/2}(h_{9/2})_{9/2}\} 16^+$
21^-		$\pi\{(h_{11/2})_{9/2}(h_{11/2})_{11/2}\} \nu\{(i_{13/2})_{13/2}(h_{9/2})_{9/2}\}$
27^-	$\pi(h_{11/2})_0 \nu\{f_{7/2}^2 h_{9/2} i_{13/2}\}$	$\pi\{(h_{11/2})_{9/2}(h_{11/2})_{11/2}\} \nu\{(i_{13/2})_{13/2}(f_{7/2})_{5/2}(h_{9/2})_{9/2}(f_{7/2})_{7/2}\}$
31^+	$\pi\{d_{5/2}^{-1}(h_{11/2}^3)_{27/2}\} 14 \nu\{f_{7/2}^2 h_{9/2} i_{13/2}\}$	$\pi\{(h_{11/2})_{9/2}(h_{11/2})_{7/2}(h_{11/2})_{11/2}(d_{5/2}^{-1})_{1/2} -\}$ $\nu\{(i_{13/2})_{13/2}(f_{7/2})_{5/2}(h_{9/2})_{9/2}(f_{7/2})_{7/2}\}$
33^-	$\pi\{d_{5/2}^{-1}(h_{11/2}^3)_{27/2}\} 14 \nu\{f_{7/2}^2 h_{9/2} i_{13/2}^2\}$	

^aExperimental assignment to the 5.088-MeV level is $I^\pi=17^+$.

the bottom of the branch. One can think of the “upper isomer’s” being due to energy hindrance [a small transition energy E_γ and thus small decay probability ($\sim E_\gamma^5$)], while the “lower isomer” is often due to a configuration

trap (see introduction to Sec. IV). The excitation pattern of ^{151}Dy was also interpreted in this spirit (Dudek, 1980). However, in many nuclei an evident decomposition of the excitation pattern into parabolic branches may be very difficult in view of a large number of possible parabolas competing and thus only the nuclei with particularly simple structure (close to doubly magic nuclei) can possibly be treated this way.

Much experimental work was performed on nuclei in the vicinity of the closed neutron shell $N=82$, notably on Gd and Tb isotopes by the Jülich group (cf. Kleinheinz, 1979). Several groups have carried out detailed theoretical analyses on these isotopes (Andersson *et al.*, 1976, 1978; Cerkaski *et al.*, 1977, 1979; Leander *et al.*, 1979; Døssing *et al.*, 1980, 1981; Dudek, 1980) in terms of the deformed independent-particle orbitals or (Kleinheinz, 1979; Broda, Kleinheinz, Lunardi, and Blomqvist, 1979; Häusser, 1979) on the basis of a spherical shell model with two-body residual interaction. Energy-level schemes can thus be interpreted in terms of configurations obtained from the spherical shell model as well as from deformed orbitals. This has been done, for example, for ^{146}Gd , ^{147}Tb , and ^{147}Gd , including most of the states below $I \sim 18$, and also including isomeric states. The agreement between the results obtained for the configura-

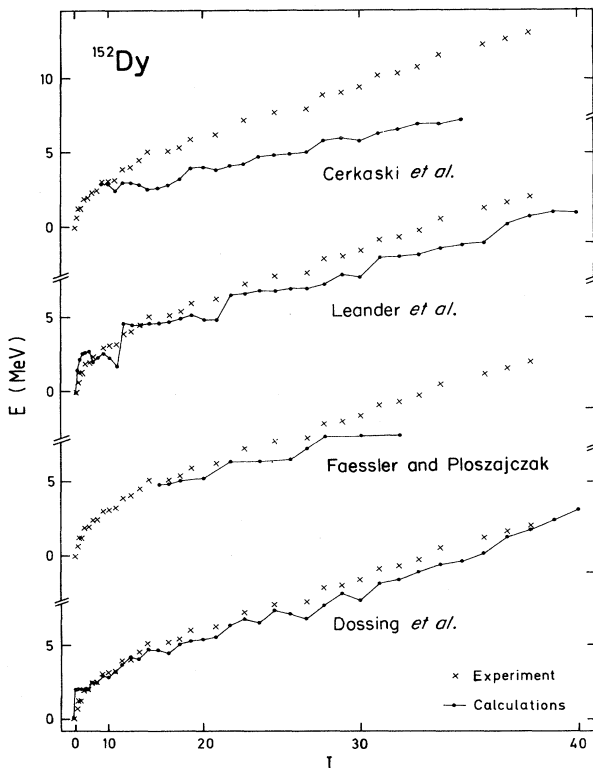


FIG. 32. Comparison of the experimental data with the calculations of the yrast line by different groups based on various assumptions on the single-particle levels and nucleonic residual interaction in the nucleus ^{152}Dy [from Døssing *et al.* (1981)].

TABLE IV. Calculated gyromagnetic factors g and magnetic moments μ for the predicted yrast traps in ^{152}Dy . (From Cerkaski *et al.*, 1979.)

I^π	g	μ
16^+	0.44	7.00
21^-	0.66	13.61
27^-	0.39	10.54
30^+	0.34	10.26
31^+	0.55	16.90

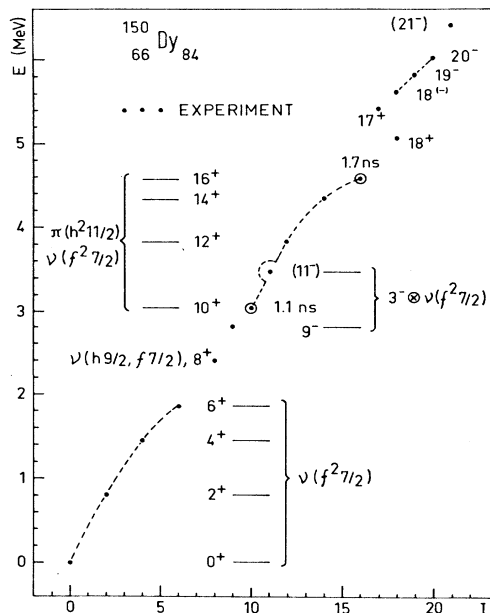


FIG. 33. Experimental high-spin excitations in ^{150}Dy (Kleinheinz, 1979). Points belonging to the same j -multiplet configuration are connected by dashed lines (Dudek, 1980).

tion assignments within the two methods is very good [cf. Kleinheinz (1979) and references quoted therein, and Dudek (1980)]. The comparison of the results calculated using the shell correction method and the experimental data

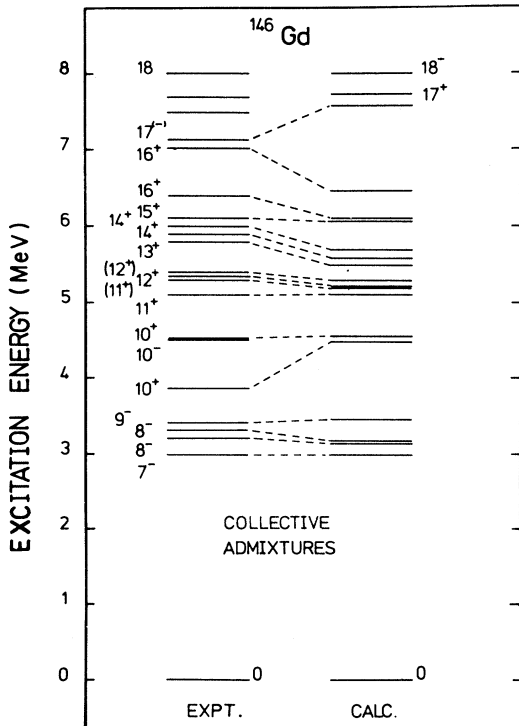


FIG. 34. High-spin excitations in ^{146}Gd . Experimental results from Kleinheinz (1979) are compared with calculations based on shell-correction plus particle-hole analysis employing the Woods-Saxon potential (Dudek *et al.*, 1982a).

for ^{146}Gd are given in Fig. 34, as an example. Figures 34 and 35 display the results of taking pairing interactions into account via the pairing correction term with blocking; also, the projection onto the correct particle number was performed. It has generally been found that inclusion of these features improves considerably the agreement with experiment. The results are very sensitive to the single-particle level spectrum used. This property can sometimes be applied for extracting information about single-particle level energy differences. This is illustrated in Fig. 35, where the experimental excited-state energies of ^{147}Tb (right-hand side) are plotted together with the single-particle Woods-Saxon levels used for the interpretation of the high-spin states (left-hand side). The proton single-particle excitations lead, among other states, to a sequence of configurations with spins $\frac{19}{2}^+, \frac{21}{2}^+, \dots, \frac{27}{2}^+$, which correspond to observed yrast states. By comparing left- and right-hand sides of the figure one can observe how the high-spin excitations can be created in terms of single-particle excitations. In addition, taking into account, for instance, the experimental difference between yrast and yrare states at $I'' = \frac{25}{2}^+$ (denoted by δ_{expt} in the figure) one can conclude that the difference between $h_{11/2}$ and $g_{7/2}$ orbital energies is exaggerated in the calculation as compared to the analogous difference for $d_{5/2}$ and $h_{11/2}$ orbitals. Thus one arrives at the conclusion that the theoretical $d_{5/2} - g_{7/2}$ difference should be diminished. The model dependence of the single-particle structure of high-spin states (due to the sensitivity for the interactions employed) is illustrated in Table V, based on results from Døssing *et al.* (1980), Dudek (1980), Kleinheinz (1979), and Häusser (1979). This table displays some of the recent results in the assignments of the configurations in terms of spherical or deformed orbitals for some isomeric high-spin states in the ^{146}Gd and ^{147}Gd nuclei. Further

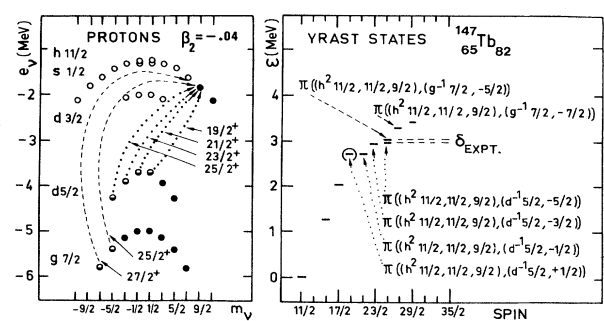


FIG. 35. Illustration of the particle-hole structure of high-spin states in $^{147}\text{ Tb}$. On the left is given the proton single particle energy e_v as a function of the angular momentum m_v calculated using the Woods-Saxon potential. The ground state is indicated by the occupied $h_{11/2}, m_v = \frac{11}{2}$ level (dot). High-spin excitations are indicated by promotions of $d_{5/2}$ or $g_{7/2}$ particles to the $h_{11/2}$ levels (with the least energy difference and maximum gain in spin). The results of the configurations are indicated in the experimental yrast spectrum on the right and in fact correspond to the observed spins, although the calculated excitation energies are systematically too large (see text). The figure is taken from Dudek (1980).

TABLE V. Configuration assignments of some calculated yrast traps in ^{146}Gd and ^{147}Gd .^a

I^π	Deformed orbitals ^b	^{146}Gd		Spherical shell model
		Deformed Woods-Saxon orbitals ^c		
10 ⁺	$\pi\{(d_{5/2}^{-2})_0 h_{11/2}^2\}$	$\pi\{(h_{11/2})_{10}^2 (d_{5/2})^{-2}\}$		$\pi\{(h_{11/2})_{10} (d_{5/2}^{-2})\}^d$
20 ⁻	$\pi\{(d_{5/2}^{-2})_0 h_{11/2}^2\} \nu\{(d_{3/2}^{-2})_0 f_{7/2} i_{13/2}\}$			
25 ⁺	$\pi\{(d_{3/2}^{-3})_{3/2} h_{11/2}^3\} \nu\{(d_{3/2}^{-2})_0 f_{7/2} i_{13/2}\}$			
^{147}Gd				
$\frac{21}{2}^+$		$\pi\{h_{11/2} d_{5/2}^{-1}\} \nu(f_{7/2})$		$\pi\{d_{5/2}^{-1} h_{11/2}\} \gamma \nu(f_{7/2})^e$
$\frac{27}{2}^-$	$\pi\{(d_{5/2}^{-2})_0 h_{11/2}^2\} \nu(f_{7/2})$	$\pi\{h_{11/2} d_{5/2}^{-1}\} \nu(i_{13/2})$		$\pi\{d_{5/2}^{-2} h_{11/2}^2\}_{10} \nu(f_{7/2})^e$
$\frac{41}{2}^-$	$\pi\{(d_{5/2}^{-2})_0 h_{11/2}^2\} \nu\{d_{3/2}^{-1} (f_{7/2} i_{13/2})_{10}\}_{21/2}^-$			
$\frac{49}{2}^+$	$\pi\{(d_{5/2}^{-2})_0 h_{11/2}^2\} \nu\{(d_{3/2}^{-2})_0 f_{7/2} h_{9/2} i_{13/2}\}_{29/2}^+$			$\pi\{d_{5/2}^{-2} h_{11/2}^2\}_{10} \nu\{h_{11/2}^{-1} i_{13/2} f_{7/2}\}_{29/2}^+e$
$\frac{59}{2}^-$	$\pi\{(d_{5/2}^{-3})_{3/2} h_{11/2}^3\} \nu\{(d_{3/2}^{-2})_0 f_{7/2} h_{9/2} i_{13/2}\}_{29/2}^+$			

^aComparison is made between various versions of the calculation.

^bDøssing *et al.*, 1980.

^cDudek, 1980.

^dKleinheinz, 1979 (no isomer observed with $I^\pi = 10^+$).

^eHäusser *et al.*, 1979, and Häusser, 1979.

comparisons among the methods show that the differences in the theoretical structure assignments to states with not too high spins ($I < 20$) are not big, and thus various approaches turn out to yield consistent results.

Observation of the quadrupole moments as a function of the excitation energy within one nucleus is of interest in view of the detection of possible shape changes. A fortunate situation where data are available occurs for ^{147}Gd (Häusser *et al.*, 1980), with measured g factors and quadrupole moments for the $\frac{13}{2}^+$, $\frac{27}{2}^-$, and $\frac{49}{2}^+$ yrast traps (see Table II). The absolute values of the quadrupole moments are 0.73, 1.26, and 3.14 e b, which would imply effective neutron charges of 2.0, 2.9, and > 3 , respectively, to bring pure shell-model values into agreement with experiment. A somewhat different neutron configuration (for instance, including the $h_{9/2}$ orbital) would decrease the effective charge without much affecting the magnetic moment. Alternatively, the large quadrupole moments have been explained (Häusser *et al.*, 1980) with bare nucleon charges by assuming that the high spins are generated by quasiparticles aligned with the rotation axis of an oblate deformed core. The deformation has been calculated to take the substantial value of $\beta_2 \sim -0.2$ for the $\frac{49}{2}^+$,

$T_{1/2} = 530$ ns isomer.

In the calculations by Cerkaski *et al.* (1979) and Døssing *et al.* (1981) (see also references quoted therein) the magnetic dipole and electric quadrupole moments of nuclear high-spin states were also obtained. The results for the magnetic moments seem generally to confirm the configuration assignments and are in line with the existing experimental data. Calculations of the quadrupole moments indicate rather weak oblate deformations in some isomeric states in ^{147}Gd which seem also to be in line with the few existing data. It is worth noting here a slight but systematic increase with spin (on the average) in the calculated oblate equilibrium deformations (cf. Figs. 28 and 29). Such an effect can be understood in terms of increasing polarization of the nuclear matter distribution in the equatorial plane of the nucleus, when more and more nucleons align their angular momenta with the symmetry axis. The experimental data, however, provide only the absolute value of the quadrupole moment, while its negative sign does not seem to be confirmed yet in a clear-cut experiment. Table VI shows a comparison between the calculated and measured values of Q and g of some of the high-spin states of ^{147}Gd (from Døssing

TABLE VI. Electromagnetic moments of observed isomers in ^{147}Gd . Column 1 lists spin and parity of the isomer. Columns 2–5 list the calculated values of the deformation parameter, the liquid-drop quadrupole moment, the “microscopic” quadrupole moment, and the gyromagnetic factor. The last three columns give the measured half-life, the quadrupole moment (absolute value), and the gyromagnetic factor. The table is taken from Døssing *et al.* (1980).

I^π	β	Calculation (Døssing <i>et al.</i> , 1980)			g	Experiment (Häusser <i>et al.</i> , 1979, 1980)		
		Q_{ld} (e b)	Q (e b)			$t_{1/2}$ (ns)	$ Q $ (e b)	g
$\frac{13}{2}^+$	-0.03	-0.52	-0.44	-0.18	22.2(5)	0.73(7)	-0.04(1)	
$\frac{27}{2}^-$	-0.05	-0.82	-1.25	0.81	26.8(7)	1.26(6)	0.84(2)	
$\frac{49}{2}^+$	-0.17	-2.78	-2.99	0.47	510(20)	3.14(17)	0.45(1)	

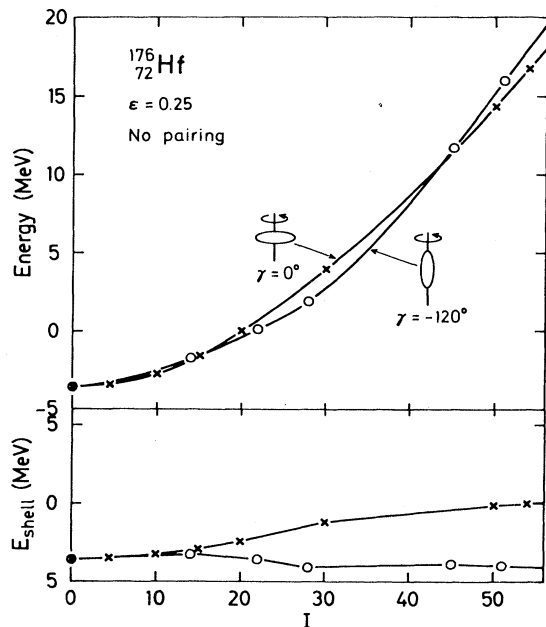


FIG. 36. The total energy (upper part) and the shell energy (lower part) plotted vs the total angular momentum I for ^{176}Hf at a fixed prolate deformation. The rotation takes place around the axis with the largest moment of inertia ($\gamma=0^\circ$, collective rotation, crosses) or, alternatively, around the axis with the smallest moment of inertia ($\gamma=-120^\circ$, noncollective rotation, open circles). The calculation was performed with the Nilsson potential [from Åberg (1978)].

et al., 1980). A significant jump in deformation at $I^\pi = \frac{49}{2}^+$ for ^{147}Gd (confirmed experimentally) is here an interesting consequence of irregularities in the intrinsic structure along the yrast line, characteristic of nuclei with the total spin aligned with the symmetry axis. According to the calculations (Døssing *et al.*, 1980), the deformation jump is due to the promotion of a neutron pair across the $N=82$ gap.

Another prediction for the existence of a rather exotic region of high spin ($I > 44$), strong deformation ($\epsilon_2 \sim 0.4, \gamma \sim 60^\circ$), and possible yrast traps was made by Døssing *et al.* (1977) (see also Bohr and Mottelson, 1977) for nuclei with $N=82$ and 84 neutrons and $Z=62-70$ protons. The region would be related to an expected strong shell effect, with nuclear shape corresponding to the ratio of axes close to 2:3. The existence of isomers in this region, however, has not been confirmed up to now experimentally.

2. The hafnium isotopes

In the above discussion we have limited ourselves only to the case of yrast traps in nuclei with oblate shape. Let us now turn our discussion to the possibility for the occurrence of yrast traps in axially symmetric nuclei of prolate shape. Although the corresponding envelope moment of inertia for the noncollective rotation in this case

($\gamma = -120^\circ$) is generally lower than that for the collective nuclear rotation ($\gamma = 0^\circ$), one may expect that in some peculiar cases a very strong shell effect may lower the noncollective states in prolate nuclei down to the yrast line, which is mainly composed of the collective ($\gamma = 0^\circ$) bands (cf. Sec. II.E). In an experimental study of ^{176}Hf Khoo *et al.* (1976) interpreted observed yrast traps as due to alignment of single-particle orbitals with the symmetry axis of a prolate deformed nucleus. A typical example may be provided by the island of nuclei around ^{176}Hf (Faessler and Ploszajczak, 1977; Åberg, 1978; Andersson *et al.*, 1978). Figure 36 illustrates the total energy and shell correction calculated for this nucleus by Åberg (1978) on the basis of the rotating Nilsson potential. It is seen that the shell effects for the noncollective rotation ($\gamma = -120^\circ$) are exceptionally large and negative, thus leading to the preference of the system for this type of motion over the collective rotation about another axis ($\gamma = 0^\circ$) in the spin region of $15 \leq I \leq 43$.

From Table VII it can be seen that the lifetimes and transition retardation factors for the Hf isotopes are in general much larger than for rare-earth nuclei (Table II). The four or six (high-spin) quasiparticle isomeric states are well described in terms of the Nilsson model with high Ω (projection of single-particle spin on the symmetry axis of a prolate deformed nucleus). Thus high- K (projection of summed single-particle spins) states are formed with less energy than is required by the collective motion at the same angular momentum. Those high- K band-heads are thus lower in energy than the ground-state band with the same spin and appear as a peculiar sort of yrast traps which can only decay by K -forbidden transitions. The Hf isotopes thus exhibit at the same time well-developed rotational bands, due to collective motion, and yrast traps as K isomers, due to quasiparticle alignment.

3. The lead region

Let us now discuss high-spin properties of nuclei around the doubly magic ^{208}Pb nucleus. A considerable amount of experimental data exists in this region for many nuclei, as can be seen from Table VIII and original papers cited there. This domain has been thoroughly analyzed by the methods of the spherical shell model, as already mentioned in Sec. II.F.

As an example, let us take the spectrum of ^{212}Rn (Fig. 37). The experimental spectrum is known up to $I^\pi = 30^+$. Calculations have been performed both for the spherical shell model [see Blomqvist (1979) and references quoted therein] and the deformed fields with the Nilsson and Woods-Saxon potentials (Andersson *et al.*, 1978; Matsuyanagi *et al.*, 1978; Døssing *et al.*, 1977; Dudek, Szymański, and Werner, 1981). Table IX lists possible configuration assignments. The similarity between the assignments reached in different ways is significant. It results from a big effect of the shell closures at $Z=82$ and $N=126$. As a consequence, only a few single-particle orbitals are active in $I < 20$ excitations (the proton $h_{9/2}$,

TABLE VII. Observed high-spin yrast isomers with $T_{1/2} \geq 1$ ns and $I \geq 10$ in the hafnium isotopes.

Nucleus	E_x (MeV)	$T_{1/2}$ (ns)	I^π	g	$ M(J) ^2$ (W.u.)	Particle configuration	References
$^{171}_{\text{Hf}}/2$	1.985	18 ± 2	$\frac{23}{2}^-$		$E1; 1.6 \times 10^{-6}$	$\pi(g_{7/2}h_{11/2})_8^- \nu(i_{13/2})_{7/2}^+$	Dracoulis and Walker, 1979
$^{173}_{\text{Hf}}$	1.984	19.5 ± 0.6	$\frac{23}{2}^-$	0.57 ± 0.02	$E1; 2.4 \times 10^{-6}$	$\pi(g_{7/2}h_{11/2})_8^- \nu(i_{13/2})_{7/2}^+$	Walker <i>et al.</i> , 1980
$^{174}_{\text{Hf}}$	3.269	$3.9 \mu\text{s}$	(12)				Kho, 1981
$^{175}_{\text{Hf}}$	1.766	1.16 ± 0.11	$\frac{23}{2}^-$		$E1; 30 \times 10^{-6}$	$\pi(g_{7/2}h_{11/2})_8^- \nu(i_{13/2})_{7/2}^+$	Dracoulis and Walker, 1980
	3.312	$3.7 \mu\text{s}$	(14^-)			$\pi(g_{7/2}h_{11/2})_8^- \nu(i_{13/2})_{7/2}^+ (h_{9/2})_{5/2}^- (h_{9/2})_{7/2}^-$	Dracoulis and Walker, 1980
	3.015	1.21 ± 0.15 μs	$(\frac{35}{2}^-)$			$\pi(g_{7/2}h_{11/2})_8^- \nu(f_{7/2}h_{9/2})_6^+$	Kho <i>et al.</i> , 1976
$^{176}_{\text{Hf}}$	2.866	$401 \mu\text{s}$	14^-			$\pi(g_{7/2}h_{11/2})_8^- \nu(f_{7/2}i_{13/2}h_{9/2}p_{3/2})_{11}^-$	Kho <i>et al.</i> , 1976
	4.377	34	19^+			$\pi(g_{7/2}h_{11/2})_8^- \nu(f_{7/2}i_{13/2}h_{9/2}h_{9/2})_{14}^+$	Kho <i>et al.</i> , 1976
	4.864	$43 \mu\text{s}$	22^-		$E2; 0.005$		Ellis and Harmatz, 1975
$^{177}_{\text{Hf}}^m$	1.315	1.08 ± 0.06 s	$\frac{23}{2}^+$		$E2; \sim 10^{-7}$		Kho, 1981
	1.343	$56 \mu\text{s}$	$\frac{19}{2}^-$				Ward and Haustein, 1971
	2.740	51 months	$\frac{37}{2}^-$				
$^{178}_{\text{Hf}}^m$	2.446	3.10 ± 1.0 yr	16^+		$E3; \sim 10^{-7}$	$\pi(g_{7/2}h_{11/2})_8^- \nu(f_{7/2}i_{13/2})_8^-$	Van Klinken <i>et al.</i> , 1980;
$^{179}_{\text{Hf}}^m$	1.106	24.8 ± 0.3 d	$\frac{25}{2}^-$			$\pi(g_{7/2}h_{11/2})_8^- \nu(i_{13/2})_{9/2}^+$	Kho and Løvhøiden, 1977
							Hübel <i>et al.</i> , 1970

$f_{7/2}, i_{13/2}$; they are described by the discussed models in a similar way, and thus the results for the high-spin structure are almost identical. For higher spins new orbitals become active (the neutron $p_{1/2}$, $g_{9/2}$, and $j_{15/2}$), and the fact that neutrons and protons contribute now in the yrast states makes the final result more sensitive with respect to small details of the models. As a consequence, the number of discrepancies among the results from various models increases for $I > 20$.

The static magnetic moments (or, equivalently, g factors) are sensitive to details of the intrinsic structure of the isomeric states. The distinct change in the g factor as a function of spin observed for $I > 20$ in ^{212}Rn is evident from Fig. 38, where the excitation energies and g factors are plotted versus $I(I+1)$. The g factors calculated on the basis of the aligned-particle configurations (Horn *et al.*, 1977) given in Table IX agree very well with the experimental values. This establishes the transition from a pure four-valence proton structure to a mixed proton-neutron configuration in the wave functions of states above $I=20$ in ^{212}Rn .

4. Collective excitations

We shall terminate this section by discussing briefly the possible excitation modes that may be superimposed on a nuclear state in which several orbitals have already been strongly aligned (for example, an yrast trap with spin I). One of the possible excitation modes is the transverse rotation of the system, i.e., the rotation about an axis perpendicular to the alignment axis (Bohr and Mottelson, 1981; Andersson, Krumlinde *et al.*, 1981). The nuclear field related to the excitation mode of this type is of the $Y_{2\pm 1}$ character ($\Delta I = \pm 1$) and may lead to the occurrence of a band with spin sequence $I, I+1, I+2, \dots$, originating from the yrast trap and extending fairly above the yrast line. Figure 39 illustrates schematically the bands calculated within the random-phase approximation for these excitations, sticking out of the yrast line (for the ^{212}Rn nucleus, Andersson, Krumlinde *et al.*, 1981). The calculated moments of inertia for the bands turn out to be rather low—in fact, considerably below the corresponding rigid-body estimates.

Another possible excitation of the system in the highly aligned state is the nonaxial vibration $\Delta I = 2$ (gamma vibration) related to the field of the $Y_{2\pm 2}$ symmetry (Bohr and Mottelson, 1981; Andersson and Krumlinde, 1977; Andersson, Krumlinde *et al.*, 1981; Böttges *et al.*, 1981). The first excited state would then have spin $(I+2)$. There are good chances that these vibrations may lead to bands lying below the rotational $\Delta I = 1$ bands in the case of a weak particle-core coupling, while for a strong coupling the transverse rotational band may lie below the $(I+2)$ vibrational band (Bohr and Mottelson, 1981). The relative importance of the two possible excitation modes and perhaps of some other relevant modes has not yet been fully analyzed and seems to require further clarifica-

TABLE VIII. Observed high-spin yrast isomers with $T_{1/2} \gtrsim 1$ ns and $I \geq 10$ or $M_y^{\text{del}} \geq 5$ in the lead region.

Nucleus	E_x (MeV)	$T_{1/2}$ (ns)	I^π	g	$ M(L) ^2$ (W.u.)	Particle configuration	References
$^{196}_{82}\text{Pb}$	$\sim 2.7^a$	2690 ± 50	12^+		$E2; 0.53 \pm 0.07$	$\nu(i_{13/2}^2)_{12}+$	Zywietz <i>et al.</i> , 1981
$^{198}_{82}\text{Pb}$	$\sim 2.8^a$	2240 ± 40	12^+		$E2; 0.67 \pm 0.07$	$\nu(i_{13/2}^2)_{12}+$	Zywietz <i>et al.</i> , 1981
$^{200}_{82}\text{Pb}$	3.10^a	194 ± 6	12^+	-0.157 ± 0.006	$E2; 0.79 \pm 0.08$	$\nu(i_{13/2}^2)_{12}+$	Mahnke <i>et al.</i> , 1979
$^{205}_{82}\text{Pb}$	3.199	217 ± 5	$\frac{25}{2}^-$	-0.067 ± 0.0011	$E2; 0.62 \pm 0.02$	$\nu(p_{1/2}^- i_{13/2}^-)_{25/2}^-$	Linden <i>et al.</i> , 1976
	5.158	71 ± 3	$\frac{33}{2}^+$	-0.159 ± 0.008	$E3; 0.09 \pm 0.01$	$\nu(i_{13/2}^-)_{33/2}^+$	Linden <i>et al.</i> , 1976
					$E2; 0.63 \pm 0.07$	$\nu(i_{13/2}^3)_{33/2}^+$	
$^{206}_{82}\text{Pb}$	4.02^a	198 ± 6	12^+	-0.155 ± 0.005	$E3; 0.17 \pm 0.02$	$\nu(i_{13/2}^-)_{12}+$	Mahnke <i>et al.</i> , 1979; Linden <i>et al.</i> , 1976;
					$E3; 0.15 \pm 0.03$	$\nu(i_{13/2}^-)_{12}+$	Bergström <i>et al.</i> , 1971
					$E3; 0.33 \pm 0.04$	$\nu(i_{13/2}^-)_{12}+$	Broda <i>et al.</i> , 1982
$^{207}_{83}\text{Bi}$	$1.932(+\Delta)$	210 ± 20	$(\frac{21}{2}^+, \frac{25}{2}^+)$	$(E2; 0.11)$			
	2.740	160 ± 30	$(\frac{29}{2}^-)$				
$^{202}_{83}\text{Bi}$	$0.598+\Delta$	3.04 ± 0.06 μs	10^-	0.255 ± 0.003	$\pi(h_{9/2})_{9/2} - \nu(i_{13/2}^-)_{13/2}^+$		Thirumala Rao <i>et al.</i> , 1981; Hübel <i>et al.</i> , 1982
$^{203}_{83}\text{Bi}$	$2.590+\Delta$	3.10 ± 50	(17^+)	0.121 ± 0.003	$\pi(h_{9/2})_{9/2} - \nu(p_{1/2}^- i_{13/2}^-)_{13/2}^+$		Thirumala Rao <i>et al.</i> , 1981; Hübel <i>et al.</i> , 1982
	1.990	90 ± 7	$(\frac{21}{2}^+)$	0.266 ± 0.004	$\pi(h_{9/2})_{9/2} - \nu(i_{13/2}^-)_{13/2}^+$		Hübel <i>et al.</i> , 1982; Lönnroth 1982
	$(1.99+\Delta)$	(~ 190)	$(\frac{25}{2}^+)$				
$^{205}_{83}\text{Bi}$	2.06	100 ± 6	$(\frac{21}{2}^+)$	0.257 ± 0.004	$\pi(h_{9/2})_{9/2} - \nu(i_{13/2}^-)_{13/2}^+$		Hübel <i>et al.</i> , 1982; Lönnroth 1982
			~ 220		$\pi(h_{9/2})_{9/2} - \nu(i_{13/2}^-)_{13/2}^+$		
	$2.06+\Delta$		$(\frac{25}{2}^+)$		$\pi(h_{9/2})_{9/2} - \nu(p_{1/2}^- i_{13/2}^-)_{25/2}^-$		Lönnroth <i>et al.</i> , 1978
$^{206}_{83}\text{Bi}$	1.045	$880 \mu\text{s}$	10^-		$\pi(h_{9/2})_{9/2} - \nu(p_{1/2}^- i_{13/2}^-)_{25/2}^-$		Lönnroth <i>et al.</i> , 1978
	3.148	15.0 ± 1.0	15^+		$\pi(h_{9/2})_{9/2} - \nu(p_{1/2}^- i_{13/2}^-)_{25/2}^-$		Blomqvist, 1979
$^{207}_{83}\text{Bi}$	2.102	$180 \mu\text{s}$	$\frac{21}{2}^+$		$\pi(h_{9/2})_{9/2} - \nu(p_{1/2}^- i_{13/2}^-)_{25/2}^-$		Blomqvist, 1979
	3.888	13	$\frac{29}{2}^-$		$\pi(h_{9/2})_{9/2} - \nu(i_{13/2}^-)_{12}^+$		Blomqvist, 1979
$^{208}_{83}\text{Bi}$	1.571	2.5 ms	10^-		$\pi(h_{9/2})_{9/2} - \nu(i_{13/2}^-)_{13/2}^+$		Blomqvist, 1979
$^{209}_{83}\text{Bi}$	2.986	18	$\frac{19}{2}^+$		$\pi(h_{9/2})_{9/2} - \nu(g_{9/2} p_{1/2}^-)_{13/2}^+$		Blomqvist, 1979
$^{205}_{84}\text{Po}$	2.224	1.73	$\frac{25}{2}^+$		$E2; 1.3$		Fant <i>et al.</i> , 1982
	3.087	83	$(\frac{29}{2}^-)$				Fant <i>et al.</i> , 1982
$^{207}_{84}\text{Po}$	$2.314+\Delta$	28	$\frac{25}{2}^+$				Fant <i>et al.</i> , 1982
$^{209}_{84}\text{Po}$	2.770	2.5 ± 0.7	$\frac{23}{2}^+$		$\pi(h_{9/2} i_{13/2})_{11} - \nu(p_{1/2}^-)_{1/2}^-$		Blomqvist, 1979; Bergström <i>et al.</i> , 1974
	4.226	118 ± 3	$\frac{31}{2}^-$		$\pi(h_{9/2} i_{13/2})_{11} - \nu(g_{9/2} p_{1/2}^-)_{1/2}^-$		Blomqvist, 1979; Bergström <i>et al.</i> , 1974
$^{210}_{84}\text{Po}$	2.849	24 ± 3	11^-	1.116 ± 0.017	$E3; 3.2 \pm 0.4$	$\pi(h_{9/2} i_{13/2})_{11}^-$	Blomqvist, 1979; Fant, 1971; Yamazaki <i>et al.</i> , 1970
	4.372	93 ± 6	13^-			$\pi(h_{9/2}^2)_{8} + \nu(g_{9/2} p_{1/2}^-)_{8}^-$	Sjoreen, Fossan, <i>et al.</i> , 1979
$^{205}_{85}\text{At}$	2.062	64 ± 2	$\frac{25}{2}^{(+)}$		$E1; 1.2 \times 10^{-6}$	$\pi(h_{9/2}^3)_{9/2} - \nu(i_{13/2}^- f_{5/2}^1)_{9/2}^-$	Sjoreen, Fossan, <i>et al.</i> , 1979
$^{207}_{85}\text{At}$	2.117	108 ± 2	$\frac{25}{2}^+$	0.30 ± 0.01	$E1; 3.6 \times 10^{-7}$	$\pi(h_{9/2}^2)_{9/2} - \nu(i_{13/2}^-)_{13/2}^+$	Fant <i>et al.</i> , 1980
$^{208}_{85}\text{At}$	1.090	46	10^-			$\pi(h_{9/2}^2 i_{13/2})_{29/2} + \nu(f_{5/2}^1)_{5/2}^-$	Fant <i>et al.</i> , 1980
	2.276	$1.5 \mu\text{s}$	(16^-)				

TABLE VIII. (Continued.)

Nucleus	E_x (MeV)	$T_{1/2}$ (ns)	I^π	g	$ M(L) ^2$ (W.u.)	Particle configuration	References
^{209}At	1.427	29	$\frac{21}{2}^-$	0.95 ± 0.02	$E2;2,8$	$\pi(h_{9/2}^3)_{21/2}^-$	Sjøren, Fossan <i>et al.</i> , 1979; Sjøren <i>et al.</i> , 1976;
	2.428	680	$\frac{29}{2}^+$	1.06 ± 0.02		$\pi(h_{9/2}^2 i_{13/2})_{29/2}^+$	Bergström <i>et al.</i> , 1975
^{210}At	1.363	27±3	11 $^+$	0.89 ± 0.03		$\pi(h_{9/2}^3)_{21/2}^- \nu(p_{1/2}^{-1})_{1/2}^-$	Sjøren, Fossan <i>et al.</i> , 1979; Sjøren <i>et al.</i> , 1976;
	2.550	580±50	15 $^-$	1.038±0.010		$\pi(h_{9/2}^2 i_{13/2})_{29/2}^- \nu(p_{1/2}^{-1})_{1/2}^-$	Rahkonen <i>et al.</i> , 1978
^{211}At	4.028	4.0±1.7 μs	19 $^+$	0.74 ± 0.03	$E3;50\pm20$	$\pi(h_{9/2}^2 i_{13/2})_{29/2}^+ \nu(g_{9/2})_{9/2}^+$	Rahkonen <i>et al.</i> , 1978
	1.416	50	$\frac{21}{2}^+$	0.917±0.016	$E2;1,8$	$\pi(h_{9/2}^3)_{21/2}^-$	Ingwersen <i>et al.</i> , 1975
^{212}At	2.641	70	$\frac{29}{2}^+$	1.073±0.31	$E3;15\pm14$	$\pi(h_{9/2}^2 i_{13/2})_{29/2}^+$	Bergström <i>et al.</i> , 1975; Ingwersen <i>et al.</i> , 1975;
	4.82	4.2 μs	$\frac{39}{2}^-$	0.72 ± 0.07	$E3;31\pm3$		Mair <i>et al.</i> , 1971
^{212}At	0.888	19.4±0.7	(11 $^+$)	0.541±0.011	$M2;0;20\pm0.01$	$\pi(h_{9/2}^2 i_{13/2})_{29/2}^- \nu(g_{9/2} p_{1/2}^{-1})_{5/-}$	Blomqvist, 1979; Maier <i>et al.</i> , 1971
					$E1;(0.53\pm0.05)\times10^{-6}$	$\pi(h_{9/2}^2 i_{13/2})_{13/2}^+ \nu(g_{9/2})_{9/2}^+$	Sjøren, Gang, <i>et al.</i> , 1979
^{208}Rn	1.543	37.4±1.4	(15 $^-$)	0.622±0.010		$\pi(h_{9/2}^3)_{21/2}^- \nu(g_{9/2})_{9/2}^+$	Sjøren, Gang, <i>et al.</i> , 1979; Häusser <i>et al.</i> , 1978
	2.615	22±4	10 $^-$	1.077±0.010		$\pi(h_{9/2}^3 i_{13/2})_{10}^-$	Mair <i>et al.</i> , 1982
^{210}Rn	2.516	22±4	10 $^-$	1.077±0.010		$\pi(h_{9/2}^3 i_{13/2})_{10}^-$	Mair <i>et al.</i> , 1982
	2.563+ Δ	64±4	11 $^-$	1.105±0.010	$E1;3.6\times10^{-7}$	$\pi(h_{9/2}^3 i_{13/2})_{11}^-$	Poletti <i>et al.</i> , 1982; Maier <i>et al.</i> , 1982
^{212}Rn	3.248	72±4	14 $^+$	1.04 ± 0.02	$E2;0,026$	$\pi(h_{9/2}^3 f_{7/2})_{14}^+$	Poletti <i>et al.</i> , 1982; Maier <i>et al.</i> , 1982
	3.812	1100±60	17 $^-$	1.040±0.101	$E2;0,101$	$\pi(h_{9/2}^3 i_{13/2})_{17}^-$	Poletti <i>et al.</i> , 1982; Maier <i>et al.</i> , 1982
^{213}Rn	4.994	11.4±0.7	20 $^+$		$E3;12,1$	$\pi(h_{9/2}^3 i_{13/2})_{20}^+$	Poletti <i>et al.</i> , 1982; Maier <i>et al.</i> , 1982
	6.469	1040±70	22 $^+$		$E2;3.5\times10^{-4}$	$\pi(h_{9/2}^3 i_{13/2})_{17}^- \nu(p_{1/2}^{-1} g_{9/2})_{5/-}$	Poletti <i>et al.</i> , 1982
^{214}Rn	7.310	44±2	25 $^-$		$E3;38$	$\pi(h_{9/2}^2 i_{13/2})_{20}^+ \nu(p_{1/2}^{-1} g_{9/2})_{5/-}$	Poletti <i>et al.</i> , 1982
	8.6	3.927+ Δ	40±2	$\frac{35}{2}^+$	$E2;0,024$		Poletti <i>et al.</i> , 1981
^{212}Rn	6.101+ Δ	28±3	$\frac{2}{2}^+$		$E3;49$		Horn <i>et al.</i> , 1977; Häusser, <i>et al.</i> , 1978
	2.859	2	12 $^+$		$E2;4,6$		Horn <i>et al.</i> , 1977; Häusser, <i>et al.</i> , 1978
^{213}Fr	3.335	8	14 $^+$		$E2;0,035$	see Table VIII	Horn <i>et al.</i> , 1977; Häusser, <i>et al.</i> , 1978
	4.044	28	17 $^-$	1.05 ± 0.02		see Table VIII	Horn <i>et al.</i> , 1977; Häusser, <i>et al.</i> , 1978
^{214}Fr	6.145	113	22 $^+$	0.72 ± 0.01		see Table VIII	Horn <i>et al.</i> , 1977; Häusser, <i>et al.</i> , 1978
	7.113	18	25 $^-$	0.71 ± 0.02	$E3;32$	see Table VIII	Horn <i>et al.</i> , 1977; Häusser, <i>et al.</i> , 1978
^{215}Fr	7.849	14	27 $^-$	0.63 ± 0.03	$E2;0,0025$	see Table VIII	Horn <i>et al.</i> , 1977; Häusser, <i>et al.</i> , 1978
	8.550	154	30 $^+$	0.657±0.003	$E3;35$	see Table VIII	Horn <i>et al.</i> , 1977; Häusser, <i>et al.</i> , 1978
^{216}Fr	1.590	510±20	$\frac{21}{2}^-$	0.888±0.004	$E2;0,04$	$\pi(h_{9/2}^5)_{21/2}^-$	Häusser <i>et al.</i> , 1976,1978
	2.537	238±6	$\frac{29}{2}^+$	1.039±0.002	$E3;26$	$\pi(h_{9/2}^4 i_{13/2})_{29/2}^+$	Häusser <i>et al.</i> , 1976,1978

^aMeasured quadrupole moments: $|\mathcal{Q}| = 0.88 \pm 0.04 \text{ e b}$ for the 3.1-MeV state in ^{200}Pb , and $0.51 \pm 0.02 \text{ e b}$ for the 4.03-MeV state in ^{206}Pb (Mahnke *et al.*, 1978). $|\mathcal{Q}| = 0.65 \pm 0.05 \text{ e b}$ for the 2.7-MeV state in ^{196}Pb , $0.75 \pm 0.05 \text{ e b}$ for the 2.8-MeV state in ^{198}Pb (Zywieltz *et al.*, 1981).

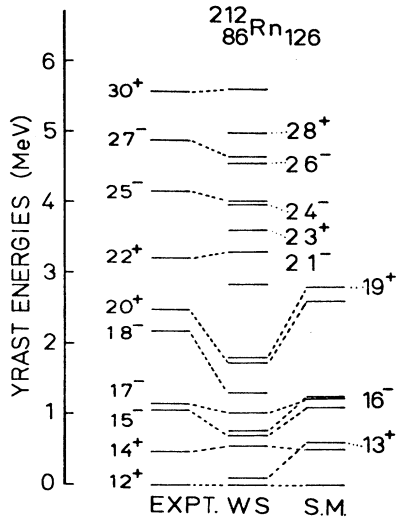


FIG. 37. The yrast spectrum of ^{212}Rn . The experimental data (for references see Table VIII) are compared with calculations based on the shell correction method with the Woods-Saxon single-particle spectrum (WS) (Dudek, 1980) and obtained within the spherical shell model (SM) (Blomqvist, 1979). The shell-model results fit slightly better to experiment, but rather severe limitation on the dimension of diagonalized matrices makes extension of the calculation to very high spin difficult. On the other hand, the shell correction method can be extended to very high spins and states of well-deformed nuclei. The shell correction method, although more "flexible" in applications, is more phenomenological.

tion, both from the experimental and the theoretical points of view.

Examples discussed in this section illustrate the richness of phenomena related to the noncollective rotation of the atomic nucleus. This field of study has in recent years experienced a great interest both from experimentalists and theoreticians. For further progress more detailed properties of highly excited isomeric states need to be measured. Particularly important are unambiguous spin and parity assignments, dipole and quadrupole moments, and decay probabilities. Specific techniques which have been used so far are discussed below in Sec. IV.B.

B. Experimental techniques and problems

1. Isotope assignment for yrast traps

Most of the observed yrast traps were excited in fusion reactions, which in general produced more than one residue. Therefore it was not always easy to identify which isotope emitted the delayed γ rays. It may occur that even more than one isotope, produced with a certain projectile-target combination and at some bombarding energy, contains isomeric states. More than one isomer may also be excited in the same isotope.

One or more of the following observations may be used for the isotopic assignment to isomeric states:

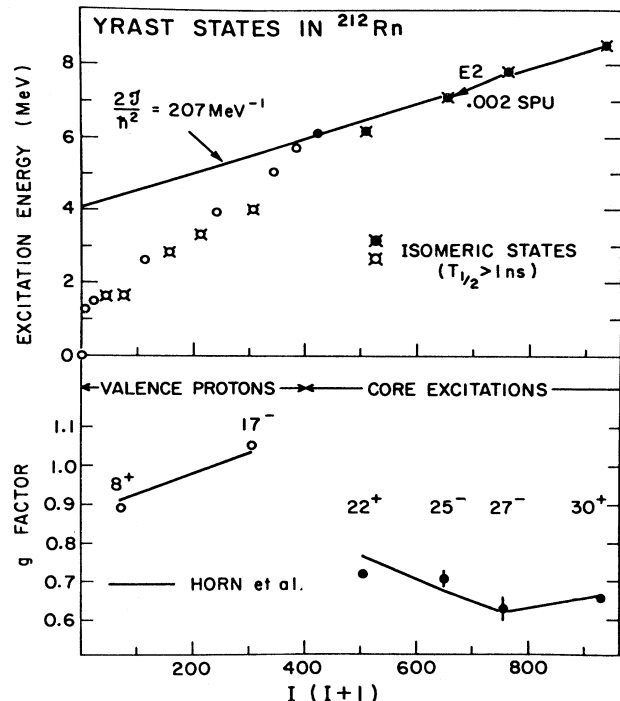


FIG. 38. Plot of the excitation energy vs $I(I+1)$ for yrast states in ^{212}Rn (upper half). The solid line represents the moment of inertia of a rigid spherical rotor. A structural change at $I \sim 20$ is evident from the g factors given in the lower part (Häusser, 1979). The solid lines are results calculated on the basis of the aligned particle configuration given in Table IX (Horn *et al.*, 1977).

- (i) the observation of delayed γ rays in coincidence with γ rays which were previously known to occur in a certain nucleus;
- (ii) the observation of known radioactive decay by known half-lives or by γ rays with known energies;

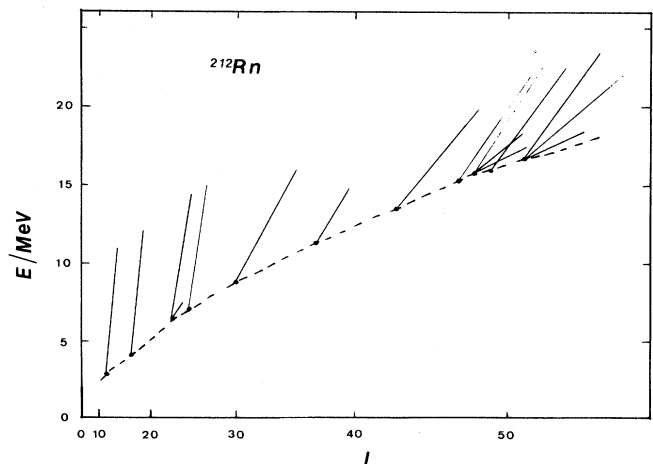


FIG. 39. An E vs I plot for the nucleus ^{212}Rn . The dashed line represents the noncollective rotation around the oblate symmetry axis. The straight lines correspond to collective rotational bands around an axis perpendicular to the symmetry axis [from Andersson *et al.* (1981)].

TABLE IX. Configuration assignments of some calculated yrast levels in ^{212}Rn .^a

I^π	Deformed Nilsson orbitals		Deformed Woods-Saxon orbitals		Deformed optimized Woods-Saxon orbitals		Spherical shell model	
	(Andersson <i>et al.</i> , 1978)		(Matsuyanagi <i>et al.</i> , 1978)		(Dudek <i>et al.</i> , 1981)		(Horn <i>et al.</i> , 1977)	
	Protons	Neutrons	Protons	Neutrons	Protons	Neutrons	Protons	Neutrons
12+	$h_{9/2}^4$		$h_{9/2}^4$		$h_{9/2}^4$		$(h_{9/2}^4)_{12+}$	
13+			$h_{9/2}^3 f_{7/2}$		$h_{9/2}^3 f_{7/2}$			
14+	$h_{9/2}^3 f_{7/2}$		$h_{9/2}^3 f_{7/2}$		$h_{9/2}^3 f_{7/2}$		$(h_{9/2}^3)_{21/2-}(f_{7/2-})$	
15-	$h_{9/2}^3 i_{13/2}$		$h_{9/2}^3 i_{13/2}$		$h_{9/2}^3 i_{13/2}$			
16-			$h_{9/2}^3 i_{13/2}$		$h_{9/2}^3 i_{13/2}$			
17-	$h_{9/2}^3 i_{13/2}$		$h_{9/2}^3 i_{13/2}$		$h_{9/2}^3 i_{13/2}$		$(h_{9/2}^3 i_{13/2})_{17-}$	
18-	$h_{9/2}^2 f_{7/2} i_{13/2}$		$h_{9/2}^2 f_{7/2} i_{13/2}$		$h_{9/2}^2 f_{7/2} i_{13/2}$			
19+			$h_{9/2}^2 i_{13/2}$		$h_{9/2}^2 i_{13/2}$			
20+	$h_{9/2}^2 i_{13/2}^2$		$h_{9/2}^2 i_{13/2}^2$		$h_{9/2}^2 i_{13/2}^2$			
21-					$h_{9/2}^2 i_{13/2}^3$			
21+			$h_{9/2}^3 i_{13/2}$	$p_{1/2}^{-1} g_{9/2}$	$p_{1/2}^{-1} g_{9/2}$			
22+	$h_{9/2}^3 i_{13/2}$	$p_{1/2}^{-1} g_{9/2}$	$h_{9/2}^3 i_{13/2}$	$p_{1/2}^{-1} g_{9/2}$	$h_{9/2} i_{13/2}^3$	$p_{1/2}^{-1} g_{9/2}$	$(h_{9/2}^3 i_{13/2})_{17-}$	$(p_{1/2}^{-1} g_{9/2})_5-$
23+	$h_{9/2}^2 f_{7/2} i_{13/2}$	$p_{1/2}^{-1} g_{9/2}$	$h_{9/2}^2 f_{7/2} i_{13/2}$	$p_{1/2}^{-1} g_{9/2}$	$h_{9/2}^2 i_{13/2} f_{7/2}$	$p_{1/2}^{-1} g_{9/2}$		
24+			$h_{9/2}^2 f_{7/2} i_{13/2}$	$p_{1/2}^{-1} i_{11/2}$	$h_{9/2}^2 i_{13/2}^2$	$p_{1/2}^{-1} g_{9/2}$		
24-					$h_{9/2}^2 i_{13/2}^2$	$p_{1/2}^{-1} g_{9/2}$		
25-	$h_{9/2}^2 i_{13/2}^2$	$p_{1/2}^{-1} g_{9/2}$	$h_{9/2}^2 i_{13/2}^2$	$p_{1/2}^{-1} g_{9/2}$	$h_{9/2}^2 i_{13/2}^2$	$p_{1/2}^{-1} g_{9/2}$	$(h_{9/2}^3 i_{13/2})_{17-}$	$(p_{1/2}^{-1} j_{15/2})_8+$
26-	$h_{9/2}^2 f_{7/2} i_{13/2}$	$p_{1/2}^{-2} g_{9/2}$	$h_{9/2}^2 f_{7/2} i_{13/2}$	$p_{1/2}^{-1} j_{15/2}$	$h_{9/2}^2 i_{13/2} f_{7/2}$	$p_{1/2}^{-1} j_{15/2}$		
27-	$h_{9/2}^3 i_{13/2}$	$p_{1/2}^{-2} g_{9/2} i_{11/2}$	$h_{9/2}^2 i_{13/2}^2$	$p_{1/2}^{-1} j_{15/2}$	$h_{9/2}^2 i_{13/2}^2$	$p_{1/2}^{-1} j_{15/2}$	$(h_{9/2}^3 i_{13/2})_{17-}$	$(g_{9/2} i_{13/2}^{-1})_{11+}$ $(j_{15/2} f_{5/2}^{-1})_{10+}$
28-	$h_{9/2}^2 f_{7/2} i_{13/2}$	$p_{1/2}^{-2} g_{9/2} i_{11/2}$	$h_{9/2}^2 f_{7/2} i_{13/2}$	$p_{1/2}^{-2} g_{9/2} i_{11/2}$	$h_{9/2}^2 i_{13/2}^2$	$p_{1/2}^{-1} j_{15/2}$		
28+					$h_{9/2}^2 i_{13/2}^2$	$p_{1/2}^{-1} j_{15/2}$		
29+			$h_{9/2}^3 i_{13/2}$	$p_{1/2}^{-2} j_{15/2} g_{9/2}$	$h_{9/2}^2 i_{13/2}^2$	$f_{5/2}^{-1} j_{15/2}$		
30+	$h_{9/2}^2 f_{7/2} i_{13/2}$	$p_{1/2}^{-2} g_{9/2} j_{15/2}$	$h_{9/2}^2 f_{7/2} i_{13/2}$	$p_{1/2}^{-2} g_{9/2} j_{15/2}$	$h_{9/2}^2 i_{13/2} f_{7/2}$	$p_{1/2}^{-2} g_{9/2} j_{15/2}$	$(h_{9/2}^3 i_{13/2})_{20+}$	$(g_{9/2} i_{13/2}^{-1})_{11+}$ $(j_{15/2} f_{5/2}^{-1})_{10+}$

^aComparison is made between various versions of the calculation method.

(iii) known experimental and theoretical cross sections for the production of certain isotopes and their variation with bombarding energy (including cross bombardments, i.e., various beam-target combinations to excite the same final nuclei);

(iv) known systematics in isotope production and high-spin isomer excitations.

Only the first of those four classes leads to unambiguous isotope assignment. The reliability of assignments based on (iii) or (iv) depends strongly on details of experimental data and combinations of the data. The entries in Tables II, VII, and VIII satisfy one or more of the above criteria.

2. Determination of excitation energies and spins

The simplest way to determine the excitation energy of an isomeric state is to add the energies of the sequentially emitted delayed γ rays, if they are known. For unambiguous spin assignments, in most cases one has to perform several conventional γ -ray spectroscopic measurements. Such measurements are often hindered by lack of information on the decay scheme. In that case, one can take advantage of the special properties of sum spectrometers and multiplicity filters. The sum spectrometer is

very well suited for measuring excitation energies for high-multiplicity cascades. Spin estimates from this method, however, are based on model assumptions relating excitation energy to spin. Unfortunately, the multiplicity of the γ -ray cascade can be determined only to a certain degree of accuracy with such a spectrometer and only if additional detectors are used.

More detailed information on spins can be obtained from experiments with multiplicity filters. They measure rather accurately the multiplicity of the delayed cascades, but yield less accurate information on the excitation energies than the sum spectrometer does. The main difficulty in interpreting the data is the transformation from multiplicity M_γ to spin I . For a ground-state rotational band this would simply be $I = 2M_\gamma$. More elaborated relations (see Sec. V) concern γ -ray cascades of a rotational nature (with a smooth dependence of \mathcal{E} on I). The nuclei discussed here, however, do not rotate collectively, and a severe deviation from such a simple relation may be expected. One may use the presently known systematics in nuclei with such complicated and irregular structure for which the multiplicities and spins have been determined independently. In the work of Jastrzebski *et al.* (1980) an empirical relation is derived between the spin of an isomer I and the number of delayed transitions M_γ^d between that isomer and the ground state with spin I_g (or another iso-

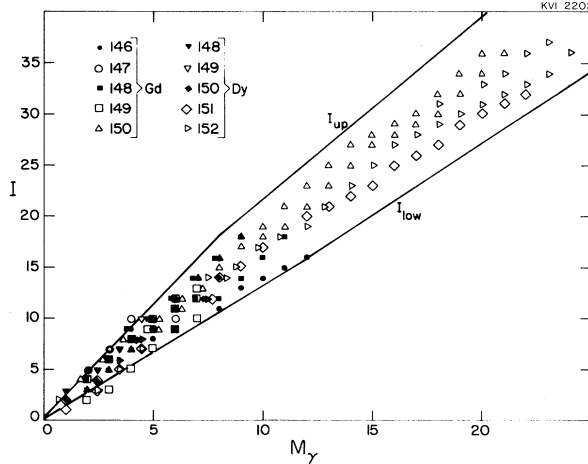


FIG. 40. The empirical relation between spins of isomeric states and the γ -ray multiplicity of the deexciting cascades extracted from cross experiments in various Gd and Dy isotopes. The spins and multiplicities were determined independently. The solid lines indicate the upper and lower estimates for spin assignments, reflecting uncertainties in the used decay schemes. This systematic may be used to assign spin limits to isomeric states from measured multiplicities [from Hageman (1981)].

mer) as $I = I_g + M_\gamma^d \Delta L$. The mean value of the average angular momentum ΔL removed by one transition varied between ~ 1.9 and ~ 1.6 , when 2–22 levels above the ground state were included. These numbers were extracted from known level schemes of ^{154}Er , ^{151}Ho , $^{152,151,150}\text{Dy}$. A similar function was determined from well-established data on $^{146-150}\text{Gd}$ and $^{148-152}\text{Dy}$ isotopes by Hageman (1981) and is presented in Fig. 40. This set of data also contains a reasonable estimate of the uncertainties involved in deriving the spin of an isomeric state from the measured multiplicity. The excitation energies are in most cases derived from the measured average multiplicities \bar{M}_γ^d , and the average γ -ray transition energy \bar{E}_γ^d in the delayed cascade as $\mathcal{E}_x = \bar{M}_\gamma^d \bar{E}_\gamma^d$.

3. Magnetic dipole and electric quadrupole moments

It was argued above that magnetic dipole moments serve as a direct test ground for the quasiparticle structure of long-lived yrast traps. From Tables II, VII, and VIII one may conclude that most of the efforts were concentrated on nuclei in the lead region. Short reviews on magnetic dipole and electric quadrupole moments of high-spin states have been presented by Häusser (1979) and Mahnke *et al.* (1979), respectively.

Detailed descriptions of various experimental methods can be found in the work of Morinaga and Yamazaki (1976). Here we will discuss only briefly the few methods commonly used in the investigations of yrast traps. When the lifetime of a nuclear excited state is sufficiently long—say, more than a few nanoseconds—then the magnetic moment may be determined from the observed time dependence of the angular distribution of the deexciting

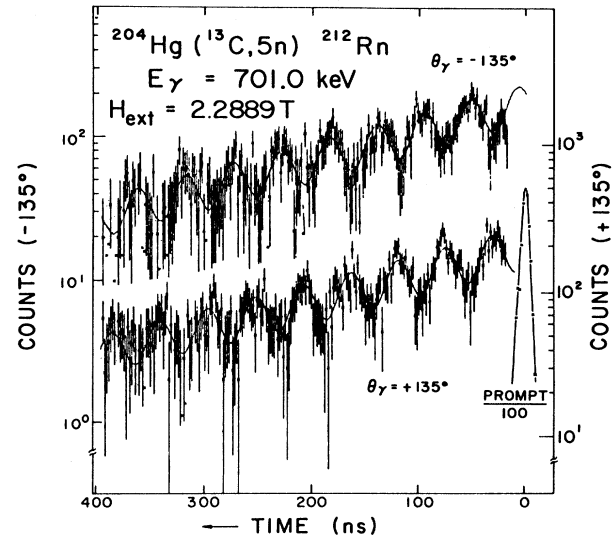


FIG. 41. The effect of an external magnetic field H_{ext} on the γ -ray intensity pattern as a function of time. The magnetic dipole moment (and spin) together with the associated asymmetric dipole γ -ray emission pattern rotate with the Larmor frequency ω around the direction of the magnetic field. The fluctuations in the γ -ray intensities observed in space-fixed ($\theta = \pm 135^\circ$) detectors as a function of time yield directly the frequency ω . The γ rays detected in this case were due to the $30^+ \rightarrow 27^-$ transition in ^{212}Rn (Häusser, 1979).

delayed γ rays. The spatial intensity distribution rotates with angular velocity ω of the Larmor precession induced by an external magnetic field H on an oriented nucleus. The initial orientation can be produced in the nuclear reaction which excites the isomeric state of interest. The relation between the gyromagnetic factor g and ω is given by $g = \omega \hbar / (\mu_N H)$, where μ_N is the nuclear magneton.

For very short lifetimes—say less than a few picoseconds—the Larmor precession due to external magnetic fields is too small. In that case the very high internal transient fields can be employed as discussed in Appendix B.

For yrast traps discussed in this section the lifetimes are sufficiently long to apply external fields and in some cases to observe even more than one full precession period by detecting delayed γ rays as a function of time. An example of such a measurement for the highest yrast isomer in ^{212}Rn with $I^\pi = 30^+$, taken from Häusser (1979), is given in Fig. 41. The rotation of the angular distribution pattern can be followed for more than eight turns in about 400 ns, which accurately determines the Larmor frequency and thus the g factor.

In contrast to the lead region, measuring magnetic moments in the rare-earth region is very difficult. This difficulty is mainly due to the paramagnetism of the lanthanides, which have an unfilled $4f$ atomic shell and which generate large internal magnetic fields acting on the nucleus. These paramagnetic ions, embedded into a solid, experience thermal fluctuations, and the rapidly fluctuating field acting on the nucleus will tend to

disorient the nuclear spin. Moreover, the paramagnetism enhances the external field due to the induction of unequally populated electronic substates. Apparently, these two disturbing effects are small only for europium and gadolinium as a slowing down material. Therefore it is not surprising that the measured g factors in the rare-earth region are restricted to the Gd isotopes (see Table II). One of the exceptions is ^{152}Dy , where these problems have been circumvented by using a lead backing as a slowing down material (Merdinger *et al.*, 1979).

Determination of quadrupole moments by making use, for instance, of the reorientation effect, as has usually been done for low-lying 2^+ states, is not possible in the case of yrast traps because of the relatively long lifetimes. In such cases quadrupole moments may be determined when the nucleus moves with certain velocity through an electric field gradient (EFG) due to the quadrupole interaction (QI) with the field. This EFG is most commonly supplied by the surrounding atoms of a crystal lattice of noncubic symmetry. The QI causes a time-dependent change in the shape of the spatial emission pattern of γ rays. This perturbation of the angular distribution of γ rays can be measured as a function of time with a pair of detectors at fixed positions—for instance, at 0° and 90° with respect to the beam axis. From the data one obtains the difference and the sum of the two normalized γ -ray time distributions represented by the quadrupole modulation function. The quadrupole moment cannot be extracted directly from a fit to the data because it is not possible to calculate the EFG reliably and subsidiary calibration experiments must be carried out. Another difficulty arises from the fact that the energy splittings of the nuclear magnetic substates due to the QI decrease quadratically with increasing spin. As a consequence the determination of the quadrupole moments becomes increasingly difficult at higher spin. Nevertheless, it appears to be possible to measure quadrupole moments—for instance, of high-spin states in ^{147}Gd —which is important when following the deformation as a function of spin. Such a measurement is possible because Gd^{3+} has an almost pure, spherical $^8S_{7/2}$ electronic ground state which keeps the magnetic hyperfine fields weak enough to observe spin relaxation times up to $\sim 1 \mu\text{s}$ (Häusser *et al.*, 1980). Measured quadrupole moments and g factors for several yrast traps are included in Tables II, VII, and VIII (for discussion see Sec. IV.A).

V. THE QUASICONTINUUM ENERGY SPECTRUM

In this section properties of the nuclear quasicontinuum spectra (qcs) will be discussed. It was argued in the previous sections that it is possible to resolve the individual gamma lines in the angular momentum region up to, say, $I \sim 30$; sometimes this limit could be shifted up to $I \sim 40$.

When the excitation energy and angular momentum increase, the number of gamma rays detected in experiment increases considerably, while their intensities generally de-

crease. It is impossible to detect the individual gamma transitions when the intensity for each transition becomes too weak and the density of levels large. This, however, does not mean the existence of overlap between most of the levels. It follows from the estimates of the level densities that the average level distance exceeds considerably the level widths. Thus it would not seem proper to call the corresponding spectrum a continuum. It is therefore usually referred to as quasicontinuum (or the region of unresolved γ rays). Its definition obviously depends on the existing technical possibilities in resolving the individual gamma lines. Thus the border line between the quasicontinuum and the region of observed individual gamma lines is rather conventional, and it may be shifted with improving techniques of detection.

The investigation of the qcs is of great importance, since it may provide valuable information on the behavior of nuclei in a vast region of high angular momenta, inaccessible by means of the ordinary methods of nuclear spectroscopy.

In this section we shall first briefly review the methods of populating the nuclear high-spin states that belong mostly to the region of the qcs (Sec. V.A). Then the experimental methods for treatment of the qcs will be discussed (Sec. V.B). Finally, in Sec. V.C we shall discuss what can be deduced about nuclear structure from the observed γ radiation of the qcs.

A. Population of the high-spin states

Atomic nuclei are about the only strong-interacting quantal objects that allow studying fast rotation corresponding to as much as 80 (or even more) units of angular momentum. Several nuclear reactions can lead to those high-spin states. Among all known reaction mechanisms the complete fusion (CF) of the bombarding ion with the target nucleus seems to be most effective for the production of high-spin states in nuclei. We shall not attempt here a detailed discussion of this reaction mechanism, as it has been extensively discussed in the literature [see, for example, Wilczynski (1973), Bass (1974), Lefort (1974), Lefort and Ngo (1978), Galin *et al.* (1974), Glas and Mosel (1974), Siwek-Wilczynska and Wilczynski (1976), Namboodiri *et al.* (1975), Birkeland *et al.* (1979), Krappe (1979), Wilczynski *et al.* (1980), and references quoted therein].

The transfer of angular momentum in the CF process obviously depends on the mass and energy of the bombarding ion and on the equilibration process of the formed compound nucleus. These effects have been studied in detail for beams varying from proton to ^{40}Ar , together with the particle (neutron) spectra [cf. Ockels *et al.* (1978), Ejiri *et al.* (1978), Sarantites, Westerberg, Halbert *et al.* (1978), Westerberg, Sarantites, Hensley *et al.* (1978), Sakai *et al.* (1979), de Voigt *et al.* (1979a, 1979b, 1982), Hillis *et al.* (1979), Hageman *et al.* (1981), Beene *et al.* (1981), Geoffroy Young *et al.* (1981), Lukasiak *et al.* (1982)].

In order to transfer as much angular momentum as possible into the compound nucleus formed in the CF process it is desirable to employ high-energy collisions with the largest possible impact parameter. However, in such collisions the cross section for the CF process is usually rather small. Some other reaction mechanisms, such as the incomplete fusion or absorptive breakup may appear more probable [see, for instance, Inamura *et al.* (1977), Siwek-Wilczynska *et al.* (1979a, 1979b), Geoffroy Young *et al.* (1979), Wilczynski *et al.* (1980), Bauer *et al.* (1980), Wu *et al.* (1979), Sujkowski (1981)].

At still higher energies and impact parameters the deep inelastic collisions, or even the quasielastic scattering may become dominant (these processes depend in general on the mass ratio of the colliding nuclei). All these mechanisms could also be employed for the production of high-spin states. However, up to now they have not been used extensively for this purpose, and thus we shall mainly concentrate on the complete fusion.

The amount of angular momentum transferred to the compound nucleus in the CF process may be estimated with a quasiclassical approach that emphasizes the importance of the critical angular momentum (Wilczynski, 1973; Bass, 1974) or the critical distance between the two ions (Lefort, 1974; Lefort and Ngo, 1976; Glass and Mosel, 1974; Namboodiri *et al.*, 1975). Several detailed analyses of the classical trajectories for the colliding nuclei have been discussed in the literature (see the papers quoted above in this section). Instead of describing the details of various approaches, we shall quote here simple formulas estimating the maximum angular momentum l_{\max} involved in the collision. Assuming that the classical turning point occurs at the radial distance between the two ions $r = r_{\min}$, we may calculate l_{\max} as

$$l_{\max} = r_{\min} \left[\frac{2\mu}{\hbar^2} \{ E_{c.m.} - V(r_{\min}) \} \right]^{1/2}. \quad (5.1)$$

Here $E_{c.m.}$ denotes the energy in the c.m. system of reference and μ the reduced mass. The potential energy V may be assumed in the form of the Coulomb energy

$$V(r) = \frac{Z_1 Z_2 e^2}{r} \quad (5.2)$$

[see, for example, Diamond and Stephens (1980)]. In a more detailed approach it includes, in addition, the contributions from the nuclear potential energy [see, for instance, Namboodiri *et al.* (1975)].

The CF reactions lead usually to the formation of compound nuclei in highly excited nuclear states ("hot" nuclei). Because of the enormous density of states at high excitation energy a statistical treatment of the deexcitation process of such nuclei is usually applied (see also Fig. 1 for illustration of the deexcitation process of a compound nucleus). Most of the excitation energy of a hot nucleus is removed from the system by emission of one or a few particles. Here, we shall discuss only the evaporation of neutrons. The probability for evaporation of a neutron tends to vanish very fast when the excitation en-

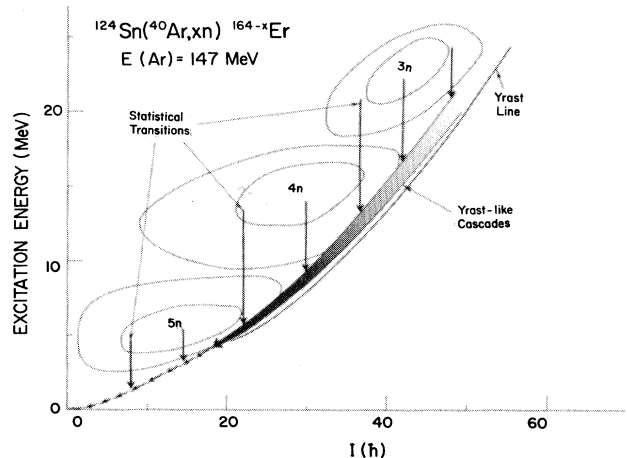


FIG. 42. Illustration of the deexcitation process of the ^{164}Er compound nucleus according to a statistical-model calculation. The contours enclose regions corresponding to γ rays emitted from the $(3-5)n$ evaporation residues (Hillis *et al.*, 1979).

ergy of the compound nucleus decreases below a certain limit (depending on the neutron separation energy). Furthermore, the neutrons are most easily evaporated from their s -state, so usually they do not carry away more than $1\frac{1}{2}$ angular momentum from the nucleus, on the average.

After the evaporation of a few neutrons the nucleus is led to the vicinity of its yrast line where no more neutrons can be evaporated. Figure 42 illustrates this situation (as does Fig. 1). From these figures it becomes evident that those reaction channels with the highest number of evaporated neutrons leave the final nuclei (evaporation residues) in states with the lowest energy and angular momentum. Thus the distribution of the cross section for nuclear reactions with various numbers of evaporated neutrons gives a rough estimate of the distribution of angular momentum in the original compound nuclei (Fig. 42).

At the final stage of the evaporation process, when no more neutrons can be emitted, the only means for further deexcitation of the nucleus is provided by the emission of cascades of gamma quanta. States at which the probabilities for neutron evaporation and for gamma-ray emission are comparable are called entry states, since they define the origin of the gamma-ray cascades. A set of entry states populated in many reactions of a certain type forms an entry line (or, more precisely, an entry region), which is usually represented as a curve (or an area) above the yrast line in the plot of energy \mathcal{E} versus angular momentum I . This situation is illustrated schematically in Fig. 43, where, in addition, the region probed by qcs studies is indicated. Figure 44 presents an example of the entry lines for various nuclear reactions leading to evaporation residues ^{160}Er and ^{164}Er . The experimental data, which are also compared with the calculations based on the statistical model, give an idea about the typical distribution of entry states above the yrast line.

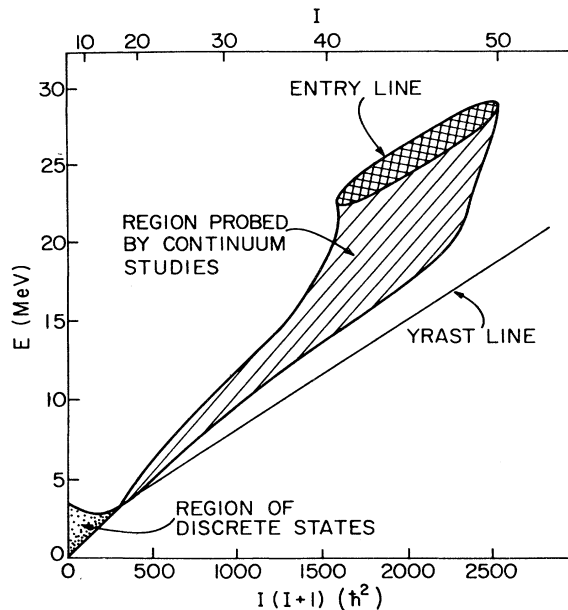


FIG. 43. Schematical γ -ray decay pattern [in the E vs I plane with $I(I+1)$ scale] of states in the entry region, populated—for example in (HI, xn) reactions—to discrete states near or on the yrast line (Khoo, 1979).

A general conclusion following from the analysis of plots of this type is that nuclear evaporation residues are very often produced in states with angular momentum considerably exceeding the highest limits that have been observed in experiments with individual gamma lines (presently corresponding to states with spins 30–40). The

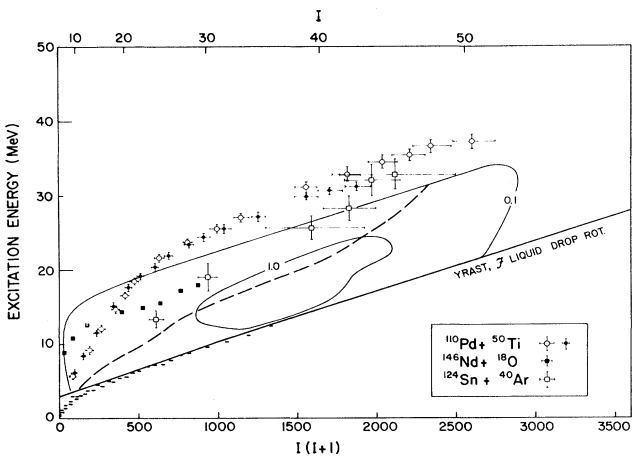


FIG. 44. The entry lines for the evaporation residues of $^{160}\text{Er}^*$ and $^{164}\text{Er}^*$ measured with ^{50}Ti (dots for 223 MeV, open circles for 204 MeV) and ^{18}O beams, respectively (Folkmann *et al.*, 1981), are shown together with the centroids of exit-channel selected entry regions from the $^{40}\text{Ar} + ^{124}\text{Sn}$ reaction at 161 and 236 MeV (Hillis *et al.*, 1979). The contours marked 0.1 and 1.0 ($\text{mb}/\text{MeV}^{-1}$) correspond to the calculated population of the evaporation residues. The entry line calculated with a statistical model (Folkmann *et al.*, 1981) is shown as a broken line.

exploration of this interesting domain has required the development of new methods and techniques. Selected aspects of this development will be discussed below.

B. Experimental analysis of the gamma cascades in the quasicontinuum spectra

When neutron evaporation from highly excited states is no longer possible, emission of cascades of gamma rays from the nucleus remains the only way for further deexcitation and removal of angular momentum. One can *a priori* think of two possible types of gamma cascades in this situation. The high-energy and generally low multipolarity (mostly dipole) gamma rays are very likely to bring the nucleus quickly into the vicinity of the yrast line without an appreciable loss in angular momentum. This type of radiation is often referred to as a statistical cascade, since it corresponds to random transitions. It follows from statistical considerations that the number of gamma rays should be an exponentially decreasing function of the transition energy. This dependence of the radiation intensity on the transition energy has been roughly confirmed by measurements. Figure 45 illustrates the result of an experiment at Berkeley (Simon *et al.*, 1977). In the logarithmic scale the high-energy part of the spectrum exhibits a linear dependence on the transition energy (indeed, the intensity decreases exponentially).

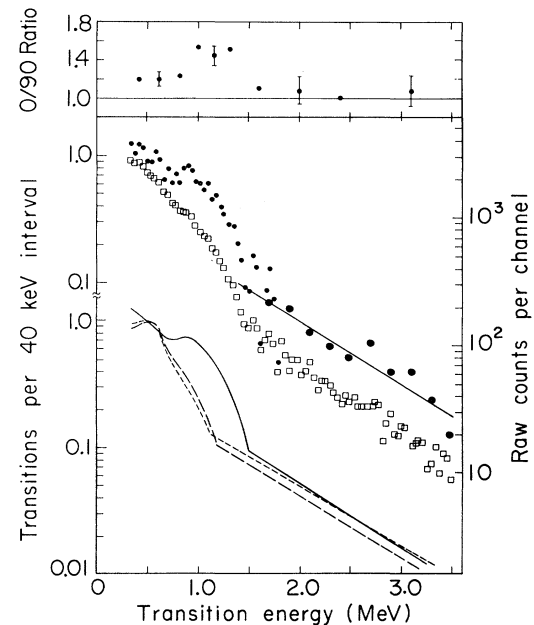


FIG. 45. The γ -rays qcs from the reaction $^{126}\text{Te}(^{40}\text{Ar}, 4n) ^{162}\text{Yb}$ at 181 MeV is given in the form of raw (squares) and also normalized unfolded (small black dots) data. The larger dots are five channel averages. At the top the $0^\circ/90^\circ$ ratio for unfolded spectra is given; at the bottom experimental unfolded spectra for the same case (solid line) and for the reactions $^{126}\text{Te}(^{40}\text{Ar}, 4n) ^{162}\text{Yb}$ at 157 MeV (long-dashed line) and $^{150}\text{Sm}(^{16}\text{O}, 4n) ^{162}\text{Yb}$ at 87 MeV (short-dashed line) (Simon *et al.*, 1977) are schematically illustrated.

The second type of gamma cascade corresponds to transitions originating usually in the yrast region and following the yrast line. The angular distribution of the gamma rays (or the 0° to 90° ratio) for these cascades often indicates the stretched (collective) $E2$ (electric quadrupole) character of these transitions (cf. top part of Fig. 45). They are commonly referred to as yrast cascades and exhibit a much more ordered character than statistical cascades. The existence of yrast cascades can be clearly seen in the lower-energy range—cf. Fig. 45—as a region of an increased intensity forming a “bump” over the extrapolation of the straight line corresponding to the statistical cascades.

Obviously, the two types of gamma cascades mentioned above do not always have to occur in a definite order in time. It may also happen that after the emission of a few statistical gamma rays, a collective $E2$ transition takes place, followed by new statistical gamma rays, etc.

Various experimental methods have been employed in order to probe the whole range of unresolved gamma spectra (i.e., the qcs region). In particular, it is important to determine the origin of the longest possible yrast cascade deexciting states with the highest angular momentum to the yrast states observed via discrete γ rays. The energies corresponding to the uppermost transitions in those cascades may be read directly from the γ -ray spectra of the type of Fig. 45 as the position of the upper edge of the “bump.” This is true if the cascades follow collective $E2$ bands thus with the highest-energy transitions on top.

Another interesting quantity is the angular momentum corresponding to those uppermost states. Experimentally, however, it is difficult to isolate long yrast cascades, because entry states are usually populated over a broad region of angular momentum in CF reactions. A lot of experimental effort has been devoted to the determination of the average value of I_{in} , i.e., the input angular momentum (Ward *et al.*, 1975; Newton *et al.*, 1975; Banashik *et al.*, 1975; Simon *et al.*, 1976; Stephens, 1977; Hagemann *et al.*, 1975; Newton *et al.*, 1977; Simpson *et al.*, 1977; Andersen *et al.*, 1978; Deleplanque, Lee *et al.*, 1978; Hillis *et al.*, 1979; de Voigt *et al.*, 1979a, 1979b; Feenstra *et al.*, 1977, 1979).

A rough estimate of the magnitude of I_{in} can be gained after the identification of the reaction channel. This identification is usually achieved by employing a Ge(Li) counter used for the detection of known discrete lines in the final nucleus. Figure 42 illustrates regions corresponding to various reaction channels. Their location in the (\mathcal{E}, I) plane may serve as a rough estimate of I_{in} .

A more direct indication is obtained by the measurements of the total number M of gamma rays in the cascades (multiplicity). The average multiplicity $\langle M \rangle$ can be measured with the help of a large number of gamma-ray (NaI) detectors working in coincidence. Such a set may be supplemented with one Ge(Li) detector, used to identify the final nucleus. Working with multidetector systems, various experimental groups have been able to determine not only the average multiplicity $\langle M \rangle$ but also

the higher moments of the gamma-ray multiplicity distribution: the variance (i.e., the width which is related to the second moment), the skewness (third moment), etc. The detailed methods are extensively treated in literature (cf. Hagemann *et al.*, 1975; Westerberg *et al.*, 1977; Westerberg, Sarantites, Young *et al.*, 1978; Lindblad, 1977; Ockels, 1978a, 1978b; Andersen *et al.*, 1978; Kerek *et al.*, 1978; Kohl *et al.*, 1978; Van der Werf, 1978; Hillis *et al.*, 1979).

Now, the question arises of how to relate the average multiplicity $\langle M \rangle$ with the angular momentum value I_{in} at the origin of the cascades. The problem would be simple if the cascades corresponded to pure stretched $E2$ bands. In order to include the possibility of other transitions (some of them statistical) different from stretched $E2$, some empirical formulas are currently used. Often a relation of the type

$$I_{in} \sim 2(\langle M \rangle - M_s) + \alpha M_s \quad (5.3)$$

is employed where parameters M_s (~ 4) and α (~ 0.5) have to be adjusted, depending on reaction mechanism, energy, etc. For further details see, for instance, Simon *et al.* (1976), Sarantites *et al.* (1976), Sarantites, Westerberg, Dayras *et al.* (1978), Hillis *et al.* (1979), de Voigt *et al.* (1979a, 1979b), Hageman *et al.* (1981), and Lukasiak *et al.* (1982).

A crucial quantity that affects the relation between $\langle M \rangle$ and I_{in} and that also bears some nuclear structure information on the qcs is the multipolarity l of the γ rays. It has already been mentioned above that the yrast cascades have predominantly a stretched $E2$ character ($l=2$) and the statistical cascades mixed stretched and nonstretched dipole ($l=1$) $E1$ character. Such information is obtained mainly from angular distribution measurements or from the intensity ratio $W(0^\circ)/W(90^\circ)$ of γ rays [cf. Banashik *et al.* (1975), Simon *et al.* (1977), Newton *et al.* (1978), Deleplanque, Byrski *et al.* (1978), Folkmann *et al.* (1981)]. Additional information on the electromagnetic character of the γ radiation is obtained from conversion electrons establishing the $E2$ character for the yrast bump and $E1$ for the statistical transitions (Feenstra *et al.*, 1977, 1979) and possibly some low-energy $M1$ transitions (Westerberg, Sarantites, Young *et al.*, 1978). Such a general idea about the gross behavior of the qcs was confirmed by several measurements of the linear polarization (Vivien *et al.*, 1979; Trautmann *et al.*, 1979; Hübel *et al.*, 1980). Significant low-energy $M1$ radiation found in the polarization experiments (in nuclei near closed shells) may indicate the existence of rotational bands in the qcs when $M1$ transitions can compete with cross-over $E2$ transitions. It should be emphasized, however, that the picture may change somewhat from nucleus to nucleus and that it also depends on the excitation process.

A sensitive measure for the collective character of transitions in the qcs can be obtained from $B(E2)$ transition probabilities. A strong $E2$ enhancement characteristic for collective rotation was concluded from the short lifetimes of the order of a few tenths of a picosecond per

transition. This conclusion was reached in early works on several nuclei ranging from ^{120}Xe to ^{184}Hg by employing the recoil distance Doppler-shift technique (Diamond *et al.*, 1969; Kutchera *et al.*, 1972; Newton *et al.*, 1973; Ward *et al.*, 1973; Rud *et al.*, 1973; Bochev *et al.*, 1975). Confirmations of that result were reported more recently by Emling *et al.* (1981) using the same technique and by Hübel *et al.* (1978, 1982) observing the Doppler shift of a large ensemble of γ rays from the qcs.

Important progress in analyzing the qcs has been made through the application of sum spectrometers. These instruments are designed mainly to measure the total gamma-ray energy by summation of the energies of the individual gamma rays of the cascade. For that purpose sum spectrometers cover a large part of the total solid angle and are optimized for detection efficiency rather than for energy resolution. They are usually applied in coincidence with one or two NaI detectors or a Ge(Li) detector used as an individual gamma-ray transition detector which may identify the reaction channel.

Several relevant quantities mentioned above, such as average values of E_γ , M , and I , can be studied in function of the total γ -ray energy of the qcs cascades. Their behavior can then be followed as a function of the excitation energy, and changes in the quantities related to different deexcitation modes (or even to different nuclear shapes) can be studied. A good example of such a study employing a sum spectrometer can be found in the works of Folkmann *et al.* (1981) and Aguer *et al.* (1981). As another example, let us mention the experiment by Körner *et al.* (1979), where the sum spectrometer was used together with other detectors in a multiplicity arrangement. The top part of Fig. 46 presents the total gamma-ray energy spectrum of the $^{124}\text{Sn} + ^{40}\text{Ar}$ (185 MeV) reaction analyzed in terms of the various reaction exit channels. The bottom part of Fig. 46 illustrates the multiplicity as a function of the total gamma-ray energy. The multiplicity value $M \sim 40$ measured in this experiment is very high. Comparison with Eq. (5.3) leads to angular momentum I of the order of 60 or 80 which is about the highest estimated liquid-drop value of angular momentum (cf. Fig. 5 for $A \sim 160$) that can be accommodated in the nucleus!

Without going into much detail, we can observe that combining sum spectrometers and multidetector arrangements may lead to the determination of the average angular momentum I_{in} at the origin of the gamma cascades as a function of the excitation energy. Figure 44 illustrates the determination of the entry line from the experiment with the sum spectrometer (Folkmann *et al.*, 1981) in comparison with other experimental (Hillis *et al.*, 1979) and theoretical estimates. From the slope of the entry line (in the \mathcal{E} -vs- I plane) one may estimate the average moment of inertia (see next section).

Experimental analysis of the qcs region is progressing steadily also through application of crystal ball spectrometers (Sarantites *et al.*, 1980; Simon, 1980). These are multidetector spectrometers able to record simultaneously the energies, angles, times of emission, etc., for all gamma

rays per individual reaction with high efficiency. In this way, the entry line and many other properties of the qcs may be determined most efficiently and accurately. First reports of the Oak Ridge group concerned experiments with a 69-NaI(Tl)-detector 4π spectrometer and a high-resolution Ge detector for identification of the evaporation residues following $^{146}\text{Nd} + (136-149)\text{-MeV } ^{20}\text{Ne}$ reactions. The deduced cross sections for the 5, 6, 7, and 8n

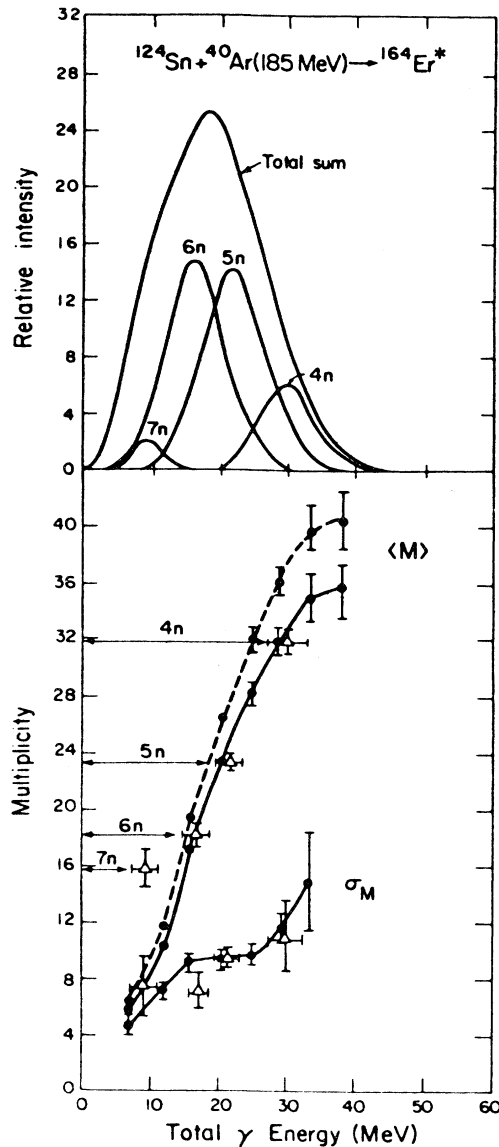


FIG. 46. The experimental total γ -ray energy spectrum and the components corresponding to the various reaction products obtained by gating on known lines in the γ -ray spectrum (top) of ^{164}Er nucleus. At the bottom the multiplicity parameters are given for 4-MeV-wide slices in the sum spectrum represented by points on the dashed (uncorrected for angular correlations) and on the solid (corrected by assuming 80% $\Delta L = 2$ quadrupoles and 20% $\Delta L = 1$ dipoles) lines. The open triangles represent the results from the Ge(Li)-multiplicity setup; in this case the total γ -ray energy is obtained by $\langle M_\gamma \rangle \langle E_\gamma \rangle$ (Körner *et al.*, 1979).

exit channels as functions of multiplicity and excitation energy and the total fusion cross section as a function of angular momentum were reproduced rather well by statistical model calculations (Sarantites *et al.*, 1982). The same group also reported entry lines and spectral γ -ray distributions (Jaäskeläinen *et al.*, 1982).

Finally, let us observe that the method of gamma-gamma energy correlations described in Sec. III.B may also lead to some valuable information about the qcs. In fact, some structures in the γ - γ coincidence plots have been seen that were not observed otherwise by means of individual gamma-ray measurements.

Most of the γ - γ -energy correlation experiments have been carried out on nuclei known to have prolate deformations at low spins, thus exhibiting regular patterns like a "central valley" (minimum of counts) in the correlation matrices as well as "bridges" (maximum of counts) related to band crossings, etc. A possible relationship between the observed width of the central valley in the coincidence plots and the moment of inertia is discussed in Sec. III.B.

When the technique is applied to more spherical nuclei, one may explore the existence of yrast traps as stepping stones to reach nuclear states with the highest angular momentum. In a study of ^{152}Er (with an isomer at ~ 12 MeV and $I \sim 33$) Baba *et al.* (1981) seem to confirm a structure typical for spherical or weakly oblate shapes up to $I \sim 50$.

We may conclude from these accounts on experimental techniques that a fascinating area of research has just been opened and that further refinements of the methods in the future should yield more quantitative results on the properties of nuclei at the highest angular momenta.

C. Nuclear structure information deduced from quasicontinuum spectra

Various calculations concerning nuclear behavior at high angular momenta can also be applied to the region of the qcs. In particular, considerable changes in nuclear shape with increasing angular momentum have been predicted (Cohen *et al.*, 1974; Bohr and Mottelson, 1974; Bengtsson *et al.*, 1975; Neergaard and Pashkevich, 1975; Neergaard *et al.*, 1976, 1977; Andersson *et al.*, 1976; Faessler *et al.*, 1976). These predictions have been described and illustrated in Secs. II.C and II.D (in particular, cf. Figs. 4–6 and 8). One of the most striking features of these calculations is the possible existence of superdeformed nuclear states corresponding to the transition over the Jacobi instability. Such an effect is well known from classical mechanics and has also been extensively discussed in astrophysics in connection with the equilibrium shapes of rotating stars and planets.

Fascinating effects are connected with the possible disappearance of the pairing correlations (phase transitions from superfluid to normal) in the rotating nuclei (cf. Sec. III.C). We have to emphasize, however, that the information on nuclear structure at high angular momentum obtained so far is rather preliminary. Thus both phe-

nomena mentioned above can neither be clearly confirmed, nor can they be ruled out on the basis of the present experimental results on the qcs.

Many experimental efforts were devoted to determination of the nuclear moments of inertia. Two methods for determining the moment of inertia \mathcal{F} have been suggested, for example, by the Berkeley group (Banashik *et al.*, 1975; Simon *et al.*, 1976, 1977). In the approach referred to as "integral," two quantities are involved: the angular momentum I_{in} at the origin of the cascade, and the gamma transition-energy E_γ . Employing a simple formula (3.16) for the rotational band, one obtains [cf. Eq. (3.17)]:

$$E_\gamma = (\hbar^2/2\mathcal{F})(4I - 2), \quad (5.4)$$

an equation that relates E_γ , I_{in} , and \mathcal{F} . The quantity \mathcal{F} determined in this way follows the definition of $\mathcal{F}^{(1)}$ [cf. Eq. (3.3)], since it is related to the first derivative of energy with respect to angular momentum ($E_\gamma = \mathcal{E}_I - \mathcal{E}_{I-2} = \Delta\mathcal{E}$). On the other hand, it is understood that Eq. (5.4) employed here is not confined to a single rotational band; it rather follows a path along many bands. Thus the quantities E_γ and I entering Eq. (5.4) are better considered averages $\langle E_\gamma \rangle$ and $\langle I_{\text{in}} \rangle$. This leads to the conclusion that $\mathcal{F}^{(1)}$ obtained in this way characterizes the envelope curve extended over many collective bands and thus should be labeled $\mathcal{F}_{\text{env}}^{(1)}$. This quantity appears to be larger than the moments of inertia $\mathcal{F}_{\text{band}}^{(1)}$ characterizing just one band [$\mathcal{F}_{\text{env}}^{(1)} > \mathcal{F}_{\text{band}}^{(1)}$], since $\mathcal{F}_{\text{env}}^{(1)}$ describes in addition the contributions to the total inertia coming from the configuration changes (band crossing).

Another (differential) method has also been proposed [cf. references above and Herskind (1980)] for determining \mathcal{F} , which is derived from the change ΔE_γ in the transition energy E_γ corresponding to the increase ΔI in angular momentum. It follows from the rotational formula (3.16) that [cf. also Eq. (3.18)]:

$$\begin{aligned} \Delta E_\gamma &= 8\hbar^2/(2\mathcal{F}) - 2E_\gamma d(\ln\mathcal{F})/dI \\ &\sim 8\hbar^2/(2\mathcal{F}_{\text{env}}^{(2)}). \end{aligned} \quad (5.5)$$

Here, the moment of inertia $\mathcal{F}_{\text{env}}^{(2)}$ has been used, since it corresponds to the second derivative of energy $\mathcal{E}(I)$, and the subscript "env" (envelope) is added again in order to indicate a path combining many bands. Finally, the moments of inertia obtained from the gamma-gamma coincidence spectra (cf. Sec. III.B) may correspond to $\mathcal{F}_{\text{band}}^{(2)}$, i.e., the dynamical moment of inertia characterizing one given rotational band.

As stated above also here, the inequality $\mathcal{F}_{\text{env}}^{(2)} > \mathcal{F}_{\text{band}}^{(2)}$ is related to the additional contribution of band crossings into $\mathcal{F}_{\text{env}}^{(2)}$. However, this relation expresses a local property of the yrast line in a region of crossing, unlike the inequality $\mathcal{F}_{\text{env}}^{(1)} > \mathcal{F}_{\text{band}}^{(1)}$. In fact, the ratio $\mathcal{F}_{\text{band}}^{(2)}/\mathcal{F}_{\text{env}}^{(2)}$ can be directly related to the relative contribution of the alignment Δi with respect to the total increase ΔI in angular momentum [cf. Bohr and Mottelson (1981)]:

$$\frac{\mathcal{F}_{\text{band}}^{(2)}}{\mathcal{F}_{\text{env}}^{(2)}} = 1 - \frac{\Delta i}{\Delta I}. \quad (5.6)$$

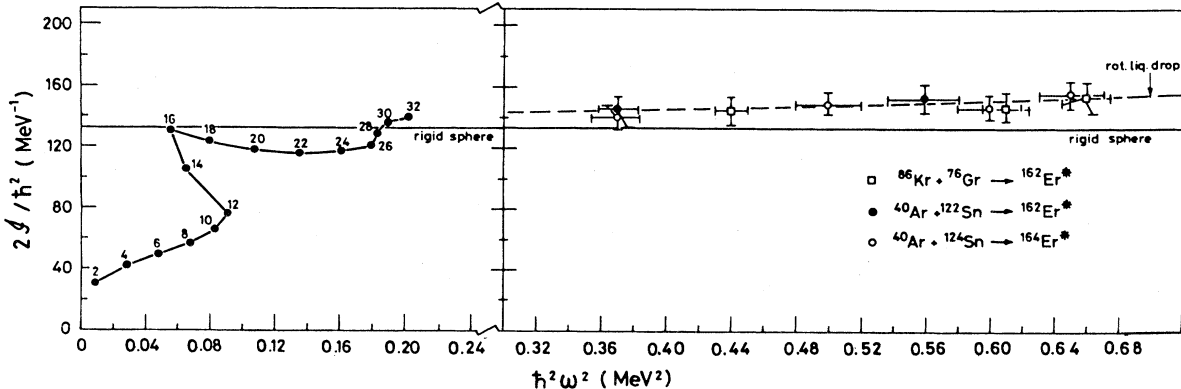


FIG. 47. Backbending plot for the Er systems produced with 161–236 MeV ^{40}Ar and 314–376 MeV ^{86}Kr beams (Hillis *et al.*, 1979). The data on the left-hand side of the figure are obtained from known transitions between discrete yrast states in ^{158}Er (Lee *et al.*, 1977). The data in the right part of the figure represent the extension of rotational bands into the quasicontinuum derived from the “collective” bump in the multiplicity spectra. The moments of inertia calculated for a rigid sphere and a rotating liquid drop are also indicated.

Nuclear moments of inertia have been discussed extensively [see, for example, Bohr and Mottelson (1975)], especially in the domain of low angular momenta. It is known (cf. Sec. III.D) that moments of inertia in superfluid nuclear states are considerably reduced as compared to the rigid-body values, \mathcal{F}_{rig} . For the normal (i.e., non-superfluid) nuclear system it was predicted long ago [Bohr and Mottelson (1955); see also Bohr and Mottelson (1975)] that the average moment of inertia should roughly coincide with that of the rigid body, \mathcal{F}_{rig} . The dependence of \mathcal{F}_{rig} on nuclear deformation has been rather well investigated on the basis of simple calculations (cf. Sec. II.F, where some estimates are given). Consequently, the variation with spin I of the moments of inertia determined experimentally could be used to obtain information on shape changes in nuclei, if other phenomena causing an increase in \mathcal{F} (such as the alignment) were ruled out.

Figure 47 illustrates the moments of inertia for some Er nuclei obtained in reactions with ^{40}Ar and ^{86}Kr leading to Er isotopes (Hillis *et al.*, 1979). The left-hand side of the figure presents a comparison with the lower-spin experiments (Lee *et al.*, 1977) performed with discrete gamma-line spectroscopy. The right-hand side of the figure illustrates the moments of inertia $\mathcal{F}_{\text{env}}^{(1)}$ obtained from multiplicity experiments. Comparison with an estimate from the rigid sphere seems to show a slight increase in $\mathcal{F}_{\text{env}}^{(1)}$ and thus perhaps also (in deformation) with increasing spin.

Another method of searching for the changes in the nuclear moment of inertia $\mathcal{F}_{\text{band}}^{(2)}$ could follow from the observation of the width of the central valley in the gamma-gamma coincidence plots (cf. Sec. III.B). As follows from Eq. (3.18) the increase in moments of inertia with angular momentum would result as a gradual decrease in the width of the central valley and vice versa. Changes of this type have indeed been observed [see, for instance, Schutz *et al.* (1982)], but no systematic behavior has yet been deduced (cf. Sec. III.B).

Experimental and theoretical investigations of the nuclear moments of inertia have been continued by many authors (Bohr and Mottelson, 1981; Leander *et al.*, 1981; Deleplanque, 1981; Deleplanque *et al.*, 1982; Zang and Åberg, 1982; Bengtsson and Ragnarsson, 1982; Stephens, 1982). The behavior of the moments of inertia for spins much above the critical value at which the superfluid pairing correlations disappear reflects important microscopic structure properties in the domain of a very fast rotation. In particular, the variation in \mathcal{F} may indicate an alignment or dealignment in consecutive neutron or proton orbitals and/or shape changes (Deleplanque *et al.*, 1982).

Moments of inertia are, of course, not the only physical quantities that can be an object of the analysis of the qcs. As an example of a different quantity, let us look for the differences in the side-feeding patterns between two isotopes of dysprosium. Side feeding of a level is defined as the population of that level which is not due to the population of the adjacent higher-spin level belonging to the same band. Figure 48(a) illustrates the result of several experiments on the gamma-ray intensities from ^{156}Dy obtained in different nuclear reactions. The ^{156}Dy nucleus is known as well deformed in the low-spin range. We can see from Fig. 48 that the intensities do not change very much with either the reaction mechanism or the ion energy. We can understand this behavior in the following way. The deformation of ^{156}Dy implies that there are definite rotational bands (channels) along the yrast line in the qcs region. Most of the intensity originating at the entry line therefore goes along these rotational bands. Thus the population of the various levels in the low-spin part of the spectrum ($I=2, 4, 6, \dots, 20$) is affected very little by either the reaction mechanism or the ion bombarding energy.

For the ^{152}Dy nucleus [cf. Fig. 48(b)], the situation is different. This nucleus is known to be spherical or weakly deformed in a rather large-spin range up to at least

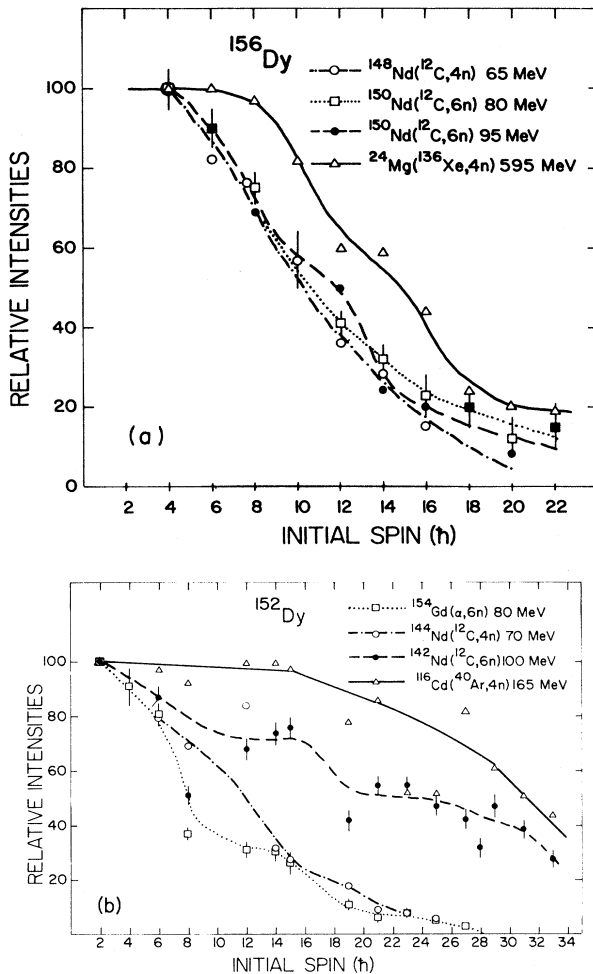


FIG. 48. Total γ -ray intensities in ^{156}Dy (a) excited in the $(^{12}\text{C},4n)$ reaction (Sukowski *et al.*, 1979), in $(^{12}\text{C},6n)$ reactions (Hageman *et al.*, 1981), and in the $(^{136}\text{Xe},4n)$ reaction (Ward *et al.*, 1979), and in ^{152}Dy (b) excited in $(\alpha,6n)$ and $(^{12}\text{C},xn)$ reactions (Hageman *et al.*, 1981) and in the $(^{40}\text{Ar},4n)$ reaction (Cornelis *et al.*, 1980).

$I \sim 40$ (cf. Sec. IV). Consequently, in its QCS there may be no rotational bands along the yrast line (or, at least, they are not so well pronounced). Hence there is no pronounced γ -ray channeling mechanism above the yrast line (which was the case in ^{156}Dy). Thus the side-feeding pattern may be entirely different, and, in particular, it may depend more sensitively both on the reaction mechanism and on the ion bombarding energy. This seems to be confirmed by the experiments with various beams and energies [see also Khoo (1980)].

One has to be careful, however, to seek explanation of the side-feeding only in the deexcitation process via collective bands of the QCS. One should also take into account the level density which increases at high spin when the number of active nucleonic orbitals increases. [See also Khoo (1980), who investigated yrast states in $^{148,150,151,152}\text{Dy}$ populated in $^{32,34}\text{S}$ induced reactions with

spins up to the valence limit, i.e., the total spin of active particles in outer shells.] The discussion above may serve as an example of the exploration of the QCS region by means of the γ -ray intensity measurements.

Several groups have initiated and performed calculations of the distribution of the gamma-radiation intensity over the whole region of QCS spectra (Liotta and Sorensen, 1978; Civitarese *et al.*, 1979; Wakai *et al.*, 1980; Leander *et al.*, 1981). These calculations are based mainly on statistical assumptions about the particle and gamma emission from highly excited compound nuclei at large angular momenta. Starting from some reasonable model assumptions, these calculations aim at reproducing properties of various physical quantities—gamma-ray intensities, average multiplicities, average side-feeding patterns, gamma-gamma energy correlations, etc.

A microscopic theory of the energy spectra in the QCS region could be provided in principle by the temperature-dependent Hartree-Fock-Bogolyubov method. Several attempts have been recently made in this direction (Tanabe and Sugawara-Tanabe, 1980; Tanabe *et al.*, 1981, 1981a; Goodman, 1981). These calculations provide the whole description of highly excited (heated) nuclei in the region above the yrast line (behavior of the pairing gap, level densities, deformation changes, etc.). For the moment, however, the results of these calculations have not yet been extensively employed in the analysis of experimental data.

We may conclude that QCS γ -ray studies have been focused mainly on bulk properties of fast rotating nuclei. For more detailed and also quantitative information it seems necessary to observe discrete γ -ray lines. In this respect, one may expect new results from multidetector Compton suppression spectrometers with high resolution, large coincidence efficiency, and with superior peak-to-background ratios presently being developed.

VI. SUMMARY

In this section we will summarize the main topics discussed in the article. Results of the studies on nuclear structure at high angular momenta and the most important conclusions are collected in Sec. VI.A. Since, however, we could not resist the temptation also to discuss the perspectives for similar research in the near future, related problems are briefly reviewed in Sec. VI.B.

A. Conclusions

High spins are most often generated in atomic nuclei by collective rotation of the nucleus as a whole, by an alignment of a few nucleonic angular momenta, and by combination of both these mechanisms.

The *collective rotation* consists of smooth adjustments in the individual nucleonic orbitals, many of which contribute coherently to the rotation of the nuclear system as a whole. The regular rotational band structures established in many well-deformed nuclei up to $I \sim 12-14$ are well

understood in terms of the collective mechanism. The yrast state structure often undergoes a sudden change at $I \sim 12-14$. It has been found that this change is the strongest in nuclei which have high- j and low- m_j single-particle levels close to the Fermi level. Extensive calculations based on the independent quasiparticle method in a rotating nuclear potential (in some versions also referred to as the HFBC method) have clearly indicated that the structure rearrangement can be associated with the alignment of the corresponding nucleonic orbitals with the axis of collective nuclear rotation. Such an alignment leads to a sudden increase in the total angular momentum and has been found experimentally in many nuclei. This phenomenon, commonly called backbending, is related to a sharp crossing between two rotational bands (i.e., those with no, or only weak interaction).

Systematic analyses of the alignment effect have established its quasiparticle character, and numerous excited rotational bands have successfully been interpreted in terms of quasiparticle excitations superimposed on the collective rotation.

Elaborate detection techniques and use of the high-energy heavy ion projectiles (up to ~ 10 MeV per nucleon) have enabled studies of discrete γ -ray transitions up to spins 30–40. This, in particular, led to discovery of the second backbending effects in several nuclei. Very detailed analysis of the excited band structure, nuclear moments, etc., have provided firm evidence for the multi-quasiparticle structure in high-spin nuclear rotation.

In *spherical or nearly spherical nuclei* individual nucleonic alignment was found to dominate the high-spin excitation pattern. The yrast sequence of these nuclei is very irregular in contrast to the smooth behavior of the yrast lines of collectively rotating nuclei. Both phenomenological and shell-model studies have confirmed the tendency toward maximum alignment (allowed by the Pauli principle) of individual nucleonic angular momenta with the total angular momentum. This in turn causes a polarization of the nucleus, giving rise to oblate shape configurations with a symmetry axis in the direction of the total angular momentum (apart from some rather exceptional cases of prolate deformed nuclei, e.g., in some Hf isotopes). Apparently, no collective rotation is allowed by quantum mechanics in such nuclear configurations, and the only mechanism of exciting high angular momenta is that via rearrangement in the individual nucleonic orbitals. This has been shown to generate isomeric (relatively long-living) states at high angular momenta.

Several properties of the high-spin isomers (excitation energies, spins, parities, lifetimes, γ -ray feeding and decay schemes, and in some cases also electromagnetic moments) have been measured. On the basis of measured hindrance in the electromagnetic transition probabilities the noncollective character of rotation in high-spin isomers has been indeed experimentally confirmed. Detailed single-particle structure of many isomeric states has been suggested theoretically and tested experimentally by measuring the corresponding magnetic dipole moments.

The degree to which isomeric states also exhibit some

collective properties has been estimated only in a few cases from measured electric quadrupole moments (in the nucleus ^{147}Gd , for example, the absolute values of the quadrupole moments were seen to increase with the excitation energy and spin of the isomeric states). Coexistence between basically single-particle excitation modes and collective vibrations have been suggested. In particular, the existence of the nuclear shape vibrations and the giant dipole (quadrupole) resonances at high-spin states have been proposed. No systematic data exist on this aspect of high-spin excitation and only future studies can possibly shed some light.

The nuclear properties at very high angular momenta (exceeding the spin limit ~ 40 accessible at present with the discrete-line spectroscopy) have also been studied. Using sum spectrometers and multiplicity filters, experimenters have measured the γ -ray energy and multiplicity distributions in several nuclei. This information, supplemented with the angular and γ - γ -energy correlation measurements, has indicated a collective character of nuclear motion in many nuclei for $I > 40$. In particular, the methods of measuring the nuclear moments of inertia at these super-high angular momenta have been designed and first results analyzed. Unfortunately, the studies concerned mainly the gross properties of the unresolved (quasicontinuum) spectra. This limitation was due to the fact that in the quasicontinuum range only the averages over many nuclear γ cascades could be measured.

No straightforward and systematic results have been obtained so far on two fascinating nuclear structure problems: the nuclear shape evolution and the disappearance of the nuclear pairing correlations at high spin. This will certainly be a subject of forthcoming analysis.

B. Perspectives

The two excitation modes—i.e., the collective rotation and the alignment of the individual orbitals—can compete in high-spin excited states. For example, an oblate system with a few aligned orbitals may rotate collectively about an axis perpendicular to the symmetry axis. Some other modes of excitation which should be investigated more extensively in the near future involve the collective vibration. A possible mode is a nonaxial shape vibration occurring simultaneously with the excitation of aligned orbitals. Other vibrational excitations including those connected with the giant resonances may also be involved. These competing mechanisms may reveal new aspects of the collective excitations characteristic for the lack of time reversal invariance in fast rotating systems.

Since the present knowledge about nuclear states at super-high angular momentum ($I > 40$) mainly concerns gross properties, one has to concentrate in the near future on the detailed properties. Gamma-ray spectroscopy may be focused on the determination of the properties of highly excited states which unambiguously reveal the nature of the band-crossing phenomena. Among other properties are the lifetimes (in the picosecond region) and the elec-

tromagnetic moments, which may shed light on the changes in nuclear shape and structure with increasing angular momentum. These measurements are particularly needed in and above the first and second backbending regions, thus at least up to spin $I \sim 30$. Extension of these detailed spectroscopic studies towards lighter nuclei (for instance, the barium region) and also towards heavier systems (e.g., the actinides) is of much interest. In particular, backbending features have been established in several lighter nuclei, but not in the actinides, although in the latter some anomalies in the rotational band structures have been observed recently.

Similar detailed information on the properties of high-spin isomers is needed in order to establish their structure. Future experiments have to prove whether very-high-spin ($I > 40$) isomers do or do not exist. Much remains to be learned about the interplay between collective and single-particle modes of excitation at various rotational frequencies.

Fast nuclear rotation may imply substantial changes in the properties of the average nuclear field. Until now, such changes were allowed for in the theoretical description mainly through appropriate variation in the nuclear deformation. At large angular velocities, however, one may expect the existence of new terms in the nuclear potential—for instance, those breaking the time reversal invariance.

Interesting information on discrete as well as on quasicontinuum states can be expected from a further development of the γ - γ -energy correlation technique. Besides improvement of the statistics one has to apply background subtraction techniques more reliable than the ones used at present or to enhance experimentally the ratio of true to random (or other background) events. The latter possibility is being exploited with systems of many Compton suppression spectrometers in coincidence. This would, in addition, allow registration of triple coincidences with sufficient statistics to remove ambiguities in the identification of long γ -ray cascades and to improve the observation of resolved weak γ -ray transitions between the very-high-spin states.

One of the fascinating present problems is the possible occurrence of the Jacobi instability in atomic nuclei at high angular momentum, sometimes referred to as "superdeformation." While this effect has been predicted by theory, no clear-cut experimental evidence seems to exist as yet. This Jacobi instability is assumed to exist in astronomical objects, where it results from a competition between the centrifugal stretching and long-range gravitational forces and may lead to the formation of double stars. However, in atomic nuclei at least two essentially different aspects can be indicated, apart from the Coulomb repulsion between protons: First, the nuclear interaction is of short-range character; second, the quantal shell structure may also play an important role.

For all these kinds of investigations one probably needs to combine high γ -ray energy resolution and large efficiency with sharp selectivity for reaction exit channels and for high-spin states. It thus seems necessary to com-

bine, for instance, sum spectrometers, multiplicity filters with several Compton suppression spectrometers [including the high-resolution Ge(Li) detectors] in compact assemblies. This may become effective if new high-density scintillation material can be applied, as, for instance, $\text{Bi}_4(\text{GeO}_4)_3$.

Another major challenge in studies of the nuclear structure is the detailed constitution of the individual γ -ray cascades which connect the highly excited entry states with the ground state. In order to reveal the nature of the cascades, one has to record all relevant parameters of the γ -ray cascades per individual nuclear reaction rather than averages over many reactions and cascades. New multidetector spectrometers called "crystal balls" have been developed for this purpose. They are designed to record in an event-by-event mode per single reaction the energies, angles, and times of emission of all γ rays with high efficiency. One spectrometer developed at Oak Ridge—St. Louis contains 72 NaI(Tl) detectors in a ball shell of 35.6 cm inner diameter and 17.8 cm thickness (Sarantites *et al.*, 1980). Another one, designed at Darmstadt-Heidelberg, contains 162 NaI(Tl) detectors in a ball shell of 50 cm inner diameter and 20 cm thickness (Simon, 1980). Those spectrometers can also be used in coincidence with Ge(Li), or particle detectors, placed in the scattering chamber inside the ball or outside it after removing one or more NaI detectors. The development of almost massless detectors (parallel-plate or avalanche detectors) makes it possible to detect particles or heavy ions inside the spectrometer without influencing the γ -ray detection.

An essential problem for future experiments is sharp selection of the initial angular momentum and excitation energy in the entry regions through the simultaneous measurement of the total γ -ray energy and the multiplicity. The instrumental spreads in these quantities may be as low as $\sim 20\%$ at full width at half maximum (FWHM) compared with ~ 50 –100% in the present sum spectrometers and multiplicity filters. An important application of combining the crystal ball with particle detectors will be found in polarization experiments in which the initial spin alignment can be detected by observing γ rays which hit a ring of detectors in one plane. This may be particularly useful when combined with the observation of emitted charged particles or heavy ions for the study of reaction processes.

It is obvious that sophisticated spectrometers on line at high-energy heavy-ion accelerators will yield a vast amount of interesting and probably also unexpected results. However, data acquisition may be very complicated, the spectrometers very expensive, the beam time limited, and the analysis presumably rather time consuming. Therefore we expect these projects to yield unique results, but only in a very limited number of cases probably concentrating on highly excited nuclei with high angular momentum. Therefore many supporting experiments may remain to be done at other nuclear physics laboratories with smaller accelerators and more beam time available. In addition, much support is expected and

needed from large and small theoretical groups, especially in stimulating new ideas. Also, extensive investigations at medium and low angular momentum have to be continued to establish the systematic trends in nuclear structure and reaction processes. In this sense, one should not forget that the extension of the present knowledge of band structures towards low spin may be as important and difficult as towards high spin.

The highly developed methods in theoretical and experimental nuclear physics with heavy- and light-ion accelerators and with advanced and conventional spectroscopic techniques common nowadays promise fascinating research and results in the field of nuclear structure in the forthcoming years.

ACKNOWLEDGMENTS

The authors would like to express their feelings of gratitude to many colleagues who provided photographic materials or other information. Particularly appreciated are comments and suggestions from Drs. F. A. Beck, A. E. L. Dieperink, O. Häusser, B. Herskind, H. Hübel, T. L. Khoo, J. C. Merdinger, R. H. Siemssen, R. S. Simon, Z. Sujkowski, J. Vervier, and A. van der Woude. One of the authors (M.d.V.) would like to thank the Free University for the opportunity to start this work during his leave of absence in Amsterdam. This work was performed as part of the research program of the "Stichting voor Fundamenteel Onderzoek der Materie" (FOM), which is financially supported by the "Nederlandse Organisatie voor Zuiver Wetenschappelijk Onderzoek" (ZWO). The work was also partly supported by the Polish-American Maria Skłodowska Fund Grant No. PF7037P. Another of us (J.D.) wishes to express his gratitude to the Danish Research Council for support during his stay at the Niels Bohr Institute, Copenhagen, where part of this study was carried out.

APPENDIX A. DETAILS OF NUCLEAR POTENTIALS

We will first recapitulate the properties of the Nilsson and Woods-Saxon spectra (Sects. 1 and 2). In Sect. 3 some systematic differences between the single-particle spectra of the two potentials will be discussed.

1. The Nilsson average potential

The first "realistic" deformed single-particle potential was introduced by Nilsson (1955). Modified since then, it has been used to calculate various nuclear properties. After some extensions both the ground and excited states in nuclei could be calculated [Nilsson *et al.* (1969), Gustafson *et al.* (1967), Andersson *et al.* (1976); see also references cited therein].

The basic constituent of the model is a deformed oscillator potential. Here we limit our discussion to the case of axial symmetry around the z axis and define

$$v_{\text{osc}} = \frac{1}{2}m[\omega_{\perp}^2(x^2+y^2)+\omega_z^2z^2], \quad (\text{A1})$$

in which the oscillator frequencies ω_{\perp} and ω_z are set to be functions of the nuclear deformation parameters. The deformation dependence is introduced after transforming the potential (A1) into the so-called stretched coordinates

$$\begin{aligned} \xi &= x[(m\omega_{\perp})/\hbar]^{1/2}, \quad \eta = y[(m\omega_{\perp})/\hbar]^{1/2} \\ z &= z[(m\omega_z)/\hbar]^{1/2}. \end{aligned} \quad (\text{A2})$$

Inserting (A2) into (A1), one obtains

$$v_{\text{osc}} = \frac{1}{2}\hbar\omega_0(\epsilon_2)\rho^2[1 - \frac{2}{3}\epsilon_2 P_2(\cos\theta_t)], \quad (\text{A3a})$$

where $\rho^2 = \xi^2 + \eta^2 + z^2$ and $\cos\theta_t = z/\rho$. Then higher multipolarity deformations—e.g., the hexadecapole deformation—are introduced by modifying Eq. (A3a):

$$\begin{aligned} v_{\text{osc}} &\xrightarrow{\text{df.}} V_{\text{osc}} = \frac{1}{2}\hbar\omega_0(\epsilon_2, \epsilon_4)\rho^2[1 - \frac{2}{3}\epsilon_2 P_2(\cos\theta_t) \\ &\quad + 2\epsilon_4 P_4(\cos\theta_t)]. \end{aligned} \quad (\text{A3b})$$

The hitherto arbitrary factor $\hbar\omega_0(\epsilon_2, \epsilon_4)$ is calculated from the condition that the volume enclosed by equipotential surfaces need not depend on the deformation (see also below). Here P_{λ} denote the Legendre polynomials.

Apparently, transformation (A2) also affects the kinetic energy term in the Schrödinger equation with the potentials v_{osc} or V_{osc} . Owing to the particular form of this transformation, the matrix elements of the kinetic energy term that connect states with different major shells N and N' cancel with the corresponding matrix elements of v_{osc} . Thus the whole Hamiltonian becomes block diagonal with respect to N if quadrupole deformation alone is used.

The deformation introduced in Eq. (A3b) contains only a quadrupole ϵ_2 and hexadecapole ϵ_4 term. Terms of any other multipolarity λ can similarly be introduced by adding $2\epsilon_{\lambda} P_{\lambda}(\cos\theta_t)$ to the right-hand side of Eq. (A3). Note that the ϵ_2 and ϵ_4 deformations are not identical with the quadrupole β_2 and hexadecapole β_4 degrees of freedom introduced as proportionality coefficients in the nuclear surface expansion (see also below):

$$R(\theta) = R_0 c(\beta_2, \beta_4)[1 + \beta_2 Y_{20}(\cos\theta) + \beta_4 Y_{40}(\cos\theta)], \quad (\text{A4})$$

where $c(\beta_2, \beta_4)$ is calculated from the constant-volume condition. The main differences originate from the stretched coordinate system used [Eq. (A2)], from the fact that $\cos\theta_t \neq \cos\theta = z/(x^2 + y^2 + z^2)^{1/2}$, and also from the fact that $\rho^2 P_{\lambda}(\cos\theta_t)$ contains a radial dependence (on x , y , and z) different from that in multipole moments defined as $\sim r^{\lambda} Y_{\lambda 0}(\cos\theta)$.

The deformed oscillator potential does not reproduce the nuclear shell structure, i.e., the magic numbers, throughout the Periodic Table. This difficulty can be overcome by adding two more terms to the Nilsson potential formula:

$$V_{\text{Nilss}} = V_{\text{osc}} - 2\kappa\hbar\dot{\omega}_0[\mathbf{l}_t \cdot \mathbf{s} - \mu(\mathbf{l}_t^2 - \langle \mathbf{l}_t^2 \rangle)], \quad (\text{A5})$$

where \mathbf{l}_t , defined in stretched coordinates, resembles the

angular momentum operator; κ and μ are adjustable constants, whereas

$$\omega_1^2 \omega_z \equiv \dot{\omega}_0^3 = \text{const} , \quad (\text{A6})$$

in order to satisfy the constant volume condition [cf. Eq. (A9) below]. It is the role of the $\mathbf{l}_t \cdot \mathbf{s}$ term to imitate the

$$H_{\text{Nilss}} = \frac{1}{2} \hbar \omega_0 (\varepsilon_2, \varepsilon_4) \left[-\Delta_{\xi \eta \beta} + \frac{2}{3} \varepsilon_2 \frac{1}{2} \left(2 \frac{\partial^2}{\partial \beta^2} - \frac{\partial^2}{\partial \xi^2} - \frac{\partial^2}{\partial \eta^2} \right) + \rho^2 - \frac{2}{3} \varepsilon_2 \rho^2 P_2(\cos \theta_t) + 2 \varepsilon_4 \rho^2 P_4(\cos \theta_t) \right] \\ - 2\kappa \hbar \dot{\omega}_0 [\mathbf{l}_t \cdot \mathbf{s} - \mu (\mathbf{l}_t^2 - \langle \mathbf{l}_t^2 \rangle_N)] , \quad (\text{A7})$$

with the first two terms in the square brackets representing the kinetic energy after one has transformed the Laplace operator Δ_{xyz} into stretched coordinates.

The Schrödinger equation with this Hamiltonian can now be solved numerically by diagonalizing expression (A7) within, for example, the harmonic oscillator basis. As is well known, in the diagonalizing methods one has to limit oneself to the finite number of basis states (basis cutoff). This is done in such a way that the number of basis states is large enough to provide sufficient accuracy, but at the same time not too large to keep the corresponding computer memory requirements acceptable. It is an important property of the Nilsson potential that the matrix elements of such operators as, for instance,

$$\varepsilon_\lambda \rho^2 P_\lambda(\cos \theta_t) \text{ for } \lambda \neq 2, \mathbf{l}_t \cdot \mathbf{s}, \text{ or } \mathbf{l}_t^2 ,$$

that connect states of different major harmonic-oscillator shells, are generally smaller than the matrix elements of the total Nilsson Hamiltonian calculated within a given shell N . (This is not generally true, but applies only to the physical range of variation of the Nilsson deformation parameters.) Since the operators listed above do not couple strongly with the various major harmonic-oscillator shells, the errors introduced by the cutoff procedure must be small.

For an adequate calculation the constants entering Eq. (A7) have to be adjusted properly. First, the volume conservation condition which says that the volume enclosed by the equipotential surface

$$V_{\text{osc}}(\xi, \eta, \beta) = \varepsilon_{\text{Fermi}} \quad (\text{A8})$$

be deformation independent gives

$$\hbar \dot{\omega}_0^3 (\varepsilon_2, \varepsilon_4) = \frac{\hbar \dot{\omega}_0}{2(1 + \frac{1}{3} \varepsilon_2)(1 - \frac{2}{3} \varepsilon_2)^{1/2}} \\ \times \int_{-1}^{+1} \frac{d(\cos \theta)}{[1 - \frac{2}{3} \varepsilon_2 P_2(\cos \theta) + 2 \varepsilon_4 P_4(\cos \theta)]^{3/2}} . \quad (\text{A9})$$

[In fact, with the form of the potential (A3b) the volume enclosed by any of the quasipotentials remains constant, provided Eq. (A9) is fulfilled.] The parameter $\hbar \dot{\omega}_0$ is usually found from the condition that the nuclear radii be reproduced. This implies that $\hbar \dot{\omega}_0$ is in general a function of the proton and neutron numbers Z and N .

nuclear spin-orbit interaction potential. The last term in Eq. (A5) deepens the effective potential well for particles residing close to the nuclear surface, i.e., in the high- j or high- l orbitals. In other words, it renders the potential more square-well-like for these orbitals.

The Nilsson single-particle Hamiltonian in its final form thus reads

$$H_{\text{Nilss}} = \frac{1}{2} \hbar \omega_0 (\varepsilon_2, \varepsilon_4) \left[-\Delta_{\xi \eta \beta} + \frac{2}{3} \varepsilon_2 \frac{1}{2} \left(2 \frac{\partial^2}{\partial \beta^2} - \frac{\partial^2}{\partial \xi^2} - \frac{\partial^2}{\partial \eta^2} \right) + \rho^2 - \frac{2}{3} \varepsilon_2 \rho^2 P_2(\cos \theta_t) + 2 \varepsilon_4 \rho^2 P_4(\cos \theta_t) \right] \\ - 2\kappa \hbar \dot{\omega}_0 [\mathbf{l}_t \cdot \mathbf{s} - \mu (\mathbf{l}_t^2 - \langle \mathbf{l}_t^2 \rangle_N)] , \quad (\text{A7})$$

One argues that the proton and neutron matter distributions should lead to similar rms radii, which in turn implies that the neutron and proton oscillator parameters should differ. It was found (Nilsson *et al.*, 1969) that in order to meet both of the above requirements one sets

$$\hbar \dot{\omega}_n = \hbar \dot{\omega}_0 \left[1 + \frac{1}{3} \frac{N - Z}{A} \right] , \quad (\text{A10a})$$

$$\hbar \dot{\omega}_p = \hbar \dot{\omega}_0 \left[1 - \frac{1}{3} \frac{N - Z}{A} \right] , \quad (\text{A10b})$$

$$\hbar \dot{\omega}_0 = 41/A^{1/3} \text{ MeV} . \quad (\text{A10c})$$

The other four parameters, two pairs of κ and μ for protons and neutrons each, are adjusted in such a way that the experimental single-particle order is reproduced optimally. The results of such a fit can be found in Nilsson *et al.* (1969).

The main advantage of Hamiltonian (A7) is that with six smooth functions of Z and N (viz., $\hbar \dot{\omega}_n$, $\hbar \dot{\omega}_p$, κ_p , μ_p , κ_n , and μ_n) a good description of the single-particle spectra is obtained. But it also contains a few disadvantages. One of them stems from the fact that the $(\mathbf{l}_t^2 - \langle \mathbf{l}_t^2 \rangle)$ term is introduced in a purely phenomenological manner in order to obtain systematic shifts of some single-particle levels with respect to the others. Its nature, in contrast to the nature of the spin-orbit term, is not a physical one. Its presence causes several difficulties in high-spin calculations, as will be discussed below. Moreover, the spin-orbit term $\sim \mathbf{l}_t \cdot \mathbf{s}$ should rather be replaced by $\mathbf{s} \cdot (\mathbf{p} \times \text{grad} \mathbf{V})$ (Bohr and Mottelson, 1969). The difference between the two expressions becomes relevant for very large distortions.

Despite these deficiencies, the Nilsson potential played and still plays an important role in studying numerous properties of nuclear structure. Its simplicity—in particular, the fact that the main harmonic-oscillator number N remains an approximately good quantum number—helped to reveal principal mechanisms in nuclear phenomena, which were later studied with more complicated methods. For a long time the results provided by Nilsson model calculations were of such quality that they could compare with those of more refined approaches. Only re-

cently has it been realized that the presence of the \mathbf{l}_t^2 term in the potential introduces some systematic effects, especially on the high- j orbitals, of importance for high-spin calculations. Some of these effects will be discussed below in Sec. 3.

The finite deformed-potential well of the Woods-Saxon type is free from most of the above deficiencies. Since, however, the corresponding Schrödinger equation is more complicated in structure, the numerical codes used to solve such an equation are also more complex. The following section will be devoted to a brief discussion of the deformed Woods-Saxon potential.

2. The Woods-Saxon average potential

Introduced initially to describe the single-particle levels of spherical nuclei, the potential

$$V_{\text{WS}} = V_c(r) + V_{\text{so}}(r) + \frac{1}{2}(1+\tau_3)V_{\text{Coul}}(r), \quad (\text{A11a})$$

where

$$V_c(r) = \frac{V_0}{1 + \exp[(r - R_0)/a]}, \quad V_0 < 0, \quad (\text{A11b})$$

and

$$V_{\text{so}}(r) = \lambda_{\text{so}} \left[\frac{\hbar}{2mc} \right]^2 \mathbf{l} \cdot \mathbf{s} \frac{1}{r} \frac{d}{dr} \left[\frac{V_0}{1 + \exp[(r - R_{\text{so}})/a]} \right] \quad (\text{A11c})$$

proved to provide a very good description of the single-particle levels. In Eqs. (A11a)–(A11c) V_0 denotes the central-potential depth parameter, and $R_0 = r_0 A^{1/3}$ ($R_{\text{so}} = r_{\text{so}} A^{1/3}$). The radius parameters r_0 and r_{so} are adjustable, A independent constants; a is a diffuseness pa-

rameter. The Coulomb potential is added for protons; it is frequently defined as an electrostatic potential generated by a uniform charge distribution, with its shape identical to that of a proton distribution (in the Nilsson potential the difference between neutrons and protons enters the potential only via numerical constants).

The strength λ_{so} of the spin-orbit potential is traditionally introduced together with the numerical factor $[\hbar/(2mc)]^2$, m denoting the nucleonic mass, in order to resemble the form of the electromagnetic spin-orbit potential obtained in a nonrelativistic limit of the Dirac equation.

The form of the Woods-Saxon potential in Eqs. (A11a)–(A11c) does not account for a possible deformation of the nucleus. In order to generalize this form, one usually introduces a parametrization of the nuclear deformation, using two auxiliary surfaces, Σ and Σ_{so} , defined by

$$\begin{aligned} \Sigma|_{\Sigma_{\text{so}}} : R(\theta) = c(\beta_2, \beta_4) R_0 |_{R_{\text{so}}} [1 + \beta_2 Y_{20}(\cos\theta) \\ + \beta_4 Y_{40}(\cos\theta)]. \end{aligned} \quad (\text{A12})$$

Here $R(\theta)$ denotes the distance from the origin of the coordinate frame to any point on the nuclear surface (axial symmetry with respect to the z axis is assumed). The quadrupole and hexadecapole deformations are denoted by β_2 and β_4 , respectively. Deformations of higher multipolarity λ can be introduced similarly by adding $\beta_\lambda Y_{\lambda 0}(\cos\theta)$ to the right-hand side of Eq. (A12). The factor $c(\beta_2, \beta_4)$ is calculated from the condition that the volume enclosed by Σ be equal to $\frac{4}{3}r_0^3 A$, independently of the deformation. A straightforward generalization of the potential in Eqs. (A11a)–(A11c) is now obtained by introducing

$$V_{\text{WS}} = \frac{V_0}{1 + \exp[\text{dist}(\mathbf{r}; \beta; R_0)/a]} - \lambda_{\text{so}} \left[\frac{\hbar}{2mc} \right]^2 \text{grad} \left[\frac{V_0}{1 + \exp[\text{dist}(\mathbf{r}; \beta; R_{\text{so}})/a_{\text{so}}]} \right] \cdot (\boldsymbol{\sigma} \times \mathbf{p}) + \frac{1}{2}(1+\tau_3)V_{\text{Coul}}(\mathbf{r}; \beta), \quad (\text{A13})$$

where $\boldsymbol{\sigma}$ and \mathbf{p} denote Pauli matrices and a linear momentum operator, respectively, and $\text{dist}(\mathbf{r}; \beta; R_0)$ [$\text{dist}(\mathbf{r}; \beta; R_{\text{so}})$] represents the distance of a point \mathbf{r} from the surface Σ (Σ_{so}). The function dist is taken with the minus sign if \mathbf{r} belongs to the nuclear interior and with the plus sign otherwise in order to provide the flat bottom and steep walls of the potential well, just as in Eqs. (A11a)–(A11c). Definition (A13) ensures that the diffuseness of the potential does not depend on the curvature of the nuclear surface, and β represents the entire set of deformation parameters [the odd-parity multipoles, e.g., $\lambda=3, 5, 7, \dots$, and also the nonaxial degrees of freedom can be included in definition (A13)].

For zero deformation the spin-orbit potential in the form of Eq. (A13) yields exactly the same result as the traditional one [Eqs. (A11a)–(A11c)]. The Coulomb po-

tential is usually generated using a classical expression for the electrostatic potential of a uniformly distributed charge enclosed by Σ ,

$$V_{\text{Coul}}(\mathbf{r}; \beta) = \frac{1}{2} \int d\mathbf{r}' \rho_{\text{charge}}(\mathbf{r}') / |\mathbf{r} - \mathbf{r}'|. \quad (\text{A14})$$

Sometimes a diffused-edge charge distribution is also introduced [see, for example, Chepurnov (1967)]. Since the solution to the Schrödinger equation with potential (A13) is obtained numerically, any particular form of the potential, or any of its parts, poses no major difficulty for the numerical procedure. Special numerical methods were devised for solving the Schrödinger equation with the deformed Woods-Saxon potential [see Pashkevich and Strutinsky (1968), Damgaard *et al.* (1969), Pauli (1973)].

The parameters of the Woods-Saxon potential were ad-

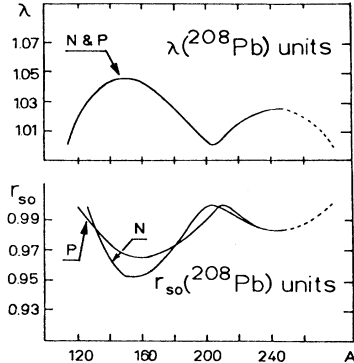


FIG. 49. Variation of the strength parameter $\lambda = \lambda_{so}$ of the spin-orbit part of the Woods-Saxon potential (upper part) and the corresponding radius parameter (bottom part) relative to the values of the ^{208}Pb nucleus. Neutron and proton curves are indicated by symbols N and P , respectively. Approximately 95% of the existing experimental data on spins and parities of odd- A nuclei have been reproduced with the above parameters at the appropriate equilibrium deformations [for more details see Dudek *et al.* (1979) and Dudek *et al.* (1980)].

justed mostly on the basis of the experimental data on the single-particle levels in spherical nuclei (Blomqvist and Wahlborn, 1960; Chepurnov, 1967; Rost, 1968; Pauli, 1973). A systematic optimization of the Woods-Saxon potential parameters for deformed medium-heavy and heavy nuclei of $A \gtrsim 40$ has recently been accomplished (Dudek and Werner, 1978; Dudek *et al.*, 1979). This optimization procedure aims at adjusting the potential parameter values by taking into account the experimental equilibrium deformations, as well as the experimental single-particle level order. To this end the experimental quadrupole and, if known, hexadecapole deformations of even-even nuclei were collected together with the ground-state spins and parities of the neighboring odd- A nuclei. On the basis of this empirical information "experimental" single-particle spectra were constructed. Then the Schrödinger equation with the potential as defined by Eq. (A13) was solved numerically at the experimental deformation values, and the two spin-orbit potential parameters, λ_{so} and $(r_0)_{so}$, were varied until agreement between the calculated and experimental single-particle level orders was achieved. The results of this analysis (Dudek and Werner, 1978; Dudek *et al.*, 1979) were the following.

(i) It was enough to vary only the two spin-orbit potential parameters specified above in order to reproduce more than 95% of the experimental data for nuclei with $A \gtrsim 40$. All other parameters were kept constant. To be more precise, the diffuseness parameters were set equal for both the central and spin-orbit potentials, and $a = a_{so} = 0.7$ fm independently of the kind of particles involved. The depth of the central part of the potential was given by

$$V_0 = V \left[1 \mp \kappa \frac{N - Z}{N + Z} \right] \quad (\text{A15})$$

for $V = -49.6$ MeV and $\kappa = 0.86$, independently of A .

(ii) The resulting dependence of the optimized values of λ_{so} and r_{so} on A turned out to be very smooth, as illustrated in Fig. 49. Characteristically for deformed nuclei, the optimal values of λ_{so} were a few percent larger and those of r_{so} a few percent smaller than the corresponding values valid for spherical nuclei.

(iii) Whereas the optimization procedure was based on the assumption that the calculated and observed single-particle level orders agree well, in many cases this assumption also provided a good description of the single-particle level distances. Figures 50(a) and 50(b) for neutrons and protons, respectively, compare the experimental and calculated levels on the example of ^{235}U and ^{249}Bk and illustrate a remarkable correspondence between the two.

Recently an attempt was made to justify the characteristic result of the optimization procedure, as depicted in Fig. 49 (Dudek, Nazarewicz, and Werner, 1980) by using the results of a microscopic theory of the average spin-orbit nuclear potential (Wong, 1968; Scheerbaum, 1976b, 1976c). For this purpose the notion of spin-saturated (*s-s*) and spin-unsaturated (*s-us*) levels was introduced: A level with a given (lj) (l denoting the single-particle orbital angular momentum, j the single-particle total angular momentum) in a spherical nucleus is called spin saturated if all $2(l+1)$ states are occupied, and spin unsaturated otherwise. On the basis of the expression for the effective nucleon-nucleon interaction g , which is represented in coordinate space as a local interaction composed of central (*c*), tensor (*t*), spin-orbit (*ls*), and quadratic spin-orbit (*q*) components,

$$g = g_c(r) + g_t(r)S_{12} + g_{ls}(r)\mathbf{l} \cdot \mathbf{s} + g_q(r)L_{12}, \quad (\text{A16})$$

Scheerbaum (1976b) demonstrated that the main contribution of spin-unsaturated orbitals to the spin-orbit splitting is due to the central and tensor rather than to the spin-orbit or quadratic spin-orbit terms in Eq. (A16). From earlier investigations (Wong, 1968; Scheerbaum, 1976a) it was known that spin-unsaturated orbitals contribute to the spin-orbit splitting with the minus sign. In order to imitate the effect of this negative contribution, in the microscopic formula for the spin-orbit potential

$$V_{so}^{\text{micro}} = \lambda'(Z, N) \left[\frac{\hbar}{2mc} \right]^2 \nabla \rho(\mathbf{r}) \cdot (\boldsymbol{\sigma} \times \mathbf{p}) \quad (\text{A17})$$

[see Bohr and Mottelson (1975)] the total density of the nuclear matter $\rho(\mathbf{r})$ was subdivided into spin-saturated core and spin-unsaturated valence terms:

$$\rho(\mathbf{r}) \rightarrow \rho_{\text{core}}^{s-s}(\mathbf{r}) - \beta \rho_{\text{valence}}^{s-\text{un}}(\mathbf{r}). \quad (\text{A18})$$

Here a phenomenological (positive) constant β is introduced (see below). After substitution Eq. (A17) reads

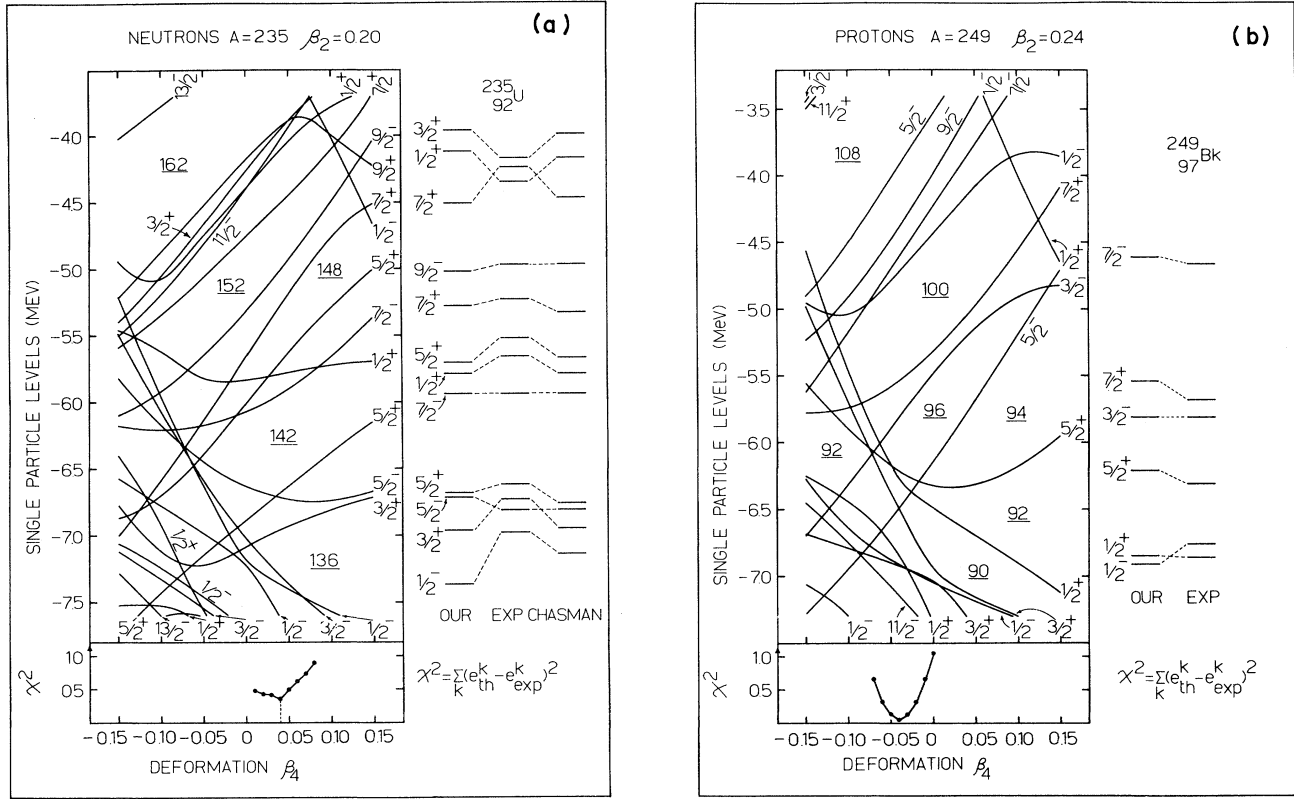


FIG. 50. (a) Single-particle neutron levels calculated with the Woods-Saxon deformed potential from Dudek *et al.* (1979). The calculated energies are compared to the experimental data and to the results of the independent theoretical study by Chasman (1978). Although only the single-particle level order (and not the level distances) was taken into account when optimizing the Woods-Saxon potential parameters, the relative distances between the calculated energies reproduce the experimental data rather well. The goodness of the calculated single-particle spectra becomes decisive for the quality of further interpretation of such high-spin phenomena as the collective band crossing and backbending or upbending effects discussed in detail in Sec. III. (b) The same as in (a) but for protons [from Dudek *et al.* (1979)].

$$V_{\text{so}}^{\text{micro}} = \lambda(Z, N) \left[\frac{\hbar}{2mc} \right]^2 \times \nabla [\rho_{\text{core}}^{s-s}(\mathbf{r}) - \beta \rho_{\text{valence}}^{s-un}(\mathbf{r})] \cdot (\boldsymbol{\sigma} \times \mathbf{p}). \quad (\text{A19})$$

This formula was not used for calculating the spin-orbit potential for individual nuclei, for which purpose the approximation would be too crude, but rather for concluding about the expected average behavior of the spin-orbit potential parameters as functions of the shell filling. Formula (A19) suggests that the contribution of the valence term will oscillate as a function of the particle number n equal to Z or N , since the partition of Z or N into core and valence parts oscillates with n . It follows (Wong, 1968) that β must be positive, and thus the effective radius of the spin-orbit potential is diminished significantly for half-filled major-shell nuclei and less significantly for magic nuclei (for illustration see Fig. 51). The corresponding effect on λ_{so} and r_{so} is shown as a function of particle number in Figs. 52 and 53. The empirical dependencies of λ_{so} and r_{so} on the particle number are consistent with the results of the semimicroscopic theory of the average spin-orbit potential.

3. Systematic differences between the single-particle spectra of the Nilsson and Woods-Saxon potentials

Although the two average field models are used alternatively for calculating the structure of high-spin states, the results of the two potentials for the single-particle spectra differ systematically. Such differences may influence just as systematically the results of further analyses that are based on the particle spectra of the two models.

Let us first illustrate the systematic shift of the Nilsson-potential single-particle levels relative to the corresponding Woods-Saxon levels as a function of the single-particle angular momentum j , for spherically shaped nuclei (see Fig. 54 for $A = 152$ single-particle spectra). The low- j orbitals of the Nilsson potential lie systematically higher than their Woods-Saxon partners, while the high- j orbitals for the Nilsson potential are slightly lower than the ones for the Woods-Saxon model.

The tendency to lower high- j orbitals in the Nilsson model can be traced back to the presence of its l_t^2 term (see Sec. 1). It creates some undesirable effects for heavier

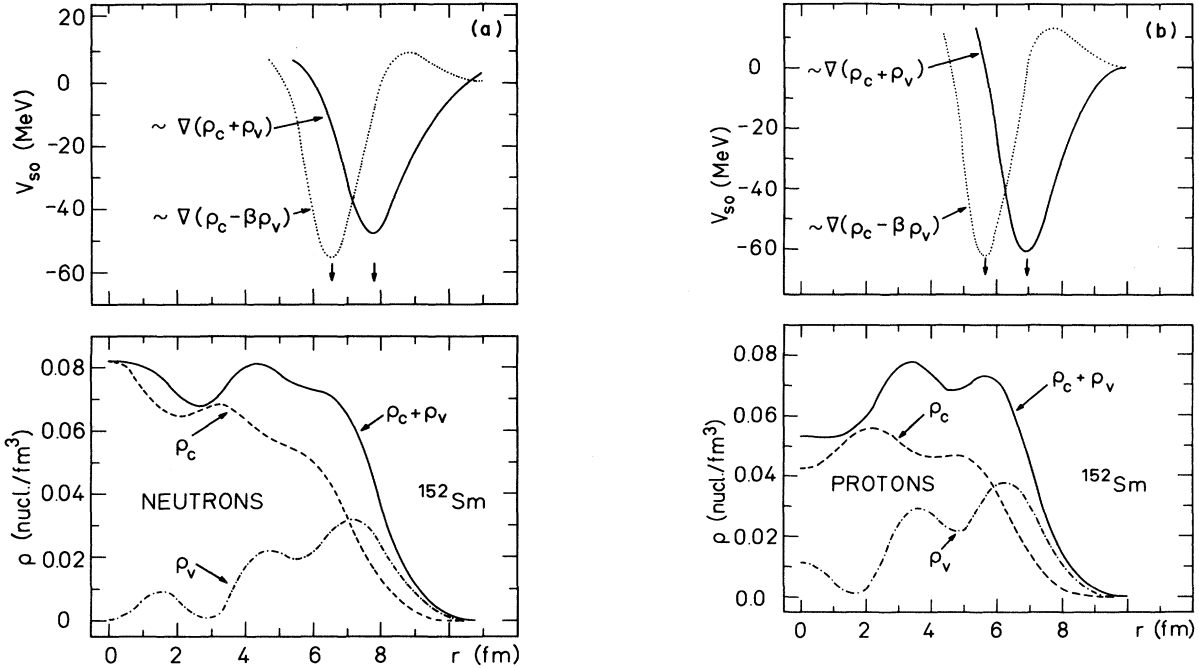


FIG. 51. (a) The calculated density of neutrons in the ^{152}Sm nucleus (bottom part) was split into contributions from the spin-saturated core (ρ_c) and the spin-unsaturated valence particle (ρ_v); a cross section of the three-dimensional distributions along the ($x=0$, $y=0$, $r=z$) plane is shown in the figure. In the top part the results corresponding to Eqs. (A17) and (A19) for the V_{so}^{micro} are given. Notice that the minimum in the curve of Eq. (A19) corresponds to an r value smaller than that of Eq. (A17). In order to account for such an effect in the Woods-Saxon potential calculations the effective radius of the spin-orbit potential has to be decreased correspondingly [cf. Figs. 53(a) and 53(b)] by $\delta r_{so} = \delta R_{so}/A^{(1/3)}$. (b) The same as in (a) but for protons. One can see the splitting into a core and a valence contributions even more pronouncedly. This splitting varies with the particle number; the smallest effect of spin-unsaturated valence particles corresponds to magic nuclei.

nuclei—i.e., for nuclei in the lead region the proton $i_{13/2}$ energy lies lower than the energy of the $f_{7/2}$ orbital and the neutron $j_{15/2}$ -state energy is lower than the energy of the $i_{11/2}$ state, in contrast to the experimental data (see Fig. 55 for the ^{208}Pb spectra). Consequently, in applications to high-spin calculations the proton $i_{13/2}$ and neutron $j_{15/2}$ levels had to be shifted arbitrarily in order to avoid artificial effects on the calculated properties of yrast lines. The thus modified single-particle spectra are

sometimes referred to as distorted modified oscillator (DMO) results [see, for instance, Andersson *et al.* (1976)].

Another important difference between the two models, again originating from the presence of the l_t^2 term in the Nilsson potential, manifests itself in the overestimates of the average moments of inertia. It was shown by Bohr and Mottelson (1975) on the basis of the Fermi gas model that the effective moment of inertia of a system of noninteracting particles is equal to the rigid-body value corre-

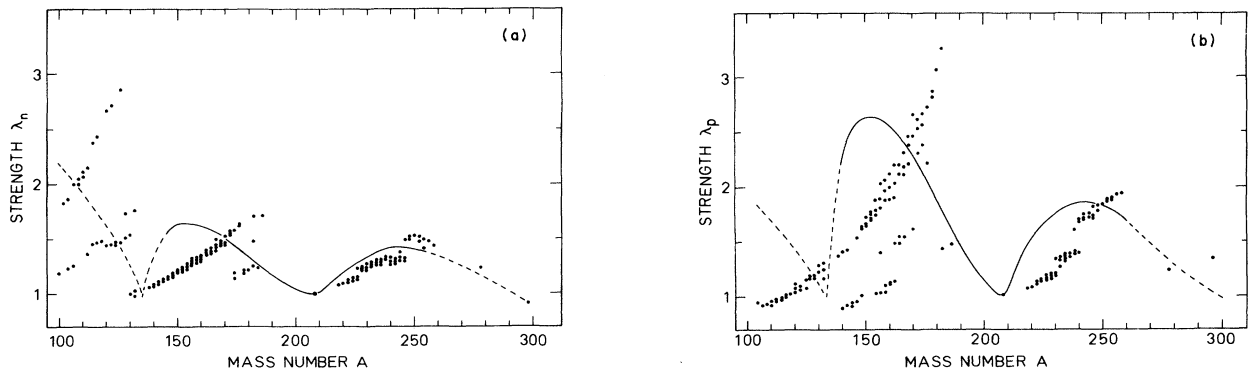


FIG. 52. (a) The calculated spin-orbit potential strength parameter $\lambda_n \equiv \lambda_{so}$ for the neutrons; the line indicates the corresponding results from Fig. 49 scaled linearly [for details see Dudek *et al.* (1980)]. (b) The calculated spin-orbit potential strength parameters $\lambda_p \equiv \lambda_{so}$ for the proton [see caption to (a) and text].

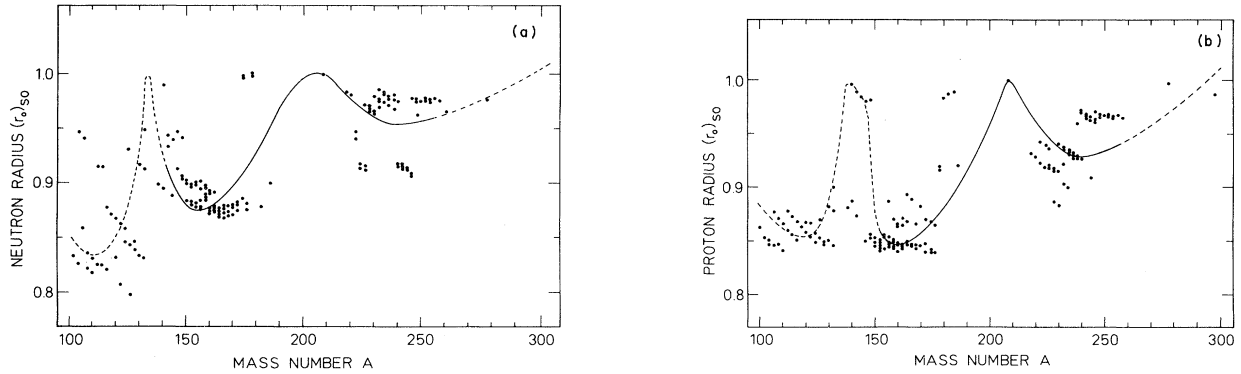


FIG. 53. (a) The neutron radius parameter $(r_0)_\text{so} = r_\text{so}$ (relative to the corresponding ^{208}Pb value) as a function of the mass number. The corresponding δr_so determining decrease in r_so for nonmagic nuclei were estimated for each nucleus separately [cf. captions to Figs. 51(a) and 51(b)]. The line corresponds to the results of Fig. 49 scaled linearly [for further details see Dudek *et al.* (1980)]. (b) The same as in (a) but for protons. Normalization to the corresponding values of ^{208}Pb is done in both (a) and (b).

sponding to the same shape as the shape imposed on the Fermi gas. Consequently, pure (i.e., without residual interactions) independent-particle potentials—such as the average field potentials of Nilsson or Woods-Saxon—are expected to provide, on the average, the rigid-body values for the moments of inertia in deformed nuclei. Using the methods presented in more detail in Sec. II.D.2, one can calculate the corresponding dependence of the total energy versus the total angular momentum resulting from the average field approach. This can be done particularly easily for nuclei that have their angular momentum aligned with the symmetry axis. The results of these calculations are presented in Fig. 56 for three potentials, the deformed harmonic-oscillator, Nilsson, and Woods-Saxon potentials, at the same deformation. The slope of the straight lines is inversely proportional to the moment of inertia \mathcal{F} , since $\mathcal{E} = (\hbar^2/2\mathcal{F})I(I+1)$. The Woods-Saxon values of the moment of inertia are only slightly higher

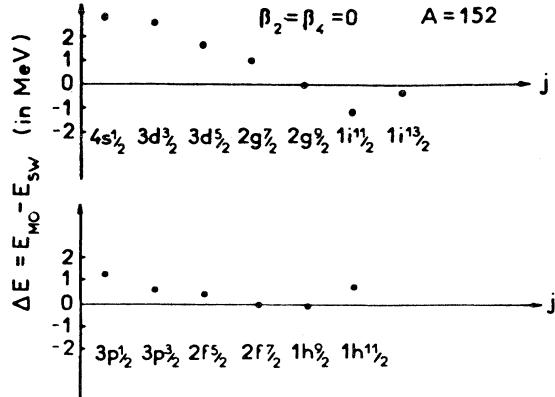


FIG. 54. A systematic difference between the single-particle level energies of the Nilsson (MO) and the Woods-Saxon (WS) models (upper part corresponding to positive and bottom part to negative parity states) [illustrative example from Cerkaski *et al.* (1979)].

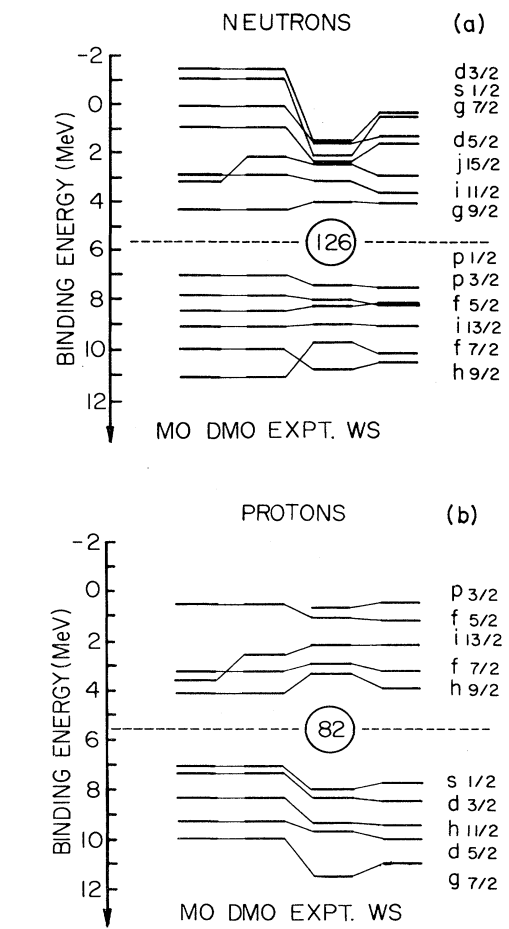


FIG. 55. (a) Systematic differences between the Nilsson model (MO) and the Woods-Saxon model (WS) for the neutron single-particle levels. For comparison the experimental data are also given. The results marked with DMO correspond to an arbitrary shift of the $j_{15/2}$ level energy, aiming at improving the agreement between the MO and the experimental results. (b) The same as in (a) but for the protons (the $i_{13/2}$ level is shifted).

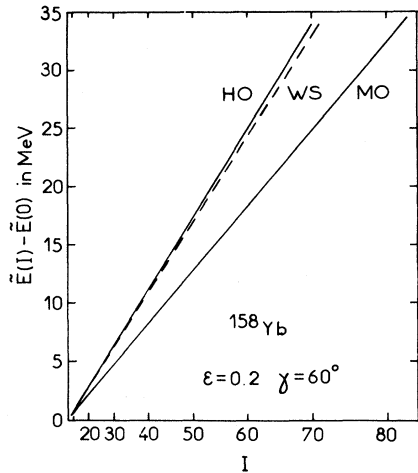


FIG. 56. The average (Stratinsky-smoothed) total energy of the ^{158}Yb nucleus calculated as a function of spin (quadratic scale used), normalized to the corresponding value at $I=0$ (for further discussion see text and Sec. II.D.2).

(about 3%) than the harmonic-oscillator values (the latter are equal to the rigid-body moment of inertia), while the Nilsson-model spectrum overestimates the moments of inertia by about 30%. By arbitrarily setting the \mathbf{l}_t^2 matrix

elements equal to zero in the calculations, one can easily demonstrate that this 30% discrepancy decreases to about a 3% discrepancy only if the \mathbf{l}_t^2 term is eliminated. Such a numerical exercise reveals the spurious introduced by the \mathbf{l}_t^2 term, which, let us recall from the discussion in Sec. 1, was introduced into the Hamiltonian (A7) in order to obtain better agreement with the experimental single-particle levels.

One can probe farther in comparing the properties of the two average field models by calculating microscopically the moments of inertia (alternatively, the first collective $I^\pi=2^+$ state energies) in the presence of residual interactions—e.g., pairing. Having first found the best parameter values for both potentials and at the same time the corresponding optimal parametrizations of the pairing Hamiltonians (for the discussion of the pairing effect see Sec. II.B), one can apply the first-order perturbation theory to the cranking Hamiltonian [Eq. (2.8)].

The resulting Inglis formula for the moment of inertia is

$$\mathcal{F} = 2\hbar \sum_{\mu, \nu} \frac{\langle \mu | j_x | \nu \rangle^2}{E_\mu + E_\nu} (u_\mu v_\nu - u_\nu v_\mu)^2 \quad (\text{A20})$$

[for a more complete version of this formula see Nilsson

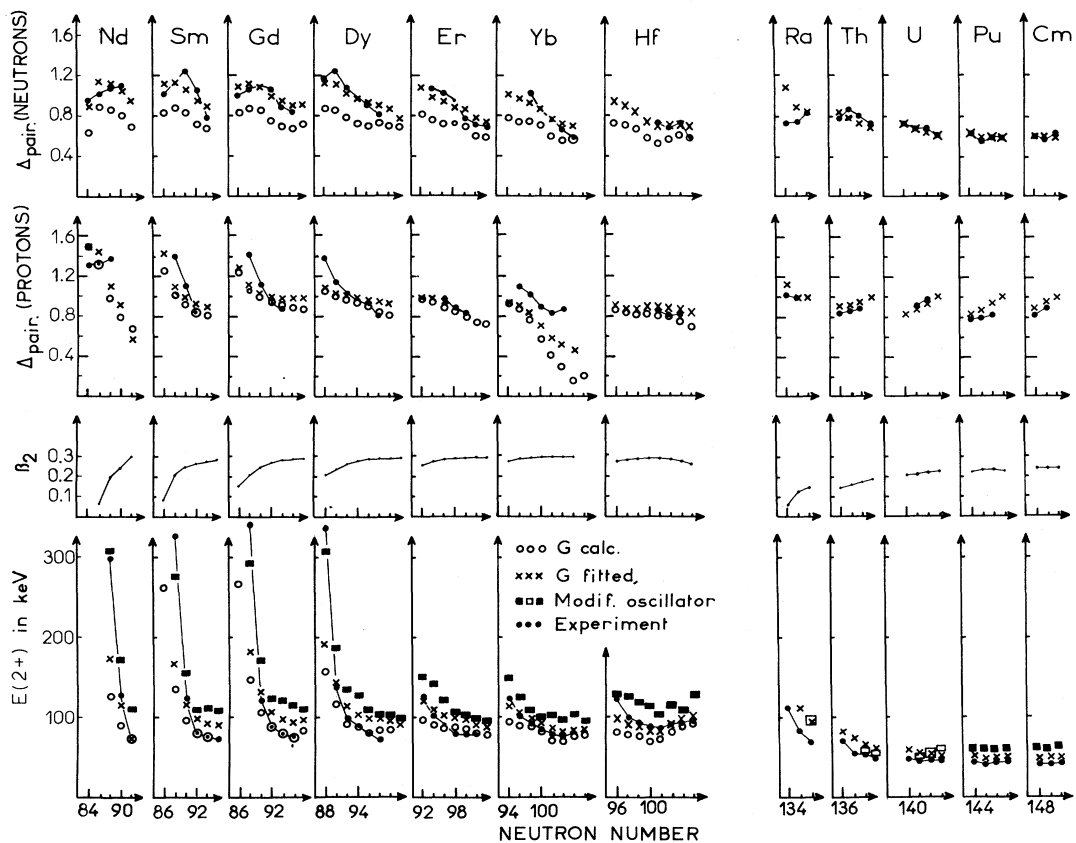


FIG. 57. Results of a systematic calculation of the first $I^\pi=2^+$ state energies (the lowest part of the figure) for some representative rare-earth and actinide nuclei. For comparison the calculated neutron and proton pairing Δ values are given, together with the corresponding empirical values obtained from the “odd-even” mass differences. Calculated equilibrium deformations are also shown [from Dudek, Majhofer, and Skalski (1980)].

and Prior (1961)], where $|\mu\rangle, |\nu\rangle$ are the Nilsson (Woods-Saxon) single-particle states and the corresponding quasiparticle energies are denoted by E_μ and E_ν .

A comparison of the moments of inertia obtained within the two models for a wide range of nuclei can illustrate the differences in their single-particle spectra. In Fig. 57 the Nilsson and Woods-Saxon potential results obtained with the above Inglis formula are shown and compared with the experimental data, together with the calculated equilibrium deformations and pairing energy gaps. One can conclude from the figure that, on the average, the Inglis values of the moment of inertia are about 10% too low (the $I^\pi=2^+$ state energies are too high) for the Nilsson model and 2–3 % too low for the Woods-Saxon model.

Figure 57 also illustrates the validity of the Inglis formula as an adiabatic approximation. The agreement between the calculated and experimental data is typically better for heavy nuclei (actinides) for which the moments of inertia are larger (and consequently the rotational frequencies corresponding to the lowest collective 2^+ states are smaller) than for the rare-earth nuclei. Since the Inglis formula is an adiabatic approximation, it follows that its goodness increases in the limit $\omega \rightarrow 0$. Moreover, for the deformation decreasing to zero—i.e., where the cranking approximation loses its meaning—the discrepancies between the calculated and experimental results quickly augment, as one can see from the figure.

Summing up, we can say that (i) there exist systematic differences between the single-particle spectra of the two potentials, (ii) they originate from the presence of an empirical I_t^2 term in the Nilsson Hamiltonian [Eq. (A7)], and (iii) these differences influence systematically the results of calculations employing their single-particle levels.

APPENDIX B: TRANSITION PROBABILITIES, LIFETIMES, AND FEEDING TIMES

Measurements of the lifetimes τ of excited nuclear states provide important information on the probabilities P of transitions between different states ($\tau \sim P^{-1}$) and thus may test the theoretical results on the structure of nuclear states.

A nuclear state with spin I is represented by the wave function $|\psi_{KM}^I\rangle$ (K denotes projection of I onto the “third” axis in a body-fixed coordinate frame, M the projection of I onto the “third” axis in a laboratory frame). In the adiabatic approximation and after the appropriate symmetrization we can express $|\psi_{KM}^I\rangle$ by

$$|\psi_{KM}^I\rangle = \left(\frac{2I+1}{16\pi^2(1+\delta_{K0})} \right)^{1/2} \times [\mathcal{D}_{MK}^I |\phi_K\rangle + (-1)^{I+K} \mathcal{D}_{M-K}^I |\phi_{\bar{K}}\rangle], \quad (\text{B1})$$

where the standard \mathcal{D} functions describe the orientation of the nucleus with respect to the laboratory frame and the intrinsic wave functions $|\phi_K\rangle$ describe the motion (of nucleons in the nucleus) in the body-fixed (rotating) coordinate frame.

The amplitudes of the electromagnetic transitions from the initial state $|\psi_{K_i M_i}^{I_i}\rangle$ to the final state $|\psi_{K_f M_f}^{I_f}\rangle$ are calculated with the help of the matrix elements

$$\langle \psi_{K_f M_f}^{I_f} | \mathcal{M}(\lambda, \mu) | \psi_{K_i M_i}^{I_i} \rangle, \quad (\text{B2})$$

where $\mathcal{M}(\lambda, \mu)$ denotes an electromagnetic transition multipole operator with multipolarity λ . By use of the Wigner-Eckart theorem we can reduce the dependence on the M and μ quantum numbers in (B2) to the Clebsch-Gordan coefficient as

$$\begin{aligned} & \langle \psi_{K_f M_f}^{I_f} | \mathcal{M}(\lambda, \mu) | \psi_{K_i M_i}^{I_i} \rangle \\ &= \frac{\langle I_i M_i \lambda \mu | I_f M_f \rangle}{(2I_f + 1)^{1/2}} \langle I_f K_f | \mathcal{M}(\lambda) | I_i K_i \rangle. \end{aligned} \quad (\text{B3})$$

In the calculation of matrix elements (B3) with wave functions given by Eq. (B1) a transformation of the multipole operator $\mathcal{M}(\lambda, \mu)$ to the intrinsic frame of reference is necessary. This transformation involves the standard functions $\mathcal{D}_{\mu\nu}^\lambda$. As a result, the matrix element (B3) factorizes into the intrinsic part, depending on the intrinsic wave functions and on some Clebsch-Gordan coefficients. We shall not discuss the details of this calculation here [cf. Bohr and Mottelson (1969)]. The quantity

$$\begin{aligned} B(\lambda; I_i K_i \rightarrow I_f K_f) &\stackrel{\text{df}}{=} \sum_{M_f(\mu)} |\langle \psi_{K_f M_f}^{I_f} | \mathcal{M}(\lambda, \mu) | \psi_{K_i M_i}^{I_i} \rangle|^2 \\ &= \frac{1}{2I_f + 1} |\langle I_f K_f | \mathcal{M}(\lambda) | I_i K_i \rangle|^2 \end{aligned} \quad (\text{B4})$$

does not depend on projections M and determines the probability $T(\lambda)$ for radiating a photon of multipolarity λ :

$$T(\lambda) = \frac{8\pi(\lambda+1)}{\lambda[(2\lambda+1)!!]^2} \frac{1}{\hbar} \left(\frac{E_\gamma}{\hbar c} \right)^{2\lambda+1} B(\lambda; I_i K_i \rightarrow I_f K_f), \quad (\text{B5})$$

where E_γ denotes the transition energy and $n!! = 1 \cdot 3 \cdot 5 \cdots n$ [cf. Blatt and Weiskopf (1952)]. The electric multipole operators are given by

$$\mathcal{M}_e(\lambda, \mu) = \sum_{q=1}^A e_q r_q^\lambda Y_{\lambda\mu}(\vartheta_q, \varphi_q) \quad (\text{B6})$$

and the magnetic multipole operators by

$$\mathcal{M}_m(\lambda, \mu) = \frac{e\hbar}{2mc} \sum_q \left[g_s s + \frac{1}{\lambda+1} g_l l \right]_q \text{grad}_q [r_q^\lambda Y_{\lambda\mu}(\vartheta_q, \varphi_q)] + \frac{e\hbar}{mc} \frac{1}{\lambda+1} g_R \int dV \mathbf{L}(\mathbf{r}) \text{grad}[r^\lambda Y_{\lambda\mu}(\vartheta, \varphi)]. \quad (\text{B7})$$

In the above relations e_q and m denote the nucleonic charge and mass, respectively; $g_1=0$ and $g_s=-3.826$ for neutrons, while $g_1=1$ and $g_s=+5.585$ for protons; $\mathbf{L}(\mathbf{r})$ is the angular momentum density in the collective motion and g_R the gyromagnetic factor associated with collective rotation ($g_R \approx Z/A$).

Connection between the multipole operator in (B6) and the electric multipole moments of the nuclear charge distribution describing its deviations from spherical symmetry is established by the corresponding expectation values; in particular, for the quadrupole moment in a state characterized by I and K we have

$$Q = \frac{\text{df.}}{\left(\frac{16\pi}{5}\right)^{1/2}} \langle \Psi_{K,M=I}^I | \mathcal{M}_e(\lambda=2, \mu=0) | \psi_{K,M=I}^I \rangle, \quad (\text{B8})$$

$$\begin{aligned} B_e(\lambda=2; I, K=0 \rightarrow I-2, K=0) &= \frac{5}{16\pi} \langle I020 | I-2, 0 \rangle^2 [Q_0(K)]^2 \\ &= 5 \langle I020 | I-2, 0 \rangle^2 B_e(\lambda=2; 2, K=0 \rightarrow 0, K=0). \end{aligned} \quad (\text{B11})$$

The following auxiliary relations are helpful for quick estimates of relevant quantities: If the mean lifetime τ_m (ps) of the initial state decaying predominantly via quadrupole transitions of energy E_γ (MeV) is known, then the “experimental” value of the reduced $B_e(\lambda=2)$ can be obtained from

$$\begin{aligned} B_e(\lambda=2; I, K=0 \rightarrow I-2, K=0) &\approx \frac{0.08156}{(E_\gamma)^5 \tau_m (1 + \alpha_{\text{tot}})} \\ &\times (e^2 b^2), \end{aligned} \quad (\text{B12})$$

where α_{tot} denotes the total electron conversion coefficient. Using the shape parametrization of the nucleus (introduced in Appendix A), one can derive a crude estimate for Q_0 :

$$Q_0(K=0) \approx \frac{3}{\sqrt{5\pi}} Z(r_0 A^{1/3})^2 \beta_2. \quad (\text{B13})$$

Most of the lifetimes and feeding times associated with collective rotation are typically of the order of picoseconds; a technique commonly applied to measure these times is the recoil distance Doppler-shift method. An example of this approach can be found in Ward *et al.* (1979); there one observes the splitting of a γ line into two components: s , originating from recoil ions which emit their γ rays after they have been stopped, and m , originating from those recoil ions which are still moving. In analyzing the spectra one obtains the survival fraction $R(d)$, defined as

$$R(d) = \frac{I_\gamma(s)}{I_\gamma(m) + I_\gamma(s)}, \quad (\text{B14})$$

where I_γ denotes the corresponding γ -ray intensities. The value $R(d)$ is determined for several distances d between the target and the stopper in order to obtain the decay

while the so-called intrinsic quadrupole moment

$$Q_0 = \left[\frac{16\pi}{5} \right]^{1/2} \langle \phi_K | \mathcal{M}_e(\lambda=2, \mu=0) | \phi_K \rangle. \quad (\text{B9})$$

Combining Eqs. (B4) and (B9) and transforming the multipole operator $\mathcal{M}(\lambda=2, \mu)$ into the intrinsic frame by means of $\mathcal{D}_{\mu\nu}^2$ functions, we obtain

$$B_e(\lambda=2; I_i K \rightarrow I_f K) = \frac{5}{16\pi} \langle I_i K 20 | I_f K \rangle^2 [Q_0(K)]^2. \quad (\text{B10})$$

For the important ground-state and Stockholm rotational bands of even-even nuclei ($K=0, I_f=I_i-2$) the above relation reduces to

curve from which the lifetimes are deduced.

Some complications in this approach arise when measuring very short lifetimes (shorter than what is needed to stop the recoil ion), since then there is no s peak in the spectrum. In such a case Ward *et al.* (1979) proposed

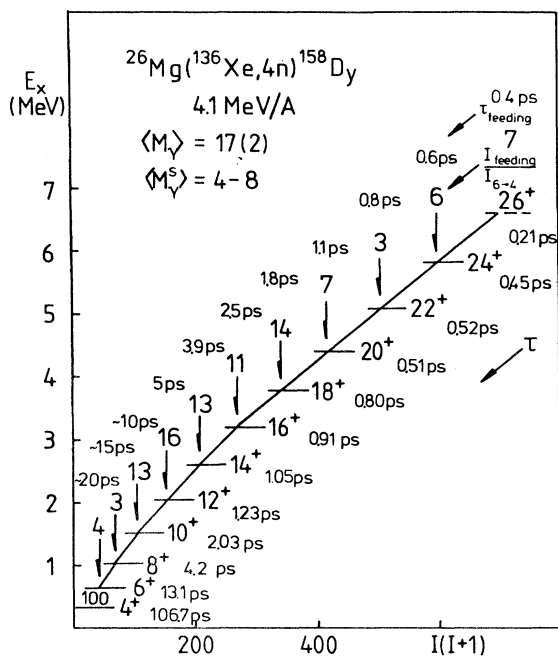


FIG. 58. Lifetimes of nuclear states in ^{158}Dy and the yrast-state feeding times of quasicontinuum γ rays deduced from recoil distance measurements. The intensities relative to the one of the $6^+ \rightarrow 4^+$ transition of the feeding γ rays are indicated. All times are given in picoseconds [from Grosse (1979) and Emling *et al.* (1981)].

to determine the survival fraction as

$$R(d) = 1 - \frac{I_\gamma(m)}{I_\gamma(m, d=\infty)}, \quad (\text{B15})$$

where $I_\gamma(m, d=\infty)$ denotes the γ -ray intensity corresponding to an infinite distance between target and stopper and thus contains the total intensity produced by the moving recoil ions. Some further details of the method can also be found in the above reference.

In the works of Grosse *et al.* (1979) and Emling *et al.* (1981) lifetimes and feeding times were obtained up to the 26^+ state in ^{158}Dy . These data are illustrated in Fig. 58.

A second means of measuring the lifetimes with the help of the Doppler effect is the Doppler-shift attenuation method (DSAM); due to the attenuation of the moving excited recoil ions in the target, the γ rays are emitted at various velocities, causing a broadening of the γ -ray spectral lines. The broadening depends on the lifetime of the decaying state.

The broadening of γ -ray lines may also occur due to the finite solid angle of the γ -ray detector. Doppler broadening can be particularly strong when one is using very-heavy-ion projectiles or detecting high-energy transitions; for instance, if the lifetime of a state decaying via $E_\gamma \sim 700$ keV is comparable with the stopping time of the recoil ion in a thick target (approximately a few picoseconds), then the linewidth is equal to the Doppler shift. For a heavy-ion induced reaction with $v/c \sim 5\%$ (typically) this width amounts to ~ 35 keV, while the unbroadened value is ~ 2 keV.

Various techniques have been developed to observe the unbroadened γ -ray lines from fast-moving recoil ions (Ward *et al.*, 1976; Grosse, 1979)—for instance, to use thin targets, or to observe γ rays in a small forward cone; one can also correct for the Doppler shift by registering the recoil velocity and angle. The latter can be done by observing coincidences between γ rays [in a Ge(Li) detector] and a particle in, say, a position-sensitive heavy-ion detector. The use of thin targets, on the other hand, may cause a significant reduction (compared to a thick target) in the γ -ray yield. In such a case it is advisable to use “sandwich” targets—i.e., a stack of several separated thin targets.

Difficulties connected with the application of DSAM are caused by strong feeding via higher-lying levels. Such complications can, however, be overcome when using MCE (multiple Coulomb excitation, which selects a given yrast cascade) and the sum spectrometer in coincidence with a Ge(Li) detector. Another difficulty is caused by our limited knowledge of the slowing-down process (attenuation of the recoil ions in the stopping material). The best way of overcoming this difficulty is apparently to measure the stopping power of the slowing-down material in the actual experiment. Various methods of determining stopping powers are reviewed by Alexander and Foster (1978); alternatively, tables [e.g., Northcliff and Schilling (1970)] are used.

It often happens that with the large angular momentum

brought into the compound nucleus several reaction channels are open; it is then particularly important to enhance detection in the channel of interest. To achieve this in techniques used so far one applies a multiplicity filter or a sum spectrometer, along with thin targets.

Another sensitive probe for the structure of nuclear states is the magnetic dipole moment. The lifetimes of states belonging to rotational bands, however, are too short (at most, a few picoseconds) to observe a Larmor precession of the nucleus due to an applied external magnetic field (as is the case for yrast traps; see, for instance, Sec. IV.B.3). It has been demonstrated recently by Rud *et al.* (1981) that observable precessions can be produced by very high internal magnetic fields during a period of $0.5 \leq t \leq 1$ ps after formation of a compound nucleus. This was achieved by utilizing the transient magnetic field interaction for nuclear recoils passing a thin foil of magnetized iron. The g factor was observed to increase from 0.2 for states with spins around 12, to 0.6 for spins around 22. These results were interpreted in terms of neutron aligned bands in the vicinity of the first backbending and of proton aligned bands below the second backbending at the yrast line, respectively (Rud *et al.*, 1981).

However, that experiment is the only one so far to yield g factors for quasicontinuum states in ^{156}Dy . The increase of the g factors at high spin has not yet been confirmed from the observation of discrete γ -ray lines. On the contrary, all values reported so far show a decrease at spins $I=4-14$, as has been summarized by Häusser (1982).

It thus appears important that further improvements of the high-spin experiments be carried out in the future. Since the gyromagnetic factors for the free proton and neutron differ significantly (even in their sign), the measurement of the magnetic moments in the rotational bands may become a valuable tool for the distinction between the proton or neutron character of the nucleonic alignment.

REFERENCES

- Åberg, S., 1978, Nucl. Phys. A **306**, 89.
- Åberg, S., and G. Leander, 1979, Nucl. Phys. A **332**, 365.
- Åberg, S., S. E. Larsson, P. Möller, S. G. Nilsson, G. Leander, and I. Ragnarsson, 1980, in *Physics and Chemistry of Fission, Proceedings, Jülich, 1979* (IAEA, Vienna), Vol. I, p. 303.
- Aguer, P., G. Bastin, A. Charmant, Y. El Masri, P. Hubert, R. V. F. Janssens, C. Michel, J. P. Thibaud, and J. Vervier, 1979, Phys. Lett. B **82**, 55.
- Aguer, P., G. Bastin, A. Péghaire, J. P. Thibaud, N. Perrin, H. Sergolle, and P. Hubert, 1981, Phys. Scr. **24**, 140 (*Nuclei at Very High Spin—Sven Gösta Nilsson in Memoriam*, Proceedings, Nobel Symposium, Örenäs, 1980, edited by Georg Leander and Hans Ryde).
- Alder, K., A. Bohr, T. Huus, B. R. Mottelson, and A. Winter, 1956, Rev. Mod. Phys. **28**, 432.
- Alexander, T. K., and J. S. Forster, 1978, Adv. Nucl. Phys. **10**, 197.

- Almberger, J., I. Hamamoto, and G. Leander, 1979, Phys. Lett. **B 80**, 153.
- Almberger, J., I. Hamamoto, and G. Leander, 1980, Nucl. Phys. A **333**, 184.
- Almberger, J., I. Hamamoto, and G. Leander, 1980a, Phys. Scr. **22**, 331.
- Andersen, O., R. Bauer, G. B. Hagemann, M. L. Halbert, B. Herskind, M. Neiman, and H. Oeschler, 1978, Nucl. Phys. A **295**, 163.
- Anderson, O., J. D. Garrett, G. B. Hagemann, B. Herskind, D. L. Hillis, and L. L. Riedinger, 1979, Phys. Rev. Lett. **43**, 687.
- Andersson, C. G., R. Bengtsson, T. Bengtsson, J. Krumlinde, G. Leander, K. Neergaard, P. Olanders, J. A. Pinson, I. Ragnarsson, Z. Szymański, and S. Åberg, 1981, Phys. Scr. **24**, 266 (*Nuclei at Very High Spin—Sven Gösta Nilsson in Memoriam*, Proceedings, Nobel Symposium, Örenäs, 1980, edited by Georg Leander and Hans Ryde).
- Andersson, C. G., G. Hellström, G. Leander, I. Ragnarsson, S. Åberg, J. Krumlinde, S. G. Nilsson, and Z. Szymański, 1978, Nucl. Phys. A **309**, 141.
- Andersson, C. G., and J. Krumlinde, 1977, Nucl. Phys. A **291**, 21.
- Andersson, C. G., J. Krumlinde, G. Leander, and Z. Szymański, 1981, Nucl. Phys. A **361**, 147.
- Andersson, C. G., S. E. Larsson, G. Leander, P. Möller, S. G. Nilsson, I. Ragnarsson, S. Åberg, R. Bengtsson, J. Dudek, B. Nerlo-Pomorska, K. Pomorski, and Z. Szymański, 1976, Nucl. Phys. A **268**, 205.
- Arima, A., M. Harvey, and K. Shimizu, 1969, Phys. Lett. B **30**, 517.
- Arima, A., and F. Iachello, 1976, Ann. Phys. **99**, 253.
- Arima, A., and F. Iachello, 1978, Ann. Phys. **111**, 201.
- Arima, A., and F. Iachello, 1979, Ann. Phys. **123**, 468.
- Asaro, F., and I. Perlman, 1952, Phys. Rev. **87**, 393.
- Asaro, F., and I. Perlman, 1953, Phys. Rev. **91**, 763.
- Auerbach, N., and I. Talmi, 1964, Phys. Lett. **10**, 297.
- Baba, C. V. K., S. Bjørnholm, O. Christensen, B. Herskind, R. M. Lieder, J. Pedersen, G. Sletten, F. Folkmann, and R. S. Simon, 1981, Phys. Scr. **24**, 290 (*Nuclei at Very High Spin—Sven Gösta Nilsson in Memoriam*, Proceedings, Nobel Symposium, Örenäs, 1980, edited by Georg Leander and Hans Ryde).
- Baklander, O., C. Baktash, J. Borggreen, J. B. Jensen, K. Kownacki, J. Pedersen, G. Sletten, D. Ward, H. R. Andrews, O. Häusser, P. Skensved, and P. Taras, 1982, Nucl. Phys. A **389**, 93.
- Banarjee, B., H. J. Mang, and P. Ring, 1973, Nucl. Phys. A **215**, 366.
- Banaschik, M. V., R. S. Simon, P. Colombani, D. P. Soroka, F. S. Stephens, and R. M. Diamond, 1975, Phys. Rev. Lett. **34**, 892.
- Bardeen, J., L. N. Cooper, and J. R. Schrieffer, 1957, Phys. Rev. **108**, 1175.
- Bass, R., 1974, Nucl. Phys. A **231**, 45.
- Bastin, G., A. Péghaire, J. P. Thibaud, S. Andre, D. Barneoud, and C. Foin, 1980, Nucl. Phys. A **345**, 302.
- Bauer, G., R. Shyam, F. Rösel, and D. Trautmann, 1980, Phys. Rev. C **21**, 2668.
- Beck, F. A., E. Bozek, T. Byrski, C. Gehringer, J. C. Merdinger, Y. Schulz, J. Styczen, and J. P. Vivien, 1979, Phys. Rev. Lett. **42**, 493.
- Beene, J. R., M. L. Halbert, D. C. Hensley, R. A. Dayras, K. Geoffroy Young, D. G. Sarantites, and J. H. Barker, 1981, Phys. Rev. C **23**, 2463.
- Bengtsson, R., 1980, J. Phys. (Paris) Colloq. **41-10**, 84 (International Conference on Nuclear Behaviour at High Angular Momentum, Strasbourg).
- Bengtsson, R., and S. Frauendorf, 1977, in *Proceedings of an International Symposium on High Spin States and Nuclear Structure, Dresden*, edited by L. Funke (ZFK, Rossendorf), p. 74.
- Bengtsson, R., and S. Frauendorf, 1979a, Nucl. Phys. A **314**, 27.
- Bengtsson, R., and S. Frauendorf, 1979b, Nucl. Phys. A **327**, 139.
- Bengtsson, R., and S. Frauendorf, 1981, Nordita preprint 78/18.
- Bengtsson, R., I. Hamamoto, and B. R. Mottelson, 1978, Phys. Lett. B **73**, 259.
- Bengtsson, R., S. E. Larsson, G. Leander, P. Möller, S. G. Nilsson, S. Åberg, and Z. Szymański, 1975, Phys. Lett. B **57**, 301.
- Bengtsson, T., M. E. Faber, G. Leander, P. Möller, M. Płoszajczak, I. Ragnarsson, and S. Åberg, 1981, Phys. Scr. **24**, 200 (*Nuclei at Very High Spin—Sven Gösta Nilsson in Memoriam*, Proceedings, Nobel Symposium, Örenäs, 1980, edited by Georg Leander and Hans Ryde).
- Bengtsson, T., and I. Ragnarsson, 1982, in *Proceedings of a Nordic Meeting on Nuclear Physics, Fuglsø*, p. 66, print Niels Bohr Institute Risø.
- Ben-Zvi, I., A. E. Blaugrund, Y. Dar, G. Goldring, J. Hess, M. W. Sachs, E. Z. Skurnik, and Y. Wolfson, 1968, Nucl. Phys. A **117**, 625.
- Bergström, I., J. Blomqvist, B. Fant, A. Filevich, G. Linden, K. G. Rensfelt, J. Szarkier, and K. Wikström, 1971, Phys. Scr. **3**, 11.
- Bergström, I., J. Blomqvist, C. J. Herrlander, K. Wikström, and B. Fant, 1974, Phys. Scr. **10**, 287.
- Bergström, I., C. J. Herrlander, Th. Lindblad, V. Rahkonen, K. G. Rensfelt, and K. Westerberg, 1975, Z. Phys. A **273**, 291.
- Bernthal, F. M., C. L. Dors, B. D. Jeltema, T. L. Khoo, and R. A. Warner, 1976, Phys. Lett. B **64**, 147.
- Bhargava, P. C., 1973, Nucl. Phys. A **207**, 258.
- Bhargava, P. C., and D. J. Thouless, 1973, Nucl. Phys. A **215**, 515.
- Bialkowski, J., B. Fant, C. J. Herrlander, L. Hildingsson, A. Johnson, W. Klamra, J. Kownacki, A. Källberg, Th. Lindblad, C. G. Lindén, T. Lönnroth, J. Starker, T. Vertse, and K. Wikström, 1981, Nucl. Phys. A **357**, 261.
- Birkelund, J. R., L. E. Tubbs, J. R. Huizenga, J. N. De, and D. Sperber, 1979, Phys. Rep. **56**, 109.
- Bjerregaard, J., B. Elbek, O. Hansen, and P. Salling, 1963, Nucl. Phys. **44**, 280.
- Blatt, M., and V. F. Weisskopf, 1952, *Theoretical Nuclear Physics* (Springer, Berlin).
- Blomqvist, J., 1979, in *Symposium on High-Spin Phenomena in Nuclei, Argonne*, edited by T. L. Khoo, print ANL/PHY-79-4, Argonne, p. 155.
- Blomqvist, J., and S. Wahlborn, 1960, Ark. Fys. **16**, 545.
- Bochev, B., S. Iliev, R. Kolpakchieva, S. A. Karamian, T. Kutsarova, E. Nadjakov, and Ts. Venkova, 1977, Nucl. Phys. A **282**, 159.
- Bochev, B., S. A. Karamyan, T. Kutsarova, E. Nadjakov, and Yu. Ts. Oganessian, 1976, Nucl. Phys. A **267**, 344.
- Bochev, B., S. A. Karamyan, T. Kutsarova, and V. G. Subbotin, 1975, Yad. Fiz. **22**, 665 [Sov. J. Nucl. Phys. **22**, 343 (1976)].
- Bohr, A., 1952, K. Dan. Vidensk. Selsk. Mat. Fys. Medd. **26**, No. 14, 1.
- Bohr, A., 1953, *Rotational States in Atomic Nuclei* (Munksgaard, Copenhagen).

- Bohr, A., 1976, Rev. Mod. Phys. **48**, 365.
- Bohr, A., I. Hamamoto, and B. R. Mottelson, 1982, Phys. Scr. **26**, 267.
- Bohr, A., and B. R. Mottelson, 1953, K. Dan. Vidensk. Selsk. Mat. Fys. Medd. **27**, No. 16, 1.
- Bohr, A., and B. R. Mottelson, 1955, K. Dan. Vidensk. Selsk. Mat. Fys. Medd. **30**, No. 1, 1.
- Bohr, A., and B. R. Mottelson, 1969 and 1975, *Nuclear Structure*, Vols. 1 and 2 (Benjamin, New York).
- Bohr, A., and B. R. Mottelson, 1974, Phys. Scr. A **10**, 13.
- Bohr, A., and B. R. Mottelson, 1977, *Proceedings of the International Conference on Nuclear Structure*, edited by T. Marumori (J. Phys. Soc. Jpn. **44**, Suppl.), p. 157.
- Bohr, A., and B. R. Mottelson, 1980, Phys. Scr. **22**, 461.
- Bohr, A., and B. R. Mottelson, 1981, Phys. Scr. **24**, 71 (*Nuclei at Very High Spin—Sven Gösta Nilsson in Memoriam*, Proceedings, Nobel Symposium, Örenäs, 1980, edited by Georg Leander and Hans Ryde).
- Bohr, A., B. R. Mottelson, and D. Pines, 1958, Phys. Rev. **110**, 936.
- Bolsterli, M., E. O. Fiset, J. R. Nix, and J. L. Norton, 1972, Phys. Rev. C **5**, 1050.
- Borggreen, J., S. Bjørnholm, O. Christensen, A. Del Zoppo, B. Herskind, J. Pedersen, G. Sletten, F. Folkmann, and R. S. Simon, 1980, Z. Phys. A **294**, 113.
- Böttges, N., A. Faessler, and M. E. Faber, 1981, J. Phys. G **7**, 321.
- Brack, M., and B. K. Jennings, 1976, Nucl. Phys. A **258**, 246.
- Broda, R., C. Günther, and B. V. Thirumala Rao, 1982, Nucl. Phys. A **389**, 366.
- Broda, R., P. Kleinheinz, P. J. Daly, M. Behar, and J. Blomqvist, 1979, in *Symposium on High-Spin Phenomena in Nuclei, Argonne*, edited by T. L. Khoo, print ANL/PHY-79-4, Argonne, p. 397.
- Broda, R., P. Kleinheinz, S. Lunardi, and J. Blomqvist, 1979, in *Symposium on High-Spin Phenomena in Nuclei, Argonne*, edited by T. L. Khoo, print ANL/PHY-79-4, Argonne, p. 389.
- Broda, R., M. Ogawa, S. Lunardi, M. R. Maier, P. J. Daly, and P. Kleinheinz, 1978, Z. Phys. A **285**, 423.
- Burde, J., E. L. Dines, S. Shih, R. M. Diamond, J. E. Draper, K. H. Lindenberger, C. Schück, and F. S. Stephens, 1982, Phys. Rev. Lett. **48**, 530.
- Byrski, T., F. A. Beck, C. Gehringer, J. C. Merdinger, Y. Schutz, and J. P. Vivien, 1980, J. Phys. (Paris) Colloq. **41-10**, 98 (International Conference on Nuclear Behavior at High Angular Momentum, Strasbourg).
- Byrski, T., F. A. Beck, C. Gehringer, J. C. Merdinger, Y. Schutz, J. P. Vivien, J. Dudek, W. Nazarewicz, and Z. Szymański, 1981, Phys. Lett. B **102**, 235.
- Carlén, L., S. Jónsson, J. Krumlinde, J. Lyttkens, M. Roy, H. Ryde, S. Strömberg, and W. Waluś, 1982, Nucl. Phys. A **381**, 155.
- Carlén, L., S. Jónsson, J. Lyttkens, H. Ryde, S. Strömberg, G. B. Hagemann, and B. Herskind, 1979, Annual Report, University of Lund, 17.
- Cerkaski, M., J. Dudek, Z. Szymański, C. G. Andersson, G. Leander, S. Åberg, S. G. Nilsson, and I. Ragnarsson, 1977, Phys. Lett. B **70**, 9.
- Cerkaski, M., J. Dudek, P. Rozmaj, Z. Szymański, and S. G. Nilsson, 1979, Nucl. Phys. A **315**, 269.
- Chasman, R., 1978, in *Proceedings of an International Symposium on Superheavy Elements, Lubbock*, edited by M. A. K. Lodhi (Pergamon, New York).
- Cherpurnov, V., A., 1967, Yad. Fiz. **6**, 955.
- Civitarese, O., A. Faessler, and M. Wakai, 1979, Phys. Lett. B **84**, 404.
- Cohen, S., F. Plasil, and W. J. Swiatecki, 1974, Ann. Phys. **82**, 557.
- Cornelis, K., R. Holzman, M. Huyse, R. V. F. Janssens, G. Lhersonneau, J. Lukasiak, C. Michel, Z. Sujkowski, M. A. Van Hove, J. Verplancke, and J. Vervier, 1980, in *Proceedings of an International Conference on Nuclear Behaviour at High Angular Momenta, Strasbourg*, print CRN, Strasbourg, 1980, p. 75.
- Cwiok, S., W. Nazarewicz, J. Dudek, J. Skalski, and Z. Szymański, 1980, Nucl. Phys. A **333**, 139.
- Daly, P. J., P. Kleinheinz, R. Broda, S. Lunardi, H. Backe, and J. Blomqvist, 1980, Z. Phys. A **298**, 173.
- Daly, P. J., P. Kleinheinz, R. Broda, A. M. Stefanini, S. Lunardi, H. Backe, L. Richter, R. Willwater, and F. Weik, 1978, Z. Phys. A **288**, 103.
- Damgaard, J., H. C. Pauli, V. V. Pashkevich, and V. M. Strutinsky, 1969, Nucl. Phys. A **135**, 432.
- Davidson, W. F., H. Beuscher, R. M. Lieder, A. Nesnakis, and C. Mayer-Böricke, 1974, Annual Report, KFA, Jülich, 86.
- Davidson, W. F., R. M. Lieder, H. Beuscher, and C. Mayer-Böricke, 1972, Phys. Scr. **6**, 251.
- Deleplanque, M. A., 1981, Phys. Scr. **24**, 158 (*Nuclei at Very High Spin—Sven Gösta Nilsson in Memoriam*, Proceedings, Nobel Symposium, Örenäs, 1980, edited by Georg Leander and Hans Ryde).
- Deleplanque, M. A., Th. Byrski, R. M. Diamond, H. Hübel, F. S. Stephens, B. Herskind, and R. Bauer, 1978, Phys. Rev. Lett. **41**, 1105.
- Deleplanque, M. A., J. P. Husson, N. Perrin, F. S. Stephens, G. Bastin, C. Schück, J. P. Thibaud, L. Hildingsson, S. Hjorth, A. Johnson, and Th. Lindblad, 1979, Phys. Rev. Lett. **43**, 1001.
- Deleplanque, M. A., H. Körner, H. Kluge, A. O. Macchiavelli, N. Bendjaballah, F. S. Stephens, and R. M. Diamond, 1982, in *Proceedings of a Nordic Meeting on Nuclear Physics, Fuglsø*, 44, print Niels Bohr Institute, Risø.
- Deleplanque, M. A., I. Y. Lee, F. S. Stephens, R. M. Diamond, and M. M. Leonard, 1978, Phys. Rev. Lett. **40**, 629.
- Deleplanque, M. A., F. S. Stephens, O. Andersen, J. D. Garrett, B. Herskind, R. M. Diamond, C. Ellegard, D. B. Fossan, D. L. Hillis, H. Kluge, M. Neiman, C. P. Roulet, S. Shih, and R. S. Simon, 1980, Phys. Rev. Lett. **45**, 172.
- Diamond, R. M., and F. S. Stephens, 1980, Ann. Rev. Nucl. Part. Sci. **30**, 85.
- Diamond, R. M., F. S. Stephens, W. H. Kelly, and D. Ward, 1969, Phys. Rev. Lett. **22**, 546.
- Domingos, J. M., G. D. Symons, and A. C. Douglas, 1972, Nucl. Phys. A **180**, 600.
- Døssing, T., K. Neergaard, K. Matsuyanagi, and H. C. Chang, 1977, Phys. Rev. Lett. **39**, 1395.
- Døssing, T., K. Neergaard, and H. Sagawa, 1980, J. Phys. (Paris) Colloq. **41-10**, 79 (International Conference on Nuclear Behaviour at High Angular Momentum).
- Døssing, T., K. Neergaard, and H. Sagawa, 1981, Phys. Scr. **24**, 258 (*Nuclei at Very High Spin—Sven Gösta Nilsson in Memoriam*, Örenäs, 1980, edited by Georg Leander and Hans Ryde).
- Draayer, J. P., C. S. Han, K. J. Weeks, and K. T. Hecht, 1981, Nucl. Phys. A **365**, 127.
- Dracoulis, G. D., C. Fahlander, and M. P. Fewell, 1980, Phys. Rev. Lett. **45**, 1831.
- Dracoulis, G. D., S. M. Ferguson, J. C. Newton, and M. G.

- Slocombe, 1977, Nucl. Phys. A **279**, 251.
- Dracoulis, G. D., and P. M. Walker, 1979, Nucl. Phys. A **330**, 186.
- Dracoulis, G. D., and P. M. Walker, 1980, Nucl. Phys. A **342**, 335.
- Dudek, J., 1980, J. Phys. (Paris) Colloq. **41-10**, 18 (International Conference on Nuclear Behaviour at High Angular Momentum, Strasbourg).
- Dudek, J., A. Majhofer, and J. Skalski, 1980, J. Phys. G **6**, 447.
- Dudek, J., A. Majhofer, J. Skalski, T. Werner, S. Cwiok, and W. Nazarewicz, 1979, J. Phys. G **5**, 1359.
- Dudek, J., W. Nazarewicz, and Z. Szymański, 1981, Phys. Scr. **24**, 309 (*Nuclei at Very High Spin—Sven Gösta Nilsson in Memoriam*, Örenäs, edited by Georg Leander and Hans Ryde).
- Dudek, J., W. Nazarewicz, and T. Werner, 1980, Nucl. Phys. A **341**, 253.
- Dudek, J., Z. Szymański, and T. Werner, 1981, Phys. Rev. C **23**, 920.
- Dudek, J., and T. Werner, 1978, J. Phys. G **4**, 1543.
- Dudek, J., A. Majhofer, W. Nazarewicz, and Z. Szymański, 1982, Phys. Lett. B **112**, 1.
- Dudek, J., Z. Szymański, T. Werner, A. Faessler, and C. Lima, 1982, Phys. Ref. C **26**, 1712.
- Durell, J. L., G. D. Dracoulis, C. Fahlander, and A. P. Byrne, 1982, Phys. Lett. B **115**, 367.
- Egido, J. L., and P. Ring, 1982a, Nucl. Phys. A **383**, 189.
- Egido, J. L., and P. Ring, 1982b, Nucl. Phys. A **388**, 19.
- Ejiri, H., T. Shibata, T. Itahashi, T. Nagai, H. Sakai, S. Nakayama, T. Kishimoto, K. Maeda, and M. Hoshi, 1978, Nucl. Phys. A **305**, 167.
- Ellis, Y. A., and B. Harmatz, 1975, Nucl. Data Sheets **16**, 135.
- Emling, H., 1981, in *Proceedings of the XIVth Masurian Summer School on Nuclear Physics, Mikolajki, Poland*, and GSI preprint 81-40 (to be published).
- Emling, H., E. Grosse, D. Schwalm, R. S. Simon, H. J. Wollersheim, D. Husar, and D. Pelte, 1981, Phys. Lett. B **98**, 169.
- Erb, K. A., J. E. Holden, I. Y. Lee, J. X. Saladin, and T. K. Saylor, 1972, Phys. Rev. Lett. **29**, 1010.
- Faber, M., M. Ploszajczak, and A. Faessler, 1979, Nucl. Phys. A **326**, 129.
- Faessler, A., R. R. Hilton, and K. R. Sandhya-Devi, 1976, Phys. Lett. B **61**, 133.
- Faessler, A., and M. Ploszajczak, 1977, Phys. Rev. C **16**, 2032.
- Faessler, A., and M. Ploszajczak, 1978, Phys. Lett. B **76**, 1.
- Faessler, A., and M. Ploszajczak, 1980, Z. Phys. A **295**, 87.
- Faessler, A., M. Ploszajczak, and K. W. Schmid, 1981, Progr. Part. Nucl. Phys. **5**, 79.
- Faessler, A., K. R. Sandhya-Devi, G. Grümmer, K. W. Schmid, and R. R. Hilton, 1976, Nucl. Phys. A **256**, 106.
- Fant, B., 1971, Phys. Scr. **4**, 175.
- Fant, B., K. Fransson, C. J. Herrlander, K. Houkanen, A. Källberg, C. G. Lindén, T. Lönnroth, and T. Weckström, 1980, Research Institute of Physics, Stockholm, Annual Report, p. 82.
- Fant, B., C. J. Herrlander, K. Houkanen, A. Källberg, V. Rahkonen, and T. Weckström, 1982, in *Proceedings of a Nordic Meeting on Nuclear Physics, Fulsø*, print Niels Bohr Institute, Risø, p. 32.
- Feeenstra, S. J., J. van Klinken, J. P. Pijn, R. V. F. Janssens, C. Michel, J. Steyaart, J. Vervier, K. Cornelis, M. Huyse, and G. Lhersonneau, 1979, Phys. Lett. B **80**, 183.
- Feeenstra, S. J., W. J. Ockels, J. van Klinken, M. J. A. de Voigt, and Z. Sujkowski, 1977, Phys. Lett. B **69**, 403.
- Fenzl, M., R. M. Lieder, H. Beuscher, W. F. Davidson, A. Nesbakis, and H. M. Jäger, 1975, Z. Phys. A **273**, 163.
- Fleckner, J., V. Mosel, P. Ring, and H. J. Mang, 1979, Nucl. Phys. A **331**, 288.
- Foin, C., S. André, D. Barneoud, G. Bastin, A. Péghaire, and J. P. Thibaud, 1982, Z. Phys. A **305**, 81.
- Folkmann, F., J. D. Garrett, G. B. Hagemann, M. N. Harakeh, B. Herskind, D. L. Hillis, S. Ogaza, H. Emling, E. Grosse, D. Schwalm, R. S. Simon, and P. O. Tjørn, 1981, Nucl. Phys. A **361**, 242.
- Fossan, D. B., and B. Herskind, 1963, Nucl. Phys. **40**, 24.
- Funk, E. G., H. J. Prask, and J. W. Mihelich, 1966, Phys. Rev. **141**, 1200.
- Gaardhøye, J. J., 1980, Ph.D. thesis, Copenhagen.
- Gaardhøye, J. J., O. Andersen, J. D. Garrett, G. B. Hagemann, B. Herskind, L. L. Riedinger, and P. O. Tjørn, 1980, in *International Conference on Nuclear Behaviour at High Angular Momentum, Strasbourg*, 101, print CRN, Strasbourg.
- Galin, J., D. Guerreau, M. Lefort, and X. Tarrago, 1974, Phys. Rev. C **10**, 1018.
- Garrett, J. D., O. Andersen, J. J. Gaardhøye, G. B. Hagemann, B. Herskind, J. Kownacki, J. C. Lisle, L. L. Riedinger, W. Walus, N. Roy, S. Jonsson, H. Ryde, M. Gutormsen, and P. O. Tjørn, 1982, Phys. Rev. Lett. **47**, 75.
- Garrett, J. D., and S. Frauendorf, 1982, Phys. Lett. B **108**, 77.
- Garrett, J. D., and B. Herskind, 1979, at Study weekend on nuclei far from stability, Daresbury Nuclear Physics Laboratory, edited by W. Gelletly, Daresbury, 22–23 September.
- Geoffroy Young, K. A., D. G. Sarantites, J. R. Beene, M. L. Halbert, D. C. Hensley, R. A. Dayras, and J. H. Barker, 1981, Phys. Rev. C **23**, 2479.
- Geoffroy Young, K. A., D. G. Sarantites, M. L. Halbert, D. C. Hensley, R. A. Dayras, and J. H. Barker, 1979, Phys. Rev. Lett. **43**, 1303.
- Glas, D., and V. Mosel, 1974, Phys. Rev. C **10**, 2620.
- Glenndinning, N. K., 1962, Phys. Rev. **127**, 923.
- Gono, Y., and T. T. Sugihara, 1974, Phys. Rev. C **10**, 2460.
- Goodman, A. L., 1974, Nucl. Phys. A **230**, 466.
- Goodman, A. L., 1976, Nucl. Phys. A **265**, 113.
- Goodman, A. L., 1979, Nucl. Phys. A **325**, 171.
- Goodman, A. L., 1981, Phys. Lett. B **103**, 163.
- Grosse, E., 1979, in *International Symposium on High Spin Phenomena in Nuclei, Argonne*, edited by T. L. Khoo, print ANL/PHY-79-4, Argonne, p. 223.
- Grosse, E., A. Balandra, H. Emling, F. Folkmann, P. Fuchs, R. B. Piercy, D. Schwalm, R. S. Simon, H. J. Wollersheim, D. Evers, and H. Ower, 1981, Phys. Scr. **24**, 337 (*Nuclei at Very High Spin—Sven Gösta Nilsson in Memoriam*, Proceedings, Nobel Symposium, edited by Georg Leander and Hans Ryde).
- Grover, J. R., 1967, Phys. Rev. **157**, 832.
- Grover, J. R., and J. Gilat, 1967a, Phys. Rev. **157**, 802.
- Grover, J. R., and J. Gilat, 1967b, Phys. Rev. **157**, 814.
- Grover, J. R., and J. Gilat, 1967c, Phys. Rev. **157**, 823.
- Grümmer, F., K. W. Schmid, and A. Faessler, 1978, Nucl. Phys. A **306**, 134.
- Grümmer, F., K. W. Schmid, and A. Faessler, 1979, Nucl. Phys. A **326**, 1.
- Gui, G. Z., G. Colombo, and E. Nolte, 1982, Z. Phys. A **305**, 297.
- Gujrathi, S. C., and J. M. Danria, 1971, Nucl. Phys. A **161**, 410.
- Gustafson, C., I. L. Lamm, B. Nilsson, and S. G. Nilsson, 1967, Ark. Fys. **36**, 613.
- Haas, B., H. R. Andrews, O. Häusser, D. Horn, J. F. Sharpey-Schafer, P. Taras, W. Trautmann, D. Ward, T. L. Khoo, and R. K. Smith, 1979, Phys. Lett. B **84**, 178.

- Haas, B., D. Ward, H. R. Andrews, O. Häusser, A. J. Ferguson, J. F. Sharpey-Schafer, T. K. Alexander, W. Trautmann, D. Horn, P. Taras, P. Skensved, T. L. Khoo, R. K. Smither, I. Ahmed, C. N. Davids, W. Kutschera, S. Levenson, and C. L. Dors, 1981, *Nucl. Phys. A* **362**, 254.
- Hageman, D. C. J. M., 1981, Ph.D. thesis, University of Groningen.
- Hageman, D. C. J. M., M. J. A. de Voigt, and J. F. W. Jansen, 1979a, *Phys. Lett. B* **84**, 301.
- Hageman, D. C. J. M., M. J. A. de Voigt, and J. F. W. Jansen, 1979b, *KVI Annual Report*, p. 68.
- Hageman, D. C. J. M., R. V. F. Janssens, J. Łukasiak, W. J. Ockels, Z. Sujkowski, and M. J. A. de Voigt, 1981, *Phys. Scr. 24*, 145 (*Nuclei at Very High Spin—Sven Gösta Nilsson in Memoriam*, Proceedings, Nobel Symposium, Örenäs, 1980, edited by Georg Leander and Hans Ryde).
- Hagemann, G. B., R. Broda, B. Herskind, M. Ischihara, S. Ogaza, and H. Ryde, 1975, *Nucl. Phys. A* **245**, 166.
- Hamamoto, I., 1976, *Nucl. Phys. A* **271**, 15.
- Hara, K., A. Hayashi, and P. Ring, 1982, *Nucl. Phys. A* **385**, 14.
- Harris, S. M., 1965, *Phys. Rev. 138*, 509B.
- Häusser, O., 1979, in *Proceedings of a Symposium on High-Spin Phenomena in Nuclei, Argonne*, edited by T. L. Khoo, print ANL/PHY-79-4, Argonne, p. 255.
- Häusser, O., 1982, in *Proceedings of a Conference on High Angular Momentum Properties in Nuclei, Oak Ridge*, edited by N. R. Johnson, ORNL, Oak Ridge, Vol. 1, p. 50.
- Häusser, O., H. R. Andrews, H. E. Mahnke, J. F. Sharpey-Schafer, M. L. Swanson, P. Taras, D. Ward, and T. K. Alexander, 1980, *Phys. Rev. Lett.* **44**, 132.
- Häusser, O., J. R. Beene, T. Faestermann, T. K. Alexander, D. Horn, A. B. McDonald, and A. J. Ferguson, 1978, *Hyperfine Interact.* **4**, 219.
- Häusser, O., J. R. Beene, A. B. McDonald, T. K. Alexander, E. D. Earle, F. C. Khanna, I. Towner, G. A. Beer, and A. Olin, 1976, *Phys. Lett. B* **63**, 279.
- Häusser, O., H. Gräf, L. Grodzins, E. Jaeschke, V. Metag, D. Habs, D. Pelte, H. Emling, E. Grosse, R. Kulessa, D. Schwalm, R. S. Simon, and J. Keinonen, 1982, *Phys. Rev. Lett.* **48**, 383.
- Häusser, O., P. Taras, W. Trautmann, D. Ward, T. K. Alexander, H. R. Andrews, B. Haas, and D. Horn, 1979, *Phys. Rev. Lett.* **42**, 1451.
- Hecht, K. T., and A. Adler, 1969, *Nucl. Phys. A* **137**, 129.
- Helppi, H., Y. H. Chung, P. J. Daly, S. R. Faber, A. Pakkanen, I. Ahmad, P. Chowdhury, Z. W. Grabowski, T. L. Khoo, R. D. Lawson, and J. Blomqvist, 1982, *Phys. Lett. B* **115**, 11.
- Herskind, B., 1980, *J. Phys. (Paris) Colloq. 41-10*, 106 (International Conference on Nuclear Behaviour at High Angular Momentum, Strasbourg).
- Hillis, D. L., J. D. Garrett, O. Christensen, B. Fernandez, G. B. Hagemann, B. Herskind, B. B. Back, and F. Folkmann, 1979, *Nucl. Phys. A* **325**, 216.
- Hilton, R. R., H. J. Mang, P. Ring, J. L. Egido, H. Herold, M. Reinecke, H. Ruder, and G. Wunner, 1981, *Nucl. Phys. A* **366**, 365.
- Holzman, R., Y. El Masri, C. Michel, M. A. Van Hove, and J. Vervier, 1980, in *International Conference on Nuclear Behaviour at High Angular Momentum, Strasbourg*, print CRN, Strasbourg, p. 79.
- Horn, D., O. Häusser, T. Faestermann, A. B. McDonald, T. K. Alexander, J. R. Beene, and C. J. Herrlander, 1977, *Phys. Rev. Lett.* **39**, 389.
- Horn, D., G. R. Young, C. J. Lister, and C. Baktash, 1980, *J. Phys. (Paris) Colloq. 41-10*, 39 (International Conference on Nuclear Behaviour at High Angular Momentum, Strasbourg).
- Horn, D., G. R. Young, C. J. Lister, and C. Baktash, 1981, *Phys. Rev. C* **23**, 1047.
- Hübel, H., D. J. Deeman, H. Grawe, H. Haas, and K. H. Maier, 1982, *Nucl. Phys. A* **382**, 56.
- Hübel, H., R. M. Diamond, P. Aguer, C. Ellegard, D. B. Fossum, H. Kluge, C. Schück, S. Shih, F. S. Stephens, and U. Smilanski, 1982, *Z. Phys. A* **304**, 225.
- Hübel, H., R. M. Diamond, F. S. Stephens, B. Herskind, and R. Bauer, 1980, *Z. Phys. A* **297**, 237.
- Hübel, H., R. A. Naumann, and P. K. Hopke, 1970, *Phys. Rev. C* **2**, 1447.
- Hübel, H., U. Smilansky, R. M. Diamond, F. S. Stephens, and B. Herskind, 1978, *Phys. Rev. Lett.* **41**, 791.
- Huus, T., and C. Zupančič, 1953, *K. Dan. Vidensk. Selsk. Mat. Phys. Medd.* **28**, No. 1, 1.
- Inamura, T., M. Ishihara, T. Fukuda, T. Shimoda, and H. Hiruta, 1977, *Phys. Lett. B* **68**, 51.
- Inglis, D. R., 1954, *Phys. Rev. 96*, 1059.
- Inglis, D. R., 1955, *Phys. Rev. 97*, 701.
- Ingwersen, H., W. Klinger, G. Schatz, and W. Withuhn, 1975, *Phys. Rev. C* **11**, 243.
- Jääskeläinen, M., D. G. Sarantites, R. Woodward, F. A. Dilmanian, H. Puchta, J. R. Beene, J. Hattula, M. L. Halbert, D. C. Hensley, and J. H. Barker, 1982, *Phys. Rev. Lett.* **49**, 1387.
- Jansen, J. F. W., Z. Sujkowski, D. Chmielewska, and R. J. de Meijer, 1976, in *Proceedings of the Third International Conference on Nuclei Far from Stability, Cargèse* (CERN 76-13), p. 415.
- Jansen, J. F. W., M. J. A. de Voigt, Z. Sujkowski, and D. Chmielewska, 1979, *Nucl. Phys. A* **321**, 365.
- Janssens, R. V. F., M. J. A. de Voigt, H. Sakai, H. Aarls, C. J. van der Poel, H. F. R. Arciszewski, D. E. C. Scherpenseel, and J. Vervieux, 1981, *Phys. Lett. B* **106**, 475.
- Jastrzebski, J., R. Kossakowski, J. Łukasiak, M. Moszyński, Z. Preibisz, S. André, J. Genevey, A. Gizon, and J. Gizon, 1980, *Phys. Lett. B* **97**, 50.
- Jett, J. H., and D. A. Lind, 1970, *Nucl. Phys. A* **155**, 182.
- Johnson, A., H. Ryde, and S. Hjorth, 1972, *Nucl. Phys. A* **179**, 753.
- Johnson, M. R., 1982, in *INS International Symposium on Dynamics of Nuclear Collective Motion, Mt. Fuji, Japan*, edited by K. Ogawa and T. Tanabe (INS, Tokyo), p. 144.
- Kearns, F., G. Varley, G. D. Dracoulis, T. Inamura, J. C. Lisle, and J. C. Willmott, 1977, *Nucl. Phys. A* **278**, 109.
- Kerek, A., J. Kihlgren, Th. Lindblad, C. Pomar, J. Szarkier, W. Waluś, O. Skeppstedt, J. Białkowski, J. Kownacki, Z. Sujkowski, and A. Zglinski, 1978, *Nucl. Instrum. Methods* **150**, 483.
- Khoo, T. L., 1979, in *Proceedings of a Symposium on High-Spin Phenomena in Nuclei, Argonne*, edited by T. L. Khoo, print ANL/PHY-79-4, Argonne, p. 95.
- Khoo, T. L., 1980, *J. Phys. (Paris) Colloq. 41-10*, 9 (International Conference on Nuclear Behavior at High Angular Momentum, Strasbourg).
- Khoo, T. L., 1981, unpublished.
- Khoo, T. L., F. M. Bernthal, R. G. H. Robertson, and R. A. Warner, 1976, *Phys. Rev. Lett.* **37**, 823.
- Khoo, T. L., and G. Løvhøiden, 1977, *Phys. Lett. B* **67**, 271.
- Khoo, T. L., R. K. Smither, B. Haas, O. Häusser, H. R. Andrews, D. Horn, and D. Ward, 1978, *Phys. Rev. Lett.* **41**, 1027.

- Kistner, O. C., C. Baktash, E. der Mateosian, D. Horn, C. J. Lister, and A. W. Sunyar, 1980, in *Proceedings of an International Conference on Nuclear Physics, Berkeley*, edited by R. M. Diamond and J. O. Rasmussen, LBL, Berkeley, p. 326.
- Kleinheinz, P., 1979, in *Proceedings of a Conference on High-Spin Phenomena in Nuclei, Argonne*, edited by T. L. Khoo, print ANL/PHY-79-4, Argonne, p. 125.
- Kleinheinz, P., R. Broda, P. J. Daly, S. Lunardi, M. Ogawa, and J. Blomqvist, 1979, *Z. Phys. A* **290**, 295.
- Kleinheinz, P., S. Lunardi, M. Ogawa, and M. R. Maier, 1978, *Z. Phys. A* **284**, 315.
- Kleinheinz, P., M. Ogawa, R. Broda, P. J. Daly, D. Haenni, H. Beuscher, and A. Kleinrahm, 1978, *Z. Phys. A* **286**, 27.
- Klinken, J. van, W. Z. Venema, R. V. F. Janssens, and G. T. Emery, 1980, *Nucl. Phys. A* **339**, 189.
- Kohl, W., D. Kolb, and I. Giese, 1978, *Z. Phys. A* **285**, 17.
- Körner, H. J., D. L. Hillis, C. P. Roulet, P. Aguer, C. Ellegaard, D. B. Fossan, D. Habs, M. Neiman, F. S. Stephens, and R. M. Diamond, 1979, *Phys. Rev. Lett.* **43**, 490.
- Krappe, H. J., 1979, in *Proceedings of a Symposium on Deep-Inelastic Fusion, Reactions with Heavy Ions, Berlin*, edited by W. von Oertzen (Springer, Berlin).
- Krumlinde, J., and Z. Szymański, 1973, *Ann. Phys. (N.Y.)* **79**, 201.
- Kurfess, J. D., and P. P. Scharenberg, 1967, *Phys. Rev.* **161**, 1185.
- Kutschera, W., D. Dehnhardt, O. C. Kistner, P. Kump, B. Povh, and H. J. Sann, 1972, *Phys. Rev. C* **5**, 1658.
- Landau, L. D., and E. M. Lifschitz, 1965, *Mekhanika* (Nauka, Moscow).
- Leander, G., C. G. Andersson, S. G. Nilsson, I. Ragnarsson, S. Åberg, J. Almberger, T. Døssing, and K. Neergaard, 1979, in *Proceedings of a Conference on High-Spin Phenomena in Nuclei, Argonne*, edited by T. L. Khoo, print ANL/PHY-79-4, Argonne, p. 197.
- Leander, G., Y. S. Chen, and B. S. Nilsson, 1981, *Phys. Scr.* **24**, 164 (*Nuclei at Very High Spin—Sven Gösta Nilsson in Memoriam*, Proceedings, Nobel Symposium, Örenäs, 1980, edited by Georg Leander and Hans Ryde).
- Lederer, C. M., and V. S. Shirley, 1978, *Tables of Isotopes* (Wiley, New York).
- Lee, I. Y., M. M. Aleonard, M. A. Deleplanque, Y. El-Masri, J. O. Newton, R. S. Simon, R. M. Diamond, and F. S. Stephens, 1977, *Phys. Rev. Lett.* **38**, 1454.
- Lee, M. A., and C. W. Reich, 1979, *Nucl. Data Sheets* **27**, 155.
- Lefort, M., 1974, *Phys. Scr. A* **10**, 101.
- Lefort, M., and Ch. Ngo, 1978, *Ann. Phys.* **3**, 5.
- Lieder, R. M., H. Beuscher, W. F. Davidson, P. Jahn, H. J. Probst, and C. Mayer-Böricker, 1972, *Z. Phys. A* **257**, 147.
- Lieder, R. M., and H. Ryde, 1978, *Adv. Nucl. Phys.* **10**, 1.
- Lindblad, Th., 1977, *Nukleonika* **22**, 1065.
- Lindén, C. G., I. Bergström, J. Blomqvist, K. G. Rensfelt, H. Sergolle, and K. Westerberg, 1976, *Z. Phys. A* **277**, 273.
- Liotta, R. J., and R. A. Sorensen, 1978, *Nucl. Phys. A* **297**, 136.
- Lisle, J. C., J. D. Garrett, G. B. Hagemann, B. Herskind, and S. Ogaza, 1981, *Nucl. Phys. A* **366**, 281.
- Lister, C. J., D. Horn, C. Baktash, E. der Mateosian, O. C. Kistner, and A. W. Sunyar, 1981, *Phys. Rev. C* **23**, 2078.
- Lister, C. J., G. R. Young, D. Cline, J. Srebrny, D. Elmore, P. A. Butler, R. Ledoux, and R. Fridieu, 1979, *Phys. Rev. C* **20**, 605.
- Lönnroth, T., 1982, *Z. Phys. A* **307**, 175.
- Lönnroth, T., L. Vegh, K. Wikström, and B. Fant, 1978, *Z. Phys. A* **287**, 307.
- Lopiparo, P. C., R. L. Rasera, and M. E. Caspari, 1972, *Nucl. Phys. A* **178**, 577.
- Łukasiak, J., D. C. J. M. Hageman, R. V. F. Janssens, Z. Sujkowski, and M. J. A. de Voigt, 1982, *Nucl. Phys. A* **379**, 125.
- Lunardi, S., M. Ogawa, H. Backe, M. Piiparinen, Y. Nagai, and P. Kleinheinz, 1979, in *Proceedings of a Symposium on High-Spin Phenomena in Nuclei, Argonne*, edited by T. L. Khoo, print ANL/PHY-79-4, Argonne, p. 403.
- Madjakov, E., 1982, *Nuclear Structure at High Spin* (Bulgarian Academy of Sciences, Sofia).
- Mahnke, H. E., E. Dafni, G. D. Sprouse, T. K. Alexander, H. R. Andrews, O. Häusser, P. Taras, and D. Ward, 1979, in *Symposium on High-Spin Phenomena in Nuclei, Argonne*, edited by T. L. Khoo, print ANL/PHY-79-4, Argonne, p. 463.
- Maier, K. H., D. J. Decman, H. Grawe, H. Haas, and W. D. Zeitz, 1982, *Hyperfine Interact.* **9**, 87.
- Maier, K. H., J. R. Leigh, F. Pühlhofer, and R. M. Diamond, 1971, *Phys. Lett. B* **35**, 401.
- Mantri, A. N., M. Diebel, and U. Mosel, 1981, *Phys. Rev. Lett.* **47**, 308.
- Marchie Van Voorthuysen, E. H. du, M. J. A. de Voigt, J. F. W. Jansen, 1977, *KVI Annual Report*, Groningen, 47.
- Mariscotti, M. A. J., G. Scharff-Goldhaber, and B. Buck, 1969, *Phys. Rev.* **178**, 1864.
- Marshalek, E. R., and A. L. Goodman, 1978, *Nucl. Phys. A* **294**, 92.
- Matsuyangi, K., T. Døssing, and K. Neergaard, 1978, *Nucl. Phys. A* **307**, 253.
- Merdinger, J. C., F. A. Beck, T. Byrski, C. Gehring, J. P. Vivien, E. Bozek, and J. Styczen, 1979, *Phys. Rev. Lett.* **42**, 23.
- Michel, C., Y. El Masri, R. Holzmann, M. A. Van Hove, and J. Vervier, 1980, *Z. Phys. A* **298**, 213.
- Michel, C., and J. Vervier, 1981, *Z. Phys. A* **299**, 149.
- Milner, W. T., F. K. McGowan, R. L. Robinson, P. H. Stelson, and R. O. Sayer, 1971, *Nucl. Phys. A* **177**, 1.
- Morinaga, H., and P. C. Gugelot, 1963, *Nucl. Phys.* **46**, 210.
- Morinaga, H., and T. Yamazaki, 1976, *In-Beam Gamma-Ray Spectroscopy* (North-Holland, Amsterdam).
- Morrison, J., A. Faessler, and C. Lima, 1981, *Nucl. Phys. A* **372**, 13.
- Mottelson, B. R., and J. G. Valatin, 1960, *Phys. Rev. Lett.* **5**, 511.
- Myers, W. D., and W. J. Swiatecki, 1967, *Ark. Fys.* **36**, 343.
- Nagai, Y., J. Styczin, M. Piiparinen, and P. Kleinheinz, 1980, *Z. Phys. A* **296**, 91.
- Namoodi, M. N., E. T. Chulick, J. B. Natowitz, and R. A. Kenefick, 1975, *Phys. Rev. C* **11**, 401.
- Neergaard, K., T. Døssing, and H. Sagawa, 1981, *Phys. Lett. B* **99**, 191.
- Neergaard, K., and V. V. Pashkevich, 1975, *Phys. Lett. B* **59**, 218.
- Neergaard, K., V. V. Pashkevich, and S. Frauendorf, 1976, *Nucl. Phys. A* **262**, 61.
- Neergaard, K., H. Toki, M. Ploszajczak, and A. Faessler, 1977, *Nucl. Phys. A* **287**, 48.
- Neskakis, A., R. M. Lieder, M. Müller-Veggian, H. Beuscher, W. F. Davidson, and C. Mayer-Böricker, 1976, *Nucl. Phys. A* **261**, 189.
- Neskakis, A., R. M. Lieder, G. Sletten, and J. D. Garrett, 1982, *Phys. Lett. B* **118**, 49.
- Newton, J. O., I. Y. Lee, R. S. Simon, M. M. Aleonard, Y. El Masri, F. S. Stephens, and R. M. Diamond, 1977, *Phys. Rev.*

- Lett. **38**, 810.
- Newton, J. O., J. C. Lisle, G. D. Dracoulis, J. R. Leigh, and D. C. Weisser, 1975, Phys. Rev. Lett. **34**, 99.
- Newton, J. O., S. H. Sie, and G. D. Dracoulis, 1978, Phys. Rev. Lett. **40**, 625.
- Newton, J. O., F. S. Stephens, and R. M. Diamond, 1973, Nucl. Phys. A **210**, 19.
- Nilsson, S. G., 1955, K. Dan. Vidensk. Selsk. Mat. Fys. Medd. **29**, No. 16, 1.
- Nilsson, S. G., and O. Prior, 1961, K. Dan. Vidensk. Selsk. Mat. Fys. Medd. **32**, No. 16, 1.
- Nilsson, S. G., C. F. Tsang, A. Sobczewski, Z. Szymański, S. Wyceck, G. Gustafson, I. L. Lamm, P. Möller, and B. Nilsson, 1969, Nucl. Phys. A **131**, 1.
- Northcliff, L. C., and R. F. Schiling, 1970, Nucl. Data Tables A **7**, 256.
- Ockels, W. J., 1978a, Ph.D. thesis, University of Groningen.
- Ockels, W. J., 1978b, Z. Phys. A **286**, 181.
- Ockels, W. J., M. J. A. de Voigt, and Z. Sujkowski, 1978, Phys. Lett. B **78**, 401.
- Ogawa, M., R. Broda, K. Zell, P. J. Daly, and P. Kleinheinz, 1978, Phys. Rev. Lett. **41**, 289.
- Pakkanen, A., Y. H. Chung, P. J. Daly, S. R. Faber, H. Helpi, J. Wilson, P. Chowdhury, T. L. Khoo, I. Ahmad, J. Borggreen, Z. W. Grabowski, and D. C. Radford, 1982, Phys. Rev. Lett. **48**, 1530.
- Pauli, H. C., 1973, Phys. Rep. **7**, 35.
- Pashkevich, V. V., and V. M. Strutinsky, 1968, Report JINR (Dubna) P2-385-1968.
- Pedersen, J., B. B. Back, F. M. Berndhal, S. Bjørnholm, J. Borggreen, O. Christensen, F. Folkmann, B. Herskind, T. L. Khoo, M. Neiman, F. Pühlhofer, and G. Sletten, 1977, Phys. Rev. Lett. **39**, 990.
- Piiparinen, M., S. Lunardi, P. Kleinheinz, H. Backe, and J. Blomqvist, 1979, Z. Phys. A **290**, 337.
- Piiparinen, M., R. Pengo, Y. Nagai, E. Harrarén, P. Kleinheinz, N. Roy, L. Carlén, H. Ryde, Th. Lindblad, A. Johnson, S. A. Hjorth, and J. Blomqvist, 1981, Z. Phys. A **300**, 133.
- Piiparinen, M., R. Pengo, Y. Nagai, P. Kleinheinz, N. Roy, L. Carlén, H. Ryde, T. Lindblad, A. Johnson, and S. A. Hjorth, 1980, in *International Conference on Nuclear Behaviour at High Angular Momentum, Strasbourg*, print CRN, Strasbourg, p. 63.
- Poletti, A. R., G. D. Dracoulis, C. Fahlander, and I. Morrison, 1981, Nucl. Phys. A **359** 180.
- Poletti, A. R., G. D. Dracoulis, C. Fahlander, and I. Morrison, 1982, Nucl. Phys. A **380**, 335.
- Pomorski, K., and B. Nerlo-Pomorska, 1977, Z. Phys. A **283**, 383.
- Prahraj, C. R., 1982, Phys. Lett. B **119** 17.
- Radford, D. C., 1980, in *International Conference on Nuclear Behaviour at High Angular Momentum, Strasbourg*, print CRN, Strasbourg, p. 157.
- Ragnarsson, I., 1978, Phys. Lett. B **80**, 4.
- Ragnarsson, I., T. Bengtsson, G. Leander, and S. Åberg, 1980, Nucl. Phys. A **347**, 287.
- Ragnarsson, I., S. G. Nilsson, and R. K. Sheline, 1978, Phys. Rep. **45**, 1.
- Ragnarsson, I., D. P. Soroka, and F. S. Stephens, 1975, Lawrence Berkeley Laboratory Annual Report, LBL-5075, p. 286.
- Rahkonen, V., I. Bergström, J. Blomqvist, O. Knuutila, K. G. Rensfelt, J. Sztarkier, and K. Westerberg, 1978, Z. Phys. A **284**, 357.
- Ratna Raju, R. D., J. P. Draayer, and K. T. Hecht, 1973, Nucl. Phys. A **202**, 433.
- Riedinger, L. L. 1980, Nucl. Phys. A **347**, 141.
- Riedinger, L. L., 1981, Phys. Scr. **24**, 312 (*Nuclei at Very High Spin—Sven Gösta Nilsson in Memoriam*, Proceedings, Nobel Symposium, Örenäs, 1980, edited by Georg Leander and Hans Ryde).
- Riedinger, L. L., O. Anderson, S. Frauendorf, J. D. Garrett, J. J. Gaardhøye, G. B. Hagemann, B. Herskind, Y. V. Makovetzky, J. C. Waddington, M. Guttormsen, and P. O. Tjøm, 1980, Phys. Rev. Lett. **44**, 568.
- Ring, P., R. Beck, and H. J. Mang, 1970, Z. Phys. **231**, 10.
- Rost, E., 1968, Phys. Lett. B **26**, 184.
- Rowe, D. J., 1970, *Nuclear Collective Motion, Models and Theory* (Methuen, London).
- Rud, N., D. Ward, H. R. Andrews, R. L. Graham, and J. S. Geiger, 1973, Phys. Rev. Lett. **31**, 1421.
- Rud, N., D. Ward, H. R. Andrews, O. Häusser, P. Taras, J. Keinonen, M. Neiman, R. M. Diamond, and F. S. Stephens, 1981, Phys. Lett. B **101**, 35.
- Ryde, H., S. A. Hjorth, D. Barnéoud, A. Johnson, G. B. Hagemann, and B. Herskind, 1973, Nucl. Phys. A **207**, 513.
- Sætre, Ø., S. A. Hjorth, A. Johnson, S. Jäger, H. Ryde, and Z. Szymański, 1973, Nucl. Phys. A **207**, 486.
- Sakai, H., H. Ejiri, T. Shibata, Y. Nagai, and K. Okada, 1979, Phys. Rev. C **20**, 464.
- Sarantites, D. G., J. H. Barker, M. L. Halbert, D. C. Hensley, R. A. Dayras, E. Eichler, N. R. Johnson, and S. A. Gronemeyer, 1976, Phys. Rev. C **14**, 2138.
- Sarantites, D. G., M. Jaäskeläinen, J. T. Hood, R. Woodward, J. H. Barker, D. C. Hensley, M. L. Halbert, and Y. D. Chan, 1980, J. Phys. (Paris) Colloq. **41**, 269 (International Conference on Nuclear Behaviour at High Angular Momentum, Strasbourg).
- Sarantites, D. G., M. Jaäskeläinen, R. Woodward, F. A. Dilmanian, D. C. Hensley, J. H. Barker, J. R. Beene, M. L. Halbert, and W. T. Milner, 1982, Phys. Lett. B **115**, 441.
- Sarantites, D. G., L. Westerberg, R. A. Dayras, M. L. Halbert, D. C. Hensley, and J. H. Barker, 1978, Phys. Rev. C **17** 601.
- Sarantites, D. G., L. Westerberg, M. L. Halbert, R. A. Dayras, D. C. Hensley, and J. H. Barker, 1978, Phys. Rev. C **18** 774.
- Sayer, R. O., E. Eichler, N. R. Johnson, D. C. Hensley, and L. L. Riedinger, 1974, Phys. Rev. C **9** 1103.
- Sayer, R. O., J. S. Smith III, and W. T. Milner, 1975, Nucl. Data Tables **15**, 85.
- Sayer, R. O., P. H. Stelson, F. K. McGowan, W. T. Milner, and R. L. Robinson, 1970, Phys. Rev. C **1**, 1525.
- Scheerbaum, R. R., 1976a, Phys. Lett. B **61**, 151.
- Scheerbaum, R. R., 1976b, Nucl. Phys. A **257**, 77.
- Scheerbaum, R. R., 1976c, Phys. Lett. B **63**, 381.
- Scholten, O., F. Iachello, and A. Arima, 1978, Ann. Phys. **115**, 325.
- Schutz, Y., J. P. Vivien, F. A. Beck, T. Byrski, C. Gehringer, J. C. Merdinger, J. Dudek, W. Nazarewicz, and Z. Szymański, 1982, Phys. Rev. Lett. **48**, 1534.
- Sie, S. H., D. Ward, J. S. Geiger, R. L. Graham, H. R. Andrews, 1977 Nucl. Phys. A **291**, 443.
- Simon, R. S., 1980, J. Phys. (Paris) Colloq. **41-10**, 281 (International Conference on Nuclear Behaviour at High Angular Momentum, Strasbourg).
- Simon, R. S., M. V. Banaschik, P. Colombani, D. P. Soroka, F. S. Stephens, and R. M. Diamond, 1976, Phys. Rev. Lett. **36**, 359.

- Simon, R. S., M. V. Banaschik, R. M. Diamond, J. O. Newton, and F. S. Stephens, 1977, Nucl. Phys. A **290**, 253.
- Simon, R. S., F. Folkmann, Ch. Briancon, J. Libert, J. P. Thibaud, R. J. Walen, and S. Frauendorf, 1980, Z. Phys. A **298**, 121.
- Simpson, J. J., P. O. Tjøm, I. Espe, G. B. Hagemann, B. Herskind, and M. Neiman, 1977, Nucl. Phys. A **287**, 362.
- Siwek-Wilczyńska, K., E. H. du Marchie van Voorthuysen, J. van Popta, R. H. Siemssen, and J. Wilczyński, 1979a, Phys. Rev. Lett. **42**, 1599.
- Siwek-Wilczyńska, K., E. H. du Marchie van Voorthuysen, J. van Popta, R. H. Siemssen, and J. Wilczyński, 1979b, Nucl. Phys. A **330**, 150.
- Siwek-Wilczyńska, K., and J. Wilczyński, 1976, Nucl. Phys. A **264**, 15..
- Sjoreen, T. P., D. B. Fossan, U. Garg, A. Neskakis, A. R. Pollett, and E. K. Warburton, 1979, in *Symposium on High-Spin Phenomena in Nuclei, Argonne*, edited by T. L. Khoo, print ANL/PHY-79-4, Argonne, p. 469.
- Sjoreen, T. P., U. Garg, and D. B. Fossan, 1978, Phys. Lett. B **76**, 397.
- Sjoreen, T. P., U. Garg, and D. B. Fossan, 1981, Phys. Rev. C **23**, 272.
- Sjoreen, T. P., U. Garg, D. B. Fossan, J. R. Beene, T. K. Alexander, E. D. Earle, O. Häusser, and A. B. McDonald, 1979, Phys. Rev. C **20**, 960.
- Sjoreen, T. P., G. Schatz, S. K. Bhattacherjee, B. A. Brown, D. B. Fossan, and P. M. S. Lesser, 1976, Phys. Rev. C **14**, 1023.
- Skaali, B., R. Kalish, J. Eriksen, and B. Herskind, 1975, Nucl. Phys. A **238**, 159.
- Stefanini, A. M., P. Kleinheinz, and M. R. Maier, 1976a, Phys. Lett. B **62**, 405.
- Stefanini, A. M., P. Kleinheinz, and M. R. Maier, 1976b, Nucl. Phys. A **258**, 34.
- Stephens, F. S., 1976, "Nuclear Structure at High Angular Momentum," in *Elementary Modes of Excitation in Nuclei*, Proceedings of the International School of Physics "Enrico Fermi," Course 69, 26 July–7 August 1976, edited by A. Bohr and R. Broglia (Società Italiana di Fisica, Bologna), p. 172.
- Stephens, F. S., 1979, in *Symposium on High-Spin Phenomena in Nuclei, Argonne*, edited by T. L. Khoo, print ANL/PHY-79-4, Argonne, p. 335.
- Stephens, F. S., 1982, in *INS International Symposium on Dynamics of Nuclear Motion, Mt. Fuji, Japan*, edited by K. Ogawa and T. Tanabe (INS, Tokyo), p. 2.
- Stephens, F. S., N. L. Lark, and R. M. Diamond, 1965, Nucl. Phys. **63**, 82.
- Strutinsky, V. M., 1967, Nucl. Phys. A **95**, 420.
- Sujkowski, Z., 1981, in *Proceedings of the XIXth Winter Meeting on Nuclear Physics, Bormio, Italy*, edited by I. Iori (University of Milano), p. 737.
- Sujkowski, Z., D. Chmielewska, R. V. F. Janssens, and M. J. A. de Voigt, 1979, Phys. Rev. Lett. **43**, 998.
- Sunyar, A. W., 1979, in *Symposium on High-Spin Phenomena in Nuclei, Argonne*, edited by T. L. Khoo, print ANL/PHY-79-4, Argonne, p. 77.
- Świątecki, W. J., J. R. Nix, and C. F. Tsang, 1969, unpublished notes.
- Szymański, Z., 1977, in *Nuclear Physics with Heavy Ions and Mesons*, edited by R. Balian, M. Rho, and G. Ripka, Les Houches, 30 (North-Holland, Amsterdam), Vol. 1, p. 297.
- Szymański, Z., 1983, *Fast Nuclear Rotation* (Oxford University, Oxford).
- Tanabe, K., K. Sugawara-Tanabe, and H. J. Mang, 1981, Nucl. Phys. A **357**, 20; 1981a, **357**, 45.
- Tanabe, K., and K. Sugawara-Tanabe, 1980, Phys. Lett. B **97**, 337.
- Thirumala Rao, B. V., R. Broda, C. Günther, A. Kleinrahm, and M. Ogawa, 1981, Nucl. Phys. A **362**, 71.
- Tippie, J. W., and R. P. Scharenberg, 1966, Phys. Rev. **141**, 1062.
- Trautmann, W., J. F. Sharpey-Schafer, H. R. Andrews, B. Haas, O. Häusser, P. Taras, and D. Ward, 1979, Phys. Rev. Lett. **43**, 991.
- Tsang, C. F., 1969, Ph.D. thesis, University of California, UCRL 18899.
- Valatin, J. G., 1961, in *Lectures in Theoretical Physics* (University of Colorado, Boulder), Vol. IV, p. 1.
- Vivien, J. P., Y. Schutz, F. A. Beck, E. Bozek, T. Byrski, C. Gehring, and J. C. Merdinger, 1979, Phys. Lett. B **85**, 325.
- Voigt, M. J. A. de, R. V. F. Janssens, H. Sakai, H. Aarts, C. J. van der Poel, D. E. C. Scherpenzeel, and H. F. R. Arciszewski, 1981, Phys. Lett. B **106**, 480.
- Voigt, M. J. A. de, K. Maeda, H. Ejiri, T. Shibata, K. Okada, T. Motobayashi, M. Sasao, T. Kishimoto, H. Suzuki, H. Sakai, and A. Shimizu, 1982, Nucl. Phys. A **379**, 160.
- Voigt, M. J. A. de, W. J. Ockels, Z. Sujkowski, A. Zglinski, and J. Mooibroek, 1979a, Nucl. Phys. A **323**, 317.
- Voigt, M. J. A. de, W. J. Ockels, Z. Sujkowski, J. Lukasiak, A. Zglinski, and A. Kerek,, 1979b, Nukleonika **24**, 425.
- Wakai, M., and A. Faessler, 1981, Z. Phys. A **303**, 335.
- Wakai, M., M. Sano, and A. Faessler, 1980, Phys. Lett. B **93**, 232.
- Walker, P. M., G. D. Dracoulis, A. Johnston, J. R. Leight, M. G. Slocombe, and I. F. Wright, 1976, J. Phys. G **2**, L197.
- Walker, P. M., D. Ward, O. Häusser, H. R. Andrews, and T. Faestermann, 1980, Nucl. Phys. A **349**, 1.
- Waluś, W., N. Roy, S. Jónsson, L. Carlén, H. Ryde, G. B. Hagemann, B. Herskind, J. D. Garrett, Y. S. Chen, J. Almberger, and G. Leander, 1981, Phys. Scr. **24**, 324.
- Ward, D., H. R. Andrews, J. S. Geiger, and R. L. Graham, 1973, Phys. Rev. Lett. **30**, 493.
- Ward, D., H. R. Andrews, O. Häusser, Y. El-Masri, M. M. Aleonard, I. Yang-Lee, R. M. Diamond, F. S. Stephens, and P. A. Butler, 1979, Nucl. Phys. A **332**, 433.
- Ward, D., H. Bertschat, P. A. Butler, P. Colombani, R. M. Diamond, and F. S. Stephens, 1975, Phys. Lett. B **56**, 139.
- Ward, D., P. Colombani, I. Y. Lee, P. A. Butler, R. S. Simon, R. M. Diamond, and F. S. Stephens, 1976, Nucl. Phys. A **266**, 194.
- Ward, T. E., and P. E. Haustein, 1971, Phys. Rev. Lett. **27**, 685.
- Warner, R. A., F. M. Bernthal, J. S. Boyno, T. L. Khoo, and G. Sletten, 1973, Phys. Rev. Lett. **31**, 835.
- Werf, S. Y. van der, 1978, Nucl. Instrum. Methods **153**, 221.
- West, R. L., E. G. Funk, A. Visvanathan, J. P. Adams, and J. W. Mihelich, 1976, Nucl. Phys. A **270**, 300.
- Westerberg, L., D. G. Sarantites, D. C. Hensley, R. A. Dayras, M. L. Halbert, and J. H. Barker, 1978, Phys. Rev. C **18**, 796.
- Westerberg, L., D. G. Sarantites, R. Lovett, J. T. Hood, J. H. Barker, C. M. Currie, and N. Mullani, 1977, Nucl. Instrum. Methods **145**, 295.
- Westerberg, L., D. G. Sarantites, K. Geoffroy Young, R. A. Dayras, J. R. Beene, M. L. Halbert, D. C. Hensley, and J. H. Barker, 1978, Phys. Rev. Lett. **41**, 96.
- Wilczyński, J., 1973, Nucl. Phys. A **216**, 386.
- Wilczyński, J., K. Siwek-Wilczyńska, J. van Driel, S. Gonggrijp, D. C. J. M. Hageman, R. V. F. Janssens, J. Lukasiak, and R. H. Siemssen, 1980, Phys. Rev. Lett. **45**, 606.

- Wilson, J., Y. H. Chung, S. R. Faber, A. Pakkanen, P. J. Daly, I. Ahmad, P. Chowdhury, T. L. Khoo, R. D. Lawson, and R. K. Smither, 1981, Phys. Lett. B **103**, 413.
- Wong, C. W., 1968, Nucl. Phys. A **108**, 481.
- Wu, J. R., C. C. Chang, H. D. Holmgren, and R. W. Koontz, 1979, Phys. Rev. C **20**, 1284.
- Yamazaki, T., T. Nomura, S. Nagamiya, and T. Katon, 1970, Phys. Rev. Lett. **25**, 547.
- Yates, S. W., I. Y. Lee, N. R. Johnson, E. Eichler, L. L. Riedinger, M. W. Guidry, A. C. Kahler, D. Cline, R. S. Simon, P. A. Butler, P. Colombani, F. S. Stephens, R. M. Diamond, R. M. Ronningen, R. D. Hichwa, J. H. Hamilton, and E. L. Robinson, 1980, Phys. Rev. C **21**, 2366.
- Zhang, J. Y., and S. Åberg, 1982, NBI preprint.
- Zolnowski, D. R., M. B. Hughes, J. Hunt, and T. T. Sugihara, 1980, Phys. Rev. C **21**, 2556.
- Zywietz, S., H. Grawe, H. Haas, and M. Menningen, 1981, Hyperfine Interact. **9**, 109.